QUINOIDAL COMPOUNDS: SYNTHESIS, GROUND-STATE GEOMETRY, PHYSICAL PROPERTIES AND APPLICATIONS

SHI XUELIANG

NATIONAL UNIVERSITY OF SINGAPORE

2015

QUINOIDAL COMPOUNDS: SYNTHESIS, GROUND-STATE GEOMETRY, PHYSICAL PROPERTIES AND APPLICATIONS

SHI XUELIANG

(*B. Sc. Soochow University*)

A THESIS SUBMITTED

FOR THE DEGREE OF DOCTOR OF PHILOSOPHY

DEPARTMENT OF CHEMISTRY

NATIONAL UNIVERSITY OF SINGAPORE

2015

Declaration

I hereby declare that this thesis is my original work and it has been written by me in its entirety, under the supervision of Dr. Chi Chunyan, (in the laboratory S9-05-01C), Chemistry Department, National University of Singapore, between August 2011 and July 2015.

I have duly acknowledged all the sources of information which have been used in the thesis.

This thesis has also not been submitted for any degree in any university previously.

The content of the thesis has been partly published in:

1) **X. Shi**, J. Chang and C. Chi, *Chem. Commun.*, **2013**, *49*, 7135 – 7137.

2) **X. Shi**, P. M. Burrezo, S. Lee, W. Zhang, B. Zheng, G. Dai, J. Chang, J. T. López Navarrete, K.-W. Huang, D. Kim, J. Casado and C. Chi, *Chem. Sci.*, **2014**, *5*, 4490 – 4503. **(Highlighted in SYNFACTS 2014, 10, 1270)**

3) **X. Shi**, S. Lee, M. Son, B. Zheng, J. Chang, L. Jing, K.-W. Huang, D. Kim and C. Chi, *Chem. Commun.*, **2015**, *51*, 13178 – 13180.

4) **X. Shi**, W. Kueh, B. Zheng, K.-W. Huang and C. Chi, *Angew. Chem. Int. Ed.*, **2015**, *54*, 14412–14416.

5) **X. Shi**, E. Quintero, S. Lee, L. Jing, T. S. Herng, B. Zheng, K.-W. Huang, J. T. López Navarrete, J. Ding, D. Kim, , J. Casado and C. Chi, *Chem. Sci.*, **2016,***7*, DOI: 10.1039/C5SC04706D.

Shi Xueliang		
Name	Signature	Date

Acknowledgement

First of all, I would like to thank my PhD supervisor Dr. Chi Chunyan for her time and patience to well train and support me during the past four years. Next I would like to express my sincere gratitude to Dr. Wu Jishan for his useful suggestions and inspiration given in every group meeting and discussion. Their guidance, suggestions, inspiration as well as tolerance during my PhD study are deeply acknowledged.

I am deeply grateful to all the past/current lab mates in Dr. Chi's group: Dr. Qu Hemi, Dr. Shao Jinjun, Dr. Ye Qun, Dr. Tong Chenhua, Dr. Dai Gaole, Dr. Gokulnath Sabapathi and Mr. Arun B. Lakshmi for their advices and help during my PhD study. I also thank the cooperation group members in Dr. Wu Jishan's group for their help and assistance. I would also thank all my collaborators including Prof. Huang Kuo-Wei, Prof. Juan Casado, Prof. Ding Jun, Prof. Dongho Kim, Dr. Zhang Wenhua, Dr. Chang Jingjing and so on. It is their help and efforts that make this thesis become true.

I also wish to thank MOE and NUS for providing me the scholarships to study in Singapore. In addition, I have greatly benefited from many staffs from chemistry department administrative office, the NMR laboratory, the Mass laboratory and the X-ray diffraction laboratory.

Finally, I would like to thank my parent for their support and understanding. I also deeply thank my wife Wu Qiuyan for her tolerance, understanding and encouragement during the four years.

Table of Contents

Publications List

1) **X. Shi**, E. Quintero, S. Lee, L. Jing, T. S. Herng, B. Zheng, K.-W. Huang, J. T. López Navarrete, J. Ding, D. Kim, , J. Casado and C. Chi, *Chem. Sci.***, 2016,***7*, DOI: 10.1039/C5SC04706D.

2) X. Yang*, **X. Shi***, Q. Miao, C. Chi, In preparation for *Chem. Sci.*. (*These authors contributed equally to this work.)

3) **X. Shi**, W. Kueh, B. Zheng, K.-W. Huang and C. Chi, *Angew. Chem. Int. Ed.*, **2015**, *54*, 14412–14416.

4) **X. Shi**, S. Lee, M. Son, B. Zheng, J. Chang, L. Jing, K.-W. Huang, D. Kim and C. Chi, *Chem. Commun.*, **2015**, *51*, 13178 – 13180.

5) Z. Zeng, **X. Shi**, Chunyan Chi, J. T. López Navarrete, J. Casado and J. Wu, *Chem. Soc. Rev.*, **2015**, *44*, 6578 – 6596.

6) **X. Shi**, P. M. Burrezo, S. Lee, W. Zhang, B. Zheng, G. Dai, J. Chang, J. T. López Navarrete, K.-W. Huang, D. Kim, J. Casado and C. Chi, *Chem. Sci.*, **2014**, *5*, 4490 – 4503. **(Highlighted in SYNFACTS 2014, 10, 1270)**

7) **X. Shi**, J. Chang and C. Chi, *Chem. Commun.*, **2013**, *49*, 7135 – 7137.

8) G. Dai, J. Chang, **X. Shi**, W. Zhang, B. Zheng, K.-W. Huang and C. Chi, *Chem. Eur. J.*, **2015**, *21*, 2019 – 2028.

9) Q. Ye, J. Chang, **X. Shi**, G. Dai, W. Zhang, K.-W. Huang, and C. Chi, *Org. Lett.*, **2014**, *16*, 3966 – 3969.

10) Q. Ye, J. Chang, K.-W. Huang, **X. Shi**, J. Wu, and C. Chi, *Org. Lett.*, **2013**, *15*, 1194 – 1197.

Summary

Quinoidal π-conjugated compounds have recently attracted increasing interest due to their unique physical properties and potential applications for organic field-effect transistors (OFETs), non-linear optics, and spin-based electronics. Various quinoidal compounds have been designed and synthesized in the last decade and typical examples are bisphenalenyls, zethrenes, indenofluorenes and so on. The most fascinating properties of quinoidal compounds are their low band gap and larger diradical character which can even lead to open-shell ground-state geometry hence resulting in their distinctive physical properties compared to the traditional aromatic π-conjugated compounds. It is believed that several factors including the quinoidal units, the fusion modes and the aromaticity/anti-aromaticity/pro-aromaticity can simultaneously determine the ground state and consequently the physical properties of quinoidal compounds. Thus fundamental understanding how these factors affect the ground-state geometry of quinoidal compounds is one of the aims of this thesis. Besides, the OFETs devices based on quinoidal compounds are also one of the objects in this thesis. In addition, we believe that instead of diene conjugation, quinoidal conjugation could be utilized as a new concept to build high order heteroacenes with bipolar/zwitterionic character.

In chapter 1 we give an overview of quinoidal compounds including their classification, their distinctive ground-state geometry and physical properties, their potential applications as well as their synthetic methodologies.

In chapter 2, a series of bisindeno-[*n*]thienoacenes (n = 1-4) were successfully synthesized *via* different strategies. The ground-state geometry and electronic properties of such series of molecules were systematically investigated by X-ray crystallographic analysis, NMR, ESR, Raman spectroscopy and theoretical calculation. This series of molecules can be regarded as anti-aromatic systems with small singlet biradical characters. It was found that with the extension of the length of quinoidal unit the molecules showed gradually increased singlet biradical character and decreased anti-aromaticity. Meanwhile, the optic and electronic properties in both neutral and charged states of the synthetic compounds were studied by one-photon absorption (OPA), two-photon absorption (TPA), cyclic voltammery and spectroelectrochemistry, which could be correlated to the chain length dependent anti-aromaticity and biradical character.

In chapter 3, a series of pro-aromatic dithiaquinoidal–[*n*]thienoacenes were successfully synthesized. The ground-state geometry and electronic properties of all molecules were systematically studied by X-ray crystallographic analysis, UV-vis spectroscopy, Raman spectroscopy and theoretical calculation. Our studies revealed that the transformation of the electronic structure from anti-aromatic in bisindeno-[*n*]thienoacenes to

pro-aromatic in dithiaquinoidal–[*n*]thienoacenes could be achieved by simply replacing the indene units by benzo-thia units. This conversion seems to promote the aromaticity and the biradical character of dithiaquinoidal–[*n*]thienoacenes and consequently affect their physical and chemical properties. Similarly, with the extension of chain length the molecules showed gradually increased singlet biradical character and increased aromaticity. The comparison between the work in chapter 2 and chapter 3 demostrated our hypothesis that both the quinoidal units and fusion modes do affect the aromaticity/anti-aromaticity/pro-aromaticity and determine the ground state of quinoidal compounds.

To further understand the fusion mode effect, pro-aromatic bisphenaleno-thieno[3,2-*b*]thiophene and anti-aromatic bisindeno-thieno[3,2-*b*]thiophene with different ground-state properties were systematically discussed and compared in chapter 4. It is found that pro-aromatic compound **BPT-TIPS** showed larger diradical character, stronger absorption, longer excited state lifetime and better redox amphotericity than anti-aromatic compound **S2-TIPS**. At the same time, solution processed OFETs based on **BPT-TIPS** with hole mobility as high as 0.26 $cm^2V^{-1}s^{-1}$ was obtained. The good OFETs performance of **BPT-TIPS** can be ascribed to its 3D ordered packing structure observed in the single crystals.

In chapter 5, the fused cyclopentadithiophenebis(dicyanovinylene) (**FCPDT**) was successfully synthesized and has been demonstrated as n-type

organic semiconductors due to the introduction of electron-withdrawing dicyanovinylene units. In particularly, field effect electron mobility as high as 0.16 $cm^2V^{-1}s^{-1}$ was achieved from **FCPDT-C16** by simple solution processing. The work in chapters 4 and 5 demostrated that, as expected, quinoidal compounds could serve as good active materials in OFETs.

In chapter 6, we designed and synthesized two quinoidal heteroacenes **1** and **3** as stable isoelectronic structures of pentacene and nonacene *via* a new synthetic approach. The unusual 1,2-sulfur migration which leads to the exclusive generation of unexpected **3** rather than the designed **2** was found in this synthetic route, and the mechanism of 1,2-sulfur migration was proposed accordingly. Meanwhile, the ground-state geometry and electronic properties of **1** and **3** were systematically investigated by X-ray crystallographic analysis, OPA, and cyclic voltammetry. All these experimental data give a same conclusion that both **1** and **3** have a typically quinoidal structure in their ground state with scarce diradical or dipolar/zwitterionic character. This work demonstrated the quinoidal conjugation could be utilized as a new concept to synthesize stable and soluble higher order acenes/heteroacenes.

In chapter 7, benzo[4,5]cyclohepta[1,2-*b*]fluorene as an isoelectronic isomer of pentacene was also designed and synthesized. The results further supported our hypothesis that instead of diene conjugation, quinoidal conjugation could be a good method to stablize high order heteroacenes. In

addition, a weak singlet diradical character and a dipolar character of such series of quinoidal heteroacenes have also been highlighted.

The work in this thesis will make supplementary contribution to understand the ground-state geometry and basic properties of quinoidal compounds.

Keywords: quinoidal, ground-state geometry, diradical, aromaticity, anti-aromaticity, pro-aromaticity, heteroacene, organic field effect transistors

List of Tables

List of Figures

List of Schemes

List of Abbreviations

AFM	atomic force microscopy
CV	cyclic voltammetry
DCM	dichloromethane
DPV	differential pulse voltammetry
DMF	dimethylformamide
DSC	differential scanning calorimetry
ESR	electron spin resonance
HOMO	highest occupied molecular orbital
LUMO	lowest unoccupied molecular orbital
MALDI-TOF	matrix-assisted laser desorption/ionization-time of flight
NBS	*N*-bromosuccinimide
NICS	nucleus independent chemical shift
NMR	nuclear magnetic resonance
ODTS	octadecyltrichlorosilane
OFETs	organic field effect transistors
OTMS	octadecyltrimethoxysilane
OTS	octadecyltrichlorosilane
PCC	pyridinium chlorochromate
POM	polarizing optical microscopy

QDM	quinodimethane
rt	room temperature (25 degrees)
SQUID	superconducting quantum interference device
TD-DFT	time-dependent density functional theory
TIPS	triisopropylsilyl
TGA	thermogravimetric analysis
THF	tetrahydrofuran
UV-Vis	ultraviolet-visible
XRD	X-ray diffraction

Chapter 1: Introduction

1.1 Quinoid and quinoidal compounds

Quinoid comes from the compound quinone. As shown in **Figure 1.1**, quinoid has a ring with one or more exocyclic double bonds resembling quinone in structure. Compared with conventional aromatic molecules, quinoidal molecules have attracted considerable interest due to their intriguing features. Firstly, quinoidal structures usually possess a much lower band gap and display a significant feature of amphoteric redox behavior compared with common aromatic structures. This feature makes quinoidal molecules good active materials in ambipolar organic field effect transistors (OFETs). Secondly, quinoidal molecules geometrically deviate from their aromatic analogues, i.e., quinoidal ones change the electron conjugation and damage the aromaticity in their aromatic analogues. However, this damage is not permanent and is reparable to some extent. Therefore, the quinoidal structures remain some aromaticity and could regain the geometry of their aromatic analogues in the form of diradicaloids by recovery of the aromaticity. Quinoidal cores/units are also the ideal fundamental bridges to build some novel molecules, which recently have been demonstrated to show open-shell biradical character compared to the closed-shell state of the conventional aromatic analogues. Without doubt, due to their obvious singlet biradical character, interesting physical properties (optical, electronic, magnetic, etc.), and potential applications for organic electronics, non-linear optics, organic

spintronics and enegy storage, quinoidal compounds have become a rising hot topic nowadays.[1]

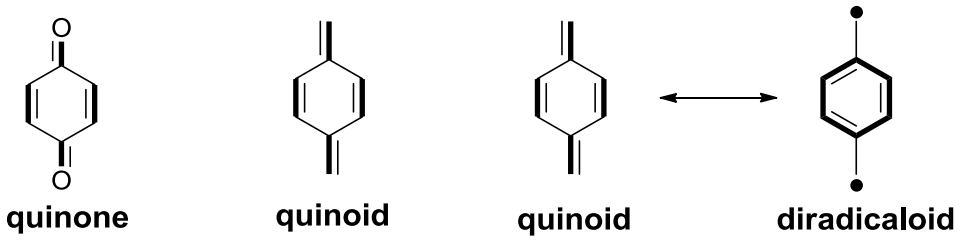

Figure 1.1 Structures of quinone, quinoid and diradicaloid.

As discussed in proceeding section, quinoid has an irresistible tendency to regain its aromatic geometry in the form of diradicaloid, which is driven by the recovery of aromaticity (**Figure 1.1**). This indicates that parent quinoidal units readily undergo dimerization, oxidation, polymerization and decomposition due to the unstable nature of diradicaloids, which have hindered the investigation and practical application based on quinoidal compounds. Hence, different strategies have been developed by chemists to stabilize such kind of semi-stable quinoidal molecules during last decades. Generally, there are two methods to stabilize such kind molecules as illustrated in **Figure 1.2**. The first one, terminal type, is to end cap the terminal methylene of quinoidal unit by some functional groups. This can both kinetically block the most reactive sites and also effectively delocalize the spin, hence, stabilize the quinoidal compounds. Furthermore, the properties such as solubility and biradical character of terminal type quinoidal compounds could at same time be tuned by choosing various functional groups as terminal substituents. By applying this method, various terminal type quinoidal

compounds have been synthesized and investigated such as quinoidal oligerthiophenes, Thiele's hydrocarbon, Chichibabin's hydrocarbon and their analogues (*vide infra*). The second approach developed recently, fusion type, is to embed the quinoidal unit into a π framework of an aromatic polycyclic hydrocarbons (PHs). This can enhance the structural rigidity and at the same time lead more efficient spin delocalization. In addition, kinetic stabilization by blocking the most reactive sites with bulky functional groups can further improve the stability and solubility. Similar to the terminal type, the properties of fusion type quinoidal compounds can also be tuned by differential fusion motifs. By using different fusion motifs, various fusion type quinoidal compounds have been designed and synthesized and typical examples are bisphenalenyls, zethrenes, indenofluorenes, quinoidal heteroacenes and their analogues (*vide infra*). Last but not least, the versatile quinoidal units give chemists a large space and opportunity to modify both types of quinoidal compounds. For example, by changing either the type of quinoidal unit or the length of it, the ground-state geometry and properties of quinoidal compounds will change accordingly. The geometry and property diversity in quinoidal compounds will lead a great interest to study the structure-properties relationship and chain length dependent properties of such series compounds.

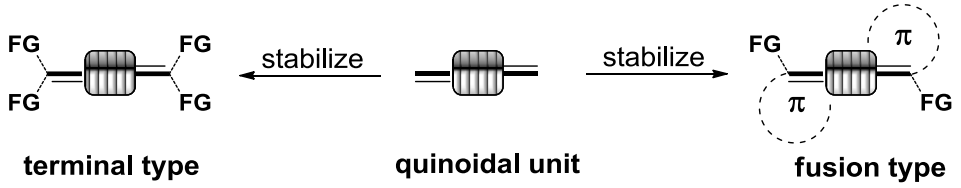

Figure 1.2 Two types of quinoidal compounds.

1.2 Terminal type quinoidal compounds

1.2.1 Quinoidal oligothiophenes and their analogues

The shortest quinoidal thiophene **1-1** in **Figure 1.3** was synthesized and developed as the alternative to the tetracyanoquinodimethan (TCNQ) in 1974 by Gronowitz and Uppström, but failed to be the electron accepter as the role of TCNQ.[2] Later, Fumio Ogura *et al.* developed the extended bi- and ter-quinoidal thiophenes **1-2** and **1-3** in 1987.[3] Both **1-2** and **1-3** could serve as electron accepter for organic metals and were considered as good TCNQ alternatives due to the better electrical conductivities. However, the development of even longer oligerthiophenes encountered poor solubility problem. This issue again hampers the synthesis of the longer quinoidal extension. To overcome this issue, Takahashi *et al.* developed a new lateral thiophene unit which is fused with a bis(butoxymethyl)cyclopentane ring to significantly improve the solubility of oligerthiophenes.[4] With this lateral thiophene unit, in 2005 the same group reported monomer to hexamer series of tetracyanoquinodimethan quinoidal oligothiophenes **1-4** – **1-9**.[5] This family of quinoidal oligothiophenes showed highly amphoteric redox behavior with very interesting properties. The oligomer series displayed strong electronic absorptions in the visible to near infrared region with a continuous energy gap decreased along with the extension of their conjugation. Interestingly, the NMR spectra of the longest two oligomers **1-8** and **1-9** showed no signals of

the tetracyanothienoquinodimethane and cyclopentane carbons, however definite signals assignable to the pendant butoxy carbons were observed. This indicated that some thermally accessible paramagnetic triplet species were involved in both **1-8** and **1-9**, which was further confirmed by ESR measurement. This system nicely demonstrates the chain length dependent properties and the increased biradical characters of quinoidal compounds with the extension of the central quinoidal units. Quinoidal oligothiophenes have also emerged as a promising class of active materials for organic electronics, especially for n-type and ambipolar OFETs due to the terminal electron deficient cyano groups. For example, the OFETs device based on **1-10** was fabricated and displayed n-type behavior with electron mobilities as high as 0.005 and 0.002 $cm^2V^{-1}s^{-1}$ for vapor and solution-deposited films, respectively.[6] The device could be further optimized and showed an ambipolar behavior with a major n-channel operation.[7] Later, Takimiya *et al.* further optimized the structure of ter- quinoidal thiophenes by changing the butyl groups in **1-10** with a bis(butoxymethyl)cyclopentane ring in **1-11** and the solution processed OFETs based on **1-11** with electron mobility as high as 0.16 $cm^2V^{-1}s^{-1}$ was obtained.[8] Recently, **1-12** and **1-13** were synthesized by Zhu's group, and the OFETs device performances based on these compounds with even higher electron mobilities than those of both **1-10** and **1-11** were achieved.[9] The better device performance may attribute to the utilization of the rigid diketopyrrolopyrrole group in **1-12** and tetrathienoquinoid core in **1-13**,

respectively. Aside from the tetracyano end-capped quinoidal oligothiophenes, quinoidal oligothiophenes with benzoquinone as terminal groups such as **1-14** – **1-16** have also been reported and exhibited low band gap and amphoteric redox behavior.[10] However, the study of their diradical character was rare and the OFETs device based on such kind structures was even less reported.

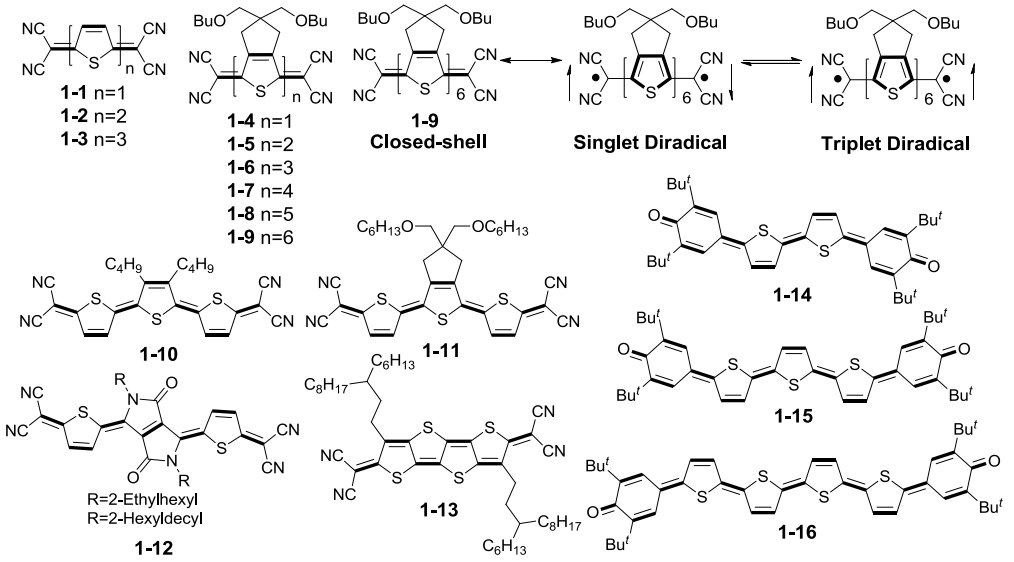

Figure 1.3 Structures of some quinoidal oligothiophenes and their analogues.

1.2.2 Thiele's hydrocarbon, Chichibabin's hydrocarbon and their analogues

More than one hundred years ago, Thiele and Chichibabin independently reported the synthesis of **1-17** and **1-18** (**Figure 1.4**) which were later termed Thiele's hydrocarbon and Chichibabin's hydrocarbon, accordingly.[11] Since that there's a long debate to be had as to the real geometry of their ground state and their intriguing properties. Both **1-17** and **1-18** are well known as singlet biradicals as their structures could be described as a resonance hybrid of a quinoidal form and singlet biradical form. In the late 1980s, low temperature

(-160 ^{0}C) and inert atmosphere X-ray crystal structures of **1-17** and **1-18** were successfully obtained and disclosed their real geometry in the solid state.[12] The large bond length alternation in the central *p*-quinoidimethans (*p*QDM) of **1-17** well revealed its quasi-quinoidal and closed-shell ground-state structure. In contrast, the bond lengths in the central section of **1-18** are intermediate between double and single bond values, ranging from 1.371-1.448 Å, indicating the significant biradical contribution to the molecular ground state of **1-18**.

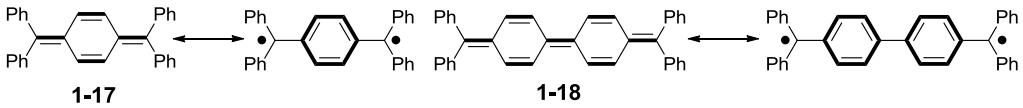

Figure 1.4 Thiele's hydrocarbon **1-17** and Chichibabin's hydrocarbon **1-18**.

Though Thiele's hydrocarbon and Chichibabin's hydrocarbon represent a typical case for the investigation of quinoidal hydrocarbons with biradical character, such kind structures are inherently reactive towards oxygen which has hampered the further studies and practical applications. Another efficient way to improve the stability of such kind of hydrocarbon is to utilize cyano groups instead of phenyl groups as terminates. This can further delocalize the spin, hence leads to the better stability than conventional Thiele's hydrocarbon and Chichibabin's hydrocarbon. With this strategy, various tetracyano-substituted quinoidal hydrocarbons were synthesized as listed in **Figure 1.5**. The synthesis, characterization and 1,6-addition reaction of TCNQ **1-19** were firstly reported by Acker and Hertler in 1962.[13] **1-19** possessess

much higher stability than Thiele's hydrocarbon **1-17** mainly due to the further spin delocalization of the terminal cyano groups in **1-19**. In that year, the particular interest in **1-19** was its strong electron acceptable ability that can form different charge-transfer complexes of **1-19**, the so-called organic metals, with electronic and magnetic properties. Its extension homologues of TNAP **1-20** and TANT **1-21** were reported later and all these electron acceptors **1-19** – **1-21** were able to form a variety of conductive complexes including TTF (tetrathiafulvalene) complexes.[14] Besides, OFETs device based on **1-20** was investigated and the n-type mobilities above 10^{-3} $cm^2V^{-1}s^{-1}$ was abtained.[15] The synthesis of even longer extended analogues of such kind of structures however encountered problems due to the stability issue. The high reactivity can be again explained by the irresistible tendency of forming diradicaloids as shown in **Figure 1.1**. Aside from the stability issue, the poor solubility of the extended analogues should also be addressed. An ingenious solution was reported by Nakamura *et al.* and the authors developed di-*p*-quinodimethane **1-22** and tri-*p*-quinodimethane **1-23** through a new molecular design (**Figure 1.5**).[16] The main idea of this design is that firstly the *p*-quinoidimethans (*p*QDM) unit was connected by carbon bridges that secured the planarity of the whole π-system. Then the 4-octyl side chains on the Ar groups together with other phenyl groups were installed to increase the solubility. At last the four cyano groups on the conjugation termini were attached to lower the HOMO level and hence stabilize the biradicaloids. Both **1-22** and **1-23** were

air-stable and thermally stable and they displayed amphoteric redox behavior. In addition, **1-23** exhibited distinctive biradical characteristics whose ground state could be described between an open-shell diradical form and a closed-shell quinoidal form. In contrast, **1-22** exhibited similar characteristics, however, with much smaller biradical character and should be formulated as a quasi-quinoidal structure.

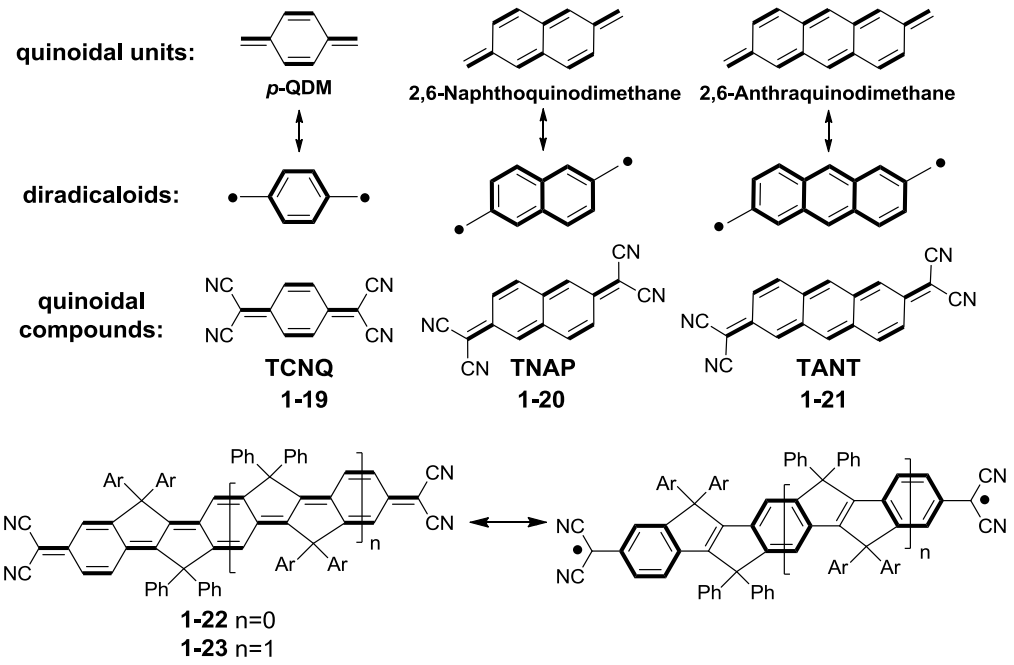

Figure 1.5 Some representative structures of tetracyano-substituted quinoidal hydrocarbons.

1.3 Fusion type quinoidal compounds

1.3.1 Bisphenalenyls

As classified in the above section, another family of quinoidal compounds is based on fusion type, which embeds the quinoidal unit into a π framework. Bisphenalenyls are the representatives which consist of *p*-quinoidimethan (*p*QDM) or other quinoidal units and two phenalenyls rings, developed mainly

by Nakasuji and Kubo *et al.*.[1g,1i] The ground-state structures of these series compounds were systematically investigated by electronic absorption, VT NMR, ESR, SQUID and X-ray crystallography together with theory calculations. Generally, **1-24** – **1-29** displayed significant singlet biradical character and with the extension of quinoidal unit the biradical character was enhanced from **1-24**, **1-25** to **1-26**, **1-27** and **1-28**, **1-29** (**Figure 1.6**).[17] The intrinsically large biradical character of such series compounds mainly attributes to the natural radical character of phenalenyl moiety and the driven force of the recovery of the aromaticity from the central quinoidal units. It is notable that the large biradical character of these series compounds leads to very interesting spin-spin interactions in their solid state (*i.e.*, in **1-25**, **1-27** and **1-29**) with very unique and strong intermolecular covalent bonding interactions between two phenalenyl rings of each two neighboring molecules. Interestingly, this intermolecular covalent bonding interaction is even stronger than the intramolecular one. This special intermolecular covalent bonding interaction in bisphenalenyls derivatives indicates their potential application as active materials of spin electronics. Some other applications such as OFETs and TPA based on these compounds were also studied. For example, OFETs device based on **1-25** exhibited ambipolar transport behavior with balanced hole and electron mobilities in the order of 10^{-3} $cm^2V^{-1}s^{-1}$.[18]

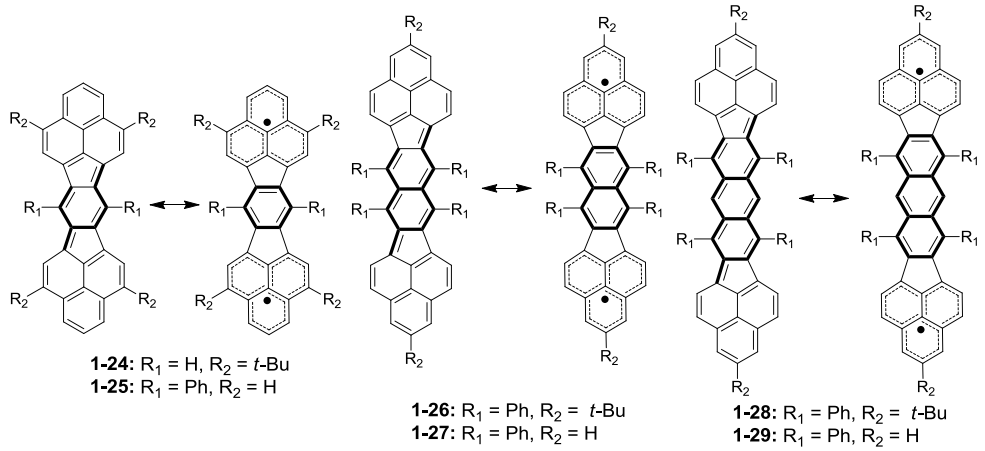

Figure 1.6 Some representative structures of bisphenalenyls.

1.3.2 Zethrenes

The parent zethrene **1-36** was first reported by Clar about 60 years ago through multi steps.[19] Later a more simple efficient method for synthesizing zethrenes was reported by Wu *et al.* in 2010.[20] The particular interest in zethrene is its intrinsic singlet biradical character which has been demonstrated by theoretical investigations, however, never confirmed by experimental studies.[21] Recently, Wu and co-workers reported the synthesis of the longer homologues of zethrene, called heptazethrene and octazethrene, and the prediction of the singlet biradical character of zethrene is thus first experimentally confirmed (**Figure 1.7**).[1a,1c,1e,1f,1h] Kinetically protected heptazethrene **1-31** showed an intense absorption band at 634 nm and sharp ^{1}H NMR signals in the aromatic region, indicating its closed-shell structure with very small biradical character.[22] Interestingly, heptazethrene diimide **1-30** displayed significantly singlet biradical character with broaden ^{1}H NMR signals in the aromatic region at room temperature.[23] Such a difference can be

explained by the relatively lower energy gap (1.0 eV) in heptazethrene diimide than that (1.47 eV) in **1-31**. A similar result was also found in the even longer zethrene homologue octazethrene **1-32**, which possessed much larger biradical character than that of **1-31**.[22] This could be easily explained by the larger resonance energy gained in **1-32** than in **1-31**. The same group again reported the two dibenzoheptazethrene isomers **1-33** and **1-34** and the ground state of both **1-33** and **1-34** was systematically investigated.[24] As a result, **1-34** showed larger biradical character and lower energy gap in comparison to **1-33**. This result may be simply due to the different annelation effect in the two compounds, thus leads to a differential conjugation contribution and energy band gap of the two compounds, though the authors explained such result by the Clar's aromatic sextet rule. Some other heptazethrene derivatives which consist of various fusion motifs such as perylene diimide and porphyrins have also been reported with small to moderate singlet biradical character.[25] Recently, one group reported the synthesis of parent zethrene **1-35** and parent dibenzozethrene **1-36** with significantly biradical character.[26] They claimed that the larger biradical character of the parent **1-35** and **1-36** than that of the conventional disubstituted zethrene derivatives was due to the substituents effect. However, the authors may mislead the readers and their conclusion may be controversial as the ESR signal they found in that work may be originated from some monoradical impurity. In summary, to date, the tunable ground-state structure of zethrene derivatives could successfully achieved and

the synthetic chemistry of zethrene family is also relatively deeply studied. Generally, the type of fusion motifs, the length of quinoidal unit together with the substituents all paly important roles to determine the ground state of zethrenes, though the substituents effect should be further investigated. The future trend of studies related to zethrene and its derivatives would focus on the real application such as OFETs, TPA, spin electronics, etc.

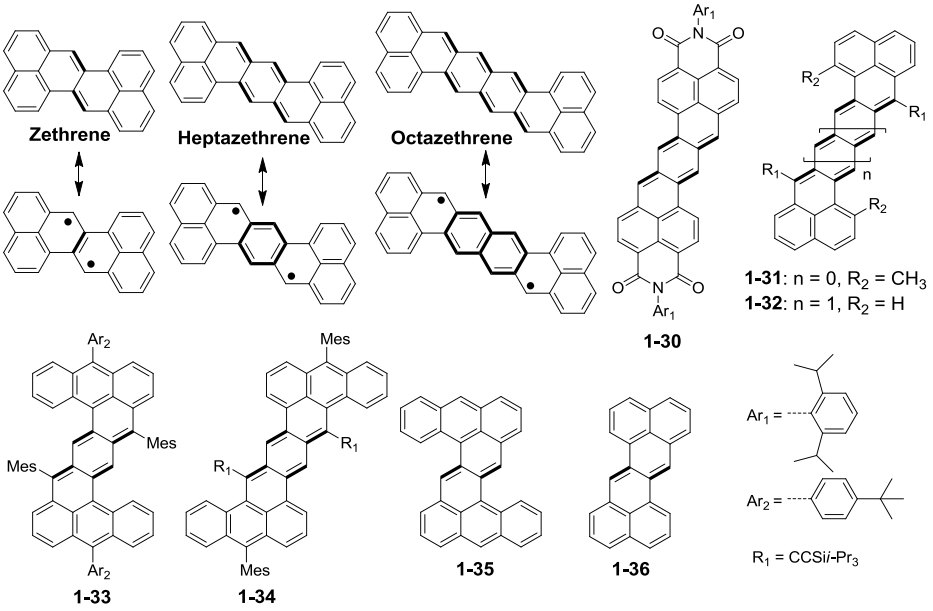

Figure 1.7 Some representative structures of zethrene and its derivatives.

1.3.3 Indenofluorenes

Indenofluorenes, which possess a 6-5-6-5-6 ring systems, are comprised of five structural isomers with quinoidal structures as shown in **Figure 1.8**. To date, aside from indeno[1,2-*a*]fluorene, all other four isomers have been synthesized and fully characterized by X-ray crystallographic analysis.[27] In 1994, Swager *et al.* first observed the generation of indeno[1,2-*b*]fluorene derivatives via a transannular cyclization reaction however failed to isolate

such compounds mostly due to the high reactivity towards oxygen.[28] In 2011, Haley *et al.* disclosed the synthesis of disubstituted indeno[1,2-*b*]fluorene derivatives such as **1-37**, **1-38** and **1-39** and the X-ray crystallographic results clearly revealed the large bond length alternation (BLA) in the central quinoidal unit in their solid states.[29] The large BLA indicated the typical quinoidal ground-state structures of indeno[1,2-*b*]fluorene derivatives with neglectable singlet biradical character. The small biradical character of indeno[1,2-*b*]fluorene derivatives was also consistent with the sharp ^{1}H NMR signals in the aromatic region, the relatively large HOMO-LUMO band gap together with the not long wavelength UV-vis absorption band. The field effect transistor based on **1-40** was also fabricated and the hole and electron mobilities extracted from **1-40** single crystal ambipolar transistors were 7×10^{-4} $cm^2V^{-1}s^{-1}$ and 3×10^{-3} $cm^2V^{-1}s^{-1}$, respectively.[30] In 2011, Haley *et al.* further reported three derivatives of indeno[1,2-*c*]fluorene **1-41**, **1-42** and **1-43**. Similar to indeno[1,2-*b*]fluorene derivatives, the X-ray crystallographic data of indeno[1,2-*c*]fluorene derivatives also showed large BLA in the central quinoidal unit, indicating the closed-shell ground structure of **1-41**, **1-42** and **1-43.**[31] The large band gap and sharp ^{1}H NMR signals in the aromatic region also supported the scarce biradical character in indeno[1,2-*c*]fluorene. The synthesis of indeno[2,1-*a*]fluorene derivative **1-44** was first repoted by Le Berre *et al.* in 1956.[32] However, **1-44** was highly reactive toward oxygen which hampered its full characterization. In 2011 the synthesis and full

characterization of indeno[2,1-*a*]fluorene derivative **1-45** were achieved by Tobe *et al.*.[33] Though the singlet biradical character of parent indeno[2,1-*a*]fluorene was estimated to be 33% on the basis of the broken-symmetry UHF calculation, the obtained disubstituted indeno[2,1-*a*]fluorene **1-45** showed small biradical character with a closed-shell ground structure confirmed by X-ray crystallographic analysis. The relatively large band gap and VT ^{1}H NMR measurement result also supported the neglectable biradical character in **1-45**. Tobe *et al.* also disclosed the synthesis and full characterization of indeno[2,1-*b*]fluorene derivative **1-46**.[34] In contrast to the other three indenofluorene isomers, **1-46** showed significant biradical character which even affected the NMR spectra. At room temperature, **1-46** showed broad ^{1}H NMR signals, however, upon cooling the signals became sharp. This indicated that some thermally accessible paramagnetic triplet species were involved in **1-46**. The paramagnetic triplet species were further detected by ESR measurement together with SQUID measurement. In summary, it is notable that among the four reported indenofluorene isomers, only the indeno[2,1-*b*]fluorene derivative **1-46** shows biradical character in its groud state. This can be explained by the number of the aromatic sextet ring gained from the closed-shell form to open-shell biradical form as in the closed-shell form only indeno[2,1-*b*]fluorene possesses one sextet, whereas other three isomers possess two, however they will all possess three in their open-shell biradical form. This “rule” predicts

that the last un-reported indeno[1,2-*a*]fluorene isomer should show significant diradicaloid character. Additionally, in contrast to bisphenalenyls and zethrene derivatives, indenofluorene derivatives show much weaker biradical character. This further indicates the important role of the fusion motifs on determining the ground-state and also the properties of the fusion type quinoidal compounds.

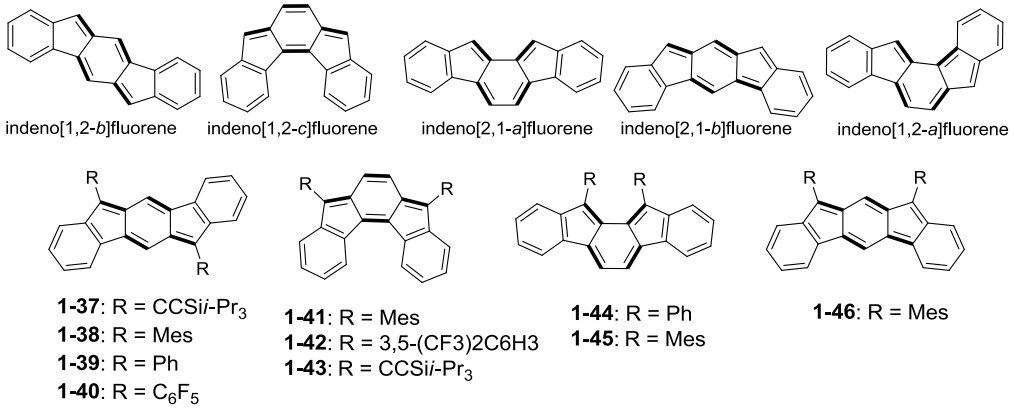

Figure 1.8 Some representative structures of indenofluorenes.

1.3.4 Quinoidal heteroacenes

Recently, our group reported the synthesis of the stable quinoidal dithiapentacene framework **1-47** and **1-48** (**Figure 1.9**).[35] Their ground-state quinoidal structures were proven by X-ray crystallographic analysis and the large BLA was found in the central quinoidal unit. Organic field effect transistors based on solution processed thin films of **1-47** and **1-48** showed a hole mobility of up to 0.032 $cm^2V^{-1}s^{-1}$. Notably, the quinoidal dithiapentacene framework showed superior stability than its corresponding pentacene analogues. Such difference could be explained by the different conjugation in two structures, i.e., quinoid-type conjugation in quinoidal dithiapentacene

framework and diene-type in conventional acene framework. In addition, acene framework such as pentacene **1-49** possesses one aromatic sextet ring, whereas **1-47** and **1-48** possess two. This work also gives us inspiration to synthesize stable and soluble high order acenes/heteroacenes with a quinoidal conjugation, called quinoidal heteroacenes.[36]

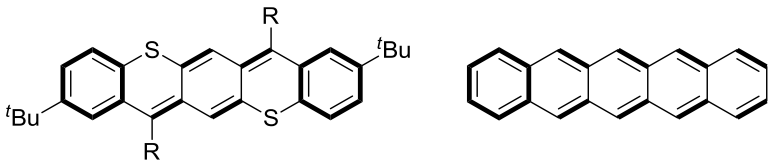

1-47: R = CCSi*i*-Pr$_3$
1-48: R = Ph

1-49

Figure 1.9 Structures of dithiapentacene and pentacene.

1.4 Synthetic methodology

1.4.1 Terminal type quinoidal compounds

The shortest quinoidal oligothiophene such as **1-1** and **1-4** have been achieved by treating 2,5-dihalothiophenes with tetracyanoethylene oxide in a refluxing condition.[2,5] TCNQ **1-19** has been synthesized from the condensation product of 1,4-cyclohexanedione and rnalononitrile.[13] However, these methods cannot be applied to synthesize even longer terminal type quinoidal compounds. To data, Takahashi's method has been mostly and widely used to prepare longer terminal type quinoidal compounds. The general of this method is that dihalo-oligomers couple with sodium dicyanomethanide under palladium catalysis followed by an oxidation reaction in the presence of various oxidants such as oxygen (from air), Br_2/water and even DDQ, which depends on the substrates (**Scheme1.1**). Most tetracyano groups end-capped

quinoidal compounds such as **1-5** – **1-13** and **1-20** – **1-23** were synthesized via this method.[5,9,16]

1.4.2 Fusion type quinoidal compounds

Different synthetic methods have been developed by chemists to construct fusion type quinoidal compounds. The most traditional and direct one is transannular cyclization route. For example, the generation of indeno[1,2-*b*]fluorene derivatives was achieved via this method by Swager *et al.*.[28] Zethrene and its derivatives such as **1-30**, **1-35** and **1-36** were also synthesized through this method.[20,23] This method is unique and straightforward and works well for the construction of small fusion type quinoidal compounds such as zethrene. However, for the construction of even longer fusion type quinoidal compounds this transannular cyclization approach meets inevitable disadvantages such as low reaction yield and the prohibition of bay region protection which usually leads unstable target compound. The second synthetic methodology, which is first widely applied in acene chemistry,[37] involves a nucleophilic addition of the corresponding diketone precursor with organolithium or Grignard reagent and subsequent reduction in the presence of $SnCl_2$. To date, most of the disubstituted fusion type quinoidal compounds were synthesized via this method. Hence, the advantages of this methodology are obvious, e.g., high reaction yield and diverse protected substitution at the bay position. The diverse protected substitution could both improve the solubility and stability of the target compounds. However, this

method also bears some drawbacks, e.g., on the one hand it does not tolerate with some precursors carrying with organolithium or Grignard reagent-sensitive active groups such as imide, ester, etc; on the other hand some Michael-type addition on the corresponding diketone precursor would be also problematic. The third synthetic methodology, which is widely applied in porphyrin chemistry, is a two-step sequence involving an intramolecular cyclization of the corresponding diol promoted by $BF_3{\cdot}OEt_2$, followed by an oxidation dehydrogenation reaction in the presence of various oxidants such as oxygen (from air), *p*-chloranil and even DDQ, which is dependent on the precursors. Hence, the choice of the oxidants is much tricky, leading this methodology to be complicated with low to moderate reaction yield.

In summary, the above literatures have shed a lot of light on how to construct and investigate quinoidal compounds, e.g., various synthetic approaches have been established; a standard characteristic method has been developed to determine the geometry of quinoidal compounds in their ground state; some potentially practical applications based on quinoidal compounds have been also proposed and investigated.

1.5 Specific gaps

Firstly, based on the above review, various factors such as the length of quinoidal units, fusion motifs and substituents can all affect the magnitude of biradical character in different quinoidal compounds. However, the study

about the relationship of these factors between the magnitude of biradical character in each quinoidal compound is still not deep. Hence, it is high imperative to find the most prominent influential factors which induce or promote the biradical character in quinoidal compounds. Secondly, to date, most studies based on quinoidal compounds just focus on the exploration of their intrinsic biradical character however a potentially existed bipolar or even zwitterionic character in quinoidal compounds may be ignored. Thirdly, the studies of practical applications based on quinoidal compounds are inadequate and urgently needed.

1.6 Objectives and significance

Based on the above limitations, the main aim of this study was to synthesize various fusion type quinoidal compounds and explore their structure-property relationship. All the target quinoidal compounds involved in this thesis are listed in **Figure 1.10**. Besides, the OFETs devices based on some quinoidal compounds were also fabricated and investigated.

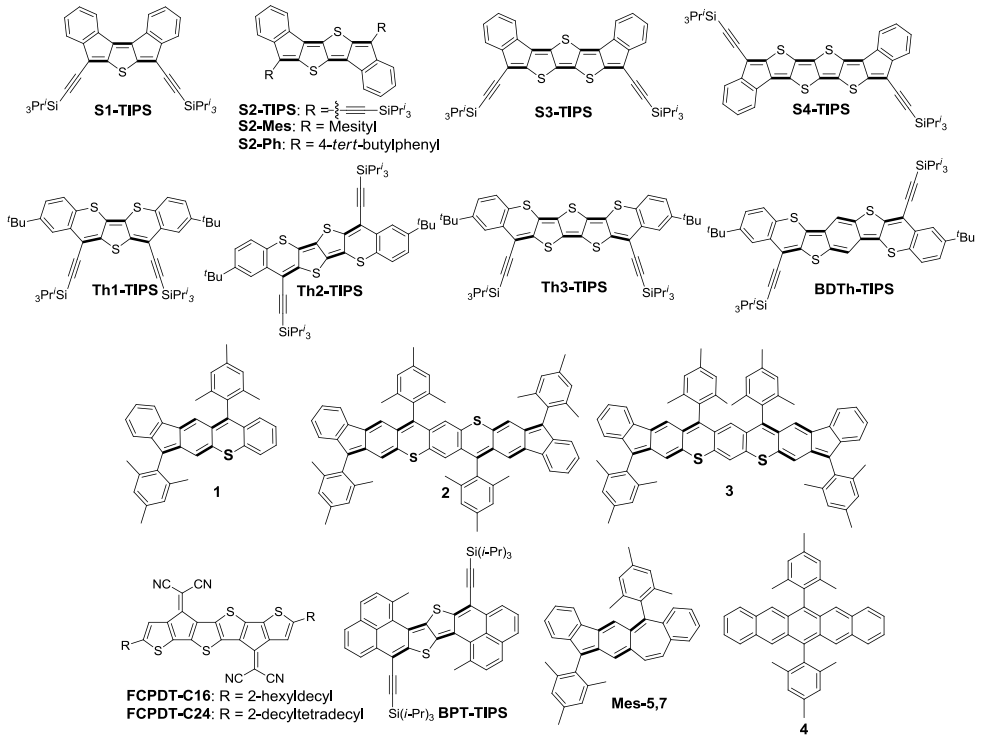

Figure 1.10 Structures of the target quinoidal compounds in this thesis.

More specifically, the objectives of this study include:

(1) To synthesize a series of quinoidal compounds, called bisindeno-[*n*]thienoacenes (**S1-TIPS**, **S2-TIPS**, **S2-Mes**, **S2-Ph**, **S3-TIPS**, **S4-TIPS**) and dithiaquinoidal–[*n*]thienoacenes (**Th1-TIPS**, **Th2-TIPS**, **Th3-TIPS**, **BDTh-TIPS**), via different synthetic methodologies and to determine the ground-state geometry and electronic structure of each quinoidal compound. In addition, the structure-aromaticity-biradical character-physical properties relationship of such series of synthetic quinoidal compounds with different chain length and fusion motifs was systematically investigated by X-ray crystallographic analysis, NMR, ESR and Raman spectroscopy, assisted by density functional theory calculations. (refer to chapter 2 and chapter 3)

(2) To synthesize quinoidal compounds (**S2-TIPS**, **BPT-TIPS, FCPDT-C16**,

and **FCPDT-C24**) and investigate the OFETs device performances based on these compounds. (refer to chapter 4 and chapter 5)

(3) To synthesize the stable high order heteroacenes with a quinoidal conjugation (**1**, **2** and **3**). Their ground-state geometry and physical properties were thoroughly studied and also compared with conventional acenes. (refer to chapter 6)

(4) To synthesize an asymmetric quinoidal compound (**Mes-5,7**) with two differential fusion motifs in one molecule and determine its ground-state geometry. The bipolar/zwitterionic character of this asymmetric quinoidal compound was preliminarily studied. Photophysical and electrochemical properties of **Mes-5,7** were also investigated and compared with those of its structural isomer **4**. (refer to chapter 7)

The results involved in this thesis would make supplementary contribution to understand the ground-state geometry and basic properties of quinoidal compounds. The various synthetic strategies which were utilized to achieve diverse quinoidal compounds in this thesis would shed light on the design and synthesis of other higher conjugated molecules with novel structures. The studies also revealed a clear structure-aromaticity-biradical character-physical properties-reactivity relationship of quinoidal compounds, which is of importance for tailored material design in the future.

Due to time and research field limit, the study of this thesis particularly focuses on the design and investigation of fusion type quinoidal compounds

and therefore terminal type ones are excluded. In addition, the mechanism and device fabrication part (which have been studied by my collaborator) involved in this thesis are not fully discussed.

Reference

[1] See review articles: (a) Z. Sun and J. Wu, *J. Mater. Chem.*, 2012, **22**, 4151. (b) J. Casado, R. Ponce Ortiz and J. T. López Navarrete, *Chem. Soc. Rev.*, 2012, **41**, 5672. (c) Z. Sun, Q. Ye, C. Chi and J. Wu, *Chem. Soc. Rev*., 2012, **41**, 7857. (d) A. Shimizu, Y. Hirao, T. Kubo, M. Nakano, E. Botek and B. Champagne, *AIP Conf. Proc.*, 2012, **1504**, 399. (e) Z. Sun, Z. Zeng and J. Wu, *Chem. Asian J.*, 2013, **8**, 2894. (f) Z. Sun and J. Wu, *Pure Appl. Chem.*, 2014, **86**, 529. (g) T. Kubo, *Chem. Rec.*, 2014, **15**, 218. (h) Z. Sun, Z. Zeng and J. Wu, *Acc. Chem. Res*., 2014, **47**, 2582. (i) T. Kubo, *Chem. Lett.*, 2015, **44**, 111.

[2] S. Gronowitz and B. Uppström, *Acta Chem. Scand., Ser. B*, 1974, **28**, 981.

[3] (*a*) K. Yui, Y. Aso, T. Otsubo and F. Ogura, *J. Chem. Soc, Chem. Commun.*, 1987, 1816. (*b*) K. Yui, H. Ishida, Y. Aso, T. Otsubo, F. Ogura, A. Kawamoto and J. Tanaka, *Bull. Chem. Soc. Jpn.*, 1989, **62**, 1547.

[4] T. Izumi, S. Kobashi, K. Takimiya, Y. Aso and T. Otsubo, *J. Am. Chem. Soc.*, 2003, **125**, 5286.

[5] T. Takahashi, K. Matsuoka, K. Takimiya, T. Otsubo and Y. Aso, *J. Am. Chem. Soc.*, 2005, **127**, 8928.

[6] T. M. Pappenfus, R. J. Chesterfield, C. D. Frisbie, K. R. Mann, J. Casado, J.

D. Raff and L. L. Miller, *J. Am. Chem. Soc.*, 2002, **124**, 4184.

[7] R. J. Chesterfield, C. R. Newman, T. M. Pappenfus, P. C. Ewbank, M. H. Haukaas, K. R. Mann, L. L. Miller and C. D. Frisbie, *Adv. Mater.*, 2003, **15**, 1278.

[8] S. Handa, E. Miyazaki, K. Takimiya and Y. Kunugi, *J. Am. Chem. Soc.*, 2007, **129**, 11684.

[9] (a) Q. Wu, R. Li, W. Hong, H. Li, X. Gao and D. Zhu, *Chem. Mater.*, 2011, **23**, 3138. (b) Y. Qiao, Y. Guo, C. Yu, F. Zhang, W. Xu, Y. Liu and D. Zhu, *J. Am. Chem. Soc.*, 2012, **134**, 4084.

[10] E. V. Canesi, D. Fazzi, L. Colella, C. Bertarelli and C. Castiglioni, *J. Am. Chem. Soc.*, 2012, **134**, 19070.

[11] (a) J. Thiele and H. Balhorn, *Chem. Ber.*, 1904, **37**, 1463. (b) A. E. Tschitschibabin, *Chem. Ber.*, 1907, **40**, 1810.

[12] L. K. Montgomery, J. C. Huffman, E. A. Jurczak and M. P. Grendze, *J. Am. Chem. Soc.*, 1986, **108**, 6004.

[13] D. S. Acker and W. R. Hertler, *J. Am. Chem. Soc*., 1962, **84**, 3370.

[14] (*a*) A. F. Garito and A. J. Heeger, *Acc. Chem. Res*., 1974, **7**, 232. (*b*) T. Yanagimoto, K. Takimiya, T. Otsubo and F. Ogura, *J. Chem. Soc*., *Chem. Commun*., 1993, 519.

[15] J. G. Laquindanum, H. E. Katz, A. Dodabalapur and A. J. Lovinger, *J. Am. Chem. Soc*., 1996, **118**, 11331.

[16] X. Zhu, H. Tsuji, K. Nakabayashi, S.-I. Ohkoshi and E. Nakamura, *J. Am.*

Chem. Soc., 2011, **133**, 16342.

[17] (a) T. Kubo, A. Shimizu, M. Sakamoto, M. Uruichi, K. Yakushi, M. Nakano, D. Shiomi, K. Sato, T. Takui, Y. Morita and K. Nakasuji, *Angew. Chem. Int. Ed.*, 2005, **44**, 6564. (b) A. Shimizu, T. Kubo, M. Uruchi, K. Yakushi, M. Nakano, D. Shiomi, K. Sato, T. Takui, Y. Hirao, K. Matsumoto, H. Kurata, Y. Morita and K. Nakatsuji, *J. Am. Chem. Soc*., 2010, **132**, 14421. (c) A. Shimizu, Y. Hirao, K. Matsumoto, H. Kurata, T. Kubo, M. Uruichi and K. Yakushi, *Chem. Commun.*, 2012, **48**, 5629.

[18] M. Chikamatsu, T. Mikami, J. Chisaka, Y. Yoshida, R. Azumi, K. Yase, A. Shimizu, T. Kubo, Y. Morita and K. Nakasuji, *Appl. Phys. Lett.*, 2007, **91**, 043506.

[19] E. Clar, K. F. Lang and H. Schulz-Kiesow, *Chem. Ber*., 1955, **88**, 1520.

[20] T.-C. Wu, C.-H. Chen, D. Hibi, A. Shimizu, Y. Tobe and Y.-T. Wu, *Angew. Chem. Int. Ed.*, 2010, **49**, 7059.

[21] M. Nakano, R. Kishi, A. Takebe, M. Nate, H. Takahashi, T. Kubo, K. Kamada, K. Ohta, B. Champagne and E. Botek, *Comput. Lett.*, 2007, **3**, 333.

[22] Y. Li, W.-K. Heng, B. S. Lee, N. Aratani, J. L. Zafra, N. Bao, R. Lee, Y. M. Sung, Z. Sun, K.-W. Huang, R. D. Webster, J. T. López Navarrete, D.-H. Kim, A. Osuka, J. Casado, J. Ding and J. Wu, *J. Am. Chem. Soc.*, 2012, **134**, 14913.

[23] Z. Sun, K.-W. Huang and J. Wu, *J. Am. Chem. Soc.*, 2011, **133**, 11896.

[24] Z. Sun, S. Lee, K. H. Park, X. Zhu, W. Zhang, B. Zheng, P. Hu, Z. Zeng,

S. Das, Y. Li, C. Chi, R. W. Li, K. W. Huang, J. Ding, D. Kim and J. Wu, *J. Am. Chem. Soc.*, 2013, **135**, 18229.

[25] (a) S. Das, S. Lee, M. Son, X. Zhu, W. Zhang, B. Zheng, P. Hu, Z. Zeng, Z. Sun, W. Zeng, R. W. Li, K. W. Huang, J. Ding, D. Kim and J. Wu, *Chem. Eur. J.*, 2014, **20**, 11410. (b) W. Zeng, M. Ishida, S. Lee, Y. Sung, Z. Zeng, Y. Ni, C. Chi, D.-H. Kim and J. Wu, *Chem. Eur. J.*, 2013, **19**, 16814.

[26] Y.-C. Hsieh, H.-Y. Fang, Y.-T. Chen, R. Yang, C.-I. Yang, P.-T. Chou, M.-Y. Kuo and Y.-T. Wu, *Angew. Chem. Int. Ed.*, 2015, **54**, 1.

[27] A. G. Fix, D. T. Chase and M. M. Haley, *Top. Curr. Chem.*, 2012, DOI: 10.1007/128_2012_376.

[28] Q. Zhou, P. J. Carroll and T. M. Swager, *J. Org. Chem*., 1994, **59**, 1294.

[29] (a) D. T. Chase, B. D. Rose, S. P. McClintock, L. N. Zakharov and M. M. Haley, *Angew. Chem. Int. Ed.*, 2011, **50**, 1127. (b) D. T. Chase, A. G. Fix, B. D. Rose, C. D. Weber, S. Nobusue, C. E. Stockwell, L. N. Zakharov, M. C. Lonergan and M. M. Haley, *Angew. Chem. Int. Ed*., 2011, **50**, 11103.

[30] D. T. Chase, A. G. Fix, S. J. Kang, B. D. Rose, C. D. Weber, Y. Zhong, L. N. Zakharov, M. C. Lonergan, C. Nuckolls and M. M. Haley, *J. Am. Chem. Soc*., 2012, **134**, 10349.

[31] A. G. Fix, P. E. Deal, C. L. Vonnegut, B. D. Rose, L. N. Zakharov and M. M. Haley, *Org. Lett*., 2013, **15**, 1362.

[32] (a) A. Étienne and A. Le Berre, *C. R. Hebd. Seances Acad. Sci.*, 1956, **242**, 1493. (b) A. Le Berre, *Ann. Chim.*, 1957, **13**, 371.

[33] A. Shimizu and Y. Tobe, *Angew. Chem. Int. Ed*., 2011, **50**, 6906.

[34] A. Shimizu, R. Kishi, M. Nakano, D. Shiomi, K. Sato, T. Takui, I. Hisaki, M. Miyata and Y. Tobe, *Angew. Chem. Int. Ed*., 2013, **52**, 6076.

[35] Q. Ye, J. Chang, X. Shi, G. Dai, W. Zhang, K. W. Huang and C. Chi, *Org. Lett*., 2014, **16**, 3966.

[36] Q. Ye and C. Chi, *Chem. Mater.*, 2014, **26**, 4046.

[37] (a) J. E. Anthony, *Chem. Rev.*, 2006, **106**, 5028. (b) J. E. Anthony, *Angew. Chem. Int. Ed.*, 2008, **47**, 452. (c) H. Qu and C. Chi, *Curr. Org. Chem.*, 2010, **14**, 2070.

Chapter 2: Anti-aromatic Bisindeno-[n]thienoacenes with Small Singlet Biradical Characters: Syntheses, Structures and Chain Length Dependent Physical Properties

2.1 Introduction

Quinoidal π-conjugated structures are fundamentally important for organic optical, electronic and magnetic materials as they are closely related to the doped state of semiconducting polymers.[1] Recent studies demonstrated that quinoidal polycyclic hydrocarbons (PHs)[2] and oligothiophenes[3] could show obvious singlet biradical character and unique optical, electronic and magnetic activity, which lead to versatile applications for organic electronics,[4] non-linear optics,[5] organic spintronics,[6] organic photovoltaics[7] and energy storage devices.[8] The fundamental subunits of the quinoidal PHs are pro-aromatic *p*-quinodimethane (*p*-QDM, **2-1**), 2,6-naphthoquinodimethane (**2-2**), 2,6-anthraquinodimethane (**2-3**), and their isomers, which are embedded into an aromatic framework (**Figure 2.1**). By using different fusion motifs, various quinoidal PHs have been designed and synthesized, and typical examples are bisphenalenyls (e.g. **2-4**) reported by Kubo *et al.*,[9] indenofluorenes (e.g. **2-5**) reported by Haley and Tobe *et al.*,[10] zethrenes (e.g. **2-6**)[11] and extended *p*-QDMs[12] reported by Wu *et al.* (**Figure 2.1**). Some of this type of hydrocarbons showed significant biradical character in the ground state due to recovery of the aromaticity of the pro-aromatic quinodimethanes

in the biradical resonance form. As a consequence, their physical properties are distinctly different from the traditional closed-shell PHs. Similarly, quinoidal oligothiophenes (**2-7**)[3] have been intensively studied due to the unique magnetic activity for higher order oligomers[13] and their promising applications for ambipolar and *n*-channel organic field effect transistors (OFETs).[14] In addition, fused α-oligothiophenes and thiophene-fused acenes, the so-called thienoacenes, have been demonstrated to be excellent organic semiconductors for OFETs by Takimiya *et al*..[15] Their quinoidal counterparts, the [*n*]thienoacenequinodimethanes (**2-8**) thus are of interest. However, synthesis of such type of molecules are challenging due to the lack of efficient synthetic method and their poor solubility.[16] Incorporation of these subunits into a polycyclic hydrocarbon framework is supposed to lead to new hybrid systems with unique physical properties but it becomes even more challenging. To the best of our knowledge, no such kind of research work has been reported. In this context, we are particularly interested in the bisindeno-[*n*]thienoacenes **2-9** – **2-12** (n = 1-4), in which a quinoidal thienoacene unit is annulated with two indene rings (**Figure 2.1**).

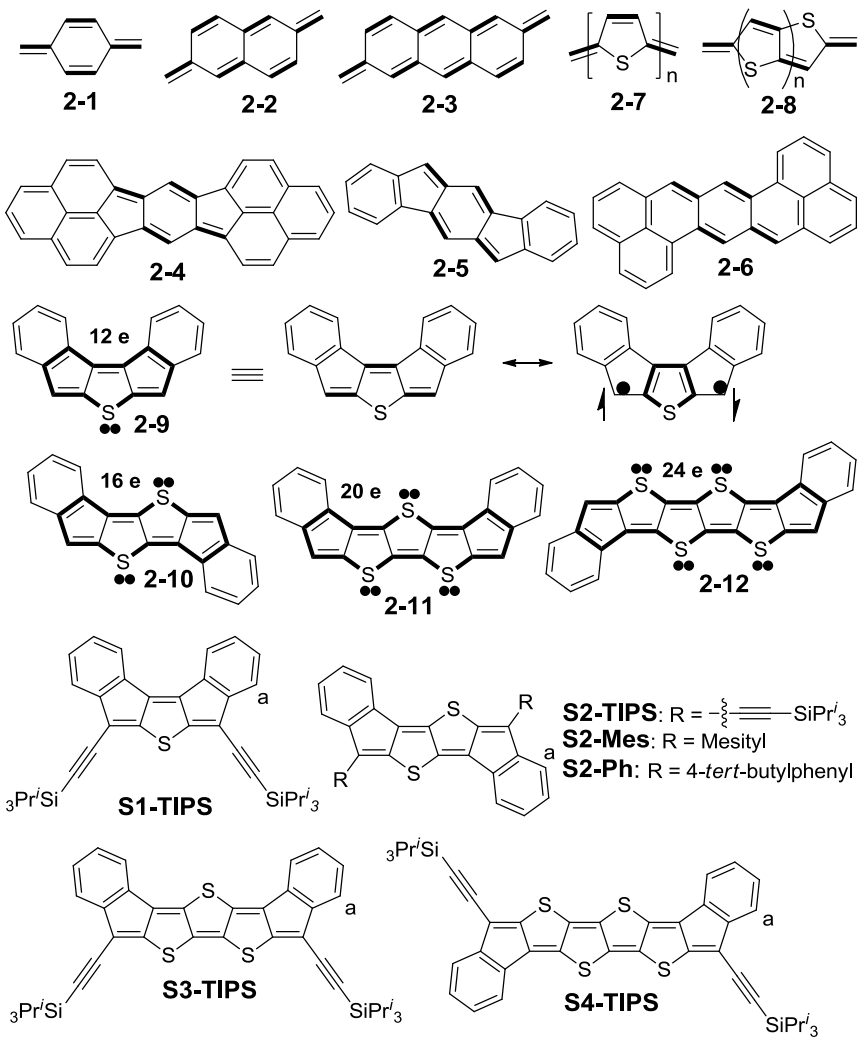

Figure 2.1 Fundamental quinodimethanes and representative quinoidal hydrocarbons and bisindeno-[*n*]thienoacenes.

Similar to the quinoidal oligothiophenes, significant contribution of the biradical resonance form to their ground-state structures can be expected due to the recovery of the aromaticity of the fused thiophene rings. Looking into the structures from another angle, this type of molecules can be regarded as dibenzannulated anti-aromatic systems containing 4n π electrons (highlighted in bold form in **Figure 2.1**) if two π electrons are counted for each sulfur atom. It is well known that anti-aromatic systems, regarding their aromatic analogues, have a pair of electrons in defect (i.e., 4n versus 4n+2) that transforms the ground electronic state from an in-phase stabilizing

combination of Kekulé structures for the aromatics into an out-of-phase combination which originates the anti-aromatic unstability. In order to mitigate such unstabilization, the highest energy bounded 4n electron pair might lead to the formation of a biradical if these two electrons are uncorrelated (in large size systems). Such interesting structural features imply their unique physical properties related to their biradical character and anti-aromaticity, as well as their interdependence or interconversion as a function of the chain length. Therefore, our particular interests of this work include: (1) their efficient synthesis; (2) their geometry and electronic structures in the ground state; (3) their chain length dependent optical, electronic and magnetic properties. In addition, the properties of their charged forms are also of interest because of the change of aromaticity upon gain or loss of one or two π electrons. Such fundamental studies will help us to better understand the role of aromaticity and biradical character on the physical properties of quinoidal systems and allow us to do tailored design in the future.

The parent compounds **2-9** – **2-12** are predicted to be unstable due to the contribution of the biradical resonance form to the ground-state structures and they are also insoluble. Therefore, their derivatives in which the most reactive sites are kinetically blocked by triisopropylsilylethynyl (TIPSE) group (**S1-TIPS**, **S2-TIPS**, **S3-TIPS**, **S4-TIPS**) or aryl groups (**S2-Mes**, **S2-Ph**) (**Figure 2.1**) were designed and synthesized. Their ground-state geometry and electronic structures were investigated by X-ray crystallographic analysis,

NMR, ESR and Raman spectroscopy, assisted by density functional theory (DFT) calculations. Their physical properties were systematically studied by different experimental techniques, including one-photon absorption (OPA), transient absorption (TA), two-photon absorption (TPA), Raman spectroscopy, cyclic voltammetry, and spectroelectrochemistry. The properties were rationally correlated to the chain length dependent anti-aromaticity and biradical character in this unique quinoidal and anti-aromatic system.

2.2 Results and discussion

2.2.1 Synthesis

The synthetic methodology used to synthesize substituted acenes,[17] indenofluorenes[10] and zethrenes[11] was utilized to obtain our target compounds. That is, the corresponding diketones were prepared first, followed by nucleophilic addition with lithiated TIPSE or aryl groups, and then by reduction of the intermediate diols with $SnCl_2$. The major challenge was the synthesis of the bisindeno-thienoacene diketones, which were achieved by different strategies.

The synthesis of **S1-TIPS** commenced with Knoevenagel type condensation reaction between diethyl thiodiglycolate (**2-13**) and benzil (**2-14**) under strong basic conditions according to a published procedure with minor modification, giving the 3,4-diphenylthiophene-2,5-dicarboxylic acid (**2-15**) in 60% yield (**Scheme 2.1**).[18] The diacid **2-15** was then treated with an excess of

thionyl chloride to afford the 3,4-diphenylthiophene-2,5-dicarbonyl chloride, and subsequent double Friedel–Crafts acylation with $AlCl_3$ gave the desired diketone **2-16** in 85% yield. Compound **S1-TIPS** was then obtained as a dark green solid in an overall 70% yield by addition of lithiated TIPSE to the diketone **2-16** followed by reductive dehydroxylation with $SnCl_2$.

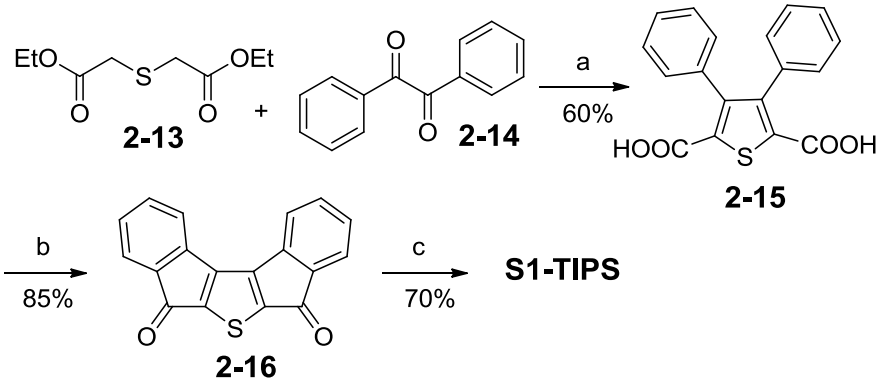

Scheme 2.1 Synthetic route to **S1-TIPS**: (a) i) CH_3ONa, EtOH, r.t. for 4 h and then 60 ^oC for 12 h; ii) NaOH, EtOH, reflux, 12 h; iii) 10% HCl (aq.); (b) i) $SOCl_2$, CH_2Cl_2, reflux; ii) $AlCl_3$, CH_2Cl_2, 0 ^oC – r.t., 12 h; (c) i) TIPSC≡CLi, THF, r.t., 12h; ii) $SnCl_2$, toluene, r.t., 12 h.

The synthesis of compounds **S2-TIPS**, **S2-Mes** and **S2-Ph** are outlined in **Scheme 2.2**. Three different substituents (TIPSE, mesityl and 4-*tert*-butylphenyl) are introduced to investigate the effect of the substituent on the physical properties. The starting compound is 2,3,5,6-tetrabromothieno[3,2-b]thiophene **2-17**, which was prepared according to reported procedure.[19] Based on our previous work, the key intermediate **2-18** was obtained in 70% yield by selective introduction of two ester groups to the α-positions of **2-17**.[20] Suzuki coupling reaction between **2-18** and phenylboronic acid gave **2-19** in 94% yield. Hydrolysis of **2-19** produced the diacid **2-20** which was treated with $SOCl_2$ and then $AlCl_3$ to give the desired

diketone **2-21** in an overall 80% yield. Subsequent addition of lithiated regents and reduction of the intermediate diols by $SnCl_2$ gave **S2-TIPS**, **S2-Mes** and **S2-Ph** in 70%, 50%, and 40% yield, respectively.

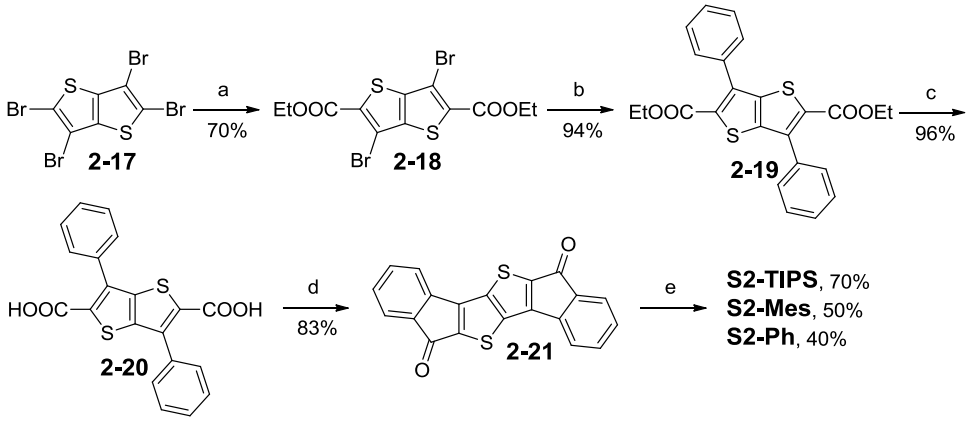

Scheme 2.2 Synthetic route to **S2-TIPS**, **S2-Mes** and **S2-Ph**: (a) i) *n*-BuLi, THF, -78 ^{o}C, 1h; ii) NC-COOEt, -78 ^{o}C – r.t., overnight; (b) $PhB(OH)_2$, $Pd(PPh_3)_4$, Na_2CO_3, toluene/H_2O, reflux, 12 h; (c) NaOH, MeOH/THF (1:1), reflux, overnight; (d) i) $SOCl_2$, CH_2Cl_2, reflux, overnight; ii) $AlCl_3$, CH_2Cl_2, 0 ^{o}C – r.t., overnight; (e) i) TIPSC≡CLi, or Mes-MgBr or 4-*tert*-butylphenylLi, 0 ^{o}C – r.t., overnight; ii) $SnCl_2$, toluene, r.t., overnight.

The synthesis of **S3-TIPS** was based on the key intermediate diketone **2-24**,[21] which was synthesized by a modified procedure in two steps from tetrabromothiophene (**2-22**) in an overall 80% yield (**Scheme 2.3**). Nucleophilic substitution and condensation reaction between **2-24** and ethyl mercaptoacetate followed by the hydrolysis of ester groups in the presence of potassium hydroxide afforded diacid **2-25** in 95% yield. Subsequent reactions following a similar protocol to that shown in **Scheme 2.1** and **Scheme 2.2** gave the target **S3-TIPS** in an overall 53% yield.

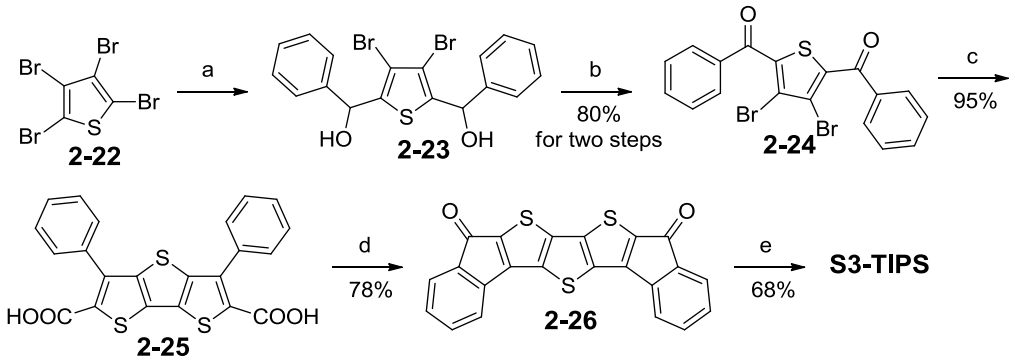

Scheme 2.3 Synthetic route to **S3-TIPS**: (a) i) *n*-BuLi, THF, -78 ^{o}C, 1 h; ii) PhCHO, -78 ^{o}C – r.t., overnight; (b) PCC, CH_2Cl_2, r.t., overnight; (c) i) HS-CH_2COOEt, KOH, EtOH, r.t. for 2 h then 55 ^{o}C overnight; ii) KOH, EtOH, reflux, overnight; iii) 10% HCl (aq.); (d) i) $SOCl_2$, CH_2Cl_2, reflux; ii) $AlCl_3$, CH_2Cl_2, 0 ^{o}C – r.t., 12 h; (e) i) TIPSC≡CLi, THF, r.t., 12h; ii) $SnCl_2$, toluene, r.t., 12 h.

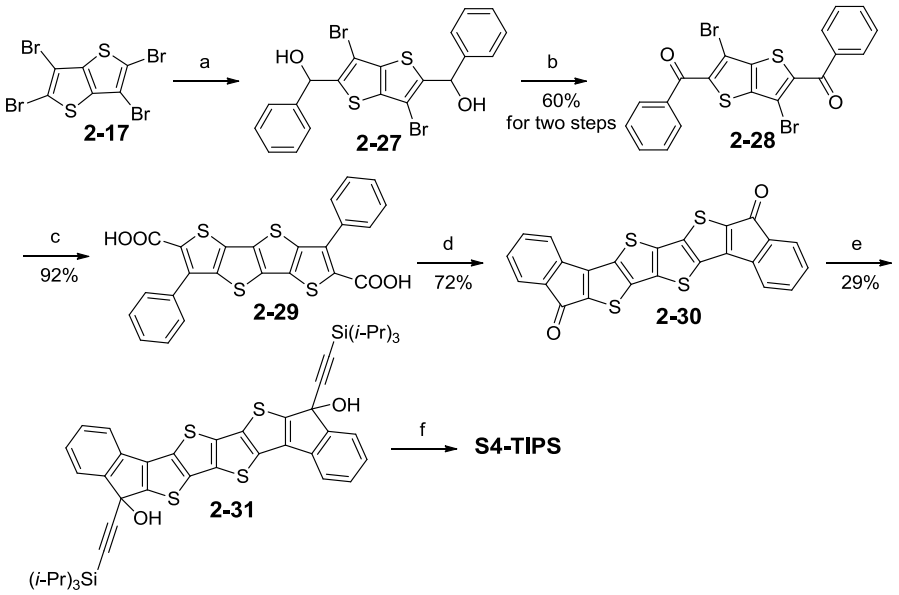

Scheme 2.4 Synthetic route to **S4-TIPS**: (a) i) *n*-BuLi, THF, -78 ^{o}C, 1 h; ii) PhCHO, -78 ^{o}C – r.t., overnight; (b) PCC, CH_2Cl_2, r.t., overnight; (c) i) HS-CH_2COOEt, KOH, EtOH, r.t. for 2 h then 55 ^{o}C overnight; ii) KOH, EtOH, reflux, overnight; iii) 10% HCl (aq.); (d) i) $SOCl_2$, CH_2Cl_2, reflux; ii) $AlCl_3$, CH_2Cl_2, 0 ^{o}C – r.t., 12 h; (e) TIPSC≡CLi, THF, r.t., 12h; f) $SnCl_2$, toluene, r.t., 30 min.

The synthesis of **S4-TIPS** utilized a similar strategy (**Scheme 2.4**). 2,3,5,6-Tetrabromothieno[3,2-b]thiophene (**2-17**) was treated with two equivalent *n*-butyllithium in THF solution at -78 ^{o}C followed by addition of

benzaldehyde to give the diol **2-27**, which was then oxidized by pyridinium chlorochromate (PCC) to give the diketone **2-28** in 60% yield for two steps. The reaction of **2-28** with ethyl mercaptoacetate and potassium hydroxide in an ethanolic solution followed by addition of excess potassium hydroxide afforded the diacid **2-29** in one pot in 92% yield. Subsequent Friedel-Crafts acylation reaction afforded the diketone **2-30** in 72% yield. Nucleophilic addition of the diketone with lithiated TIPSE gave the diol **2-31** in 29% yield after column chromatography purification. Similar reduction of the diol **2-31** by $SnCl_2$ in different solvents (chloroform, toluene, THF etc.) under inert atmosphere gave the target compound **S4-TIPS**, which however is extremely reactive. The reaction was also conducted in deuterated solvents such as $CDCl_2CDCl_2$ under Ar and monitored by NMR spectrometry (**Figure 2.2**). The reaction completed in 30 minutes with the formation of the desired **S4-TIPS**, which was confirmed by MALDI-TOF mass spectrometry (MS), but at the same time, side products formed. The reaction in dry toluene was also followed by UV-vis-NIR absorption spectroscopic measurements and similarly, the formation of the **S4-TIPS** was accompanied by simultaneous decomposition of the product (**Figure 2.3**). Attempted separation of **S4-TIPS** by column chromatography or recrystallization all failed due to its high reactivity to oxygen, protonated reagents and silica gel, and complicated mixture mainly containing O_2-addition products were detected by MALDI-TOF MS (**Figure 2.4**). Attempts to replace the TIPSE group by other

bulky or electron-deficient aryl groups also failed to give stable compounds. The high reactivity of **S4-TIPS** is believed to be associated to its large biradical character (*vide infra*). Nevertheless, the sufficient lifetime ($t_{1/2}$ ~ 3h in N_2) allows us to probe its basic optical properties.

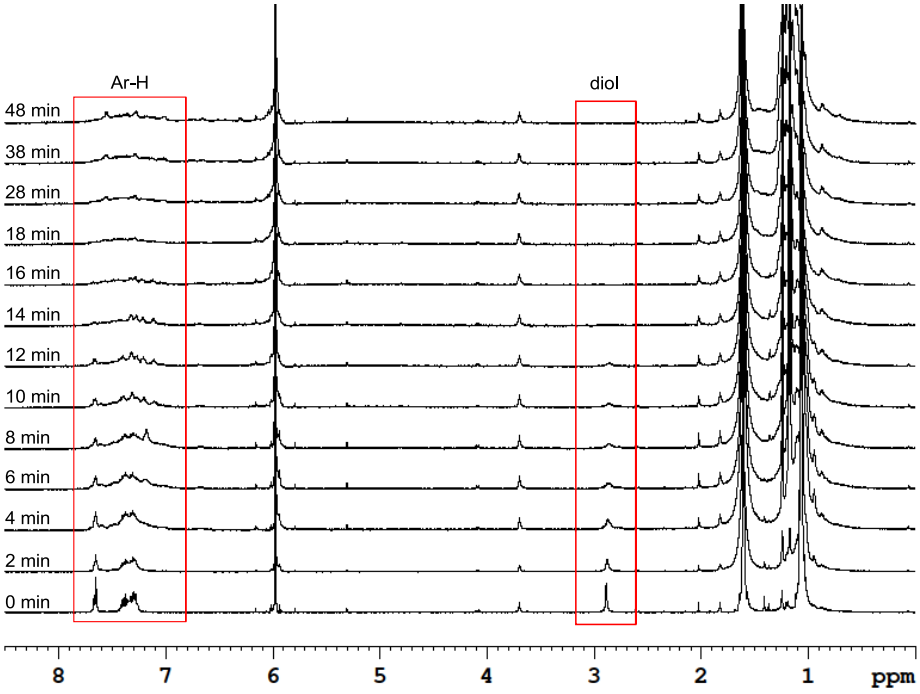

Figure 2.2 The in situ generation of **S4-TIPS** by reduction of **2-31** in $CDCl_2CDCl_2$ under Ar followed by ^1H NMR (500 MHz, $C_2D_2Cl_4$, rt).

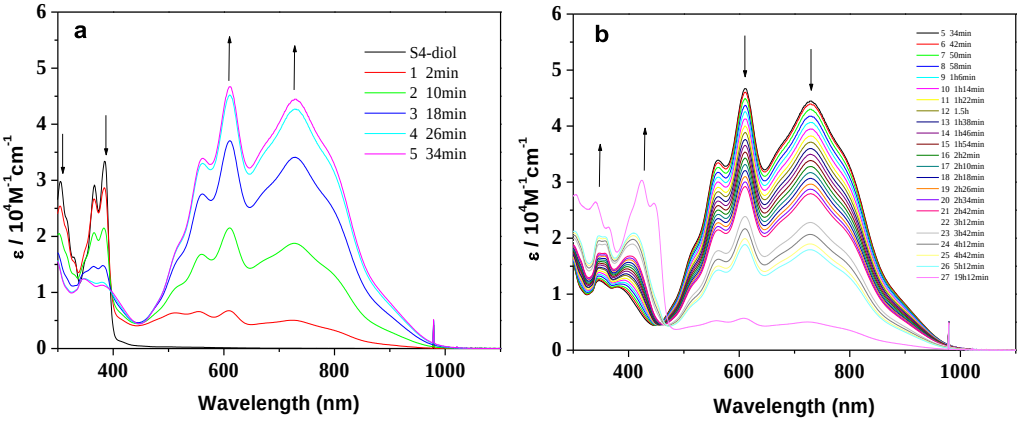

Figure 2.3 UV-vis-NIR absorption spectra of **S4-TIPS** during the reduction of compound **2-31** by $SnCl_2$ in dry toluene under argon atmosphere. The arrows show the changes of the spectra during the reduction reaction. (a) The spectra recorded in 0-34 min after addition of $SnCl_2$. (b) The spectra recorded in 34 min-19 h after addition of $SnCl_2$.

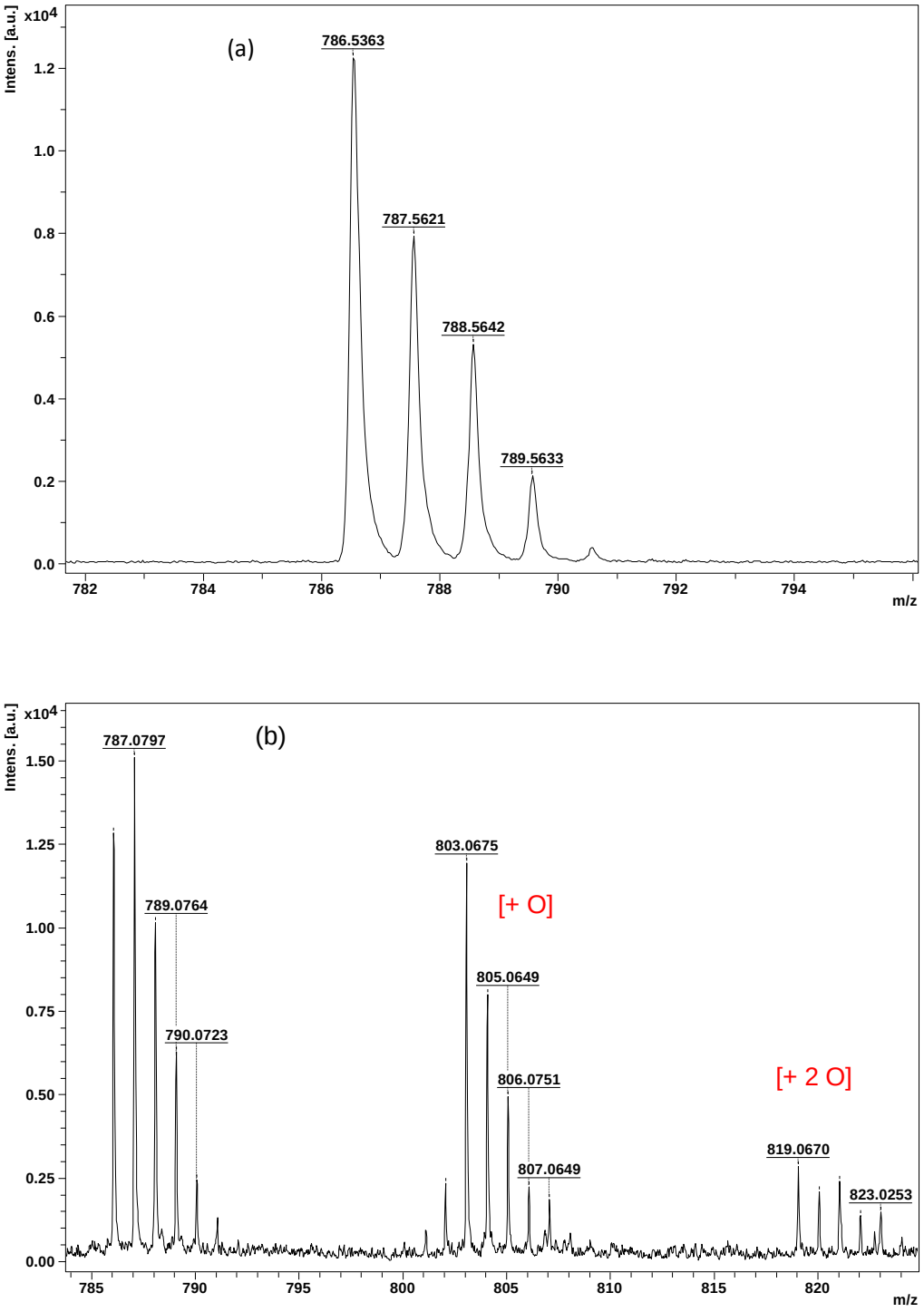

Figure 2.4 MALDI-TOF mass spectra of the freshly prepared **S4-TIPS** (a) and its decomposition products (b).

2.2.2 Electronic absorption spectropscopy

The steady-state OPA spectra of all the bisindeno-[*n*]theinoacenes are

shown in **Figure 2.5** and the data are collected in **Table 2.1**. The frontier molecular orbital profiles, energy diagrams and the absorption spectra were also calculated by time-dependent (TD) DFT (B3LYP/6-31G*) (**Figure 2.6**). Two major bands were observed for all compounds. For **S1-TIPS**, the first intense band at 444 nm can be assigned to the HOMO-1→LUMO transition (*f* = 0.7393, 442.8 nm by TD DFT). The second weaker band at 684 nm is correlated to the HOMO→LUMO transition (*f* = 0.1511, 729.7 nm by TD DFT). Interestingly, such an electronic absorption spectrum is very similar to that of indeno[2,1-*c*]fluorene (**2-32**) derivative (**Figure 2.7**).[10d] This is not surprising if we consider that the core of **S1-TIPS** is actually an isoelectronic structure of **2-32**, a dibenzannulated *as*-indacene. Similarly, compound **S3-TIPS** showed one intense band at 554 nm (HOMO-2→LUMO, *f* = 1.051, 530.7 nm by TD DFT) and one weaker band at 687 nm (HOMO→LUMO, *f* = 0.6399, 720.3 nm by TD DFT). The core of **S3-TIPS** can be regarded as an isoelectronic structure of the extended dibenzannulated *as*-indacene **2-34** (**Figure 2.7**). The optical energy gap (E_g^{opt} = 1.37 eV) of **S3-TIPS** determined from the lowest energy absorption onset is smaller than **S1-TIPS** (E_g^{opt} = 1.51 eV) due to extended π-conjugation. Compounds **S2-TIPS**, **S2-Mes** and **S2-Ph** exhibited a different band structure from **S1-TIPS**/**S3-TIPS**, with one intense band at 450/423/442 nm (HOMO-2→LUMO) and one intense band at 606/546/610 nm (HOMO→LUMO), respectively. The band structure is somehow similar to the absorption spectrum of its isoelectronic structure

fluoreno[4,3-*c*]fluorene (**2-33**), an extended dibenzannulated *s*-indacene (**Figure 2.7**).[10e] The relatively larger optical band gap of **S2-TIPS** (E_g^{opt} =1.58 eV) compared to **S1- TIPS** is interesting and could be related to the different fusion mode (*as*-indacene *vs. s*-indacene). Variation of the substituents has obvious effect on the absorption wavelength, but not on the band shape. In particular, the absorption maxima of **S2-Mes** shift significantly to higher energy side in comparison to **S2-TIPS** and **S2-Ph**. This can be attributed to the larger dihedral angle between the mesityl and bisindeno- thienothiophene core, which leads to diminished π-conjugation. This claim is evidenced by the X-ray crystallographic structures of **S2-Mes** (dihedral angle: 71.4°) and **S2-Ph** (dihedral angle: 36.2°) (*vide infra*). DFT calculations also showed that the HOMO and LUMO are less delocalized along the mesityl than 4-*tert*-phenyl unit (**Figure 2.5**). The *in situ* generated **S4-TIPS** showed a similar band structure to **S2-TIPS**, which is reasonable considering that its isoelectronic structure **2-35** is an analogue of **2-33** (**Figure 2.7**). The spectrum is however largely red-shifted. No fluorescence was observed for all compounds, indicating an ultrafast relaxation process of the excited state which is related to the anti-aromaticity of these molecules. Looking into each electronic transition in more details (**Figure 2.5**), the first absorption band at higher energy in these compounds can be correlated to the excitations within molecular orbitals mainly involving the external benzene rings and that are grouped in pairs of vibronic components of the same excitation (HOMO-1/HOMO-2→LUMO).

The longer wavelength absorption band can be assigned to the transition mainly involving innermost anti-aromatic indacene-thienoacene unit (HOMO→LUMO). It is worthy to highlight the longest wavelengths for the lowest energy lying absorptions of the smaller compounds (**S1-TIPS** and **S2-TIPS**) which is a spectroscopic signature of anti-aromatic compounds.[22] This small gap also promotes very fast deactivation channels (e.g. vibrational relaxation) for the singlet excited state such as observed by the disappearance of fluorescence.

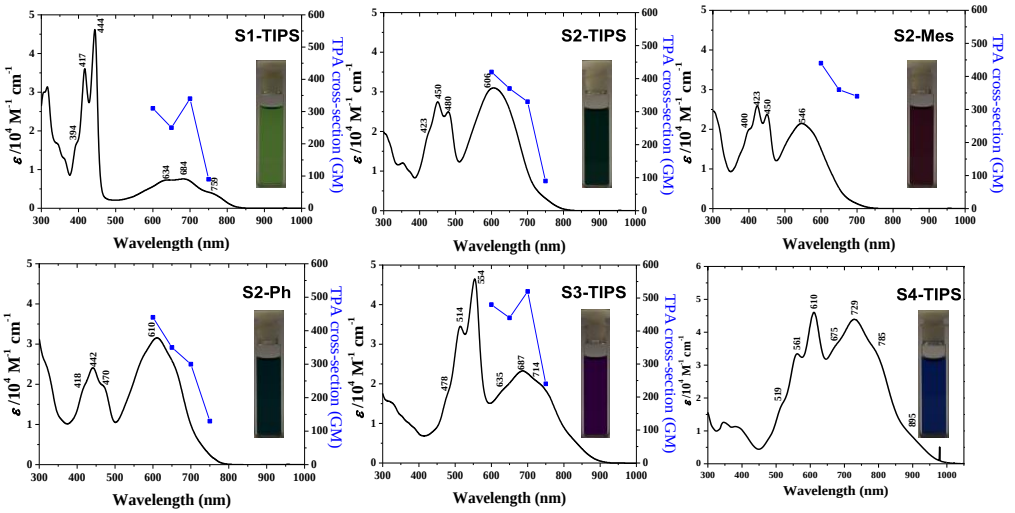

Figure 2.5 One-photon absorption spectra (solid lines and left vertical axes) in $CHCl_3$ and two-photon absorption (TPA) spectra in toluene (blue symbols and right vertical axes) of **S1-TIPS**, **S2-TIPS**, **S2-Mes**, **S2-Ph**, **S3-TIPS** and **S4-TIPS**. TPA spectra are plotted at $\lambda_{ex}/2$. The TPA spectrum of **S4-TIPS** was not recorded due to its high reactivity. Insert are the photos of the solutions.

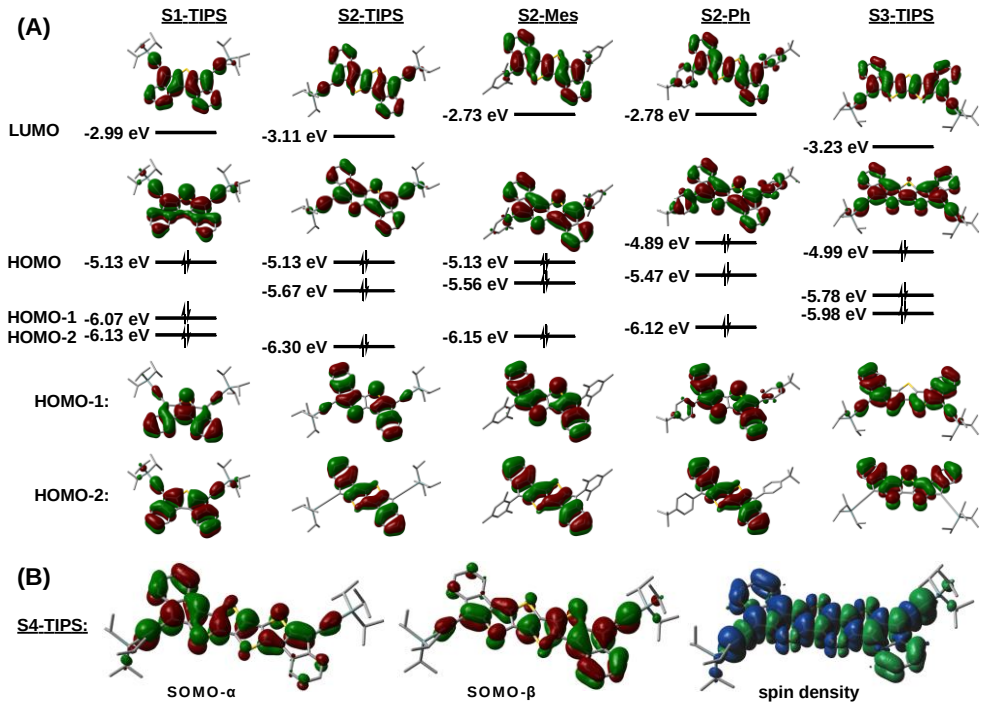

Figure 2.6 (A) Calculated (B3LYP/6-31G**) frontier molecular orbital profiles and energy diagrams of **S1-TIPS**, **S2-TIPS**, **S2-Mes**, **S2-Ph** and **S3-TIPS**. (B) The calculated (UCAM-B3LYP/6-31G*) singly occupied molecule orbital profiles and spin density distribution of the singlet biradical of **S4-TIPS**.

Table 2.1 Summary of photophysical and electrochemical data[a]

Comp	$E_{1/2}^{ox}$ (V)	$E_{1/2}^{red}$ (V)	HOMO (eV)	LUMO (eV)	E_g^{EC} (eV)	E_g^{opt} (eV)	τ (ps)	$\sigma^{(2)}_{max}$ (GM) (λ_{ex})
S1-TIPS	0.70	-1.62	-5.41	-3.69	1.72	1.51	1.9 (τ_1)	340
		-1.52					11 (τ_2)	(1400 nm)
		-1.21						
S2-TIPS	0.62	-1.42	-5.35	-3.75	1.60	1.58	1.1 (τ_1)	420
		-1.08					10 (τ_2)	(1200 nm)
S2-Mes	0.63	-1.39	-5.16	-3.64	1.52	1.71	1.2 (τ_1)	440
		-1.22					12 (τ_2)	(1200 nm)
S2-Ph	0.43	-1.52	-5.13	-3.82	1.31	1.58	1.1 (τ_1)	440
	0.84	-1.22					11 (τ_2)	(1200 nm)
S3-TIPS	0.40	-1.28	-5.30	-3.68	1.62	1.37	0.6 (τ_1)	520
	0.98	-1.02					7 (τ_2)	(1400 nm)
S4-TIPS	-	-	-	-	-	1.27	-	-

[a] $E_{1/2}^{ox}$ and $E_{1/2}^{red}$ are half-wave potentials of the oxidative and reductive waves, respectively, with potentials vs Fc/Fc^+ couple. HOMO = − (4.8 + E_{ox}^{onset}) and LUMO = − (4.8 + E_{red}^{onset}), where E_{ox}^{onset} and E_{red}^{onset} are the onset potentials of the first oxidative and reductive waves, respectively. E_g^{EC}: electrochemical band gap. E_g^{opt}: optical band gap estimated from the absorption onset. τ: singlet excited lifetime obtained from TA. $\sigma^{(2)}_{max}$: maximum TPA cross section. λ_{ex}: excitation wavelength in TPA measurements.

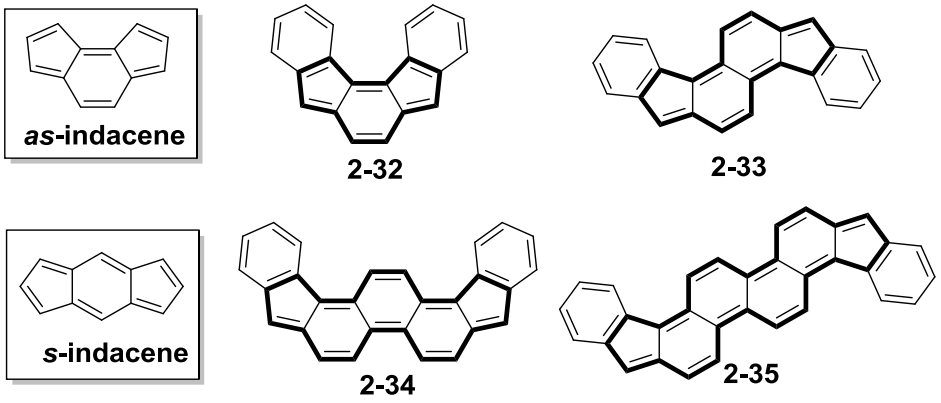

Figure 2.7 Structures of *as*-/*s*- indacene and isoelectronic polycyclic hydrocarbons of **2-9** – **2-12**.

2.2.3 TA and TPA measurements

Femtosecond TA measurements were utilized to explore the excited-state dynamics of **S1-TIPS**, **S2-TIPS**, **S2-Mes**, **S2-Ph** and **S3-TIPS** (**Figure 2.8** and **Figure 2.9**). The TA spectrum of **S1-TIPS** displayed an intense excited-state absorption (ESA) band in a broad range of 450-750 nm. It did not show any perceptible ground-state bleach (GSB) signal due to the strong ESA contribution. The decay profiles probed at 505 nm were fitted by a double exponential function with the time constants of 1.9 and 11 ps (**Table 2.1**). Such a short singlet excited-state lifetime is in good agreement with its non-fluorescence nature.[23] The TA spectrum of **S2-TIPS** exhibited two distinct ESA bands at 490-540 nm/690-850 nm and two GSB bands that well match their steady-state absorption spectra. **S2-Mes** and **S2-Ph** displayed similar TA spectrum to that of **S2-TIPS**. The singlet excited-state lifetimes of **S2-TIPS**, **S2-Mes** and **S2-Ph** were measured to be 10, 12 and 11 ps, respectively (**Table 2.1**), which are similar to that of **S1-TIPS**. The TA spectrum of **S3-TIPS**

showed an intensive ESA band in the 570-650 nm along with two strong GSB signals in the 470-575 and 650-850 nm. Short singlet excited-state lifetime was also observed for **S3-TIPS** (~ 7 ps, **Table 2.1**). The short excited-state lifetimes observed for all compounds indicate an ultrafast relaxation process, which is a common phenomenon for most anti-aromatic systems and singlet biradicaloids.[24, 11, 12]

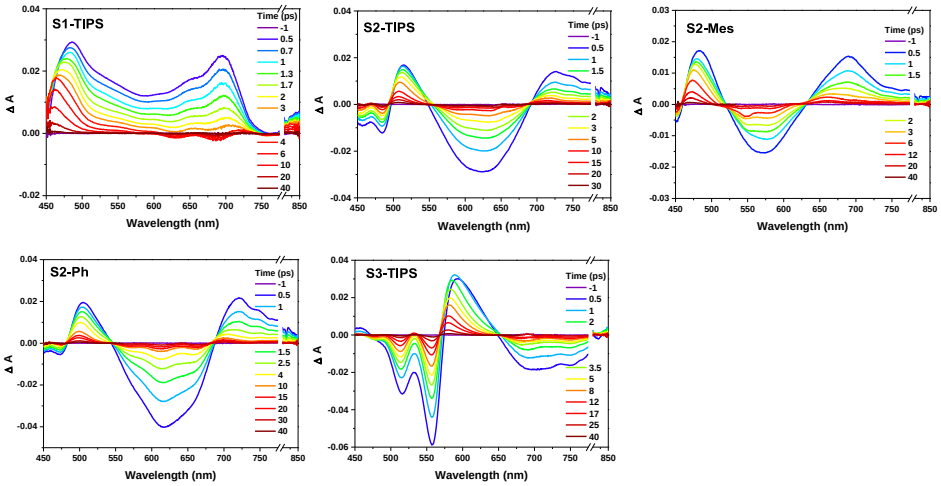

Figure 2.8 Femtosecond transient absorption spectra of **S1-TIPS**, **S2-TIPS, S2-Mes, S2-Ph** and **S3-TIPS** measured in toluene with photoexcitation at 650, 650 and 700 nm, respectively.

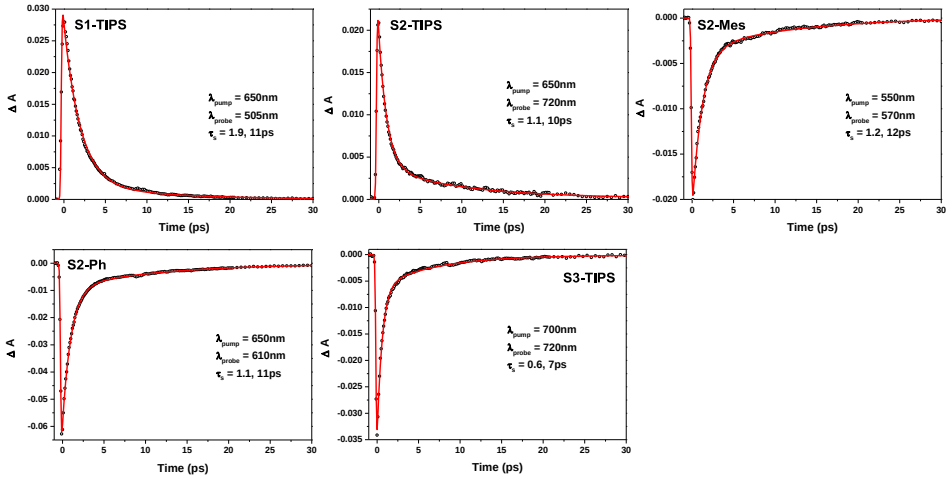

Figure 2.9 Time decay profiles of **S1-TIPS**, **S2-TIPS**, **S2-Mes**, **S2-Ph** and **S3-TIPS**.

TPA measurements were also conducted for **S1-TIPS**, **S2-TIPS**, **S2-Mes**, **S2-Ph** and **S3-TIPS** in toluene by Z-scan technique in the NIR region from 1200 to 1500 nm where one-photon absorption contribution is negligible (**Figure 2.5** and **Figure 2.10**).[25] Owing to the extension of π-conjugation, the maximum TPA cross section values ($\sigma^{(2)}_{max}$) were increased from 340 GM (λ_{ex}: 1400 nm) for **S1-TIPS** to 420 GM (λ_{ex}: 1200 nm) for **S2-TIPS** and to 520 GM (λ_{ex}: 1400 nm) for **S3-TIPS**. The $\sigma^{(2)}_{max}$ values of **S2-Mes** and **S2-Ph** are similar to that of **S2-TIPS** (**Table 2.1**). Previous studies on singlet biradicaloids showed that chromophores with a small or moderate singlet biradical character usually exhibited strong third-order NLO response with large TPA cross sections.[26, 5, 11, 12] On the other hand, chromophores with an anti-aromatic character usually display smaller TPA cross sections compared with the corresponding aromatic counterparts.[27] The observed moderate TPA cross sections can be explained by the unique property of our systems, that is, they can be regarded as anti-aromatic systems which possess a small biradical character at the same time.

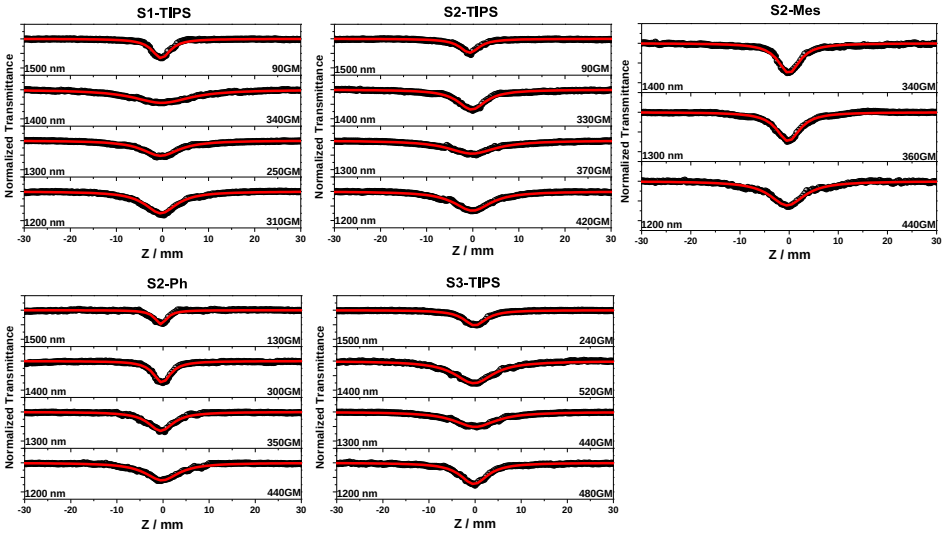

Figure 2.10 Z-scan curves by photoexcitation in the range of 1200-1500 nm. We have always confirmed our experimental condition using Styryl-9M as a reference molecule before proceeding to actual measurements. Also, in every measurement we have ensured that the Rayleigh ranges, even though with fluctuations, reside in a certain range.

2.2.4 *Ground-state geometry and electronic structures*

Single crystals suitable for X-ray crystallographic analysis were obtained for all final products except for **S4-TIPS** (due to its high reactivity) by slow diffusion of acetonitrile into $CHCl_3$ solution.[28] The Oak Ridge Thermal Ellipsoid Plot (ORTEP) drawings and 3D packing structures are shown in **Figure 2.11**. The π-frameworks (bisindeno[*n*]thienoacene) of all the molecules are almost planar. **S1-TIPS** show a lamellar packing structure and in each layer, the molecules form a head-to-tail closely stacked polymer chain *via* π-π interactions between the bisindenothiophene cores (π-π distance: 3.41 Å). For **S2-TIPS**, two molecules form an anti-parallel packed dimer *via* π-π interactions (distance: 3.382 Å) and [S ··S] interactions (distance: 3.677 Å), which further stacks into a columnar structure. No π-stacking was observed for **S2-Mes** due to the bulky mesityl substituent. **S2-Ph** also showed a π-stacked

columnar structure but with relatively large π-π distance (3.48 Å). No close π-stacking was observed for **S3-TIPS**. The observed close packing in **S1-TIPS**, **S2-TIPS** and **S2-Ph** indicated that they could serve as potential semiconductors in OFETs. Actually, our preliminary field effect transistor tests on the spin-coated thin films of **S2-TIPS** showed an average field effect hole mobility of 0.016 $cm^2V^{-1}s^{-1}$ in N_2 and 0.01 $cm^2V^{-1}s^{-1}$ in air.

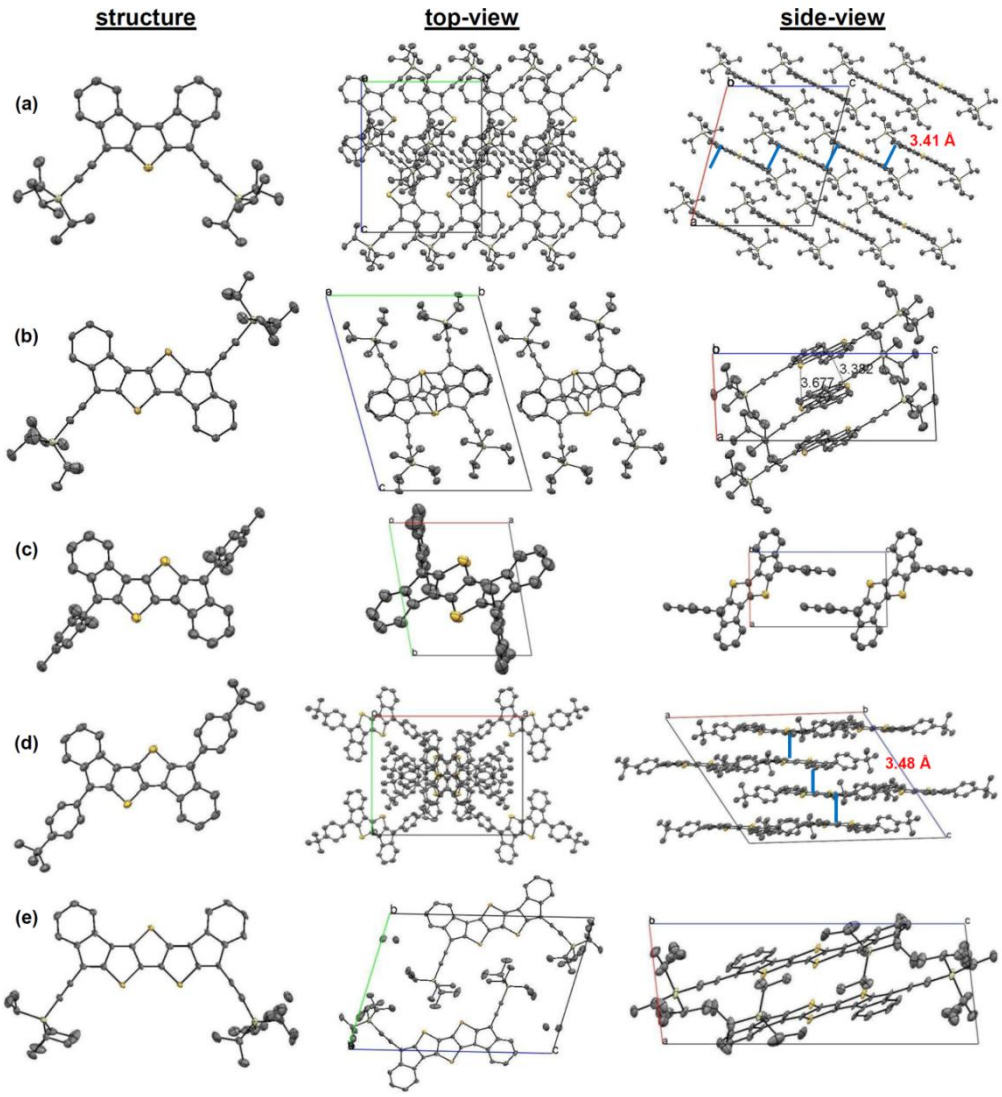

Figure 2.11 X-ray crystallographic structures and packing structures of (a) **S1-TIPS**, (b) **S2-TIPS**, (c) **S2-Mes**, (d) **S2-Ph** and (e) **S3-TIPS**. Hydrogen atoms are omitted for clearance.

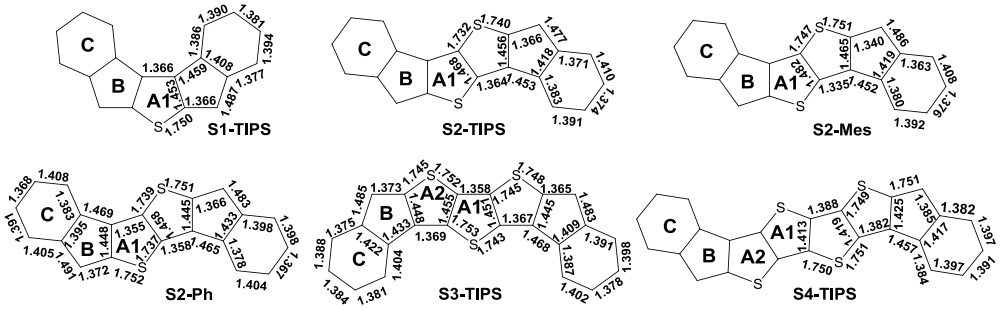

Figure 2.12 Selected bond lengths for **S1-TIPS**, **S2-TIPS**, **S2-Mes**, **S2-Ph** and **S3-TIPS** from their crystallographic structures, and calculated bond lengths for the singlet biradical of **S4-TIPS**.

Bond length analysis was performed to better analyze the ground-state geometry (**Figure 2.12**). In all cases, large bond length alternation was observed for the central biscyclopenta-thienoacene core, indicating a typical quinoidal structure with anti-aromatic character. The outmost two benzene rings however showed less bond length alternation, indicating their large aromatic character.

DFT calculations (both UB3LYP/6-31G* and UCAM-B3LYP/6-31G*)[29] were conducted to understand the ground-state electronic structures. It was found that all the **S1-S3** series molecules indeed favor a closed-shell ground state. However, for **S4-TIPS**, the energy of its singlet biradical state is 4.0 and 3.6 kcal/mol lower than the triplet biradical and closed-shell state, respectively, thus suggesting a singlet biradical ground state. The calculated SOMO-α and SOMO-β profiles showed a disjoint character, with the spins evenly distributed along the whole π-conjugated framework (**Figure 2.6** B). The singlet biradical character y_0 values were calculated as 0.03 for **S3-TIPS** and 0.202 (<S**2>= 0.8808) for **S4-TIPS**, while ignorable for **S1-TIPS** and **S2-TIPS**. Therefore, the singlet biradical character increases with the

extension of chain length. The high reactivity of the **S4-TIPS** thus can be rationalized by its significant biradical character. The calculated geometry of the singlet biradical of **S4-TIPS** also showed large bond length alternation (**Figure 2.12**), indicating that the quinoidal resonance form contributes most to the ground state.

Nucleus independent chemical shift (NICS) calculations were conducted to understand the trend of aromaticity of each ring (**Figure 2.12** and **Table 2.2**).[30] From **S1-TIPS** to **S4-TIPS**, the NICS(1)zz values for the central thiophene ring (ring A1) become more negative, indicating an increase of aromaticity with the extension of the chain length, which is in accordance with the increased biradical character. The cyclopenta-subunit (ring B) showed large positive NICS(1)zz values, indicating a typical anti-aromatic character of central $4n$ π electron system, which is annulated and stabilized by two aromatic benzene rings (ring C) possessing large negative NICS(1)zz values. For **S3-TIPS** and **S4-TIPS**, the innermost thiophene ring (ring A1) is more aromatic than the neighbouring thiophene rings (ring A2).

Table 2.2 Calculated (UCAM-B3LYP/6-31G*) NICS(1)zz values for the rings A1-C of **S1-TIPS**, **S2-TIPS**, **S2-Mes**, **S2-Ph**, **S3-TIPS** and **S4-TIPS**. The rings are labeled in **Figure 4.12**.

Compound	**A1**	**A2**	**B**	**C**
S1-TIPS	7.55	NA	15.93	-19.29
S2-TIPS	4.08	NA	10.11	-21.48
S2-Mes	3.46	NA	8.94	-22.06
S2-Ph	3.59	NA	9.58	-21.15
S3-TIPS	-2.10	NA	10.07	-20.92
S4-TIPS	-6.63	-2.62	11.76	-19.90

In consistence with the change of the aromaticity and singlet biradical character with the extension of chain length, the ^{1}H NMR resonance peak for the proton *a* (see label in **Figure 2.1**) showed graduate shift to the low-field from 7.13 ppm for **S1-TIPS** to 7.17 ppm for **S2-TIPS** and to 7.25 ppm for **S3-TIPS** (**Figure 2.13**). Compound **S4-TIPS** exhibited broadened NMR spectrum at room temperature which could be ascribed to the existence of small amount of thermally excited triplet diradicals. ESR measurements on the *in situ* generated **S4-TIPS** in toluene showed a single-line ESR spectrum (g_e = 2.003) and the intensity decreases when temperature is lowered (**Figure 2.14**). This is a typical phenomenon for most systems with a singlet biradical ground state.[9-12] With the decrease of the temperature, the singlet-triplet equilibrium shifts to the lower energy singlet state, thus leading to a decrease of the magnetic susceptibility. Unfortunately, due to the difficulty to obtain pure sample, the exact singlet-triplet energy gap could not be determined by variable temperature ESR. **S4-TIPS** represents the largest size compound in which the destabilizing bounded electron pair (the highest energy pair of the 4*n* electrons) might get uncorrelated and, such as described for anti-aromatic systems, would permit the formation of a highly unstable biradical species as confirmed by the data recorded for it.

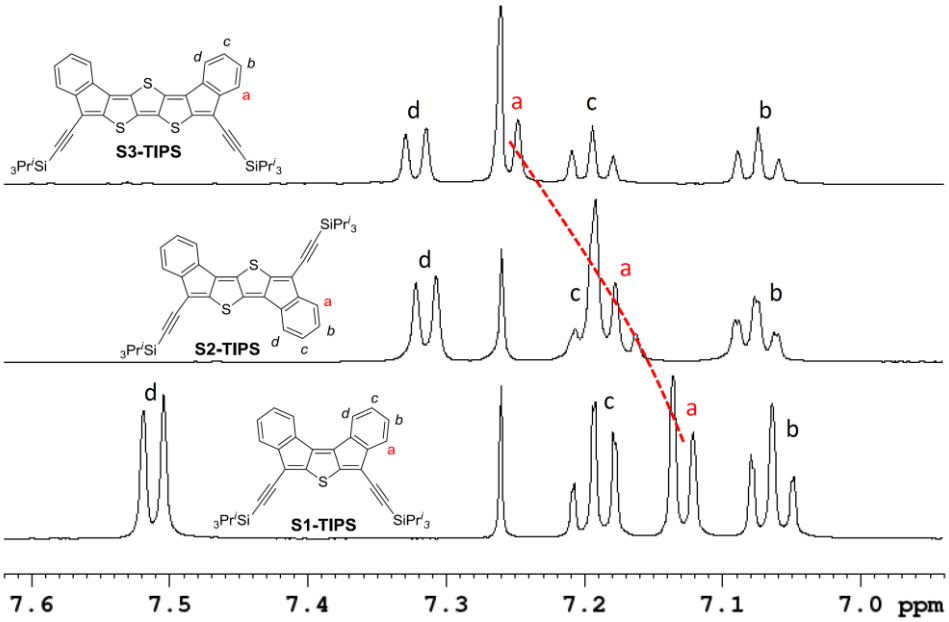

Figure 2.13 Combined ^{1}H NMR spectra (aromatic region) of **S1-TIPS**, **S2-TIPS** and **S3-TIPS** in $CDCl_3$ (500 MHz). The resonance for proton "*d*" in **S1-TIPS** located at low field mainly due to the de-shielding effect from the second terminal benzene ring.

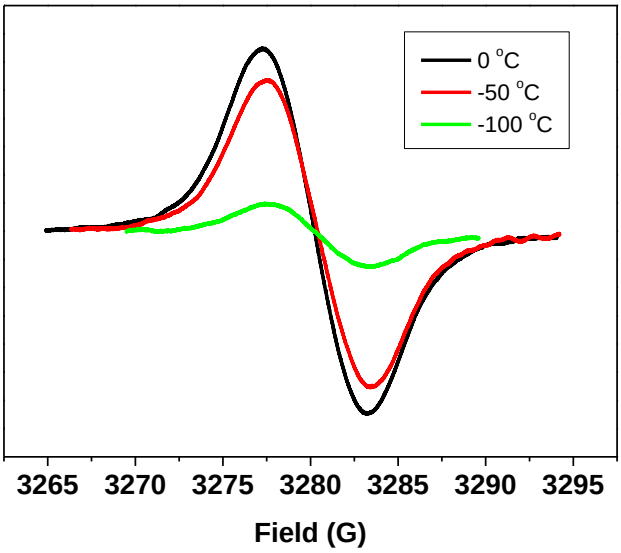

Figure 2.14 VT ESR spectra of the *in situ* generated **S4-TIPS** in dry toluene.

2.2.5 *Raman spectroscopic measurements*

Raman spectroscopy has been proved to be a powerful tool to evaluate the electronic ground state and to understand macroscopic magnetic and optical data of π-conjugated systems.[3, 11-13] Therefore, the Raman spectra of **S1-TIPS**, **S2-TIPS** and **S3-TIPS** were recorded in powder form with different excitation

wavelengths (**Figure 2.15**). The Raman spectrum of **S1-TIPS** clearly highlights a strong bond-length alternation pattern with two intense bands dominating the spectrum at high frequencies values (denoting short C=C distances) at 1633 and 1525 cm^{-1} due to the C=C stretching modes, ν (C=C), of the cyclopentene double bonds and of the quinoidal thiophene, respectively. Quinoidal thiophene Raman bands typically appear close to 1400 cm^{-1}, a frequency value indicative of bond length equalization along the quinoidal conjugated path, in strong contrast with that at 1525 cm^{-1} in **S1-TIPS** revealing an accentuation of the bond length alternation pattern.[13d,13e]

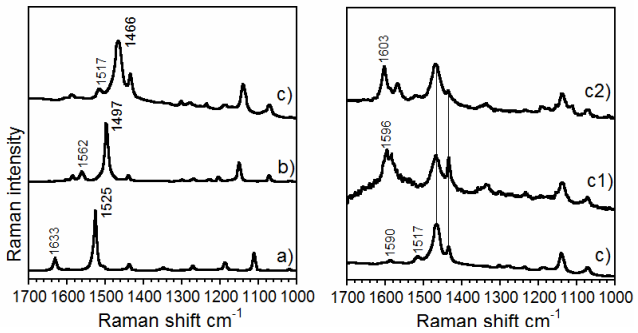

Figure 2.15 Left: 1064 nm FT-Raman spectra of a) **S1-TIPS**, b) **S2-TIPS**, and c) **S3-TIPS**. Right: spectra of **S3-TIPS** taken with the excitation wavelengths at: c) 1064 nm, c1) 785 nm and c2) 532 nm.

The Raman spectra disclosed a very large change of the vibrational properties of the ground state as the dominating ν(C=C) bands move to lower frequencies at 1562/1497 and 1517/1466 cm^{-1} in **S2-TIPS** and **S3-TIPS**, respectively. This Raman behavior is consistent with a reduction of the bond length alternation pattern but still significantly expressed for **S2-TIPS** and **S3-TIPS**. Strong bond length alternation is a well-known property of even-parity anti-aromatic systems as the inherent unstability provokes the ground state distortion towards a strongly C=C/C-C bond length alternated

path. Besides the high frequency denoting a large bond length alternation, the concomitant decrease of the Raman frequencies is in agreement with a significant conjugation within the quinoidal thienoacene core. Going in Raman resonance with the main absorption bands of **S3-TIPS** at 516/553 nm (with the 532 nm laser Raman excitation) and at 686 nm (with the 785 nm Raman laser excitation), we observed the relative intensification of the 1600 cm^{-1} bands due to the largest involvement of the outermost benzenes in the whole anti-aromatic path.

The Raman spectra of aromatic thienoacenes are characterized by the scarce variability of the strongest Raman bands as a function of the number of fused thiophene rings which is a consequence of the all-*cis* cross-conjugated disposition of the successive double bonds.[13] This behavior contrasts with that found in **S1-TIPS** – **S3-TIPS** series where a great dependence of the Raman bands is detected with the number of thiophene units which is in accordance with the persistence of the quinoidal forms in the thiophene rings in the three compounds. On the basis of the high ν (C=C) frequency values reflecting a large C=C/C-C bond alternation, **S1-TIPS** – **S3-TIPS** can also be formulated as thieno-quinoidal anti-aromatic molecules with small biradical characters, which is in agreement with the above X-ray analysis and theoretical calculations.

2.2.6 *Electrochemical and spectroelectrochemical studies*

The electrochemical properties of **S1-S3** series were investigated by cyclic voltammetry in dry CH_2Cl_2 solution (**Figure 2.16**). All compounds showed amphoteric redox behavior with multiple (quasi-) reversible redox waves. **S1-TIPS** exhibited three reduction waves (half-wave potential $E_{1/2}^{red}$ = -1.62, -1.52, -1.21 V *vs* Fc^+/Fc) and one oxidation wave (half-wave potential $E_{1/2}^{ox}$ = 0.70 V *vs* Fc^+/Fc), indicating its high tendency to accept or loss electrons to form stable charged species. **S2-TIPS** displayed two reduction waves ($E_{1/2}^{red}$ = -1.42, -1.08 V) and one oxidation wave ($E_{1/2}^{ox}$ = 0.62 V), while **S3-TIPS** showed two reduction waves ($E_{1/2}^{red}$ = -1.28, -1.02 V) and two oxidation waves ($E_{1/2}^{ox}$ = 0.40, 0.98 V). The HOMO and LUMO energy levels were deduced from the onset potentials of the first oxidation (E_{ox}^{onset}) and the first reduction wave (E_{red}^{onset}), according to the following equations: HOMO = -(4.8 + E_{ox}^{onset}) and LUMO = - (4.8 + E_{red}^{onset}), where the potentials are calibrated to $E(Fc^+/Fc)$ (**Table 2.1**).

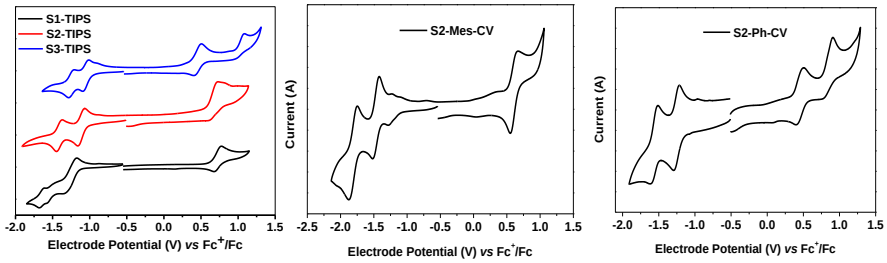

Figure 2.16 Cyclic voltammograms of **S1-TIPS**, **S2-TIPS, S3-TIPS** and **S2-Mes, S2-Ph** in dry CH_2Cl_2 containing 0.1 M Bu_4NPF_6 as the supporting electrolyte, AgCl/Ag as the reference electrode, Au as the working electrode, Pt wire as the counter electrode, and a scan rate of 50 mV s^{-1}. The potential was externally calibrated against the ferrocene/ferrocenium redox couple.

The multistage reversible redox waves and the large separation between

the redox waves allow us to quantitatively attain the singly and doubly charged species by electrochemistry. UV-Vis-NIR spectroelectrochemical measurements were thus conducted for **S1-TIPS** – **S3-TIPS** in CH_2Cl_2 containing 0.1 M *n*-Bu_4NPF_6 as the supporting electrolyte by applying different electrode potentials and the absorption spectra were monitored by UV-vis-NIR spectrometer. For all three compounds, one electron extraction (oxidation) gave rise to the corresponding radical cations apparently characterized by two absorption bands (**Figure 2.17**). The common feature is that the high energy absorption appeared in the high energy tail of the absorption band of the neutral compound, very close to it, being only well resolved in the case of **S3-TIPS** with a clear maximum at 719 nm. The second absorptions of these radical cations scarcely change with the molecular size, and are at 904, 921 and 928 nm for **S1-TIPS**, **S2- TIPS** and **S3-TIPS**, respectively. According to the anti-aromatic framework, one electron extraction gives rise to a molecular species containing one aromatic thienoacene unit, one anti-aromatic cyclopentadienyl cation, and one benzylic radical (**Scheme 2.5**), that is, the radical cations have a pseudo-aromatic character and are reasonably stable. Further oxidation is expected to give one aromatic thienoacene and two anti-aromatic cyclopentadienyl cations (**Scheme 2.5**), which are thus unstable and difficult to attain by electrochemistry.

One-electron electrochemical reduction of the three neutral compounds gave rise to spectra characterized by two well differentiated groups of

absorptions likely corresponding to two different excitations with vibronic structure (**Figure 2.18**). One band appeared at the higher energy side of the neutral species (666/524/686 nm for **S1-TIPS**, **S2-TIPS** and **S3-TIPS**, respectively) and another band was observed at the lower energy side (1201/1188/1371 nm for **S1-TIPS**, **S2-TIPS** and **S3-TIPS**, respectively). The band shape and intensity are similar to those of many aromatic polycyclic hydrocarbons such as acenes[17] and rylenes,[31] indicating an aromatic character of the radical anions. In fact, one-electron reduction should give one aromatic thienoacene unit, one aromatic cyclopentadienyl anion, and one benzylic radical (**Scheme 2.5**), which can explain the high stability of the radical anions. The second follow-up reduction gave rise to dianions with absorption spectra typical of aromatic thiophene and fused α-oligothiophenes,[15a-c] with absorption maximum at 279, 340 and 457 nm for **S1-TIPS**, **S2-TIPS** and **S3-TIPS**, respectively (**Figure 2.18**). This reveals that for the dianions the structures have become fully aromatic within the thiophene rings, which can be easily elucidated by the formation of one aromatic thiophene/thienoacene unit and two aromatic cyclopentadienyl anions (**Scheme 2.5**). Our system provides a nice example of the competition between aromatic and anti-aromatic cores and how they transform from one to the other depending on the number of added or extracted electrons.

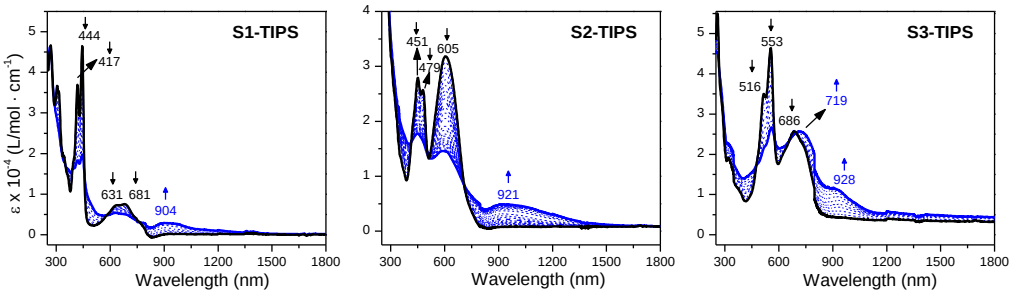

Figure 2.17 UV-Vis-NIR absorption spectra of **Sn-TIPS** (n = 1, 2, 3) obtained during their potentiostatic oxidation in intervals of 50 mV. Blue lines: radical cation spectra.

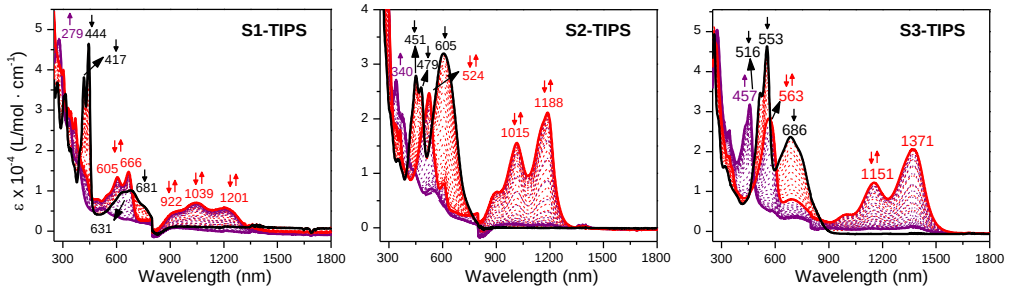

Figure 2.18 UV-Vis-NIR absorption spectra of **Sn-TIPS** (n = 1, 2, 3) obtained during their potentiostatic reduction in intervals of 50 mV. Red line: radical anion spectra. Purple line: dianion spectra.

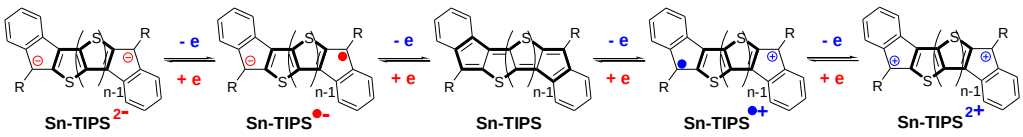

Scheme 2.5 Schematic presentation of the oxidation and reduction processes of **Sn-TIPS** (n = 1, 2, 3)

2.3 Conclusion

In summary, a series of alkynyl or aryl substituted bisindeno-[*n*]thienoacenes (n = 1-4) were successfully synthesized *via* different strategies. This series of molecules can be regarded as anti-aromatic systems with small singlet biradical characters. Their ground-state geometry and electronic structures were carefully studied by various experimental techniques (X-ray crystallographic analysis, NMR, ESR and Raman

spectroscopy) and DFT calculations, and all of these data interpreted in the context of their anti-aromaticity. It was found that with the extension of chain length the molecules showed gradually increased singlet biradical character and decreased anti-aromaticity. In particular, the longest molecule **S4-TIPS** showed a singlet biradical ground state with a small-to-moderate biradical character (y_0 = 0.202). As a result, it displayed high reactivity. Their optical and electronic properties were systematically investigated by OPA, TPA, TA and cyclic voltammetry and revealed chain length dependent behavior. The observed short singlet excited state lifetime, moderate TPA cross section and amphoteric redox behavior all are related to their anti-aromaticity and singlet biradical character. The transformation from anti-aromatic to pseudo-aromatic/aromatic systems was conducted by electrochemical oxidation and reduction followed by UV-Vis–NIR spectroscopic measurements. Again, the aromaticity of the corresponding charged species can be used to well interpret their absorption spectra and stability. Our work provided the first study on a quinoidal thienoacene/polycyclic hydrocarbon hybrid system and disclosed the close relation between the anti-aromaticity, singlet biradical character and their unique physical properties, which sheds light on the rational material design in the future.

2.4 Experiments

2.4.1 *General experimental methods*

All reagents were purchased from commercial sources and used without further purification. Anhydrous dichloromethane (DCM) and *N*,*N*-dimethylformamide (DMF) were distilled from CaH_2. Anhydrous toluene and THF were distilled from sodium benzophenone immediately prior to use. The ^{1}H NMR and ^{13}C NMR spectra were recorded in solution of $CDCl_3$ or DMSO-d_6 on Bruker DRX 500 NMR spectrometer with tetramethylsilane (TMS) as the internal standard. Abbreviations for signal coupling are as follows: s, singlet; d, doublet; t, triplet; q, quartet; m, multiplet; br, broad. MALDI-TOF mass spectra were recorded on a Bruker Autoflex instrument. High resolution (HR) EI mass spectra were recorded on Agilent 5975C DIP/MS mass spectrometer. HR ACPI mass spectra were recorded on a MicrOTOF-QII instrument. UV-vis-NIR absorption spectra were recorded on a Shimadzu UV-1700 and UV-3600 spectrometer. The electrochemical measurements were carried out in anhydrous DCM with 0.1 M tetrabutylammonium hexafluorophosphate (Bu_4NPF_6) as the supporting electrolyte at a scan rate of 0.05 V/s at room temperature under the protection of nitrogen. A gold disk was used as working electrode, platinum wire was used as counting electrode, and Ag/AgCl (3M KCl solution) was used as reference electrode. The potential was calibrated against the ferrocene/ferrocenium couple. Continuous wave X-band ESR spectra were

obtained with a Bruker ELEXSYS E500 spectrometer using a variable temperature Bruker liquid nitrogen cryostat.

1064 nm FT–Raman spectra were obtained in an FT–Raman accessory kit (FRA/106–S) of a Bruker Equinox 55 FT–IR interferometer. A continuous–wave Nd–YAG laser working at 1064 nm was employed for excitation. A germanium detector operating at liquid nitrogen temperature was used. Raman scattering radiation was collected in a back–scattering configuration with a standard spectral resolution of 4 cm^{-1}. 1000–3000 scans were averaged for each spectrum. Raman spectra with the excitation lasers at 532, 633 and 785 nm were collected by using the 1×1 camera of a Bruker Senterra Raman microscope by averaging spectra during 50 minutes with a resolution of 3–5 cm^{-1}. A CCD camera operating at -50 ℃ was used for the Raman detection.

In situ UV-Vis-NIR spectroelectrochemical studies were conducted on a Cary 5000 spectrophotometer from Varian operating in a maximal 175-3300 nm range. A C3 epsilon potentiostat from BASi was used for the electrolysis using a thin layer cell from a demountable omni cell from Specac. In this cell a three electrodes system was coupled to conduct *in situ* spectroelectrochemistry. A Pt gauze was used as the working electrode, a Pt wire as the counter electrode and a Ag wire as the pseudo-reference electrode. The spectra were collected a constant potential electrolysis and the potentials were changed in interval of 100 mV. The electrochemical medium used was 0.1 M

(n-$C_4H_9)_4NPF_6$ in fresh distilled CH_2Cl_2, at room temperature with sample concentrations of 10^{-3} M.

The femtosecond time-resolved transient absorption spectrometer used for this study consisted of a femtosecond optical parametric amplifier (Quantronix, Palitra-FS) pumped by a Ti:sapphire regenerative amplifier system (Quantronix, Integra-C) operating at 1 kHz repetition rate and an accompanying optical detection system. The generated OPA pulses had a pulse width of ~100 fs and an average power of 1 mW in the range 450 to 800 nm, which were used as pump pulses. White light continuum (WLC) probe pulses were generated using a sapphire window (3 mm thick) by focusing of small portion of the fundamental 800 nm pulses, which were picked off by a quartz plate before entering into the OPA. The time delay between pump and probe beams was carefully controlled by making the pump beam travel along a variable optical delay (Newport, ILS250). Intensities of the spectrally dispersed WLC probe pulses were monitored by miniature spectrograph (OceanOptics, USB2000+). To obtain the time-resolved transient absorption difference signal (ΔA) at a specific time, the pump pulses were chopped at 500 Hz and absorption spectra intensities were saved alternately with or without pump pulse. Typically, 4000 pulses were used to excite samples and to obtain the TA spectra at a particular delay time. The polarization angle between pump and probe beam was set at the magic angle (54.7^o) using a Glan-laser polarizer with a half-wave retarder to prevent polarization-dependent signals. The

cross-correlation fwhm in the pump-probe experiments was less than 200 fs, and chirp of WLC probe pulses was measured to be 800 fs in the 400-800 nm regions. To minimize chirp, all reflection optics were used in the probe beam path, and a quartz cell of 2 mm path length was employed. After completing each set of fluorescence and TA experiments, the absorption spectra of all compounds were carefully checked to rule out the presence of artifacts or spurious signals arising from, for example, degradation or photo-oxidation of the samples in question.

The two-photon absorption spectrum was measured in the NIR region using the open-aperture Z-scan method with 130 fs pulses from an optical parametric amplifier (Light Conversion, TOPAS) operating at a repetition rate of 1 kHz generated from a Ti:sapphire regenerative amplifier system (Spectra-Physics, Hurricane). After passing through a 10 cm focal length lens, the laser beam was focused and passed through a 1 mm quartz cell. Since the position of the sample cell could be controlled along the laser beam direction (z axis) using the motorcontrolled delay stage, the local power density within the sample cell could be simply controlled under constant laser intensity. The transmitted laser beam from the sample cell was then detected by the same photodiode as used for reference monitoring. The on-axis peak intensity of the incident pulses at the focal point, I_0, ranged from 40 to 60 GW cm^{-2}. For a Gaussian beam profile, the nonlinear absorption coefficient can be obtained by curve fitting of the observed open-aperture traces $T(z)$ with the following

equation:

$$T(z)=1-\frac{\beta I_0(1-e^{-\alpha_0 l})}{2\alpha_0[1+(z/z_0)^2]}$$

where α_0 is the linear absorption coefficient, l is the sample length, and z_0 is the diffraction length of the incident beam. After the nonlinear absorption coefficient has been obtained, the TPA cross section $\sigma^{(2)}$ of one solute molecule (in units of GM, where 1 GM = 10^{-50}cm^4 s photon^{-1} molecule^{-1}) can be determined by using the following relationship:

$$\beta=\frac{10^{-3}\sigma^{(2)}N_A d}{h\nu}$$

where N_A is the Avogadro constant, d is the concentration of the compound in solution, h is the Planck constant, and ν is the frequency of the incident laser beam.

2.4.2 Detailed synthetic procedures and characterization data

Compound 2-15

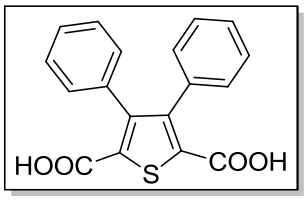

This compound was synthesized according to a published procedure with minor modification (*Macromolecules,* 2005, **38**, 19.). To a mixture of diethyl thiodiacetate (**2-13**, 2 g, 9.70 mmol) and benzil (**2-14**, 2.04 g, 9.70 mmol) in ethanol (30 mL), NaOMe (1.57 g, 29.10 mmol) was added as a solid. The

mixture was stirred at room temperature for 4 h and then stirred at 60 ^{o}C for 12 h. After cooling down to room temperature NaOH (1.60 g, 40.00 mmol) and additional ethanol (20 mL) were added to the above reaction mixture. The mixture was heated to reflux for additional 12 h. The alcohol was evaporated and 10% HCl was slowly added. During this period diacid **2-15** was precipitated. After filtration, a pale yellow solid was obtained. The crude product was purified by washing with hexane (30 mL) and DCM (30 mL) to give a white solid (1.89 g, 60% yield). ^{1}H NMR (500 MHz, DMSO-d_6, ppm): δ = 13.26 (br, 1H), 7.15-7.14 (m, 3H), 7.01-6.99 (m, 2H); ^{13}C NMR (125 MHz, DMSO-d_6, ppm): δ = 162.28, 147.76, 134.87, 132.90, 129.79, 127.15, 127.12. HR MS (EI): calcd for $C_{18}H_{12}O_4S$ (M^+), 324.0456; found, 324.0447 (error: -2.78 ppm).

Compound 2-16

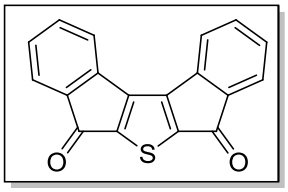

Compound **2-15** (973 mg, 3.00 mmol) was dissolved in anhydrous DCM (30 mL), followed by the addition of excess of thionyl chloride (2 ml). To this mixture anhydrous DMF (1-2 drops) was added at room temperature. The resultant mixture was heated at reflux overnight. During this period the insoluble diacid **2-15** became soluble in DCM. After cooling down the solvent was removed under reduced pressure to afford crude acid chloride. This

intermediate compound was dissolved in anhydrous DCM (30 mL) then anhydrous $AlCl_3$ (1.60 g, 12.00 mmol) was added carefully at 0 ℃. The resultant mixture was allowed to warm up to room temperature and stirred overnight, then slowly quenched by 10% HCl solution, extracted with large amount of DCM. The combined organic phase was washed with 10% HCl and brine. The organic phase was dried over anhydrous Na_2SO_4 and the solvent was removed under reduced pressure. The crude product was purified by column chromatography (silica gel, DCM) to afford compound **2-16** as an orange solid (735 mg, 85% yield). ^{1}H NMR (500 MHz, $CDCl_3$, ppm): δ = 7.62 (d, *J* = 7.0 Hz, 1H), 7.51 (dd, *J* = 7.1 Hz, 1H), 7.44 (d, *J* = 6.8 Hz, 1H), 7.32 (dd, *J* = 7.1 Hz, 1H). ^{13}C NMR spectrum was not obtained due to its poor solubility. HR MS (EI): calcd for $C_{18}H_8O_2S$ (M^+), 288.0245; found, 288.0236 (error: -3.12 ppm). Anal. Calcd for $C_{18}H_8O_2S$: C, 74.98; H, 2.80; S, 11.12; found: C, 74.95; H, 2.72; S, 11.08.

Compound S1-TIPS

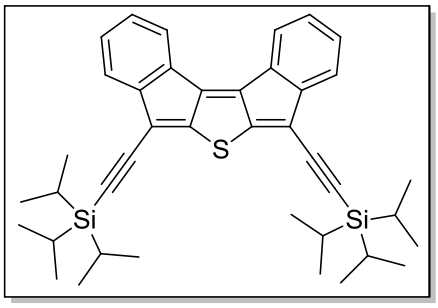

To a solution of triisopropylsilylacetylene (1.10 g, 6.00 mmol) in anhydrous THF (30 mL) at 0 ^{o}C was added dropwise *n*-BuLi (1.6 M in hexanes, 3.75 mL,

6.00 mmol). The solution was stirred for 30 min at 0 ^{o}C. Then diketone **2-16** (288 mg, 1.00 mmol) was added as solid in one portion. The mixture was slowly warmed to room temperature and stirred overnight. During this period the insoluble diketone disappeared and the solution became clear. The reaction was quenched with 10% HCl solution (10 mL) and extracted in $CHCl_3$. The organic layer was dried (Na_2SO4), filtered, and evaporated to dryness under vacuum. After that the crude diol was dissolved in dry toluene (20 mL) and degassed by bubbling through argon. $SnCl_2$ (758.5 mg, 4.00 mmol) was added to the mixture and stirred overnight. During this period the color of the reaction mixture became green-to-blue. The resulting solution was then filtered and the filtrate was subsequently evaporated to dryness. The residue was purified by column chromatography (silica gel, hexane: DCM = 5: 1). Compound **S1-TIPS** was further purified by recrystallization from CH_3CN/CH_2Cl_2 as a dark green solid (430 mg, 70% yield). ^{1}H NMR (500 MHz, $CDCl_3$, ppm): δ = 7.51 (d, *J* = 7.2 Hz, 1H), 7.19 (dd, *J* = 7.5 Hz, 1H), 7.13 (d, *J* = 7.2 Hz, 1H), 7.06 (dd, *J* = 7.6 Hz, 1H), 1.17-1.15 (br, 21H); ^{13}C NMR (125 MHz, $CDCl_3$, ppm): δ = 153.75, 148.86, 144.01, 130.75, 130.16, 125.76, 124.34, 120.66, 116.29, 105.87, 99.68, 18.70, 11.25. HR MS (EI): calcd for $C_{40}H_{50}SSi_2$ (M^+), 618.3172; found, 618.3167 (error: -0.81 ppm).

Compound 2-18

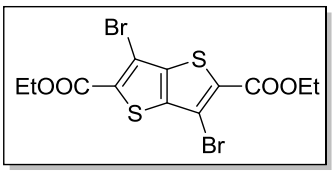

Under argon and anhydrous condition at -78 ^{o}C, *n*-BuLi (1.6 M in hexane, 6.25 mL, 10.00 mmol) was slowly added to a solution of 2,3,5,6-tetrabromothieno[3,2-b]thiophene (**2-17**, 2.28 g, 5.00 mmol) in THF (40 mL) and the mixture was stirred for 1 h. Ethyl cyanoformate (1 mL, 10.00 mmol) was added by syringe at -78 ^{o}C. The reaction was slowly warmed to room temperature and stirred overnight. The reaction was quenched by water at 0 ^{o}C. All of the organic solvents were removed and the organic precipitate was collected by filtration. The crude product was washed with hexane and methanol to give pure compound **2-18** as a white solid (1.55 g, 70% yield). ^{1}H NMR (500 MHz, $CDCl_3$, ppm): δ = 4.43 (q, J = 7.1 Hz, 4H), 1.42 (t, J = 7.2 Hz, 6H); ^{13}C NMR (125 MHz, $CDCl_3$, ppm): δ = 160.48, 142.46, 132.04, 109.55, 62.13, 14.19. HR MS (EI): calcd for $C_{12}H_{10}Br_2O_4S_2$ (M^+), 441.8367; found, 441.8365 (error: -0.45 ppm).

Compound 2-19

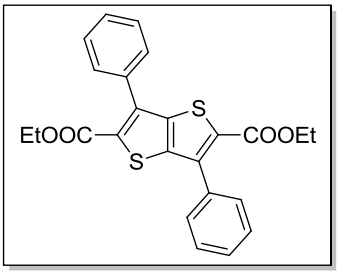

Phenylboronic acid (488 mg, 4 mmol), **2-18** (442 mg, 1.00 mmol), and Na_2CO_3 (424 mg, 4.00 mmol) were dissolved in water (3 mL) and toluene (15 mL). $Pd(PPh_3)_4$ (70 mg) was added as a catalyst and the mixture was refluxed for 12 h. After cooling down cold methanol was added and a white precipitate was formed. The crude product was collected by filtration and further purified by column chromatography (silica, hexane: DCM = 1: 1) to give a white solid (410 mg, 94% yield). ^{1}H NMR (500 MHz, $CDCl_3$, ppm): δ = 7.60-7.59 (m, 2H), 7.51-7.46 (m, 3H), 4.25 (q, *J* = 7.2 Hz, 2H), 1.23 (t, *J* = 7.0 Hz, 3H); ^{13}C NMR (125 MHz, $CDCl_3$, ppm): δ =161.92, 142.53, 140.70, 133.64, 131.32, 129.03, 128.83, 128.32, 61.41, 14.00. HR MS (EI): calcd for $C_{24}H_{20}O_4S_2$ (M^+), 436.0803; found, 436.0805 (error: 0.46 ppm).

Compound 2-20

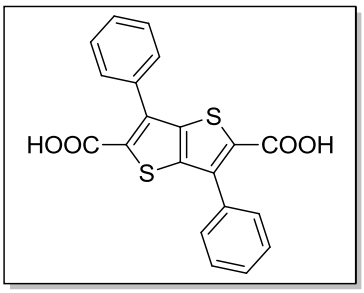

Compound **2-19** (436 mg, 1.00 mmol) was dissolved in methanol and THF (20 mL, 1:1 v/v), followed by the addition of sodium hydroxide (240 mg, 6.00 mmol). This mixture was heated at reflux overnight. The solvent was removed under reduced pressure after the reaction was completed. To the residue then concentrated hydrochloric acid was added. The precipitate formed was

collected by filtration and washed with water and a little amount of DCM, then dried in vacuum to afford product **2-20** as a white solid (365 mg, 96% yield). ^{1}H NMR (500 MHz, DMSO-d_6, ppm): δ = 13.40 (br, 1H), 7.62-7.61 (m, 2H), 7.53-7.48 (m, 3H); ^{13}C NMR (125 MHz, DMSO-d_6, ppm): δ =162.56, 141.41, 139.39, 133.28, 132.23, 128.98, 128.80, 128.38. HR MS (EI): calcd for $C_{20}H_{12}O_4S_2$ (M^+), 380.0177; found, 380.0159 (error: -4.74 ppm).

Compound 2-21

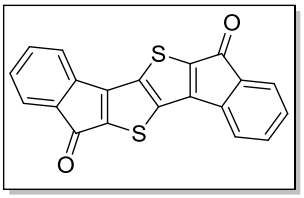

Compound **2-20** (380 mg, 1.00 mmol) was added in anhydrous DCM (20 mL), followed by the addition of excess of thionyl chloride (1 mL). To this mixture anhydrous DMF (1-2 drops) was added at room temperature. The resultant mixture was heated at reflux overnight. During this period the insoluble diacid **2-20** became soluble in DCM. After cooling down the solvent was removed under reduced pressure to afford crude acid chloride. This intermediate compound was dissolved in anhydrous DCM (20 mL) then anhydrous $AlCl_3$ (533 mg, 4.00 mmol) was added carefully at 0 ℃. The resultant mixture was allowed to warm up to room temperature and stirred overnight, then slowly quenched by 10% HCl solution to form a red precipitate. The crude precipitate was rinsed with 10% NaOH, MeOH, DCM and THF until the washings were colorless, giving **2-21** as an insoluble red solid (286 mg, 83% yield). Both ^{1}H

NMR and ^{13}C NMR data were not obtained due to its poor solubility. HR MS (EI): calcd for $C_{20}H_8O_8S_2$ (M^+), 343.9966; found, 343.9962 (error: -1.16 ppm). Anal. Calcd for $C_{20}H_8O_2S_2$: C, 69.75; H, 2.34; S, 18.62; found: C, 69.55; H, 2.08; S, 18.97.

Compound S2-TIPS

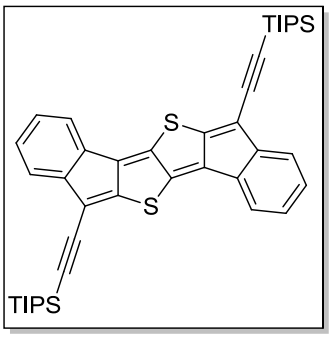

To a solution of triisopropylsilylacetylene (1.10 g, 6.00 mmol) in anhydrous THF (30 mL) at 0 ^oC was added dropwise *n*-BuLi (1.6 M in hexane, 3.75 mL, 6.00 mmol). The solution was stirred for 30 min at 0 ^oC. Then diketone **2-21** (344 mg, 1.00 mmol) was added as solid in one portion. The mixture was slowly warmed to room temperature and stirred overnight. During this period the insoluble diketone disappeared and the solution became clear with strong blue fluorescence. The reaction was quenched with 10% HCl solution (10 ml) and extracted in $CHCl_3$. The organic layer was dried (Na_2SO4), filtered, and evaporated to dryness under vacuum. After that the crude diol was dissolved in dry toluene (20 mL) and degassed by bubbling through Ar. $SnCl_2$ (758.5 mg, 4.00 mmol) was then added to the mixture and stirred overnight. During this period the color of the reaction mixture became deep blue. The resulting blue

solution was then filtered and the filtrate was subsequently evaporated to dryness. The residue was purified by column chromatography (silica gel, hexane: DCM = 5: 1). Compound **S2-TIPS** was further purified by recrystallization from CH_3CN/CH_2Cl_2 as a dark blue solid (472 mg, 70% yield). ^1H NMR (500 MHz, $CDCl_3$, ppm): δ = 7.31 (d, *J* = 7.4 Hz, 1H), 7.21-7.16 (m, 2H), 7.09-7.05 (m, 1H), 1.19-1.17 (br, 21H); ^{13}C NMR (125 MHz, $CDCl_3$, ppm): δ = 150.11, 147.30, 146.96, 139.41, 129.60, 128.78, 125.50, 122.63, 120.71, 114.74, 105.40, 99.99, 18.76, 11.30. HR MS (EI): calcd for $C_{42}H_{50}S_2Si_2$ (M^+), 674.2892; found, 674.2893 (error: 0.15 ppm).

Compound S2-Mes

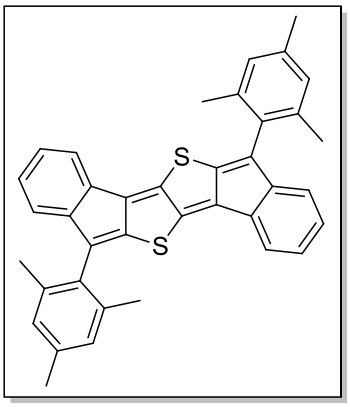

To a solution of **2-21** (344 mg, 1.00 mmol) in anhydrous THF (30 mL) at 0 ^oC was added dropwise mesitylmagnesium bromide (1.0 M in ether, 6 mL, 6.00 mmol). The mixture was slowly warmed to room temperature and stirred overnight. During this period the insoluble diketone disappeared and the solution became clear. The reaction was quenched with 10% HCl solution (10 ml) and extracted in $CHCl_3$. The organic layer was dried (Na_2SO4), filtered,

and evaporated to dryness under vacuum. After that the crude diol was dissolved in dry toluene (20 mL) and degassed with Ar. $SnCl_2$ (758.5 mg, 4.00 mmol) was then added to the mixture and stirred overnight. During this period the color of the reaction mixture became brown. The resulting brown solution was then filtered and the filtrate was subsequently evaporated to dryness. The residue was purified by column chromatography (silica gel, hexane: DCM = 5: 1). Compound **S2-Mes** was further purified by recrystallization from CH_3CN/CH_2Cl_2 as a dark solid (275 mg, 50% yield). ^{1}H NMR (500 MHz, $CDCl_3$, ppm): δ = 7.33 (d, *J* = 7.0 Hz, 1H), 7.10-7.03 (m, 2H), 6.98 (s, 2H), 6.72 (d, *J* = 7.3 Hz. 1H), 2.36 (s, 3H), 2.22 (s, 6H); ^{13}C NMR (125 MHz, $CDCl_3$, ppm): δ =147.99, 147.12, 144.69, 138.55, 137.78, 137.09, 132.34, 130.33, 128.99, 128.33, 128.23, 124.56, 122.68, 120.53, 21.14, 20.23. HR MS (EI): calcd for $C_{38}H_{30}S_2$ (M^+), 550.1789; found, 550.1799 (error: 1.82 ppm).

Compound S2-Ph

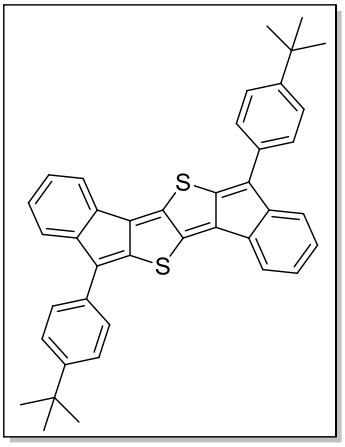

To a solution of 1-bromo-4-*tert*-butylbenzene (1.28 g, 6.00 mmol) in anhydrous THF (30 ml) at -78 ^{o}C was added dropwise *n*-BuLi (1.6 M in

hexane, 3.75 mL, 6.00 mmol). The solution was stirred for 1 h at -78 ^{o}C. Then diketone **2-21** (344 mg, 1.00 mmol) was added as solid in one portion. The mixture was slowly warmed to room temperature and stirred overnight. During this period the insoluble diketone disappeared and the solution became clear. The reaction was quenched with 10% HCl solution (10 ml) and extracted in $CHCl_3$. The organic layer was dried (Na_2SO_4), filtered, and evaporated to dryness under vacuum. After that the crude diol was dissolved in dry toluene (20 mL) and degassed with Ar. $SnCl_2$ (758.5 mg, 4.00 mmol) was added to the mixture and stirred overnight. During this period the color of the reaction mixture became deep blue. The resulting blue solution was then filtered and the filtrate was subsequently evaporated to dryness. The residue was purified by column chromatography (silica gel, DCM). Compound **S2-Ph** was further purified by recrystallization from CH_3CN/CH_2Cl_2 as a dark blue solid (232 mg, 40% yield). ^{1}H NMR (500 MHz, $CDCl_3$, ppm): δ = 7.65 (d, *J* = 8.3 Hz, 2H), 7.54-7.51 (m, 3H), 7.41 (d, *J* = 7.2 Hz. 1H), 7.20 (dd, *J* = 7.5 Hz, 1H), 7.11 (dd, *J* = 7.4 Hz, 1H), 1.39 (s, 9H). This compound has a poor solubility and the ^{13}C NMR was not obtained. HR MS (EI): calcd for $C_{40}H_{34}S_2$ (M^+), 578.2102; found, 578.2096 (error: -1.04 ppm). Anal. Calcd for $C_{40}H_{34}S_2$: C, 83.00; H, 5.92; S, 11.08; found: C, 82.65; H, 6.10; S, 10.98.

Compound 2-24

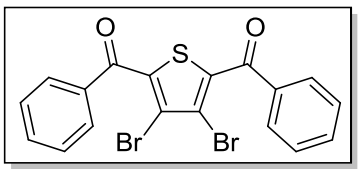

Under argon and anhydrous condition at -78 ^{o}C, *n*-BuLi (1.6 M in hexane, 6.25 mL, 10.00 mmol) was slowly added to a solution of tetrabromothiophene (**2-22**, 2.00 g, 5.00 mmol) in THF (40 mL) and the mixture was stirred for 1 h at this temperature. Benzaldehyde (1.06 g, 10.00 mmol) was added by syringe at -78 ^{o}C. The reaction was slowly warmed to room temperature and stirred overnight. The reaction was quenched by water at 0 ^{o}C. The organic solvent was removed and the organic precipitate was collected by filtration. The precipitate was washed with hexane to give the diol intermediate (**2-23**) which used for the next step reaction without further purification and characterization.

The above diol intermediate was dissolved in 40 mL of DCM. PCC (3.23 g, 15 mmol) was slowly added into the solution by portions. The reaction was stirred overnight at room temperature and the resulting mixture was poured into water and extracted with DCM. The combine extracts were dried (Na_2SO_4), the solvent removed under vacuum and the residue purified by column chromatography (silica gel, hexane: ethyl acetate (EA) = 5: 1). The title compound **2-24** was obtained as colorless oil (1.80 g, 80% yield). ^{1}H NMR (500 MHz, $CDCl_3$, ppm): δ = 7.89-7.87 (m, 2H), 7.67-7.64 (m, 1H), 7.54-7.50 (m, 2H); ^{13}C NMR (125 MHz, $CDCl_3$, ppm): δ = 187.28, 139.14,

136.19, 134.00, 130.00, 128.73, 119.10. HR MS (EI): calcd for $C_{18}H_{10}Br_2O_2S$ (M^+), 447.8768; found, 447.8768 (error: -1.16 ppm).

Compound 2-25

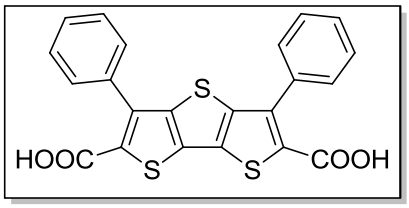

Ethyl mercaptoacetate (1.20 g, 10 mmol) and compound **2-24** (1.80 g, 4 mmol) were dissolved in 30 mL of ethanol. KOH (1.12 g, 20 mmol) was added to the above reaction mixture. The reaction was stirred at room temperature for 2 h then stirred at 50-60 ℃ overnight. During this period the precipitate would be formed. Then excess of KOH (3g) was added and the reaction was heated to reflux for 24 h. After cooling down the alcohol was evaporated and 10% HCl was slowly added. During this period diacid **2-25** was precipitated. After filtration, a pale yellow solid was obtained. The crude product was purified by washing with hexane (30 mL) and DCM (30 mL) to give a pale yellow solid (1.66 g, 95% yield). ^{1}H NMR (500 MHz, DMSO-d_6, ppm): δ = 13.35 (br, 1H), 7.56-7.54 (m, 2H), 7.49-7.43 (m, 3H); ^{13}C NMR (125 MHz, DMSO-d_6, ppm): δ =162.67, 144.73, 140.06, 133.39, 131.81, 130.64, 128.92, 128.68, 128.32. HR MS (EI): calcd for $C_{22}H_{12}O_4S_3$ (M^+), 435.9898; found, 435.9902 (error: -0.92 ppm).

Compound 2-26

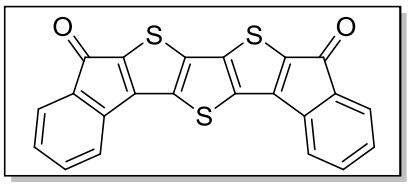

Compound **2-25** (873 mg, 2.00 mmol) was added in anhydrous DCM (20 mL), followed by the addition of excess of thionyl chloride (3 mL). To this mixture anhydrous DMF (1-2 drops) was added at room temperature. The resultant mixture was heated at reflux overnight. After cooling down the solvent was removed under reduced pressure to afford crude acid chloride. This intermediate compound was dissolved in anhydrous DCM (20 mL) then anhydrous $AlCl_3$ (1.07g, 8.00 mmol) was added carefully at 0 ℃. The resultant mixture was allowed to warm up to room temperature and stirred overnight, then slowly quenched by 10% HCl solution to form a red precipitate. The crude precipitate was rinsed with 10% NaOH, MeOH, DCM and THF until the washings were colorless, giving **2-26** as an insoluble red solid (624 mg, 78% yield). Both ^{1}H NMR and ^{13}C NMR data were not obtained due to its poor solubility. HR MS (EI): calcd for $C_{22}H_8O_2S_3$ (M^+), 399.9686; found, 399.9690 (error: 1.00 ppm). Anal. Calcd for $C_{22}H_8O_2S_3$: C, 65.98; H, 2.01; S, 24.02; found: C, 65.68; H, 2.34; S, 23.98.

Compound S3-TIPS

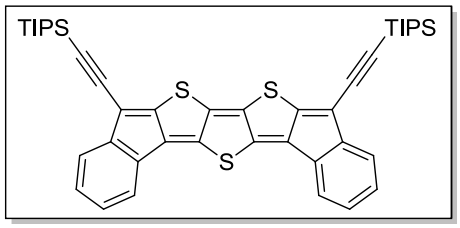

To a solution of triisopropylsilylacetylene (1.10 g, 6.00 mmol) in anhydrous THF (30 ml) at 0 ^{o}C was added dropwise *n*-BuLi (1.6 M in hexane, 3.75 mL, 6.00 mmol). The solution was stirred for 30 min at 0 ^{o}C. Then diketone **2-26** (400 mg, 1.00 mmol) was added as solid in one portion. The mixture was slowly warmed to room temperature and stirred overnight. During this period the insoluble diketone disappeared and the solution became clear with strong blue fluorescence. The reaction was quenched with 10% HCl solution (10 ml) and extracted in $CHCl_3$. The organic layer was dried (Na_2SO_4), filtered, and evaporated to dryness under vacuum. After that the crude diol was dissolved in dry toluene (20 mL) and degassed with Ar. $SnCl_2$ (758.5 mg, 4.00 mmol) was added to the mixture and stirred overnight. During this period the color of the reaction mixture became purple. The resulting purple solution was then filtered and the filtrate was subsequently evaporated to dryness. The residue was purified by column chromatography (silica gel, hexane: DCM = 5: 1). Compound **S3-TIPS** was further purified by recrystallization from CH_3CN/CH_2Cl_2 as a black solid (497 mg, 68% yield). ^{1}H NMR (500 MHz, $CDCl_3$, ppm): δ = 7.32 (d, *J* = 7.4 Hz. 1H), 7.25 (d, *J* = 6.1 Hz. 1H), 7.19 (dd, *J* = 7.5 Hz, 1H), 7.07 (dd, *J* = 7.5 Hz, 1H), 1.19-1.17 (br, 21H); ^{13}C NMR (125

MHz, $CDCl_3$, ppm): δ = 148.88, 146.62, 143.96, 142.99, 138.56, 129.26, 128.56, 125.11, 122.10, 120.76, 113.22, 105.48, 100.41, 18.74, 11.31. HR MS (EI): calcd for $C_{44}H_{50}S_3Si_2$ (M^+), 730.2613; found, 730.2607 (error: -0.82 ppm).

Compound 2-27

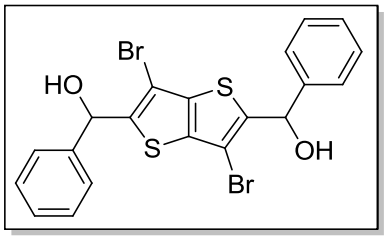

Under argon and anhydrous condition at -78 °C, *n*-BuLi (1.6 M in hexane, 6.25 mL, 10.00 mmol) was slowly added to a solution of 2,3,5,6-tetrabromothieno[3,2-b]thiophene (**2-17**, 2.28 g, 5.00 mmol) in THF (40 mL) and the mixture was stirred for 1 h. Benzaldehyde (1.06 g, 10.00 mmol) was added by syringe at -78 °C. The reaction was slowly warmed to room temperature and stirred overnight. The reaction was quenched by water at 0 °C. The organic solvent was removed and the organic precipitate was collected by filtration. The precipitate was washed with hexane to give the white diol intermediate which used for the next step reaction without further purification and characterization.

Compound 2-28

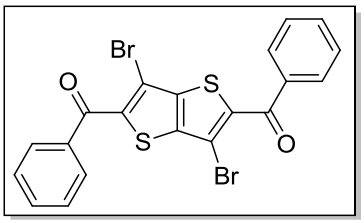

The above diol intermediate was dissolved in 40 mL of DCM. PCC (3.23 g, 15 mmol) was slowly added into the solution by portions. The reaction was stirred overnight at room temperature and the resulting mixture was poured into water and extracted with dichloromethane. The combine extracts were dried (Na_2SO_4), the solvent removed in vacuo and the residue purified by column chromatography (silica gel, hexane: EA = 5: 1). The title compound **2-28** was obtained as white solid (1.52 g, 60% yield) ^{1}H NMR (500 MHz, $CDCl_3$, ppm): δ = 7.89 (d, *J* = 7.1 Hz. 2H), 7.66 (m, 1H), 7.53 (m, 2H); ^{13}C NMR (125 MHz, $CDCl_3$, ppm): δ = 187.80, 142.90, 139.79, 136.97, 133.51, 129.78, 128.60, 107.71. HR MS (EI): calcd for $C_{20}H_{10}Br_2O_2S_2$ (M^+), 505.8468; found, 505.8468 (error: 0 ppm).

Compound 2-29

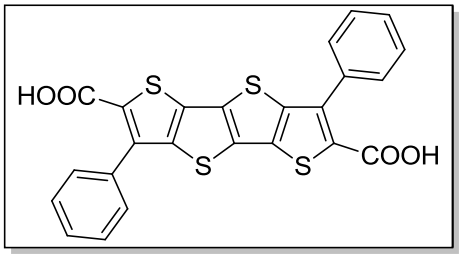

Ethyl mercaptoacetate (300 mg, 2.5 mmol) and compound **2-28** (506 mg, 1 mmol) were dissolved in 20 mL of ethanol. KOH (224 mg, 5 mmol) was

added to the above reaction mixture. The reaction was stirred at room temperature for 2 h then stirred at 50-60 ℃ overnight. Then excess of KOH (1g) was added and the reaction was heated to reflux for 24 h. After cooling down the alcohol was evaporated and 10% HCl was slowly added. During this period diacid **2-29** was precipitated. After filtration, a pale yellow solid was obtained. The crude product was purified by washing with hexane (30 mL) and DCM (30 mL) to give a pale yellow solid (453 mg, 92% yield). ^{1}H NMR (500 MHz, DMSO-d_6, ppm): δ = 13.28 (br, 1H), 7.65-7.61 (m, 2H), 7.55-7.48 (m, 3H). ^{13}C NMR data were not obtained due to its poor solubility. HR MS (APCI): calcd for $C_{24}H_{13}O_4S_4$ $(M + H)^+$, 492.9697; found, 492.9674 [$(M+H)^+$] (error: -4.67 ppm). Anal. Calcd for $C_{24}H_{12}O_4S_4$: C, 58.52; H, 2.46; S, 26.04; found: C, 58.42; H, 2.64; S, 26.32.

Compound 2-30

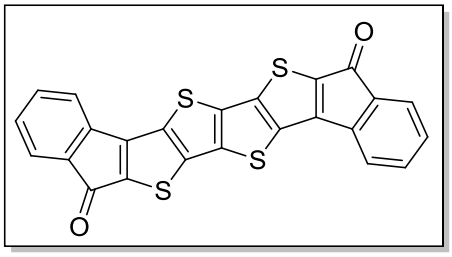

Compound **2-29** (492 mg, 1.00 mmol) was added in anhydrous DCM (20 mL), followed by the addition of excess of thionyl chloride (2 mL). To this mixture anhydrous DMF (1-2 drops) was added at room temperature. The resultant mixture was heated at reflux overnight. After cooling down the solvent was removed under reduced pressure to afford crude acid chloride. This

intermediate compound was dissolved in anhydrous DCM (20 mL) then anhydrous $AlCl_3$ (533 mg, 4.00 mmol) was added carefully at 0 ℃. The resultant mixture was allowed to warm up to room temperature and stirred overnight, then slowly quenched by 10% HCl solution to form a red precipitate. The crude precipitate was rinsed with 10% NaOH, MeOH, DCM and THF until the washings were colorless, giving **2-30** as an insoluble red solid (329 mg, 72% yield). Both ^{1}H NMR and ^{13}C NMR data were not obtained due to its poor solubility. HR MS (APCI): calcd for $C_{24}H_9O_2S_4$ $(M + H)^+$, 456.9485; found, 456.9480 $[(M+H)^+]$ (error: -1.09 ppm). Anal. Calcd for $C_{24}H_8O_2S_4$: C, 63.13; H, 1.77; S, 28.09; found: C, 62.85; H, 2.02; S, 27.98.

Compound 2-31

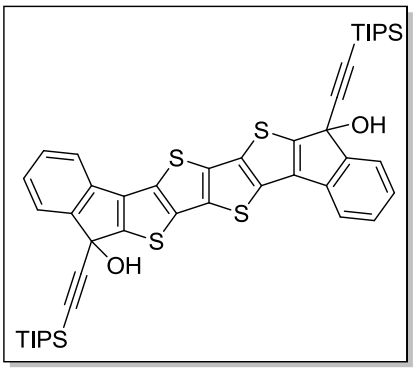

To a solution of triisopropylsilylacetylene (730 mg, 4.00 mmol) in anhydrous THF (30 mL) at 0 ^{o}C was added dropwise *n*-BuLi (1.6 M in hexane, 2.50 ml, 4.00 mmol). The solution was stirred for 30 min at 0 ^{o}C. Then diketone **2-30** (228 mg, 0.50 mmol) was added as solid in one portion. The mixture was slowly warmed to room temperature and stirred overnight. During this period

the insoluble diketone disappeared and the solution became clear with strong blue fluorescence. The reaction was quenched with 10% HCl solution (10 mL) and extracted in ethyl acetate. The combine extracts were dried (Na_2SO_4), the solvent removed under vacuum and the residue was purified by column chromatography (silica gel, hexane: EA = 6: 1). The resulting solid was washed with hexane to obtain the title compound **2-31** as off-white solid (120 g, 29% yield). The low yield was due to the column chromatography process because the title diol compound was very easily to attach on the silica gel. ^{1}H NMR (500 MHz, $C_2D_2Cl_4$, ppm): δ = 7.64 (m, 1H), 7.38-7.23 (m, 3H), 2.90 (s, 1H), 1.10-1.03 (br, 21H). ^{13}C NMR data were not obtained due to its poor solubility. HR MS (APCI): calcd for $C_{46}H_{53}O_2S_4Si_2$ [$(M+H)^+$], 821.2467; found, 821.2487 (error: 2.44 ppm). Anal. Calcd for $C_{46}H_{52}O_2S_4Si_2$: C, 67.27; H, 6.38; S, 15.62; found: C, 67.39; H, 6.68; S, 15.30.

In situ generation of S4-TIPS

Compound **2-31** was dissolved in dry toluene (or THF, $CHCl_3$ etc.) and excessive dry $SnCl_2$ was added. The mixture was shacked to facilitate reaction. The reaction was carefully conducted under argon atmosphere and followed by ^{1}H NMR (in dry $CDCl_2CDCl_2$, **Figure 2.2**) and UV-vis-NIR measurements (in dry toluene, **Figure 2.3**). The reaction completed in about 30 mins but the products gradually decomposed simultaneously even under Ar protection. The formation of the **S4-TIPS** was confirmed by the MALDI-TOF mass

spectrometry for the freshly prepared sample (**Figure 2.4a**). Upon contact with air, it quickly decomposed with the major products as the oxygen addition species (**Figure 2.4b**).

References

[1] (a) J. L. Brédas and G. B. Street, *Acc. Chem. Res.*, 1985, **18**, 309. (b) L. M. Tolbert, *Acc. Chem. Res.*, 1992, **25**, 561. (c) T. Nishinaga, A. Wakamiya, D. Yamazaki and K. Komatsu, *J. Am. Chem. Soc.*, 2004, **126**, 3163. (d) D. Yamazaki, T. Nishinaga, N. Tanino and K. Komatsu, *J. Am. Chem. Soc.*, 2006, **128**, 14470. (e) M. Banerjee, S. V. Lindeman and R. Rathore, *J. Am. Chem. Soc.*, 2007, **129**, 8070. (f) M. Banerjee, R. Shukla and R. Rathore, *J. Am. Chem. Soc.*, 2009, **131**, 1780. (g) S. R. González, Y. Ie, Y. Sao, J. T. López Navarrete and J. Casado, *J. Am. Chem. Soc.*, 2011, **133**, 16350. (h) S. R. González, M. Carmen Tuiz Delgado, R. Caballero, P. De la Cruz, F. Langa, J. T. López Navarrete and J. Casado, *J. Am. Chem. Soc.*, 2012, **134**, 5675.

[2] See review articles: (a) Z. Sun and J. Wu, *J. Mater. Chem.*, 2012, **22**, 4151. (b) Z. Sun, Q. Ye, C. Chi and J. Wu, *Chem. Soc. Rev.*, 2012, **41**, 7857. (c) A. Shimizu, Y. Hirao, T. Kubo, M. Nakano, E. Botek and B. Champagne, *AIP Conf. Proc.*, 2012, **1504**, 399. (d) Z. Sun, Z. Zeng and J. Wu, *Chem. Asian J.*, 2013, **8**, 2894. (e) M. Abe, *Chem. Rev.*, 2013, **113**, 7011. (f) Z. Sun and J. Wu, *Pure Appl. Chem.*, 2014, **86**, 529.

[3] See review articles: (a) J. Casado, R. P. Ortiz and J. T. López Navarrete,

Chem. Soc. Rev., 2012, **41**, 5672. (b) J. Casado and J. T. López Navarrete, *Chem. Records,* 2011, **11**, 45.

[4] (a) M. Chikamatsu, T. Mikami, J. Chisaka, Y. Yoshida, R. Azumi and K. Yase, *Appl. Phys. Lett.,* 2007, **91**, 043506. (b) D. T. Chase, A. G. Fix, S. J. Kang, B. D. Rose, C. D. Weber, Y. Zhong, L. N. Zakharov, M. C. Lonergan, C. Nuckolls and M. M. Haley, *J. Am. Chem. Soc.,* 2012, **134**, 10349.

[5] K. Kamada, K. Ohta, T. Kubo, A. Shimizu, Y. Morita, K. Nakasuji, R. Kishi, S. Ohta, S.-I. Furukawa, H. Takahashi and M. Nakano, *Angew. Chem. Int. Ed.,* 2007, **46**, 3544.

[6] (a) Y. W. Son, M. L. Cohen and S. G. Louie, *Phys. Rev. Lett.,* 2006, **97**, 216803. (b) V. Dediu, L. E. Hueso, I. Bergenti and C. Tliani, *Nat. Mater.,* 2009, **8**, 707. (c) V. Dediu, L. E. Hueso and I. Bergenti, "Spin transport in organic semiconductors" (chapter 22) in the book, "Handbook of spin transport and magnetism", Taylor & Francis Group, 2012.

[7] (a) M. B. Smith and J. Michl, *Chem. Rev.,* 2010, **110**, 6891. (b) J. Lee, P. Jadhav, P. D. Reusswig, S. R. Yost, N. J. Thompson, D. N. Congreve, E. Hontz, T. Van Voorhis and M. Baldo, A. *Acc. Chem. Res.*, 2013, **46**, 1300.

[8] (a) Y. Morita, S. Nishida, T. Murata, M. Moriguchi, A. Ueda, M. Satoh, K. Arifuku, K. Sato and Takui, T. *Nat. Mater.,* 2011, **10**, 947. (b) J.-Y. Shin, T. Yamada, H. Yoshikawa, K. Awaga and H. Shinokubo, *Angew. Chem. Int. Ed.,* 2014, **53**, 3096.

[9] (a) K. Ohashi, T. Kubo, T. Masui, K. Yamamoto, K. Nakasuji, T. Takui, Y.

Kai and I. Murata, *J. Am. Chem. Soc.*, 1998, **120**, 2018. (b) T. Kubo, M. Sakamoto, M. Akabane, Y. Fujiwara, K. Yamamoto, M. Akita, K. Inoue, T. Takui and K. Nakasuji, *Angew. Chem. Int. Ed.*, 2004, **43**, 6474. (c) T. Kubo, A. Shimizu, M. Sakamoto, M. Uruichi, K. Yakushi, M. Nakano, D. Shiomi, K. Sato, T. Takui, Y. Morita and K. Nakasuji, *Angew. Chem. Int. Ed.*, 2005, **44**, 6564. (d) A. Shimizu, M. Uruichi, K. Yakushi, H. Matsuzaki, H. Okamoto, M. Nakano, Y. Hirao, K. Matsumoto, H. Kurata and T. Kubo, *Angew. Chem. Int. Ed.*, 2009, **48**, 5482. (e) A. Shimizu, T. Kubo, M. Uruichi, K. Yakushi, M. Nakano, D. Shiomi, K. Sato, T. Takui, Y. Hirao, K. Matsumoto, H. Kurata, Y. Morita and K. Nakasuji, *J. Am. Chem. Soc.*, 2010, **132**, 14421. (f) A. Shimizu, Y. Hirao, K. Matsumoto, H. Kurata, T. Kubo, M. Uruichi and K. Yakushi, *Chem. Commun.*, 2012, **48**, 5629.

[10] (a) D. T. Chase, B. D. Rose, S. P. McClintock, L. N. Zakharov and M. M. Haley, *Angew. Chem. Int. Ed.*, 2011, **50**, 1127. (b) A. Shimizu and Y. Tobe, *Angew. Chem. Int. Ed.*, 2011, **50**, 6906. (c) A. G. Fix, D. T. Chase and M. M. Haley, *Top. Curr. Chem.*, 2012, DOI: 10.1007/128_2012_376. (d) A. G. Fix, P. E. Deal, C. L. Vonnegut, B. D. Rose, L. N. Zakharov and M. M. Haley, *Org. Lett.*, 2013, **15**, 1362. (e) B. D. Rose, C. L. Vonnegut, L. N. Zakharov and M. M. Haley, *Org. Lett.*, 2013, **14**, 2426. (f) A. Shimizu, R. Kishi, M. Nakano, D. Shiomi, K. Sato, T. Takui, I. Hisaki, M. Miyata and Y. Tobe, *Angew. Chem. Int. Ed.*, 2013, **52**, 6076. (g) H. Miyoshi, S. Nobusue, A. Shimizu, I. Hisaki, M. Miyatab and Y. Tobe, *Chem. Sci.*, 2014, **5**, 163. (h) B. S. Young, D. T. Chase, J.

L. Marshall, C. L. Vonnegut, L. N. Zakharov and M. M. Haley, *Chem. Sci.*, 2014, **5**, 1008.

[11] (a) R. Umeda, D. Hibi, K. Miki and Y. Tobe, *Org. Lett.*, 2009, **11**, 4104. (b) T. C. Wu, C. H. Chen, D. Hibi, A. Shimizu, Y. Tobe and Y. T. Wu, *Angew. Chem. Int. Ed.*, 2010, **49**, 7059. (c) Z. Sun, K.-W. Huang and J. Wu, *Org. Lett.*, 2010, **12**, 4690. (d) Z. Sun, K.-W. Huang and J. Wu, *J. Am. Chem. Soc.*, 2011, **133**, 11896. (e) Y. Li, W.-K. Heng, B. S. Lee, N. Aratani, J. L. Zafra, N. Bao, R. Lee, Y. M. Sung, Z. Sun, K.-W. Huang, R. D. Webster, J. T. López Navarrete, D. Kim, A. Osuka, J. Casado, J. Ding and J. Wu, *J. Am. Chem. Soc.*, 2012, **134**, 14913. (f) W. Zeng, M. Ishida, S. Lee, Y. Sung, Z. Zeng, Y. Ni, C. Chi, D.-H. Kim and J. Wu, *Chem. Eur. J.*, 2013, **19**, 16814. (g) Z. Sun, S. Lee, K. Park, X. Zhu, W. Zhang, B. Zheng, P. Hu, Z. Zeng, S. Das, Y. Li, C. Chi, R. Li, K. Huang, J. Ding, D. Kim and J. Wu, *J. Am. Chem. Soc.*, 2013, **135**, 18229. (h) Z. Sun and J. Wu, *J. Org. Chem.*, 2013, **78**, 9032; (i) L. Shan, Z.-X. Liang, X.-M. Xu, Q. Tang and Q. Miao, *Chem. Sci.*, 2013, **4**, 3294. (j) J. L. Zafra, R. C. González Cano, M. C. R. Delgado, Z. Sun, Y. Li, J. T. López Navarrete, J. Wu and J. Casado, *J. Chem. Phys.*, 2014, **140**, 054706. (k) Y. Li, K.-W. Huang, Z. Sun, R. D. Webster, Z. Zeng, W. D. Zeng, C. Chi, K. Furukawa and J. Wu, *Chem. Sci.*, 2014, **5**, 1908**.**

[12] (a) X. Zhu, H. Tsuji, H. Nakabayashi, S. Ohkoshi and E. Nakamura, *J. Am. Chem. Soc.*, 2011, **133**, 16342. (b) Z. Zeng, Y. M. Sung, N. Bao, D. Tan, R. Lee, J. L. Zafra, B. S. Lee, M. Ishida, J. Ding, J. T. López Navarrete, Y. Li, W.

Zeng, D. Kim, K.-W. Huang, R. D. Webster, J. Casado and J. Wu, *J. Am. Chem. Soc.*, 2012, **134**, 14513. (c) Z. Zeng, M. Ishida, J. L. Zafra, X. Zhu, Y. M. Sung, N. Bao, R. D. Webster, B. S. Lee, R.-W. Li, W. Zeng, Y. Li, C. Chi, J. T. López Navarrete, J. Ding, J. Casado, D. Kim and J. Wu, *J. Am. Chem. Soc.*, 2013, **135**, 6363. (d) Z. Zeng, S. Lee, J. L. Zafra, M. Ishida, X. Zhu, Z. Sun, Y. Ni, R. D. Webster, R.-W. Li, J. T. López Navarrete, C. Chi, J. Ding, J. Casado, D. Kim and J. Wu, *Angew. Chem. Int. Ed.*, 2013, **52**, 8561. (e) Z. Zeng, S. Lee, J. L. Zafra, M. Ishida, N. Bao, R. D. Webster, J. T. López Navarrete, J. Ding, J. Casado, D. Kim and J. Wu, *Chem. Sci.* 2014, **5**, 3072.

[13] (a) V. Hernández, S. Calvo Losada, J. Casado, H. Higuchi and J. T. López Navarrete, *J. Phys. Chem. A*, 2000, **104**, 661. (b) J. Casado, T. M. Pappenfus, K. R. Mann, E. Ortí, P. M. Viruela, B. Milián, V. Hernández and J. T. López Navarrete, *ChemPhysChem*, 2004, **5**, 529. (c) T. Takahashi, K. I. Matsuoka, K. Takimiya, T. Otsubo, Y. Aso, *J. Am. Chem. Soc.*, 2005, **127**, 8928. (d) R. P. Ortiz, J. Casado, V. Hernandez, J. T. López Navarrete, P. M. Viruela, E. Orti, K. Takimiya and T. Otsubo, *Angew. Chem. Int. Ed*., 2007, **46**, 9057. (e) R. P. Ortiz, J. Casado, S. R. González, V. Hernández, J. T. López Navarrete, P. M. Viruela, E. Ortí, K. Takamiya and T. Otsubo, *Chem. Eur. J.*, 2010, **16**, 470. (f) E. V. Canesi, D. Fazzi, L. Colella, C. Bertarelli and C. Castiglioni, *J. Am. Chem. Soc.*, 2012, **134**, 19070.

[14] (a) T. M. Pappenfus, R. J. Chesterfield, C. D. Frisbie, K. R. Mann, J. Casado, J. D. Raff and L. L. Miller, *J. Am. Chem. Soc.*, 2002, **124**, 4184. (b) R.

J. Chesterfield, C. R. Newman, T. M. Pappenfus, P. C. Ewbank, M. H. Haukaas, K. R. Mann, L. L. Miller and C. D. Frisbie, *Adv. Mater.*, 2003, **15**, 1278. (c) R. P. Ortiz, A. Facchetti, T. J. Marks, J. Casado, M. Z. Zgierski, M. Kozaki, V. Hernández, J. T and López Navarrete, *Adv. Funct. Mater.*, 2009, **19**, 386. (d) Y. Suzuki, E. Miyazaki and K. Takimiya, *J. Am. Chem. Soc.*, 2010, **132**, 10453.

[15] (a) X. Zhang, A. Côté and A. J. Matzger, *J. Am. Chem. Soc.*, 2005, **127**, 10502. (b) K. Xiao, Y. Liu, T. Qi, W. Zhang, F. Wang, J. Gao, W. Qiu, Y. Ma, G. Cui, S. Chen, X. Zhan, G. Yu, J. Qin, W. Hu and D. Zhu, *J. Am. Chem. Soc.*, 2005, **127**, 13281. (c) T. Okamoto, K. Kudoh, A. Wakamiya and S. Yamaguchi, *Chem. Eur. J.*, 2007, **13**, 548. (d) E.-G. Kim, V. Coropceanu, N. E. Gruhn, R. S. Sánchez-Carrera, R. Snoeberger, A. J. Matzger and J. L. Brédas, *J. Am. Chem. Soc.*, 2007, **129**, 13072. (e) K. Takimiya, S. Shinamura, I. Osaka and E. Miyazaki, *Adv. Mater.*, 2011, **23**, 4347. (f) A. N. Sokolov, S. Atahan-Evrenk, R. Mondal, H. B. Akkermanl, R. S. Sánchez-Carrera, S. Granados-Focil, S. Schrier, S. C. B. Mannsfeld, A. P. Zoombelt, Z. Bao and A. Aspuru-Guzik, *Nat. Commun.*, 2011, **2**, 437. (g) K. Niimi, S. Shinamura, I. Osaka, E. Miyazaki and K. Takimiya, *J. Am. Chem. Soc.*, 2011, **133**, 8732. (h) W. Xie, K. Willa, Y. Wu, R. Häusermann, K. Takimiya, B. Batlogg and C. D. Frisbie, *Adv. Mater.*, 2013, **25**, 3478. (i) T. Yokota, K. Kuribara, T. Tokuhara, U. Zschieschang, H. Klauk, K. Takimiya, Y. Sadamitsu, M. Hamada, T. Sekitani and T. Someya, *Adv. Mater.*, 2013, **25**, 3639.

[16] (a) K. Yui, H. Ishida, Y. Aso, T. Otsubo, F. Ogura, A. Kawamoto and J. Tanaka, *Bull. Chem. Soc. Jpn.*, 1989, **62**, 1547. (b) Q. Wu, R. Li, W. Hong, H. Li, X. Gao and D. Zhu, *Chem. Mater.*, 2011, **23**, 3138.

[17] (a) J. E. Anthony, *Chem. Rev.*, 2006, **106**, 5028. (b) J. E. Anthony, *Angew. Chem. Int. Ed.*, 2008, **47**, 452. (c) H. Qu, C. Chi, *Curr. Org. Chem.*, 2010, **14**, 2070.

[18] A. Henckens, K. Colladet, S. Fourier, T. J. Cleij, L. Lutsen, J. Gelan and D. Vanderzande, *Macromolecules*, 2005, **38**, 19.

[19] L. S. Fuller, B. Iddon and K. A. Smith, *J. Chem. Soc., Perkin Trans. 1*, 1997, 3465.

[20] (a) X. Shi, J. Chang and C. Chi, *Chem. Commun.*, 2013, **49**, 7135. (b) T. Kunz and P. Knochel, *Chem. Eur. J.*, 2011, **17**, 866.

[21] D. T. Tùng, D. T. Tuân, N. Rasool, A. Villinger, H. Reinke, C. Fischer and P. Langer, *Adv. Synth. Cat.*, 2009, **351**, 1595.

[22] (a) F. Dietz, N. Tyutyulkov and M. Rabinovitz, *J. Chem. Soc. Perkin Trans. 2*, 1993, 157. (b) F. Dietz, M. J. Rabinovitz, A. Tadjer and N. Tyutyulkov, *J. Chem. Soc. Perkin Trans. 2*, 1995, 735.

[23] J. Lakowicz, *Principles of Fluorescence Spectroscopy*, Kluwer Academic/Plenum Publishers, New York, Boston, Dordrecht, London, Moscow, 1999.

[24] (a) E. M. Giacobbe, G, Q. Mi, M. T. Colvin, B. Cohen, A. Ramana, A. M. Scott, S. Yeganeh, T. J. Marks, M. A. Ratner and M. R. Wasielewski, *J. Am.*

Chem. Soc., 2009, **131**, 3700. (b) K. Ishii, Y. Hirose, H. Fujitsuka, O. Ito and N. Kobayashi, *J. Am. Chem. Soc.*, 2001, **123**, 702.

[25] M. Sheik-Bahae, A. A. Said, T.-H. Wei, D. J. Hagan and E. W. Van Stryland, *IEEE J. Quant. Electr.,* 1990, **26**, 760. Our TPA set-up is 1200-2400nm, and the maximum TPA cross-section values cannot be assigned.

[26] M. Nakano, R. Kishi, A. Takebe, M. Nate, H. Takahashi, T. Kubo, K. Kamada, K. Ohta, B. Champagne aned E. Botek, *Comput. Lett.,* 2007, **3**, 333.

[27] (a) M. Pawlicki, H. A. Collins, R. G. Denning and H. L. Anderson, *Angew. Chem. Int. Ed.,* 2009, **48**, 3244. (b) T. K. Ahn, J. H. Kwon, D. Y. Kim, D. W. Cho, D. H. Jeong, S. K. Kim, M. Suzuki, S. Shimizu, A. Osuka and D. Kim, *J. Am. Chem. Soc.,* 2005, **127**, 12856. (c) Y. Tanaka, S. Saito, S. Mori, N. Aratani, H. Shinokubo, N. Shibata, Y. Higuchi, Z. S. Yoon, K. S. Kim, S. B. Noh, J. K. Park, D. Kim and A. Osuka, *Angew. Chem. Int. Ed.,* 2008, **47**, 681. (d) J. M. Lim, Z. S. Yoon, J.-Y. Shin, K. S. Kim, M.-C. Yoon and D. Kim, *Chem. Commun.,* 2009, 261.

[28] CCDC number, **S1-TIPS**: 1004903, **S2-TIPS**: 1004904, **S2-Mes**: 1004905, **S2-Ph**: 1004906, **S3-TIPS**: 1004907.

[29] (a) T. Yanai, D. Tew and N. Handy, *Chem. Phys. Lett.,* 2004, **393**, 51. (b) R. Seeger and J. A. Pople, *J. Chem. Phys.,* 1977, **66**, 3045.

[30] H. Fallah-Bagher-Shaidaei, C. S. Wannere, C. Corminboeuf, R. Puchta and P.v.R, Schleyer, *Org. Lett.,* 2006, **8**, 863.

[31] T. Weil, T. Vosch, J. Hofkens, K. Peneva and K. Müllen, *Angew. Chem. Int. Ed.*, 2010, **49**, 9068.

Chapter 3: Pro-aromatic Dithiaquinoidal–[*n*]thienoacenes with Small to Moderate Singlet Biradical Characters: Synthesis, Structures and Chain Length Dependent Physical Properties

3.1 Introduction

As reviewed in the preceding chapter 1 introduction section, recent studies demonstrated that aromaticity and biradical character played important roles on determining the ground-state structures and physical properties of quinoidal polycyclic hydrocarbons[1] and oligothiophenes[2], a kind of molecular materials showing promising applications for organic electronics, photonics and spintronics. Based on the reported literatures to date, generally there are three factors, including the length of quinoidal unit, the type of fusion motifs together with the substituents, which can simultaneously affect the singlet biradical characters of the fusion type quinoidal compounds (**Figure 3.1**).

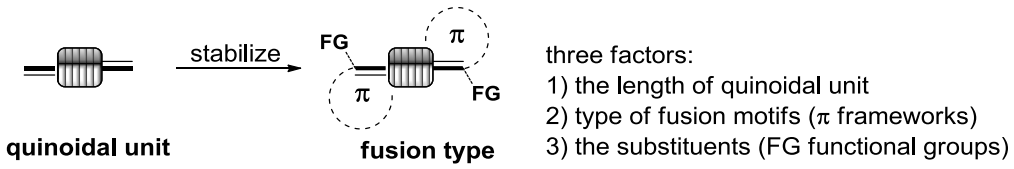

Figure 3.1 Fusion type quinoidal structure and three factors related to its singlet biradical character.

In chapter 2, we discussed the synthesis of a new type of hybrid system, called bisindeno-[*n*]thienoacenes (*n* = 1-4), by annulation of quinoidal fused α-oligothiophenes with two indene units (**Figure 3.2**). The obtained molecules

can be regarded as anti-aromatic systems containing $4n$ π electrons with small singlet biradical characters (y_0). The chain length (length of quinoidal unit) dependent properties were systematically studied. It was found that with the extension of the chain length the molecules showed a gradually increasing singlet biradical character and decreasing antiaromaticity.

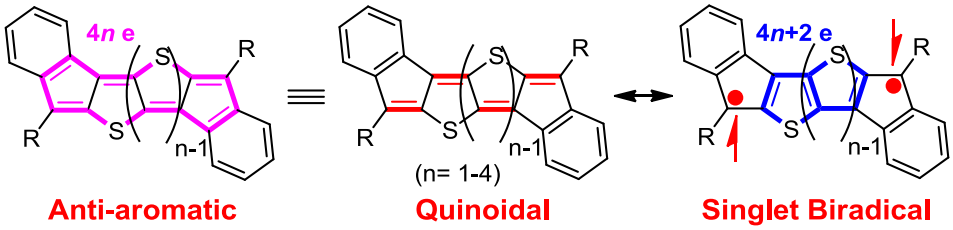

Figure 3.2 Resonance structures of bisindeno-[*n*]thienoacenes (*n* = 1-4).

Based on the work of chapter 2, in this chapter we designed and synthesized a series of quinoidal compounds, called dithiaquinoidal–[*n*]thienoacenes, by annulation of quinoidal fused *α*-oligothiophenes with two benzo-thia units (**Figure 3.3**). The structural features of such series of compounds and those of bisindeno-[*n*]thienoacenes are of interest. As can be seen, the great structural similitude between bisindeno-[*n*]thienoacenes and dithiaquinoidal–[*n*]thienoacenes is obvious that they remain the same quinoidal unit (quinoidal fused *α*-oligothiophenes) in the central of their structures. In contrast, the biggest structural difference between these two series of compounds is also distinct that they have the differential type of fusion motifs at the side of their structures (indene units in bisindeno-[*n*]thienoacenes *vs* benzo-thia units in dithiaquinoidal–[*n*]thienoacenes). Therefore, to understand the properties

correlation between such two series of compounds is one of the objectives in this chapter. Besides, the purpose of this work also involves: (1) the efficient synthesis of dithiaquinoidal–[*n*]thienoacenes; (2) their chain length dependent optical and electronic properties; (3) their geometry and electronic structures in the ground state. This work will help us better understand the anti-aromaticity (in bisindeno-[*n*]thienoacenes) and pro-aromaticity (in dithiaquinoidal–[*n*]thienoacenes) correlation, which further gives rise to the different singlet biradical characters (y_0) in these two series of compounds.

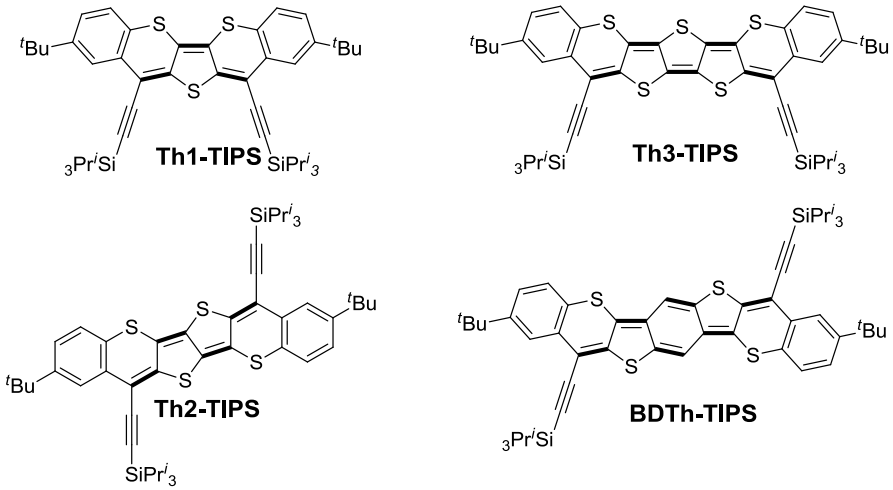

Figure 3.3 The strcutures of dithiaquinoidal–[*n*]thienoacenes.

3.2 Results and discussion

3.2.1 Synthesis

The synthetic methodology used to synthesize substituted acenes,[3] indenofluorenes[4] and zethrenes[5] was utilized to obtain our target compounds. That is, the corresponding diketones were prepared first, followed by nucleophilic addition with lithiated TIPSE, and then by reduction of the intermediate diols with $SnCl_2$. With this strategy, the synthesis of

dithiaquinoidal–[*n*]thienoacenes was successfully achieved.

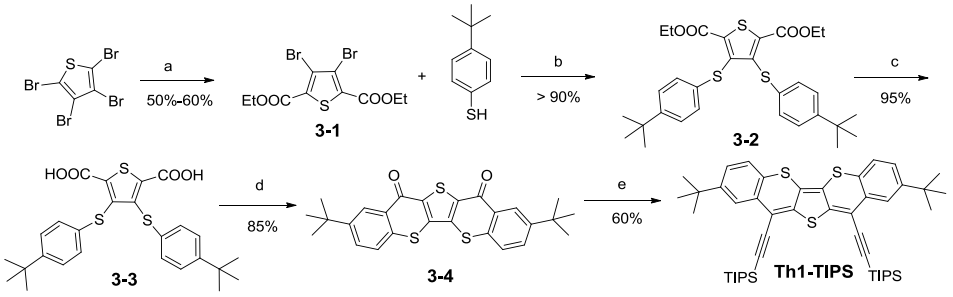

Scheme 3.1 Synthetic route to **Th1-TIPS**. *Reagents and conditions*: (a) i) *n*-BuLi, dry THF, -78 ^{o}C; ii) NCCOOEt, -78 ^{o}C – r.t., overnight; iii) H_2O, 0 ^{o}C; (b) $Pd_2(dba)_3$, dppf, DMF, $^{i}Pr_2NEt$, 100 ^{o}C, overnight; (c) i) NaOH, EtOH, reflux overnight; ii) 10% HCl (aq.); (d) i) $SOCl_2$, DMF, dry dichloromethane, reflux; ii) $AlCl_3$, dry dichloromethane, 0 ^{o}C – r.t., overnight; (e) i) TIPSCCLi, THF, 0 ^{o}C – r.t.; ii) $SnCl_2$, 6 h.

The synthetic route to **Th1-TIPS** is shown in **Scheme 3.1**. The diester compound **3-1** was obtained from two consecutive steps in one-pot reaction according to the literature[6] with a minor modification. Firstly, the tetrabromothiophene underwent Lithium-Halogen Exchange (lithiation) with two equivalent *n*-butyl lithium under -78 ^{o}C in dry THF solution to selectively give dilithiated intermediate at α-positions of thiophene ring, which easily reacted with ethyl cyanoformate to give product **3-1** in 50% to 60% yield. Subsequently, the compound **3-1** underwent palladium-catalyzed cross-coupling reaction[7] with 4-*tert*-butylbenzenethiol to give compound **3-2** in a very good yield (90%). Compound **3-2** was then hydrolyzed and acidified to form diacid **3-3**. Diacid **3-3** was then converted into the corresponding carboxylic acid chloride by reaction with thionyl chloride in dry dichloromethane (DCM). Subsequent double Friedel–Crafts acylation with aluminium chloride afforded the desired diketone **3-4** in a good yield. Compound **Th1-TIPS** was then obtained as a dark purple solid in an overall

60% yield by addition of lithiated TIPSE to the diketone **3-4** followed by reductive dehydroxylation with $SnCl_2$.

The synthesis of **Th2-TIPS** and **Th3-TIPS** utilized a similar strategy as that of **Th1-TIPS**, and the synthetic routes are outlined in **Scheme 3.2** and **Scheme 3.3**, respectively. Starting from their corresponding tetrabromo compounds **2-17**[8] and **3-8**[9,10], which were synthesized according to the literatures though multi steps, two ester groups were then selectively introduced into α-position of **2-17** and **3-8** to give the dibromo-diester compounds **2-18** and **3-9**, respectively. **2-18** and **3-9** then coupled with 4-*tert*-butylbenzenethiol to form products **3-5** and **3-10** by using palladium catalyst. The hydrolysis of **3-5** and **3-10** followed by acidification gave the diacid **3-6** and **3-11**, which were converted into the corresponding carboxylic acid chloride by reaction with thionyl chloride in dry dichloromethane (DCM). Subsequent double Friedel–Crafts acylation with aluminium chloride afforded the desired diketone **3-7** and **3-12** in very high yield. Last but not least, addition of lithiated TIPSE to the diketone **3-7** and **3-12** and reduction of the intermediate diols by $SnCl_2$ gave **Th2-TIPS** and **Th3-TIPS** in 75% and 60% yield, respectively.

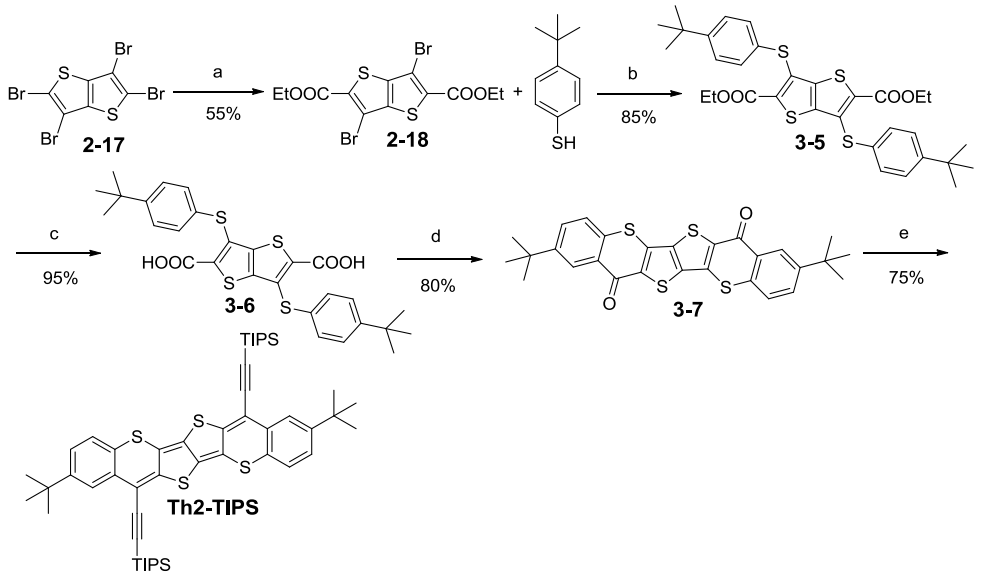

Scheme 3.2 Synthetic route to **Th2-TIPS**. *Reagents and conditions*: (a) i) *n*-BuLi, dry THF, -78 °C; ii) NCCOOEt, -78 °C – r.t., overnight; iii) H_2O, 0 °C; (b) $Pd_2(dba)_3$, dppf, DMF, $^{i}Pr_2NEt$, 100 °C, overnight; (c) i) NaOH, EtOH, reflux overnight; ii) 10% HCl (aq.); (d) i) $SOCl_2$, DCM, reflux; ii) $AlCl_3$, dry DCM, 0 °C – r.t., overnight; (e) i) TIPSCCLi, dry THF, 0 °C – r.t.; ii) $SnCl_2$, 6 h.

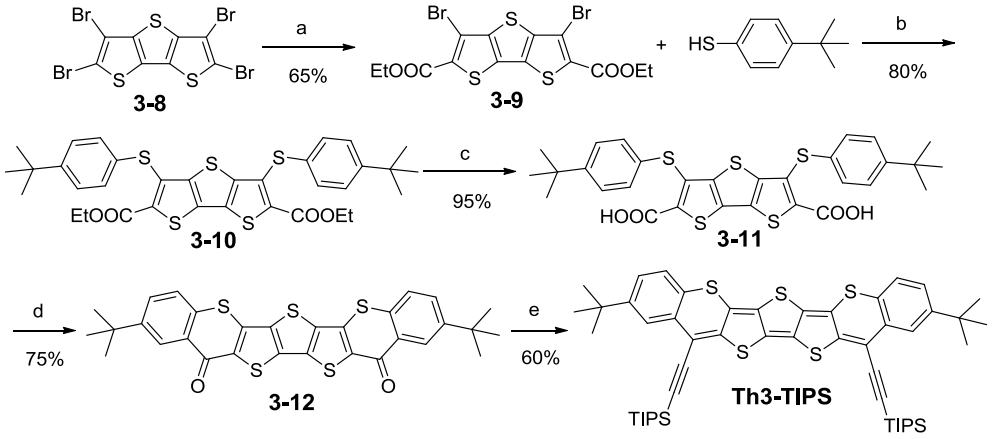

Scheme 3.3 Synthetic route to **Th3-TIPS**. *Reagents and conditions*: (a) i) *n*-BuLi, dry THF, -78 °C; ii) NCCOOEt, -78 °C – r.t., overnight; iii) H_2O, 0 °C; (b) $Pd_2(dba)_3$, dppf, DMF, $^{i}Pr_2NEt$, 100 °C, overnight; (c) i) NaOH, EtOH, reflux overnight; ii) 10% HCl (aq.); (d) i) $SOCl_2$, DCM, reflux; ii) $AlCl_3$, dry DCM, 0 °C – r.t., overnight; (e) i) TIPSCCLi, dry THF, 0 °C – r.t.; ii) $SnCl_2$, 6 h.

The synthetic route to **BDTh-TIPS** shown in **Scheme 3.4** is slightly different from the routes of **Th1-TIPS**, **Th2-TIPS** and **Th3-TIPS**. Instead of dibromo-diester compounds **3-1**, **2-17** and **3-9**, the ditriflate-diester compound **3-13**, which was prepared according to a reported procedure[11], was directly used to undergo nucleophilic substitution reaction with

4-*tert*-butylbenzenethiol to give compound **3-14** under base condition as the triflate is a good leaving group, and a good reaction yield (>90%) was obtained in this step. Subsequent reactions following a similar protocol to that shown in **Scheme 3.1**, **Scheme 3.2** and **Scheme 3.3** gave the target compound **BDTh-TIPS** in an acceptable yield.

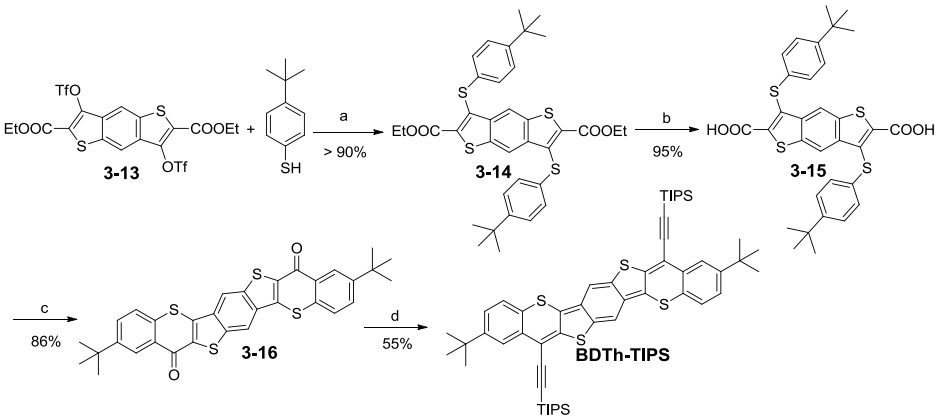

Scheme 3.4 Synthetic route to **BDTh-TIPS**. *Reagents and conditions*: (a) K_2CO_3, DMF, r. t., 12 h; (b) i) NaOH, EtOH, reflux overnight; ii) 10% HCl (aq.); (c) i) $SOCl_2$, DMF, dry dichloromethane, reflux; ii) $AlCl_3$, dry dichloromethane, 0 ^oC - rt., overnight; (d) i) TIPSCCLi, THF, 0 ^oC – r.t.; ii) $SnCl_2$, 6 h.

3.2.2 Photophysical, electrochemical and spectroelectrochemical studies

The UV-vis absorption spectra of all compounds are shown in **Figure 3.4** and the data are collected in **Table 3.1**. The absorption spectra of the **Th1-TIPS** – **Th3-TIPS** compounds show a unique main band in the visible region which contrasts with the spectra of their parent **S1-TIPS** – **S3-TIPS** compounds (**Figure 2.5** in Chapter 2) which have two main bands in this region, in particular, their long wavelength absorption has a distinctive broad structure and blue-shifts with the increase of the molecular size, two features attributed to the emergence of the anti-aromatic property. In contrast, in these

series of compounds the main absorption continuously red-shifts with the increment of the number of thiophenes (from ≈ 550 nm in **Th1-TIPS** to ≈ 680 nm in **Th3-TIPS** and ≈ 700 nm in **BDTh-TIPS**) highlighting that the replacement of the indene units by benzo-thia units seems to remove the anti-aromatic feature giving way to the appearance of the pro-aromatic thienoquinoidal structure. From **Th2-TIPS (Th3-TIPS)** to **BDTh-TIPS**, the red-shift is small and the absorption band gets concomitantly broadened two features which suggest the transformation of the quinoidal-thienoacene structure into a pseudo-aromatic shape. Another noticeable observation is that the absorption spectra of **Th1-TIPS**, **Th2-TIPS** and **Th3-TIPS** all display a shoulder peak at the shorter wavelength of the maximum absorption band, which is normal for closed-shell polycyclic hydrocabons, while that of **BDTh-TIPS** displays a shoulder peak at the longer wavelength, which indicates that the electronic ground state of **BDTh-TIPS** is potential open-shell configuration with singlet biradical character.

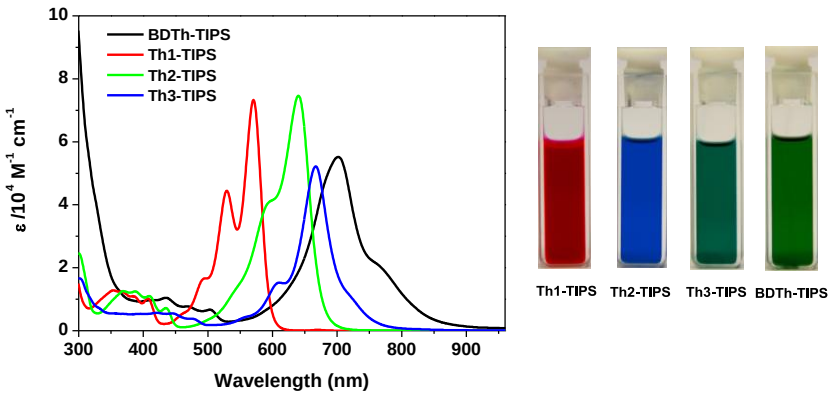

Figure 3.4 UV-vis-NIR absorption spectra of **Th1-TIPS**, **Th2-TIPS**, **Th3-TIPS** and **BDTh-TIPS** recorded in DCM. Right are the photos of the solutions of each compound.

Table 3.1 Summary of photophysical and electrochemical data[a]

Comp	λ_{max}(abs) (nm)	ε (10^4 M^{-1} cm^{-1})	$E_{1/2}^{ox}$ (V)	$E_{1/2}^{red}$ (V)	HOMO (eV)	LUMO (eV)	E_g^{EC} (eV)	E_g^{opt} (eV)
Th1-TIPS	570	4.86	0.05	-1.83	-4.77	-3.06	1.71	2.05
			0.55	-2.11				
Th2-TIPS	640	4.87	-0.13	-1.71	-4.56	-3.17	1.39	1.90
			0.32	-1.90				
Th3-TIPS	667	4.72	-0.25	-1.59	-4.42	-3.35	1.07	1.65
			0.14	-1.80				
BDTh-TIPS	702	4.74	-0.26	-0.83	-4.39	-3.40	0.99	1.46
			0.07	-1.73				

[a] $E_{1/2}^{ox}$ and $E_{1/2}^{red}$ are half-wave potentials of the oxidative and reductive waves, respectively, with potentials vs Fc/Fc^+ couple. HOMO = − (4.8 + E_{ox}^{onset}) and LUMO = − (4.8 + E_{red}^{onset}), where E_{ox}^{onset} and E_{red}^{onset} are the onset potentials of the first oxidative and reductive waves, respectively. E_g^{EC}: electrochemical band gap. E_g^{opt}: optical band gap estimated from the absorption onset.

The electrochemical properties of all compounds were investigated by cyclic voltammetry (CV) and differential plus voltammetry (DPV) in dry dichloromethane solution (**Figure 3.5**). All compound display amphoteric redox behavior with four-stage (quasi-) reversible redox waves. **Th1-TIPS** exhibited two reversible oxidation waves at $E_{1/2}^{ox}$ = 0.05 V, 0.55 V and two quasi-reversible reduction waves at $E_{1/2}^{red}$ = -1.83 V, -2.11 V. **Th2-TIPS** and **Th3-TIPS** also displayed two oxidation waves at $E_{1/2}^{ox}$ = -0.13 V, 0.32 V and $E_{1/2}^{ox}$ = -0.25 V, 0.14 V as well as two reduction waves at $E_{1/2}^{red}$ = -1.71 V, -1.90 V and $E_{1/2}^{red}$ = -1.59 V, -1.80 V, respectively. Similarly, **BDTh-TIPS** showed two oxidation waves at $E_{1/2}^{ox}$ = -0.26 V, 0.07 V and two reduction waves at $E_{1/2}^{red}$ = -0.83 V, -1.73 V. The HOMO and LOMO energy levels were estimated from the onset potentials of the first oxidation and reduction wave by the following correlation: HOMO = - (E_{ox}^{onset} + 4.8) eV and LUMO = - (E_{red}^{onset} + 4.8) eV, where the potentials are calibrated to $E(Fc^+/Fc)$ (**Table**

3.1). As can be seen from **Table 3.1**, the electrochemical energy band gaps (E_g^{EC}) of target molecules also decrease with increase of conjugation length from **Th1-TIPS** to **BDTh-TIPS**, which is consistent with those obtained from the optical offset. The small energy band gaps of these series of compounds indicate that they could be potentially used as semiconducting materials in ambipolar organic field effect transistors (OFETs) with a small hole/electron injection barrier.

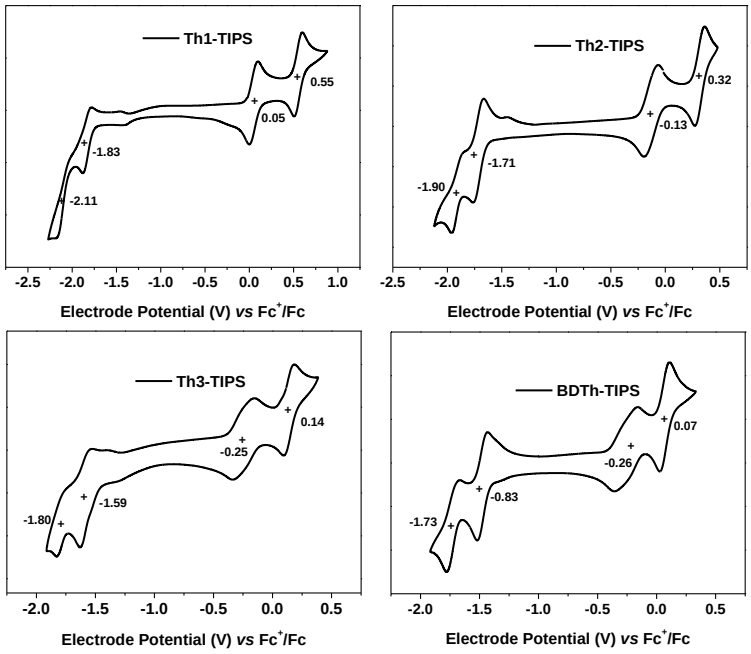

Figure 3.5 Cyclic voltammograms of **Th1-TIPS**, **Th2-TIPS, Th3-TIPS** and **BDTh-TIPS** in dry CH_2Cl_2 containing 0.1 M Bu_4NPF_6 as the supporting electrolyte, AgCl/Ag as the reference electrode, Au as the working electrode, Pt wire as the counter electrode, and a scan rate of 50 mV s^{-1}. The potential was externally calibrated against the ferrocene/ferrocenium redox couple.

Figure 3.6 shows the electronic absorption spectra of the four compounds in their different redox states according with their electrochemical properties on the cyclic voltammetries. **BDTh-TIPS** shows amphoteric electrochemical redox behavior (**Figure 3.5**) what allows us to record the spectra of the

positive and negatively charged species. Upon electrochemical reduction, the disappearance of the neutral band at 700 nm gives rise to the growth of two weak features at 927 and 379 nm, a two-band pattern characteristic of open shell molecules with one semi-occupied orbital or the anion radical. The aromatization of the partial quinoidal thiophenes and benzene of the neutral biradical drives the formation of the anion species. In comparison with their anti-aromatic bisindenothienoacene (chapter 2) analogues, the largest similitude of this **BDTh-TIPS** radical anion is with the radical cations of **Sn-TIPS** (n = 1-3).

One electron oxidation of **BDTh-TIPS** gives rise to the appearance, at the initial stage of the oxidation, of two weak bands at 1327 and 1614 nm which quickly convert into a spectrum with stronger bands at 625, 1377 and 1738 nm. During this first oxidation, the two described spectra coexist. Contrarily to the case of the anion radical, now, the 625/1377/1738 nm spectrum of the radical cation of **BDTh-TIPS** is surprisingly similar to that described for the radical anions of the **Sn-TIPS** (n = 1-3) anti-aromatic bisindenothienoacenes. We have also recorded the UV-Vis-NIR absorption spectra of the radical cations of **Th1-TIPS**, **Th2-TIPS** and **Th3-TIPS** in **Figure 3.6** which show quite similar patterns to that of **BDTh-TIPS**. The adjustment of the low energy bands to the reciprocal of the chain length provides a good linear regression with a similar tendency to that of the neutral bands. We can argue that while the quinoidal path provides the condition for electron conjugation in the neutrals, in the

radical cations oxidation on one of the non-thiophenic sulfur allows conjugation or charge delocalization with the other at the origin of the similar neutral/radical cation chain length dependence.

One electron oxidation of the radical cation produces the clearance of the NIR bands and the growth of intense absorptions in the visible 500-600 nm region. We assign the characteristic bands of the dication to the bands at 495 nm in the dication of **Th2-TIPS**, at 602 nm in the dication of **Th3-TIPS** and at 655 nm in the spectrum of the dicationic species of **BDTh-TIPS**. The correlation of these dicationic bands to a linear regression with 1/n provides a much greater slope than in the radical cations likely revealing the strongest pinning of the electron wavefunction. We have also represented the variation λ_{max} (eV) - 1/n for neutral thienoacenes and obtained a very similar behavior than that found for our dications in consonance with the progressive aromatization of the initial quinoidal structure of **Thn-TIPS** & **BTh** after two-electron extraction. The aromatization of the structure of the dications can explain the more localized character of the wavefunction in these double oxidized species.

The great similitude between the UV-Vis-NIR absorption spectra of the radical cation and anion, and viceversa, of the anti-aromatic bisindeno-[*n*]thienoacenes and of our pro-aromatic dithiaquinoidal–[*n*]thienoacenes is reminiscent of the similarity between the clear two reduction waves of the former and of the two oxidation waves of the

latter.

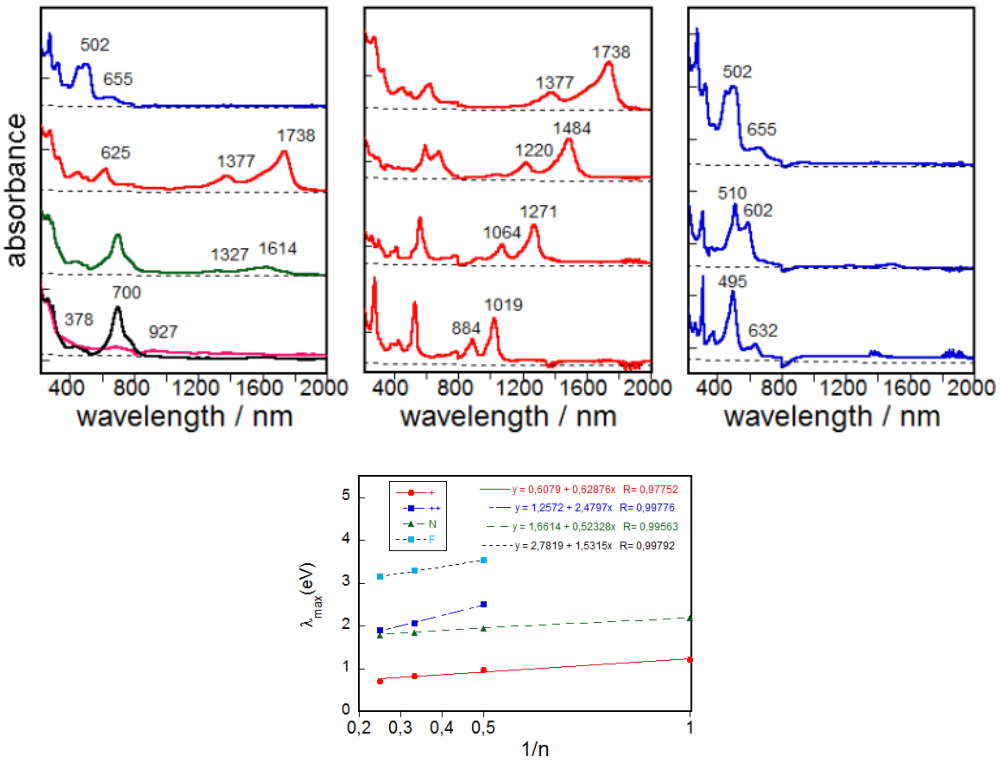

Figure 3.6 Top left: UV-Vis-NIR spectra obtained by electrochemical redox treatment of the neutral **BDTh-TIPS** (black line), radical anion (purple line), radical cation-1 (green line), radical cation (red line) and dication (blue line). Top middle: spectra of the radical cations of **Th1-TIPS**, **Th2-TIPS**, **Th3-TIPS** and **BDTh-TIPS** (from the bottom to the top). Top right: spectra of the dications of **Th2-TIPS**, **Th3-TIPS** and **BDTh-TIPS** (from the bottom to the top). Bottom: representation of the absorption maxima as a function of the reciprocal of the chain length.

3.2.3 *Raman spectroscopic measurements*

Figure 3.7 shows the Raman spectra of the four compounds. There are two main characteristics in the frequency and intensity behavior: 1) there is a main band that dominates the spectra of **Th1-TIPS** – **Th3-TIPS** and that progressively downshifts from 1434 cm^{-1} in **Th1-TIPS** to 1358 cm^{-1} in **Th3-TIPS** whose frequency positions is typical of quinoidal tetracyano oligothiophenes. The overall shift is of 76 cm^{-1} which compares with the 61

cm^{-1} in the **S1-TIPS** – **S3-TIPS** compounds (**Figure 2.15** in Chapter 2) in agreement with a more efficient electron delocalized system free of any anti-aromatic electron pinning effects. 2) On **Th2-TIPS (Th3-TIPS)** to **BDTh-TIPS**, the main Raman band downshifts only by ≈ 4 cm^{-1} and develops a low frequency component at 1347 cm^{-1} suggesting that the downshift of this frequency band with the number of ring collapses on **BDTh-TIPS** or is close to collapse. Furthermore, a new band at 1423 cm^{-1} appears which is between the frequencies of the main bands of **Th1-TIPS** and **Th2-TIPS** allowing it to be assigned as a quinoidal feature in **BDTh-TIPS**. This spectral behavior can be accounted for a saturation of the quinoidization effect from **Thn-TIPS** (n = 1-3) to **BDTh-TIPS** likely resulting from a pseudo-aromatization in the central benzene of the conjugated backbone accompanied by a portion of quinoidal contribution on the thiophenes rings. A similar behavior has been reported in a quinoidal tetracyano-quaterthiophene and ascribed to the formation of a biradicaloid singlet ground electronic state with a pseudo-aromatic (pseudo-quinoidal) central (peripheral) structure on its rings.

Temperature-Variable Raman experiments on **BDTh-TIPS** in **Figure 3.7** are pertinent to scan the evolution of the biradical ground electronic state (singlet) into the lowest energy lying excited state (triplet). On heating up to 140 ℃, the most noticeable finding is the coalescence of the 1423 cm^{-1} thieno-quinoidal band and the simultaneous emergence of two new medium bands at 1466/1451 cm^{-1}. Characteristic Raman bands around 1460 cm^{-1} have

been reported for aromatic thienoacene cores meaning that the clearance of the quinoidal band (1423 cm^{-1}) is at the expenses of the rise of aromatic ones (1466/1451 cm^{-1}). In addition the pre-existing most intense Raman scatterings around 1350 cm^{-1} enlarge their separation from low temperature (7 cm^{-1}) to high (12 cm^{-1}) temperature revealing the transformation between two species, one at low temperature with a less defined aromatic structure (pseudo-aromatic or singlet with incipient biradical structure) and another at high temperatures with more distinguished aromatic feature typical of biradical triplets.

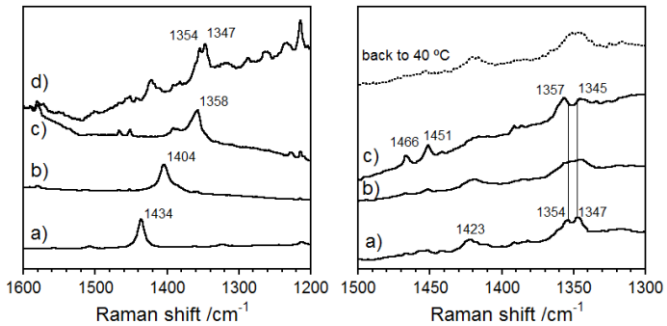

Figure 3.7 Left: 785 nm Raman spectrain solid state of: a) **Th1-TIPS**, b) **Th2-TIPS**, c) **Th3-TIPS** and d) **BDTh-TIPS**. Right: Raman spectra of **BDTh-TIPS** in solid state at a) -140 ℃, b) 40 ℃, c) +140 ℃.

3.2.4 *Ground-state geometry and electronic structures*

Single crystals suitable for X-ray crystallographic analysis were obtained for **Th1-TIPS**, **Th2-TIPS** and **Th3-TIPS** by slow diffusion of acetonitrile or methanol into their solution. The crystal growth of **BDTh-TIPS** is still in progress. The Oak Ridge Thermal Ellipsoid Plot (ORTEP) drawings and 3D packing structures are shown in **Figure 3.8**. The π-frameworks (dithiaquinoidal–[*n*]thienoacenes) of all the molecules are almost planar. All

molecules crystallize in a triclinic lattice system, with space group P -1. Whereas **BDTh-TIPS** crystallize in a monoclinic lattice system, with space group P2(1)/n. For **Th1-TIPS**, two molecules form an anti-parallel packed dimer *via* π-π interactions with a distance about 3.57 Å within the dimer (side view, a). The average distance between adjacent dimers was more than 4.2 Å hence no close π-stacking was observed between each dimer (top view, a). For **Th2-TIPS**, two molecules also form an anti-parallel packed dimer *via* π-π interaction, which further arranges into a columnar packing pattern (top view, b) with lamellar structure in each column, and the average π-stacking distance between two molecules is 3.51 Å (side view, b). For **Th3-TIPS,** similar to **Th1-TIPS** and **Th2-TIPS**, two of the **Th3-TIPS** molecules also form a dimer *via* π-π interaction (distance: 3.37 Å) in packing structure. Furthermore, **Th3-TIPS** packs into columnar stacks (top view, c) as well with lamellar structure in each column, where each pair of two adjacent packing dimers intersects with each other in column (side view, c). **BDTh-TIPS** shows a π-stacked columnar structure (top view, d) with a closeπ-π distance about 3.35 Å (side view, d). The observed close packing in **Th2-TIPS**, **Th3-TIPS** and **BDTh-TIPS** indicates that they could serve as potential semiconductors in OFETs because such a closed packing structure can facilitate the charge transport process and hence improve the charge carrier mobility.

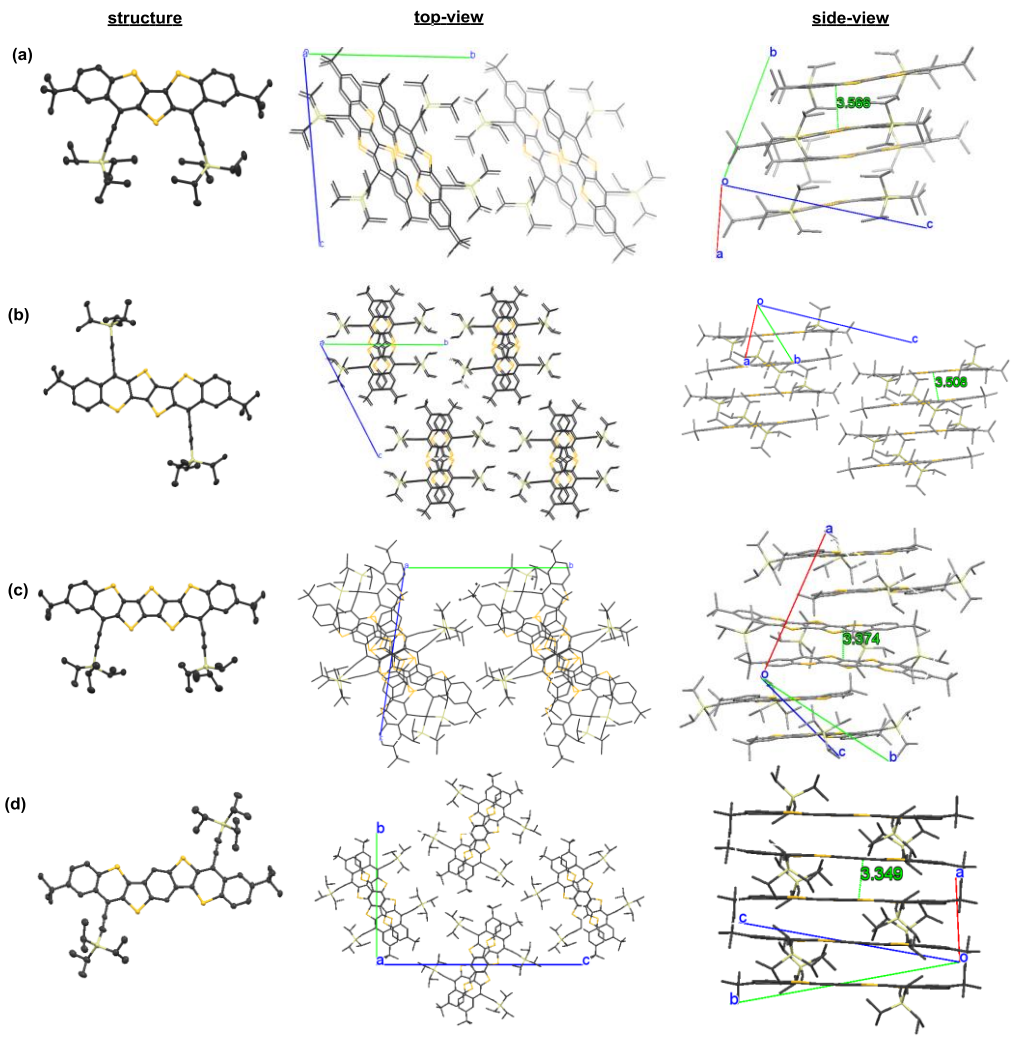

Figure 3.8 X-ray crystallographic structures and packing structures of (a) **Th1-TIPS**, (b) **Th2-TIPS**, (c) **Th3-TIPS** and (d) **BDTh-TIPS**. Hydrogen atoms are omitted for clearance.

Bond length analysis was performed to better analyze the ground-state geometry (**Figure 3.9**). The asymmetric unit contains two halves molecule for the compound **Th2-TIPS**, **Th3-TIPS** and **BDTh-TIPS** hence two groups of bond length analysis data were collected for them. In all cases, large bond length alternation was observed for the central quinoidal-thieno core (quinoidal unit), indicating a typical quinoidal structure. The outmost two benzene rings however showed less bond length alternation, indicating their large aromatic character.

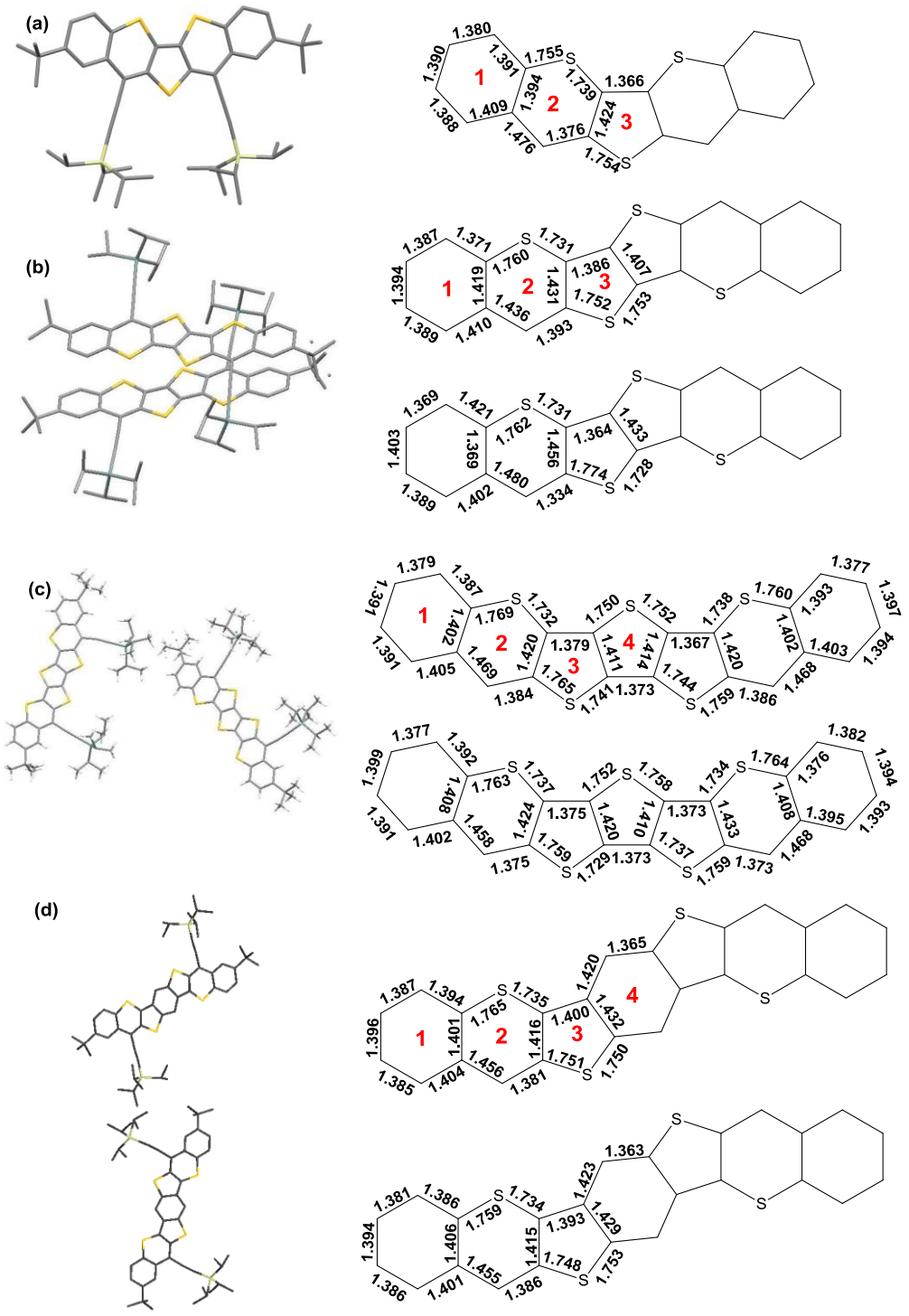

Figure 3.9 Selected bond lengths for **Th1-TIPS**, **Th2-TIPS**, **Th3-TIPS** and **BDTh-TIPS** from their crystallographic structures.

DFT calculations (both UB3LYP/6-31G* and UCAM-B3LYP/6-31G*) were conducted to understand the ground-state electronic structures. The result showed that the shortest molecule **Th1-TIPS** indeed favors a closed-shell

ground state. However, for **Th2-TIPS**, **Th3-TIPS** and **BDTh-TIPS**, the energy of their singlet biradical state is lower than the triplet biradical and closed-shell state, thus suggesting a singlet biradical ground state. The calculated SOMO-α and SOMO-β profiles showed a disjoint character, with the spins evenly distributed along the whole π-conjugated framework (**Figure 3.10**). The singlet diradical character y_0 values were calculated as 0.024, 0.182 and 0.382 for **Th2-TIPS**, **Th3-TIPS** and **BDTh-TIPS**, respectively, while ignorable for **Th1-TIPS**. Therefore, the singlet diradical character increases with the extension of chain length. Though the chain length is almost the same in **Th3-TIPS** and **BDTh-TIPS,** the later one shows the significantly larger diradical character, which mostly ascribes to the different quinoidal unit in these two molecules. That is, instead of thiophene ring (ring 4 in **Figure 3.9**) in **Th3-TIPS**, benzene ring (ring 4 in **Figure 3.9**) in **BDTh-TIPS** would lead to more aromaticity/resonance energy hence promotes the diradical character in **BDTh-TIPS**. Another noticeable observation is that **Th2-TIPS** and **Th3-TIPS** have remarkable larger diradical character than their parent **S2-TIPS** and **S2-TIPS** compounds which have negligible diradical character. Considering their structural similarity, such difference must be associated with their differential fusion mode. This revealed that removing the two indene units in **Sn-TIPS** and replacing them by two benzo-thia units in **Thn-TIPS** could somehow promote the biradical character of **Thn-TIPS** and consequently affect their physical and chemical properties. These results also

demonstrated that the properties of quinoidal compounds are both largely dependent on the length of the central quinoidal units and the two-side fusion motifs in their structures.

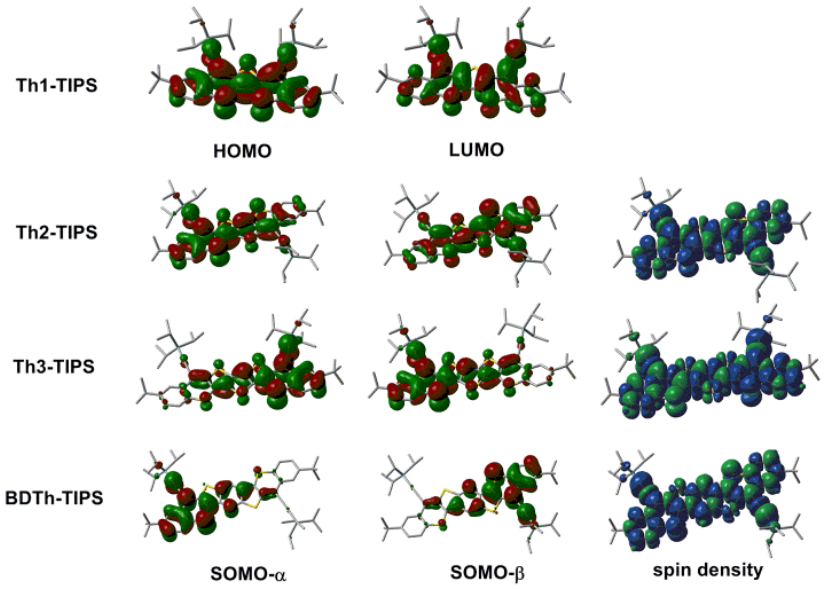

Figure 3.10 Calculated (B3LYP/6-31G**) frontier molecular orbital profiles of **Th1-TIPS** and calculated (UCAM-B3LYP/6-31G*) singly occupied molecule orbital profiles and spin density distribution of the singlet biradical of **Th2-TIPS**, **Th3-TIPS** and **BDTh-TIPS**.

Nucleus independent chemical shift (NICS) calculations were conducted to understand the trend of aromaticity of each ring (**Figure 3.9** and **Table 3.2**). From **Th1-TIPS** to **Th2-TIPS**, to **Th3-TIPS** and to **BDTh-TIPS** the NICS(1)zz values for the central quinoidal ring (ring 3 and ring 4) become more negative, indicating an increase of aromaticity with the extension of the chain length, which is in accordance with the increased biradical character. At the same time, in contrast to their parent **Sn-TIPS** compounds, the NICS(1)zz values for the central quinoidal ring (ring 3 and ring 4) of **Thn-TIPS** and **BDTh-TIPS** are more negative, indicating the larger aromaticity in **Thn-TIPS** and **BDTh-TIPS** while **Sn-TIPS** are typical anti-aromatic. The benzo-thia unit

(ring 2) showed large positive NICS(1)zz values, indicating a typical anti-aromatic character. Such anti-aromatic benzo-thia unit is further annulated and stabilized by two aromatic benzene rings (ring 1) possessing large negative NICS(1)zz values. As a consequence, the anti-aromatic character of the sulfur six member ring is been "diluted" by the outmost aromatic benzene rings (ring 1) and central modestly aromatic quinoidal unit (ring 3 and ring 4) which leads to a unique pro-aromatic system.

Table 3.2 Calculated (UCAM-B3LYP/6-31G*) NICS(1)zz values for the rings 1-4 of **Thn-TIPS** and **BDTh-TIPS**. The rings are labeled in **Figure 5**.

Comp	**1**	**2**	**3**	**4**
Th1-TIPS	-21.865	8.521	-2.849	NA
Th2-TIPS	-21.429	9.208	-4.004	NA
Th3-TIPS	-21.209	9.229	-6.715	-7.390
BDTh-TIPS	-21.2732	8.0904	-7.9735	-17.8326

3.3 Conclusion

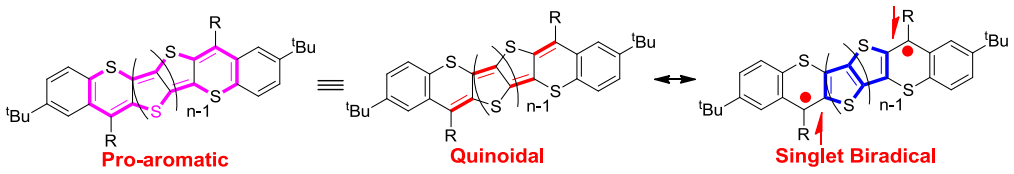

Figure 3.11 Resonance structures of dithiaquinoidal–[*n*]thienoacenes (*n* = 1-3).

In summary, a series of dithiaquinoidal thienoacenes were successfully synthesized. Their ground-state geometry and electronic structures were systematically studied by various experimental techniques (X-ray crystallographic analysis, NMR and Raman spectroscopy) and DFT calculations. Our studies revealed that the transformation of the electronic structure from anti-aromatic in bisindeno-[*n*]thienoacenes to pro-aromatic in

dithiaquinoidal–[*n*]thienoacenes could be achieved by simply replacing the indene units by benzo-thia units. This conversion seems to promote the aromaticity and the biradical character of **Thn-TIPS** and **BDTh-TIPS** and consequently affect their physical and chemical properties. Additionally, with the extension of chain length the molecules showed gradually increased singlet biradical character and increased aromaticity. In particular, the molecule **BDTh-TIPS** showed a singlet biradical ground state with a moderate biradical character (y_0 = 0.382). Their optical and electronic properties were also carefully investigated by OPA and cyclic voltammetry and revealed their chain length dependent behavior. The transformation from pro-aromatic to pseudo-aromatic/aromatic systems was conducted by electrochemical oxidation and reduction followed by UV-Vis–NIR spectroscopic measurements. Our work provided the first study on the fusion mode effect on the aromaticity, biradical character and physical properties of quinoidal compounds. Hence, this work revealed the close relation between the aromaticity, singlet biradical character and distinctive physical properties, which will make supplementary contribution to understand the ground-state geometry and basic properties of quinoidal compounds.

3.4 Experiments

3.4.1 General experimental methods

Refer to the section of *2.4.1 General experimental methods* in chapter 2.

3.4.2 Detailed synthetic procedures and characterization data

Compound 3-1

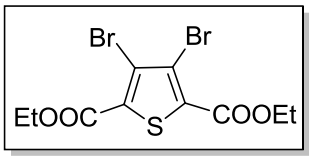

A 250 ml round-bottomed flask was charged with tetrabromothiophene (2 g, 5 mmol) and freshly-distilled THF (60 mL) under argon atmosphere. Upon cooling to -78 ^{o}C, *n*-butyl lithium (5 mL, 2.0 M in hexanes, 10 mmol) was added drop wise to the solution in the course of 30 min under an inert atmosphere. The reaction mixture was maintained at -78 ^{o}C with stirring for a further 150 min. ethyl cyanoformate (1.1 mL, 10 mmol) was added in one portion and the mixture was warmed slowly to ambient temperature overnight. The reaction was quenched by water at 0 ^{o}C. All of the organic solvents were removed and the organic precipitate was collected by filtration. The crude product was washed with hexane and methanol to give pure compound **3-1** as a white solid (1.16 g, 60% yield). ^{1}H NMR (500 MHz, $CDCl_3$, ppm): δ = 4.41 (q, *J* = 7.1 Hz, 2H), 1.40 (t, *J* = 7.2 Hz, 3H); ^{13}C NMR (125 MHz, $CDCl_3$, ppm): δ = 159.52, 132.15, 121.72, 62.35, 14.12. HR MS (EI): calcd for $C_{10}H_{10}Br_2O_4S$ (M^+), 383.86665; found, 383.86653(error: -0.32 ppm).

Compound 3-2

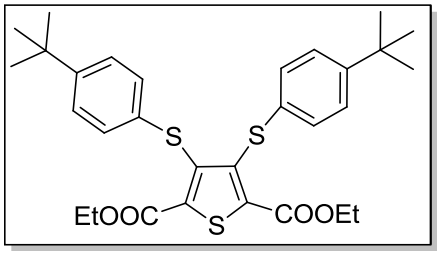

To a solution of $Pd_2(dba)_3$ (46 mg, 0.050 mmol) and dppf (56 mg, 0.100 mmol) in DMF (15 ml) were added compound **3-1** (386 mg, 1.0 mmol),

4-tert-butylbenzenethiol (665 mg, 4.0 mmol), and $^{i}Pr_2NEt$ (0.9 mL, 5.2 mmol) at room temperature. The solution was heated to 100 ^{o}C and stirred overnight. Upon cooling to room temperature, the reaction was then quenched by addition of water and extracted with ethyl acetate. The organic layer was washed with 10% hydrochloric acid solution and dried over anhydrous Na_2SO_4. The solvent was removed under vacuum and the residue was purified by column chromatography (silica, hexane: DCM =4:1) to give compound **3-2** as yellowish oil (500 mg, 90% yield). ^{1}H NMR (500 MHz, $CDCl_3$, ppm): δ = 7.19 (d, *J* = 8.4 Hz, 2H), 7.05 (d, *J* = 8.5 Hz, 2H), 4.26 (q, *J* = 7.1, 2H), 1.25 (m, 12H); ^{13}C NMR (125 MHz, $CDCl_3$, ppm): δ = 160.30, 149.41, 14176, 137.71, 133.06, 128.62, 125.86, 61.95, 34.38, 31.20, 14.01. HR MS (EI): calcd for $C_{30}H_{36}O_4S_3$ (M^+), 556.17758; found, 556.17889 (error: 2.37 ppm).

Compound 3-3

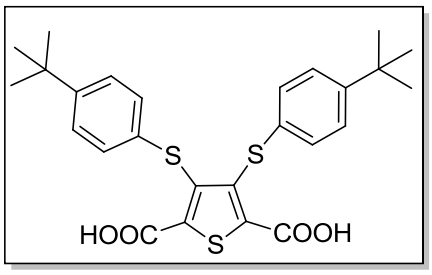

Compound **3-2** (1.1 g, 2 mmol) was dissolved in 60 mL ethanol, followed by the addition of an excess of sodium hydroxide (0.8 g). This mixture was heated to reflux overnight. The solvent was removed by rotary evaporator after the reaction was completed. To the residue then 10% hydrochloric acid solution was added. The precipitate formed was collected by filtration and

washed with water and hexane, then dried under vacuum to afford compound **3-3** as yellow solid (950 mg, 95% yield). ^{1}H NMR (500 MHz, DMSO-d_6, ppm): δ = 13.88 (br, 1H), 7.24 (d, *J* = 8.6 Hz, 2H), 6.93 (d, *J* = 8.5 Hz, 2H), 1.21 (s, 9H); ^{13}C NMR (125 MHz, DMSO-d_6, ppm): δ = 160.92, 148.53, 139.65, 139.12, 133.19, 127.35, 125.85, 34.08, 30.95. HR MS (EI): calcd for $C_{26}H_{28}O_4S_3$ (M^+), 500.11497; found, 500.11534 (error: 0.73 ppm).

Compound 3-4

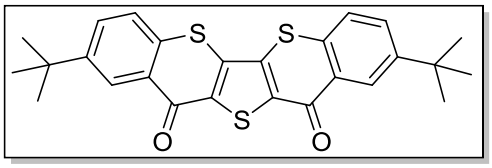

Compound **3-3** (500 mg, 1 mmol) was added in anhydrous DCM (30 mL) in 100 mL two-neck round bottom flask, followed by the addition of excess of thionyl chloride (1 mL). To the mixture anhydrous DMF (1-2 drops) was added at room temperature. The reaction mixture was heated at reflux overnight. After cooling down the solvent was removed by rotary evaporator to afford crude acyl chloride. This intermediate compound was re-dissolved in anhydrous DCM (20 mL) then anhydrous $AlCl_3$ (533 mg, 4.00 mmol) was added carefully at 0 ℃. The resultant mixture was allowed to warm up to room temperature and stirred overnight. The reaction mixture was slowly quenched by 10% HCl solution and extracted with DCM. The organic layer

was washed with 10% hydrochloric acid solution and dried over anhydrous Na_2SO_4. The solvent was removed under vacuum and the residue was purified by column chromatography (silica, DCM). Compound **3-4** was further purified by recrystallization from MeOH/CH_2Cl_2 as a yellow solid (394 mg, 85% yield). ^{1}H NMR (500 MHz, $CDCl_3$, ppm): δ = 8.69 (s, 2H), 7.77 (d, *J* = 8.5 Hz, 2H), 7.67 (d, *J* = 8.5 Hz, 2H), 1.43 (s, 9H); ^{13}C NMR (125 MHz, $CDCl_3$, ppm): δ = 175.42, 151.55, 137.56, 134.58, 133.18, 130.48, 128.99, 126.82, 125.43, 35.16, 31.18. HR MS (EI): calcd for $C_{26}H_{24}O_2S_3$ (M^+), 464.09385; found, 464.09419 (error: 0.75 ppm).

Compound Th1-TIPS

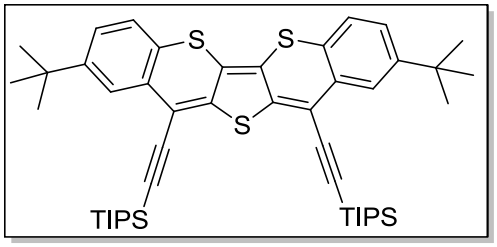

To a solution of triisopropylsilylacetylene (365 mg, 2. mmol) in anhydrous THF (20 mL) at 0 ^{o}C was added drop wise *n*-BuLi (2 M in cyclohexane, 1 mL, 2 mmol). The solution was stirred for 30 min at 0 ^{o}C. Then diketone **3-4** (116 mg, 0.25 mmol) was added in one portion. The mixture was slowly warmed to room temperature and stirred overnight. After that, $SnCl_2$ (190 mg, 1 mmol) was added and the solution became red immediately. Upon completion of the reaction as monitored by TLC, the resulting solution was filtered over anhydrous Na_2SO_4 and the solvent was subsequently removed by rotary

evaporator. The residue was purified by column chromatography (aluminium oxide, hexane: DCM =8:1). Compound **Th1-TIPS** was further purified by recrystallization from MeOH/CH_2Cl_2 as a dark red solid (120 mg, 60% yield). ^{1}H NMR (500 MHz, $CDCl_3$, ppm): δ = 7.87 (s, 1H), 7.18 (d, *J* = 8.2 Hz, 1H), 7.11 (d, *J* = 8.3 Hz, 1H), 1.32 (s, 9H), 1.20 (s, 21H); ^{13}C NMR (125 MHz, $CDCl_3$, ppm): δ =150.08, 144.37, 128.90, 125.40, 124.89, 124.65, 124.38, 121.59, 106.19, 103.96, 103.11, 34.67, 31.17, 18.83, 11.29. HR MS (EI): calcd for $C_{48}H_{66}S_3Si_2$ (M^+), 794.38652; found, 794.38554 (error: 0.75 ppm).

Compound 3-7

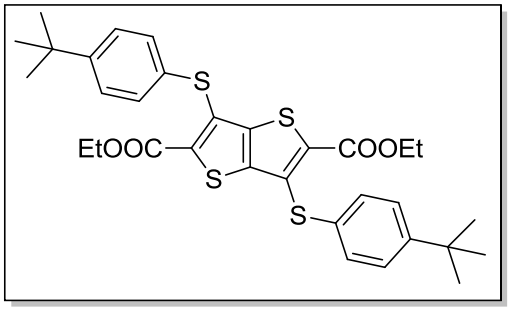

To a solution of $Pd_2(dba)_3$ (46 mg, 0.050 mmol) and dppf (56 mg, 0.100 mmol) in DMF (15 ml) were added compound **2-18** (442 mg, 1.0 mmol), 4-*tert*-butylbenzenethiol (665 mg, 4.0 mmol), and ^{i}Pr$_2$NEt (0.9 mL, 5.2 mmol) at room temperature. The solution was heated to 100 ^{o}C and stirred overnight. Upon cooling to room temperature, the reaction was then quenched by addition of water and extracted with ethyl acetate. The organic layer was washed with 10% hydrochloric acid solution and dried over anhydrous Na_2SO_4. The solvent was removed under vacuum and the residue was purified

by column chromatography (silica, hexane: DCM = 4:1) to give compound **3-5** as a pale yellow solid (515mg, 85% yield). ^{1}H NMR (500 MHz, $CDCl_3$, ppm): δ = 7.54 (d, *J* = 8.4 Hz, 2H), 7.42 (d, *J* = 8.2 Hz, 2H), 4.27 (q, *J* = 7.1, 2H), 1.38 (s, 9H), 1.28 (t, *J* = 7.1 Hz 3H); ^{13}C NMR (125 MHz, $CDCl_3$, ppm): δ = 162.06, 153.90, 140.65, 135.94, 135.07, 127.37, 126.37, 126.30, 61.31, 34.87, 31.26, 14.25. HR MS (EI): calcd for $C_{32}H_{36}O_4S_4$ (M^+), 612.14965; found, 612.14940 (error: -0.41ppm).

Compound 3-6

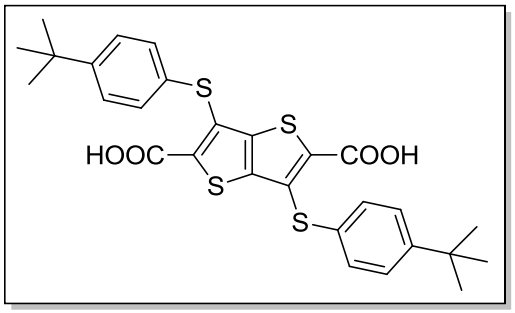

Compound **3-5** (1.2 g, 2 mmol) was dissolved in a mixture solvent (80 mL ethanol/20 mL THF), followed by the addition of an excess of sodium hydroxide (1.2g). This mixture was heated to reflux overnight. The solvent was removed by rotary evaporator after the reaction was completed. To the residue then 10% hydrochloric acid solution was added. The precipitate formed was collected by filtration and washed with water and hexane, then dried under vacuum to afford compound **3-6** as yellow solid (1.1 g, 95% yield). ^{1}H NMR (500 MHz, DMSO-d_6, ppm): δ = 13.42 (br, 1H), 7.52 (d, *J* = 8.2 Hz, 2H), 7.47 (d, *J* = 8.2 Hz, 2H), 1.31 (s, 9H); ^{13}C NMR data was not obtained

due to its poor solubility. HR MS (EI): calcd for $C_{28}H_{28}O_4S_4$ (M^+), 556.08705; found, 556.08629 (error: -1.36 ppm).

Compound 3-7

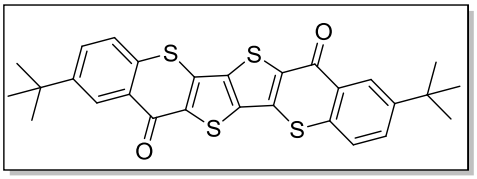

Compound **3-6** (607 mg, 1 mmol) was added in anhydrous DCM (30 mL) in 100 mL two-neck round bottom flask, followed by the addition of excess of thionyl chloride (1 mL). To the mixture anhydrous DMF (1-2 drops) was added at room temperature. The reaction mixture was heated at reflux overnight. After cooling down the solvent was removed by rotary evaporator to afford crude acyl chloride. This intermediate compound was re-dissolved in anhydrous DCM (25 mL) then anhydrous $AlCl_3$ (533 mg, 4.00 mmol) was added carefully at 0 ℃. The resultant mixture was allowed to warm up to room temperature and stirred overnight. The reaction mixture was slowly quenched by 10% HCl solution to give a yellow precipitate. After filtration, the crude precipitate was washed with methanol, hexane and acetone until the filtrate was colorless, giving compound **3-7** as an insoluble yellow solid (457 mg, 80% yield). Both ^1H NMR and ^{13}C NMR data were not obtained due to its poor solubility. HR MS (EI): calcd for $C_{28}H_{24}O_2S_4$ (M^+), 520.06592; found, 520.06520 (error: -1.38 ppm).

Compound Th2-TIPS

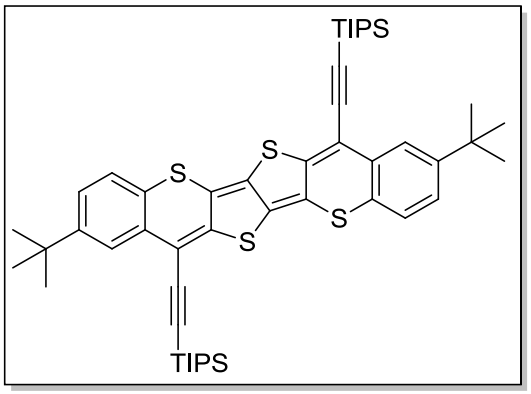

To a solution of triisopropylsilylacetylene (365 mg, 2 mmol) in anhydrous THF (20 mL) at 0 ^{o}C was added dropwise *n*-BuLi (2 M in cyclohexane, 1 mL, 2 mmol). The solution was stirred for 30 min at 0 ^{o}C. Then diketone **3-7** (114 mg, 0.2 mmol) was added in one portion. The mixture was slowly warmed to room temperature and stirred overnight. During this period the insoluble diketone disappeared and the solution became clear. After that, $SnCl_2$ (190 mg, 1 mmol) was added and the solution became deep blue immediately. Upon completion of the reaction as monitored by TLC, the resulting solution was filtered over anhydrous Na_2SO_4 and the solvent was subsequently removed by rotary evaporator. The residue was purified by column chromatography (aluminium oxide, hexane: DCM =8:1). Compound **Th2-TIPS** was further purified by recrystallization from MeOH/CH_2Cl_2 as a dark blue solid (135 mg, 75% yield). ^{1}H NMR (500 MHz, benzene-d_6, ppm): δ = 8.02 (s, 1H), 6.85 (d, *J* = 8.3 Hz, 1H), 6.75 (d, *J* = 8.3 Hz, 1H), 1.29-1.28 (br, 21H), 1.25 (s, 9H); ^{13}C NMR (125 MHz, benzene-d_6, ppm): δ =150.25, 150.10, 134.71, 129.47, 125.51, 125.32, 125.06, 124.71, 117.65, 108.60, 104.44, 104.35, 34.69, 31.26,

19.12, 11.79. HR MS (EI): calcd for $C_{50}H_{66}S_4Si_2$ (M^+), 850.35860; found, 850.35777 (error: -0.97 ppm).

Compound 3-9

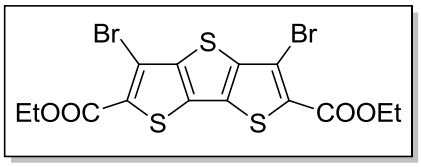

A 250 ml round-bottomed flask was charged with tetrabromo compound **3-8** (511 mg, 1 mmol) and freshly-distilled THF (60 mL) under argon atmosphere. Upon cooling to -78 ^oC, n-butyl lithium (1.0 mL, 2.0 M in hexanes, 2 mmol) was added dropwise to the solution in the course of 30 min under an inert atmosphere. The reaction mixture was maintained at -78 ^oC with stirring for a further 30 min. ethyl cyanoformate (0.3 mL, 2.1mmol) was added in one portion and the mixture was warmed slowly to ambient temperature overnight. The reaction was quenched by water at 0 ^oC. All of the organic solvents were removed and the organic precipitate was collected by filtration. The crude product was washed with hexane and methanol to give pure compound **3-9** as a white solid (324 mg, 65% yield). ^1H NMR (500 MHz, $CDCl_3$, ppm): δ = 4.43 (q, J = 7.1 Hz, 2H), 1.43 (t, J = 7.2 Hz, 3H); ^{13}C NMR (125 MHz, $CDCl_3$, ppm): δ = 160.59, 146.06, 132.46, 129.29, 110.48, 62.01, 14.24. HR MS (EI): calcd for $C_{14}H_{10}Br_2O_4S_3$ (M^+), 495.81080; found, 495.81087 (error: 0.14 ppm).

Compound 3-10

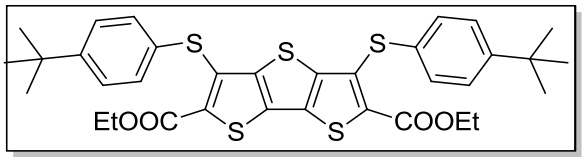

To a solution of $Pd_2(dba)_3$ (46 mg, 0.050 mmol) and dppf (56 mg, 0.100 mmol) in DMF (15 ml) were added compound **3-9** (498 mg, 1.0 mmol), 4-*tert*-butylbenzenethiol (665 mg, 4.0 mmol), and $^{i}Pr_2NEt$ (0.9 mL, 5.2 mmol) at room temperature. The solution was heated to 100 ^{o}C and stirred overnight. Upon cooling to room temperature, the reaction was then quenched by addition of water and extracted with ethyl acetate. The organic layer was washed with 10% hydrochloric acid solution and dried over anhydrous Na_2SO_4. The solvent was removed under vacuum and the residue was purified by column chromatography (silica, hexane: DCM = 4:1) to give compound **3-10** as yellowish solid (535mg, 80% yield). ^{1}H NMR (500 MHz, $CDCl_3$, ppm): δ = 7.29 (s, 2H), 7.26 (s, 2H), 4.39 (q, *J* = 7.1, 2H), 1.38 (t, *J* = 7.1 Hz 12H); ^{13}C NMR (125 MHz, $CDCl_3$, ppm): δ = 161.77, 152.28, 146.25, 134.86, 133.46, 131.95, 127.95, 127.78, 126.14, 61.61, 34.73, 31.28, 14.28. HR MS (EI): calcd for $C_{34}H_{36}O_4S_5$ (M^+), 668.12172; found, 668.12103 (error: -1.03 ppm).

Compound 3-11

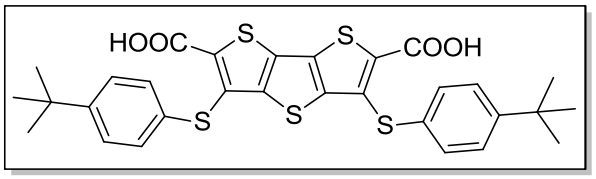

Compound **3-10** (669 mg, 1 mmol) was dissolved in a mixture solvent (80 mL ethanol/20 mL THF), followed by the addition of an excess of sodium hydroxide (1.2g). This mixture was heated to reflux overnight. The solvent was removed by rotary evaporator after the reaction was completed. To the residue then 10% hydrochloric acid solution was added. The precipitate formed was collected by filtration and washed with water and hexane, then dried under vacuum to afford compound **3-11** as yellow solid (581 mg, 95% yield). ^{1}H NMR (500 MHz, DMSO-d_6, ppm): δ = 13.65 (br, 1H), 7.35 (d, J = 8.3 Hz, 2H), 7.24(d, J = 8.3 Hz, 2H), 1.31 (s, 9H); ^{13}C NMR (125 MHz, DMSO-d_6, ppm): δ = 162.41, 151.78, 144.98, 132.73, 132.21, 131.34, 130.08, 127.39, 126.22, 34.43, 30.94. HR MS (APCI): calcd for $C_{30}H_{28}O_4S_5$ [$(M+H)^+$], 613.0664; found, 613.0656 (error: 1.2 ppm).

Compound 3-12

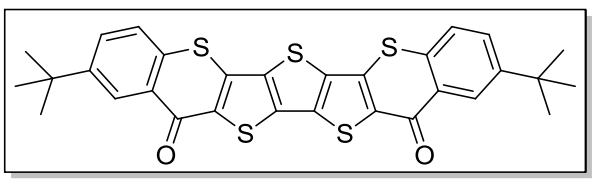

Compound **3-11** (612 mg, 1 mmol) was added in anhydrous DCM (30 mL) in 100 mL two-neck round bottom flask, followed by the addition of excess of

thionyl chloride (1 mL). To the mixture anhydrous DMF (1-2 drops) was added at room temperature. The reaction mixture was heated at reflux overnight. After cooling down the solvent was removed by rotary evaporator to afford crude acyl chloride. This intermediate compound was re-dissolved in anhydrous DCM (25 mL) then anhydrous $AlCl_3$ (533 mg, 4.00 mmol) was added carefully at 0 ℃. The resultant mixture was allowed to warm up to room temperature and stirred overnight. The reaction mixture was slowly quenched by 10% HCl solution to give a yellow precipitate. After filtration, the crude precipitate was washed with methanol, hexane and acetone until the filtrate was colorless, giving compound **3-12** as an insoluble yellow solid (432 mg, 80% yield). Both ^{1}H NMR and ^{13}C NMR data were not obtained due to its poor solubility. HR MS (APCI): calcd for $C_{30}H_{25}O_2S_5$ $[(M+H)^+]$, 577.0453; found, 577.0451 (error: 0.3ppm).

Compound Th3-TIPS

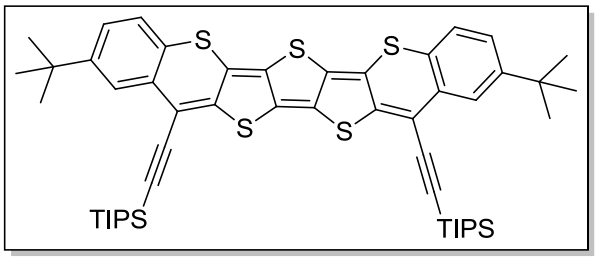

To a solution of triisopropylsilylacetylene (365 mg, 2. mmol) in anhydrous THF (20 mL) at 0 ^{o}C was added dropwise *n*-BuLi (2 M in cyclohexane, 1 mL, 2 mmol). The solution was stirred for 30 min at 0 ^{o}C. Then diketone **3-12** (115 mg, 0.2 mmol) was added in one portion. The mixture was slowly warmed to

room temperature and stirred overnight. During this period the insoluble diketone disappeared and the solution became clear. After that, $SnCl_2$ (190 mg, 1 mmol) was added and the solution became blue-green immediately. Upon completion of the reaction as monitored by TLC, the resulting solution was filtered over anhydrous Na_2SO_4 and the solvent was subsequently removed by rotary evaporator. The residue was purified by column chromatography (aluminium oxide, hexane: DCM =8:1). Compound **Th3-TIPS** was further purified by recrystallization from MeOH/CH_2Cl_2 as a dark blue solid (108 mg, 60% yield). ^{1}H NMR (500 MHz, benzene-d_6, ppm): δ = 8.00 (s, 1H), 6.90-6.70 (m, 2H), 1.26-1.23 (br, 21H), 1.12 (s, 9H); ^{13}C NMR data was not obtained due to its poor solubility. HR MS (APCI): calcd for $C_{52}H_{66}S_5Si_2$ [$(M+H)^+$], 907.3379; found, 907.3379 (error: 0 ppm).

Compound 3-14

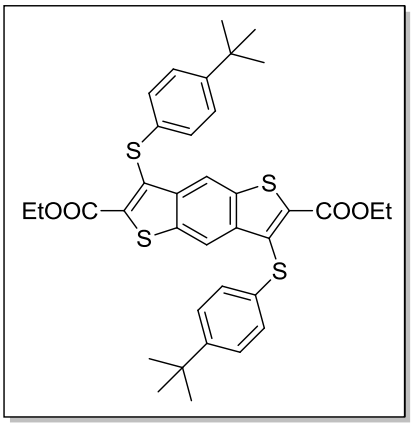

4-*tert*-butylbenzenethiol (1.33 g, 8 mmol) and K_2CO_3 (1.11 g, 8 mmol) were added to 40 mL dry DMF and the mixture was stirred at room temperature for 30 minutes. After that, compound **3-13** (1.26 g, 2 mmol) was added as solid in

one portion to this reaction mixture and stirred overnight. Then the mixture was poured into cold 10% hydrochloric acid solution and extracted with ethyl acetate. The organic layer was washed with 10% hydrochloric acid solution and dried over anhydrous Na_2SO_4. The solvent was removed under vacuum and the residue was purified by column chromatography (silica, hexane: DCM = 2: 1) to give compound **3-14** as pare yellow solid (1.21 g, 91% yield). ^{1}H NMR (500 MHz, $CDCl_3$, ppm): δ = 8.35 (s, 1H), 7.24 (d, *J* = 8.6 Hz, 2H), 7.16 (d, *J* = 8.4 Hz, 2H), 4.39 (q, *J* = 7.2 Hz, 2H), 1.35 (t, *J* = 7.2 Hz, 3H), 1.26 (s, 9H); ^{13}C NMR (125 MHz, $CDCl_3$, ppm): δ = 161.52, 149.64, 140.23, 137.21, 137.06, 132.22, 130.02, 128.22, 126.17, 119.44, 62.01, 34.43, 31.19, 14.13. HR MS (EI): calcd for $C_{36}H_{38}O_4S_4$ (M^+), 662.1653; found, 662.1662 (error: 1.36 ppm).

Compound 3-15

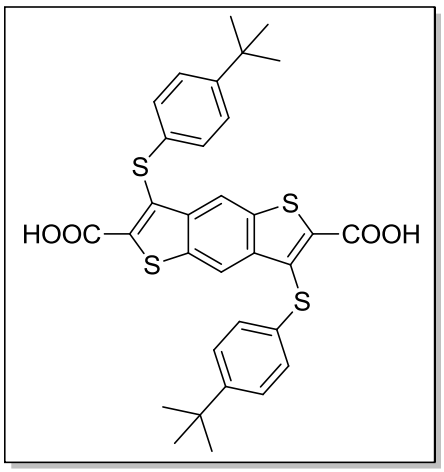

Compound **3-14** (1.33 g, 2 mmol) was dissolved in 60 mL ethanol, followed by the addition of an excess of sodium hydroxide (1.2 g). This mixture was heated to reflux overnight. The solvent was removed under reduced pressure

after the reaction was completed. To the residue then 10% hydrochloric acid solution was added. The precipitate formed was collected by filtration and washed with water and hexane, then dried in vacuum to afford compound **3-15** as yellow solid (1.15 g, 95% yield). ^{1}H NMR (500 MHz, DMSO-d_6, ppm): δ = 13.95 (br, 1H), 8.54 (s, 1H), 7.28 (d, *J* = 8.4 Hz, 2H), 7.13 (d, *J* = 8.6 Hz, 2H), 1.20 (s, 9H); ^{13}C NMR (125 MHz, DMSO-d_6, ppm): δ = 162.23, 149.03, 139.81, 139.72, 136.43, 132.06, 127.78, 127.61, 126.21, 119.28, 34.12, 30.90. HR MS (EI): calcd for $C_{32}H_{30}O_4S_4$ (M^+), 606.1027; found, 606.1005 (error: -3.63 ppm).

Compound 3-16

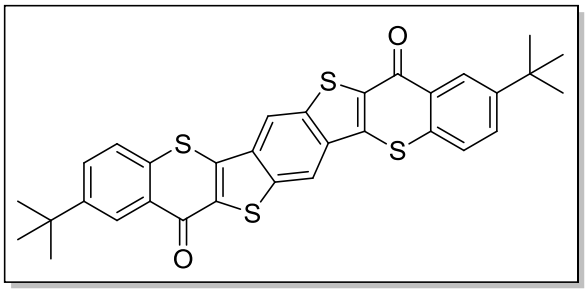

Compound **3-15** (607 mg, 1 mmol) was added in anhydrous DCM (30 mL), followed by the addition of excess of thionyl chloride (1 mL). To this mixture anhydrous DMF (1-2 drops) was added at room temperature. The resultant mixture was heated at reflux overnight. During this period the insoluble diacid **3-15** became soluble in DCM. After cooling down the solvent was removed under reduced pressure to afford crude acid chloride. This intermediate compound was re-dissolved in anhydrous DCM (20 mL) then anhydrous $AlCl_3$ (533 mg, 4.00 mmol) was added carefully at 0 ℃. The resultant mixture was

allowed to warm up to room temperature and stirred overnight, then slowly quenched by 10% HCl solution to form a yellow precipitate. The crude precipitate was rinsed with MeOH, hexane and acetone until the washings were colorless, giving compound **3-16** as an insoluble yellow solid (491 mg, 85% yield). Both ^{1}H NMR and ^{13}C NMR data were not obtained due to its poor solubility. HR MS (APCI): calcd for $C_{32}H_{27}O_2S_4$ $[(M+H)^+]$, 571.0894; found, 571.0895 (error: 0.18 ppm).

Compound BDTh-TIPS

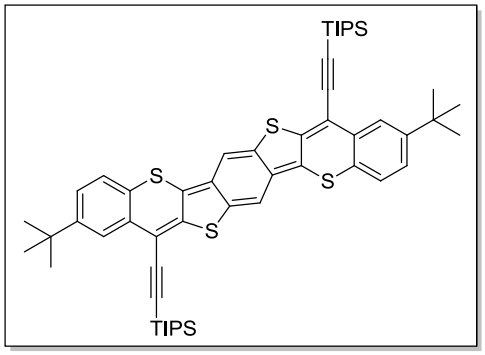

To a solution of triisopropylsilylacetylene (365 mg, 2. mmol) in anhydrous THF (20 mL) at 0 ^{o}C was added dropwise *n*-BuLi (2 M in cyclohexane, 1 mL, 2 mmol). The solution was stirred for 30 min at 0 ^{o}C. Then diketone **3-16** (115 mg, 0.2 mmol) was added as solid in one portion. The mixture was slowly warmed to room temperature and stirred overnight. During this period the insoluble diketone disappeared and the solution became clear. After that, $SnCl_2$ (190 mg, 1 mmol) was added to the resulting mixture and the solution became deep blue immediately. Upon completion of the reaction as monitored by TLC, the resulting blue solution was then filtered and the filtrate was subsequently

evaporated to dryness. The residue was purified by column chromatography (aluminium oxide, hexane: DCM = 8: 1). Compound **BDTh-TIPS** was further purified by recrystallization from MeOH/CH_2Cl_2 as a dark blue solid (100 mg, 55% yield). ^{1}H NMR (500 MHz, toluene-d_8, ppm): δ = 8.03 (s, 1H), 6.95-6.80 (br, 2H), 6.69 (s, 1H), 1.33-1.30 (br, 21H), 1.27 (s, 9H); ^{13}C NMR data was not obtained due to its poor solubility. HR MS (APCI): calcd for $C_{54}H_{69}S_4Si_2$ [$(M+H)^+$], 901.3821; found, 901.3813 (error: -0.89 ppm).

References

[1] See review articles: (a) Z. Sun and J. Wu, *J. Mater. Chem.*, 2012, **22**, 4151. (b) Z. Sun, Q. Ye, C. Chi and J. Wu, *Chem. Soc. Rev.*, 2012, **41**, 7857. (c) A. Shimizu, Y. Hirao, T. Kubo, M. Nakano, E. Botek and B. Champagne, *AIP Conf. Proc.*, 2012, **1504**, 399. (d) Z. Sun, Z. Zeng and J. Wu, *Chem. Asian J.*, 2013, **8**, 2894. (e) M. Abe, *Chem. Rev.*, 2013, **113**, 7011. (f) Z. Sun and J. Wu, *Pure Appl. Chem.*, 2014, **86**, 529. (g) T. Kubo, *Chem. Rec.*, 2014, **15**, 218. (h) Z. Sun, Z. Zeng and J. Wu, *Acc. Chem. Res.*, 2014, **47**, 2582. (i) T. Kubo, *Chem. Lett.*, 2015, **44**, 111.

[2] See review articles: (a) J. Casado, R. P. Ortiz and J. T. López Navarrete, *Chem. Soc. Rev.*, 2012, **41**, 5672. (b) J. Casado and J. T. López Navarrete, *Chem. Records*, 2011, **11**, 45.

[3] (a) J. E. Anthony, *Chem. Rev.*, 2006, **106**, 5028. (b) J. E. Anthony, *Angew.*

Chem. Int. Ed., 2008, **47**, 452. (c) H. Qu and C. Chi, *Curr. Org. Chem.*, 2010, **14**, 2070.

[4] (a) D. T. Chase, B. D. Rose, S. P. McClintock, L. N. Zakharov and M. M. Haley, *Angew. Chem. Int. Ed.* 2011, **50**, 1127. (b) A. Shimizu and Y. Tobe, *Angew. Chem. Int. Ed.*, 2011, **50**, 6906. (c) A. G. Fix, D. T. Chase and M. M. Haley, *Top. Curr. Chem.*, 2012, DOI: 10.1007/128_2012_376. (d) A. Shimizu, R. Kishi, M. Nakano, D. Shiomi, K. Sato, T. Takui, I. Hisaki, M. Miyata and Y. Tobe, *Angew. Chem. Int. Ed.*, 2013, **52**, 6076.

[5] (a) Y. Li, W.-K. Heng, B. S. Lee, N. Aratani, J. L. Zafra, N. Bao, R. Lee, Y. M. Sung, Z. Sun, K.-W. Huang, R. D. Webster, J. T. López Navarrete, D.-H. Kim, A. Osuka, J. Casado, J. Ding and J. Wu, *J. Am. Chem. Soc.*, 2012, **134**, 14913. (b) Z. Sun, S. Lee, K. H. Park, X. Zhu, W. Zhang, B. Zheng, P. Hu, Z. Zeng, S. Das, Y. Li, C. Chi, R. W. Li, K. W. Huang, J. Ding, D. Kim and J. Wu, *J. Am. Chem. Soc.*, 2013, **135**, 18229.

[6] D. T. Tứng, D. T. Tuấn, N. Rasool, A. Villinger, H. Reinke, C. Fischer, and P. Langer, *Adv. Synth. Catal.* 2009, **351**, 1595.

[7] T. Okauchi, K. Kuramoto and M. Kitamura, *Synlett*, 2010, **19**, 2891.

[8] L. S. Fuller, B. Iddon and K. A. Smith, *J. Chem. Soc., Perkin Trans. 1*, 1997, 3465.

[9] T. H. Kwon, V. Armel, A. Nattestad, D. R. MacFarlane, U. Bach, S. J. Lind, K. C. Gordon, W. Tang, D. J. Jones and A. B. Holmes, *J. Org. Chem.*, 2011, **76**, 4088–4093.

[10] K. Yui, H. Ishida, Y. Aso, T. Otsubo, F. Ogura, A. Kawamoto and J. Tanaka, *Bull. Chem. Soc. Jpn.*, 1989, **62**, 1547.

[11] S. Ota, S. Minami, K. Hirano, T. Satoh, Y. Ie, S. Seki, Y. Aso and M. Miura, *RSC Adv.*, 2013, **3**, 12356.

Chapter 4: Pro-aromatic Bisphenaleno-thieno[3,2-*b*]thiophene *versus* Anti-aromatic Bisindeno-thieno[3,2-*b*]thiophene: Different Ground-state Properties and Applications for Field-effect Transistors

4.1 Introduction

Quinoidal π-conjugated molecules recently have attracted increasing interest due to their unique physical properties (low band gap and open-shell diradical character) and potential applications for field-effect transistors (FETs), non-linear optics, and spin-based electronics.[1] Various quinoidal polycyclic aromatic hydrocarbons (PAHs)[2] and their thiophene-based analogues[3] have been synthesized and some of them have been successfully applied in ambipolar or *n*-channel FETs.[4] However, fundamental understanding of how the fusion mode and the aromaticity/anti-aromaticity/pro-aromaticity affect the ground state and consequently the physical properties is of importance. Recently, our group and Haley's group independently reported the synthesis and properties of a series of quinoidal bisindeno-[*n*]thienoacenes (**Sn-TIPS**) (*n* = 1-4), which can be regarded as an *anti-aromatic* system containing an annulene framework with 4*m* π-electrons (**Figure 4.1**).[5] These molecules also displayed small to moderate diradical character in the ground state due to the recovery of the aromaticity of the central thienoacene moiety in the diradical form (**Figure**

4.1). Analogues of this system are the bisphenaleno-thienoacenes in which the two indeno- units are replaced by two phenaleno- moieties, and the resulting quinoidal system is now *pro-aromatic* and an open-shell diradical resonance form can be drawn too (**Figure 4.1**). A comparison between these two systems will provide insights into the correlations between the aromaticity, the ground state, and the physical properties. Therefore, in this work, a pro-aromatic bisphenaleno-thieno[3,2-*b*]thiophene (**BPT-TIPS**) was synthesized and its ground state and physical properties were compared with its anti-aromatic counterpart, the bisinedno-thieno[3,2-*b*]thiophene (**S2-TIPS**) (**Figure 4.1**). Our studies clearly showed their distinctively different ground-state electronic structure and physical properties. Moreover, ordered 3D packing structure was observed in single crystals, qualifying **BPT-TIPS** as a new high performance semiconductor.

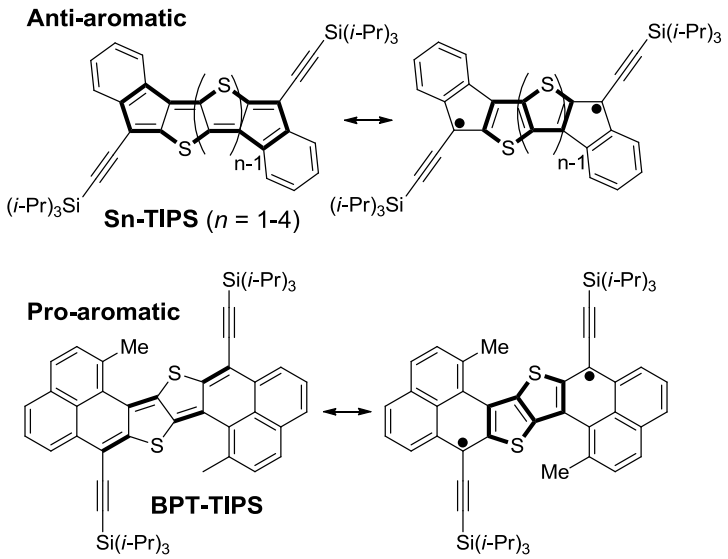

Figure 4.1 Structures of anti-aromatic bisindeno-thienoacenes **Sn-TIPS** (*n* = 1-4) and pro-aromatic bisphenaleno-thieno[3,2-*b*]acenes **BPT-TIPS**.

4.2 Results and discussion

4.2.1 Synthesis

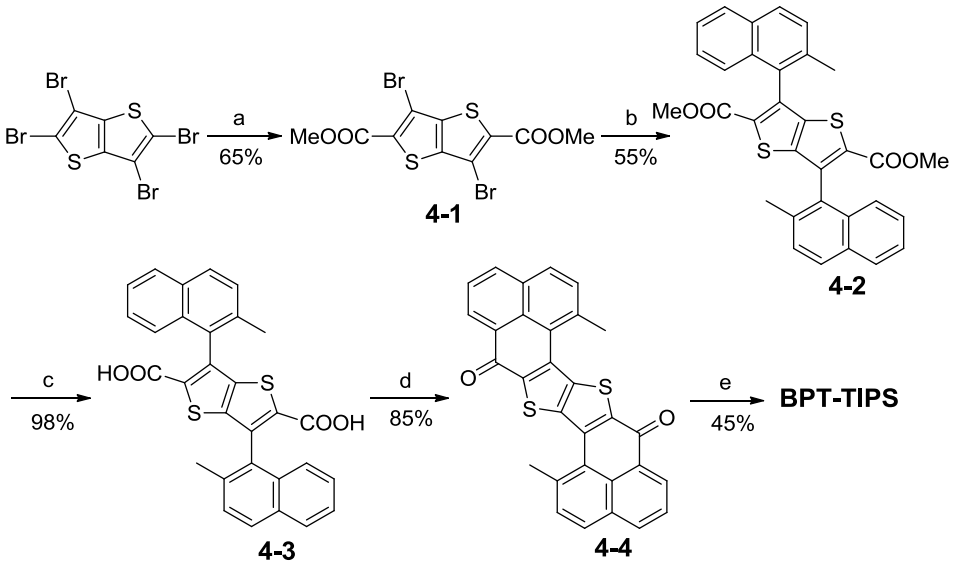

Scheme 4.1 Synthetic route to **BPT-TIPS**: (a) i) *n*-BuLi, THF, -78 ^{o}C, 1 h; ii) NC-COOMe, -78 ^{o}C – r.t., overnight; (b) 2-methylnaphthalen-1-yl-1-boronic acid (4 equiv.), $Pd(PPh_3)_4/K_2CO_3$, toluene/EtOH/water (3:1:1), one drop aliquat 336, reflux, overnight; (c) i) NaOH, MeOH/THF (1:1), reflux overnight; ii) 10% HCl (aq.); (d) i) $SOCl_2$, dry CH_2Cl_2, reflux; ii) $AlCl_3$, dry CH_2Cl_2, 0 ^{o}C - rt., overnight; (e) i) triisopropylsilyl ethynyl lithium, THF, 0 ^{o}C – r.t.; ii) $SnCl_2$, toluene, r.t., 12 h.

The key intermediate for the synthesis of **BPT-TIPS** was the α,α-di-ester substituted thieno[3,2-*b*]thiophene (TT) (**4-1**), which was obtained by regio-selective lithiation of 2,3,5,6-tetrabromo- TT followed by quenching with methyl cyanoformate (**Scheme 4.1**). Suzuki coupling between **4-1** and 2-methylnaphthale-1-yl-boronic acid gave **4-2** in 55% yield. Hydrolysis of **4-2** followed by acidification gave the diacid **4-3** in quantitative yield, which was converted into the corresponding carboxylic acid chloride with thionyl chloride in dry CH_2Cl_2. Subsequent double Friedel–Crafts acylation with $AlCl_3$ afforded the desired diketone **4-4** in 85% yield. Finally, addition of triisopropylsilyl ethynyl lithium to the diketone **4-5** and reduction of the

intermediate diols by $SnCl_2$ gave the targeted compound **BPT-TIPS** in 45% yield.

4.2.2 Photophysical and electrochemical properties

Compound **BPT-TIPS** is a soluble and stable material, displaying a blue colour in CH_2Cl_2, while **S2-TIPS** exhibits a deep green colour (**Figure 4.2a**). **BPT-TIPS** shows a well-resolved electronic absorption spectrum in CH_2Cl_2 with an intense *p*-band at 682 nm (log ε = 5.03; ε: molar extinction coefficient in M^{-1} cm^{-1}), which is similar to many closed-shell PAHs such as acenes[6] and closed-shell quinoidal compounds such as heptazethrene.[2b] This observation also indicates that **BPT-TIPS** likely has a closed-shell electronic structure in the ground state. **S2-TIPS** exhibits a very different absorption spectrum with a broad longest-wavelength absorption band centered at 606 nm which is much weaker than that in **BPT-TIPS**, in accordance with its anti-aromatic character. Femtosecond transient absorption measurement was conducted to explore the excited-state dynamics of **BPT-TIPS** in toluene. The spectrum exhibits ground-state bleach signal around 690 nm and a broad weak excited-state absorption band in 450-600 nm spectra region (**Figure 4.3**). The singlet excited-state lifetime (τ) was estimated to be 5.3 ns, which is much longer than that of the anti-aromatic **S2-TIPS** (τ_1 = 1.1 ps, τ_1 = 10 ps).[5b] Two-photon absorption (TPA) measurements were also conducted for **BPT-TIPS** in toluene by Z-scan technique in the NIR region from 1300 to 1500 nm (**Figure 4.4**) and a maximum TPA cross section value ($\sigma^{(2)}_{max}$) of 620 GM (λ_{ex}: 1400

nm), which is slightly higher than that for **S2-TIPS** ($\sigma^{(2)}_{max}$ = 520 GM, λ_{ex}: 1400 nm) under the same condition.[5b]

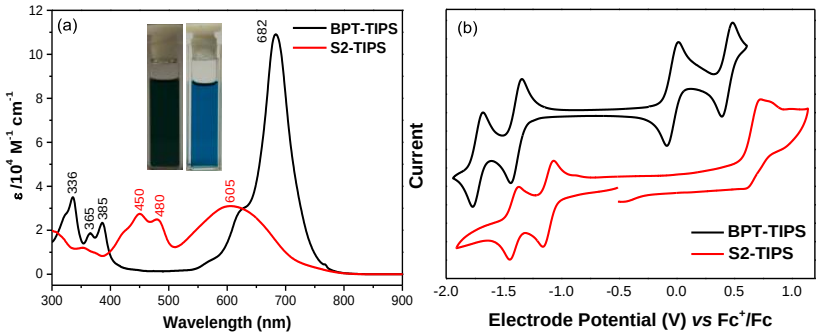

Figure 4.2 (a) Electronic absorption spectra of **BPT-TIPS** and **S2-TIPS** in CH_2Cl_2; insert are the photos for the solutions of **S2-TIPS** (left) and **BPT-TIPS** (right). (b) Cyclic voltammograms of **BPT-TIPS** and **S2-TIPS** in CH_2Cl_2 containing 0.1 M $TBAPF_6$.

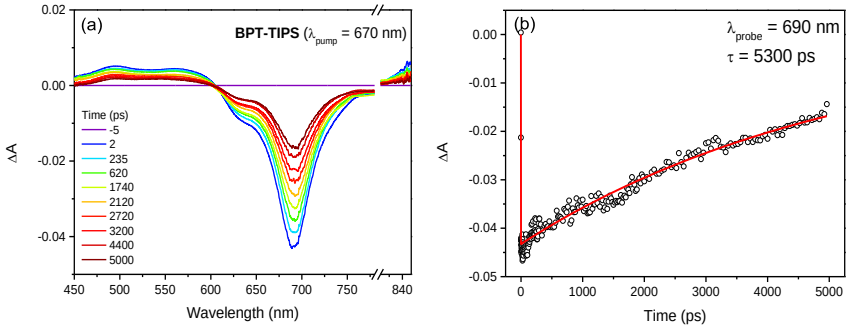

Figure 4.3 (a) Femtosecond transient absorption spectra（TA）spectrum of **BPT-TIPS** recorded in toluene (pump at 670 nm) and (b) the decay curve probed at 690 nm.

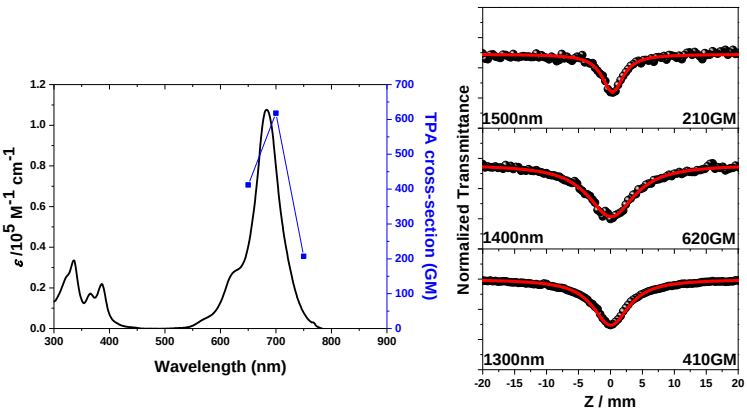

Figure 4.4 One-photon absorption spectrum (solid line and left vertical axes) and two-photon absorption spectrum (blue symbols and right vertical axes) and Z-scan curve of **BPT-TIPS**.

BPT-TIPS displays excellent amphoteric redox behavior with two reversible oxidation waves ($E_{1/2}^{ox}$ = -0.03, -0.44 V *vs* Fc^{+}/Fc) and two reversible reduction waves ($E_{1/2}^{red}$ = -1.73, -1.38 V *vs* Fc^{+}/Fc) (**Figure 4.2b**). The HOMO and LUMO energy levels were estimated to be -4.64 eV and -3.40 eV from the onset of the first oxidation and reduction wave, respectively. Compared with the anti-aromatic **S2-TIPS** which has a HOMO/LUMO level of -5.35/-3.75 eV (Eg = 1.60 eV) and is easily reduced but hard to be oxidized, the pro-aromatic **BPT-TIPS** can be easily oxidized and reduced to the corresponding radical cations/anions and dications/dianions. Such difference can be explained by the aromatic nature of both the cationic and anionic forms of **BPT-TIPS**, but for **S2-TIPS** its cationic forms are unstable due to the anti-aromatic nature of the cyclopentadienyl cation while its anionic forms are stable due to the aromatic character of the cyclopentadienyl anion.

4.2.3 Ground-state geometry

BPT-TIPS shows sharp NMR spectra even at elevated temperatures and it is ESR silent, indicating its closed-shell nature in the ground state. However, broken symmetry DFT calculation (UCAM-B3LYP/6-31G*) predicted that **BPT-TIPS** has an open-shell singlet diradical ground state, with a small diradical character (y = 18.6%) and a large singlet-triplet energy gap ($E_{S\text{-}T}$ = -13.3 kcal/mol). Under same computation method, **S2-TIPS** was predicted to be a typical closed-shell system with an ignorable diradical character. X-ray crystallographic analysis (at 100 K) further elaborated their ground-state

geometry (**Figure 4.5**).[7] The molecule is distorted from planarity due to the repulsion between the methyl groups and the TT unit (**Figure 4.5a**). Large bond length alternation was found in the central TT-quinodimethane moiety of both **BPT-TIPS** and **S2-TIPS** (**Figure 4.5b**), indicating that closed-shell quinoidal form contributes most to the ground-state structure in both cases. However, NICS(1)zz calculations distinguished their different electronic structures. For **BPT-TIPS**, the NICS(1)zz values for the central two rings 1 and 2 are negative but much less negative than the outmost two rings 3 and 4, indicating a small aromatic character of the rings 1 and 2 which can be correlated to its intrinsic pro-aromaticity. In contrast, the central two rings 1 and 2 in **S2-TIPS** possess positive NICS(1)zz values, implying a typical anti-aromatic character.

Molecules of **BPT-TIPS** are packed into a 1D infinite head-to-tail chain with a short average π-stacking distance of 3.34 Å (**Figure 4.5c**). The top view shows that the stacking is through phenalenyl-phenalenyl interaction, which is similar to the multi-center covalent bonding in the biphenalenyls[2a] but the distance is in the typical π-π stacking distance range (3.3-3.6 Å). Spin density distribution of the singlet diradical of **BPT-TIPS** shows that the spins are evenly distributed along the whole π-conjugated framework (**Figure 4.6**), which thus explains the decreased covalent character of the phenalenyl-phenalenyl interactions. The 1D polymer chains are then further stacked into a compact 3D network (side view, **Figure 4.5c**), which is

desirable for efficient charge transport.

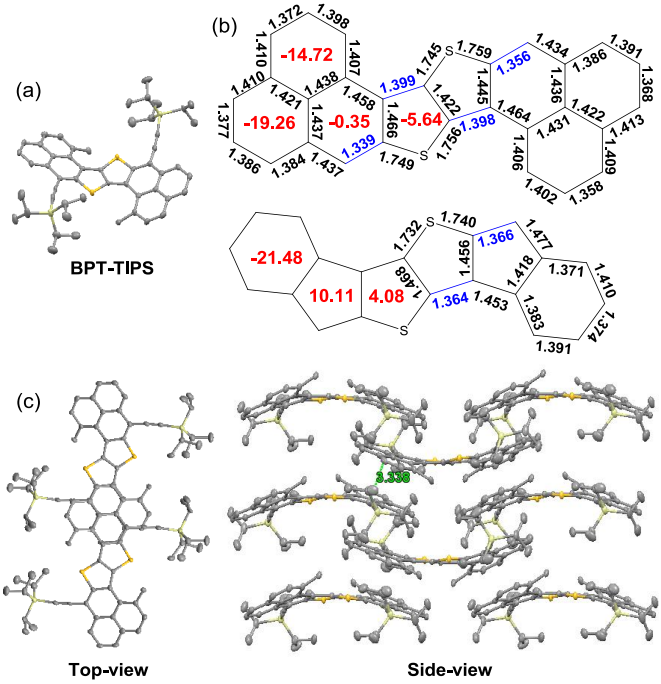

Figure 4.5 (a) X-ray crystallographic structure of **BPT-TIPS**, hydrogen atoms are omitted for clearance; (b) selected bond length analysis from the single-crystal structures and calculated NICS(1)zz values (red numbers); (c) 3D packing structures of **BPT-TIPS**.

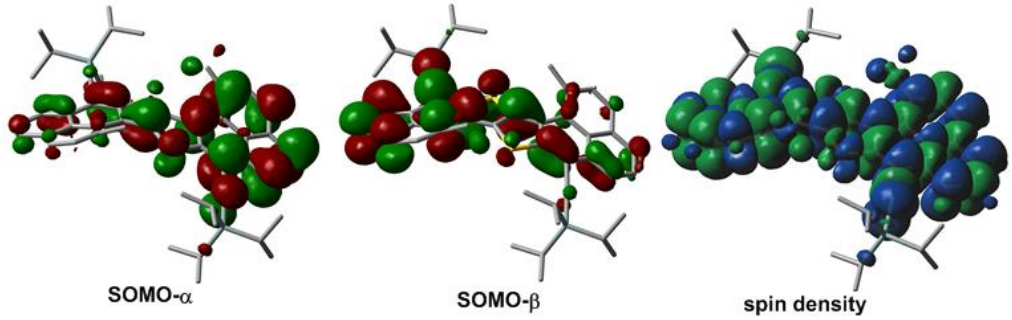

Figure 4.6 The calculated (UCAM-B3LYP/6-31G*) singly occupied molecule orbital profiles and spin density distribution of the singlet biradical of **BPT-TIPS**.

4.2.4 *Organic field effect transistor and thin film characterization*

Bottom-gate, top-contact FETs were thus fabricated and used to evaluate the charge transporting properties of **BPT-TIPS** in both drop-casted and spin-coated thin films (**Table 4.1**). All of the devices exhibited *p*-type operation with well-defined saturation behavior in nitrogen (**Figure 4.7**). An average field effect hole mobility of 0.14 $cm^2V^{-1}s^{-1}$ with a threshold voltage

(V_{th}) of 4 V and a current on/off ratio of 10^4 was measured for the spin-coated thin films on OTS modified substrates. When processed with drop casting method, large crystal domain was achieved, and as a result, the hole mobility was improved to 0.26 $cm^2V^{-1}s^{-1}$ without shifting the V_{th}. The different performance can be further correlated to the small surface roughness and high crystallinity of the drop-casted thin films as measured by AFM and XRD (**Figure 4.8 – 4.12**). Under similar processing conditions, the thin films of **S2-TIPS** showed much lower field-effect hole mobility (0.016 $cm^2V^{-1}s^{-1}$), which presumably can be ascribed to its separated columnar superstructure observed in the single crystals.[5b]

Table 4.1 The electrical parameters of the field effect transistors based on **BPT-TIPS**.

	Solution deposition	Annealing Temp	In N2		
			$\mu[cm^2V^{-1}s^{-1}]$	V_T [V]	On/off
1	Spin	As-spun	0.14	4	10^4
2	Spin	A120 °C	0.06	6	10^4
3	Drop	As-cast	0.26	5	10^4
4	Drop	A120 °C	0.15	5	10^4

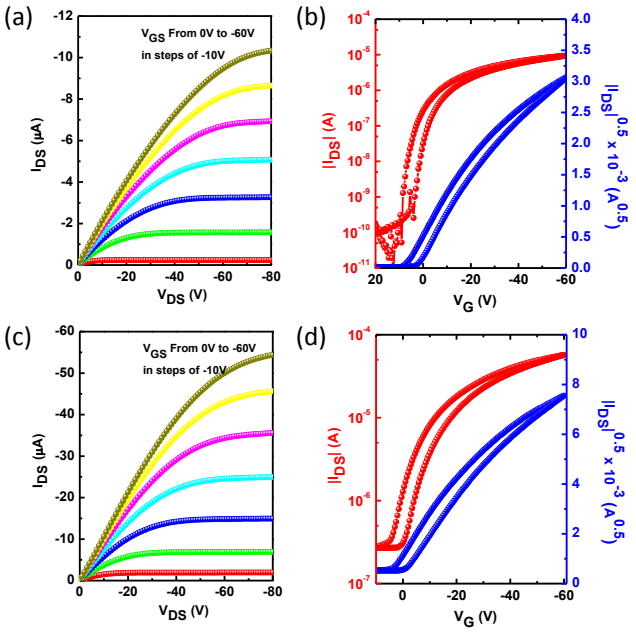

Figure 4.7 The output (a, c) and transfer (b, d) curves of the **BPT-TIPS** OFETs based on spin coated and drop casted thin films on OTS modified substrates.

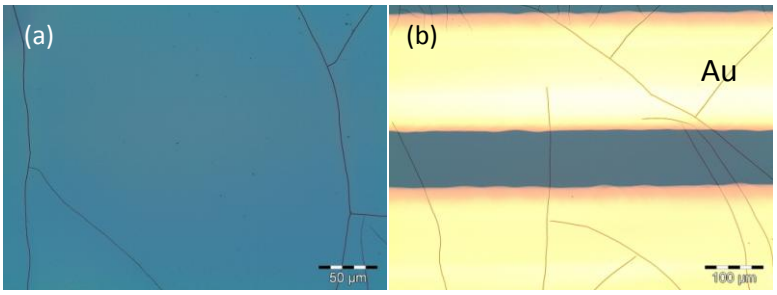

Figure 4.8 The optical microscopy images of the **BPT-TIPS** thin films drop casted onto OTS modified substrates (a) and the OFET device based on this films (b).

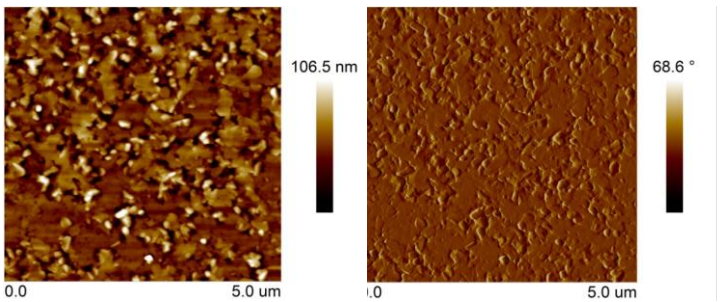

Figure 4.9 The AFM images of the **BPT-TIPS** thin films spin coated onto the OTS modified substrates.

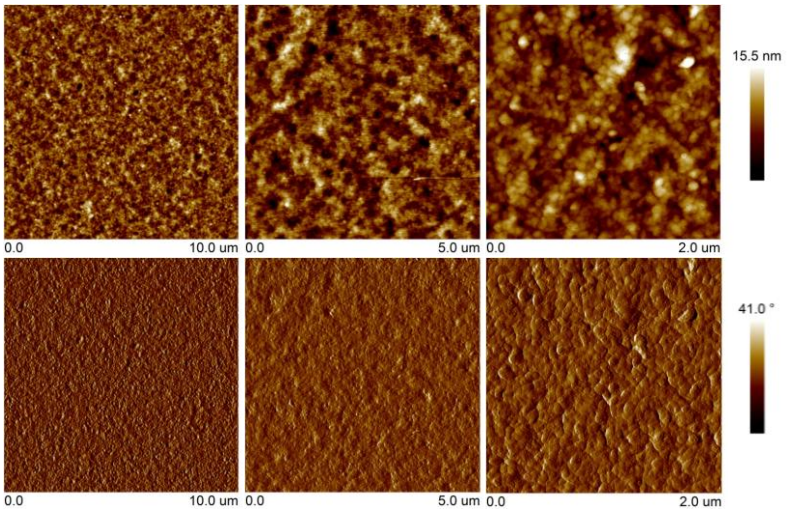

Figure 4.10 The AFM images of the **BPT-TIPS** thin films drop casted onto the OTS modified substrates with different data scale.

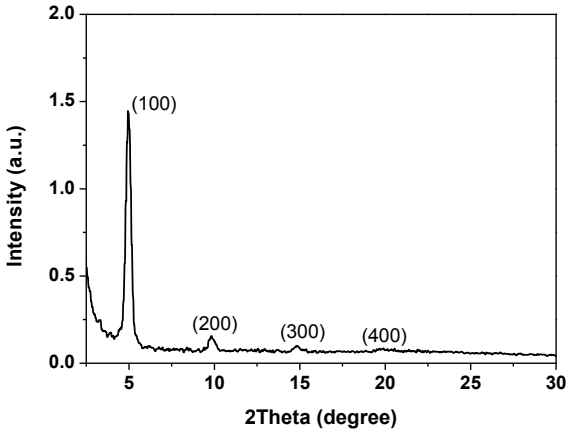

Figure 4.11 The thin film XRD pattern of **BPT-TIPS** thin films spin coated onto the OTS modified substrates.

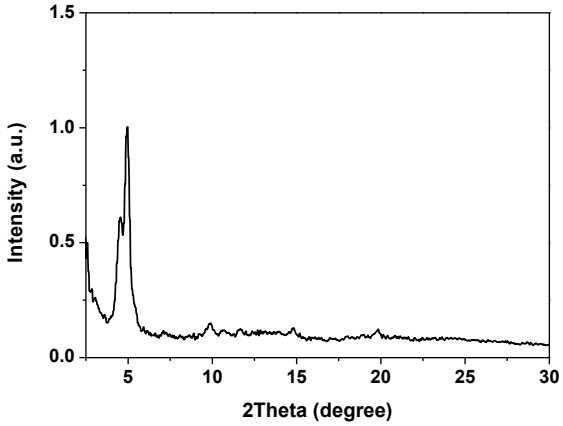

Figure 4.12 The thin film XRD pattern of **BPT-TIPS** thin films drop casted onto the OTS modified substrates.

4.3 Conclusion

In summary, we demonstrate that the quinoidal **BPT-TIPS** has distinctively different ground-state electronic structure and physical properties from its analogue **S2-TIPS**, which can be correlated to their respective pro-aromatic and anti-aromatic character. Our studies indicate that a pro-aromatic system exhibits a larger diradical character, longer excited state lifetime and better redox amphotericity than its anti-aromatic counterparts, which is important information for future molecular design. The 3D ordered packing structure of this diradicaloid molecule led to a relatively high charge carrier mobility, which also paved the way to design materials for spin-dependent charge transport studies in next stage.

4.4 Experiments

4.4.1 *General experimental methods*

Refer to the section of *2.4.1 General experimental methods* in Chapter 2.

The device fabrication is as following: The SiO_2/Si substrate was cleaned with acetone and isopropanol, and then immersed in a piranha solution for 8 minutes. Followed by rinsing with deionized water, and then treated with octadecyltrimethoxysilane (OTMS) spin coated from 10 mM trichloroethylene solution, and treated with ammonia vapor for 7h, or octadecyltrichlorosilane (ODTS) immersed in 3 mM hexadecane solution for 16h in N_2.

4.4.2 Detailed synthetic procedures and characterization data

Compound 4-1

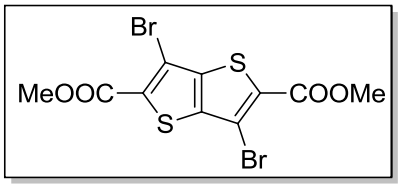

Under argon and anhydrous condition at -78 ^{o}C, *n*-BuLi (1.6 M in hexane, 6.25 mL, 10.00 mmol) was slowly added to a solution of 2,3,5,6-tetrabromothieno[3,2-b]thiophene (2.28 g, 5.00 mmol) in THF (40 mL) and the mixture was stirred for 1 h. Methyl cyanoformate (851 mg, 10.00 mmol) was added by syringe at -78 ^{o}C. The reaction was slowly warmed to room temperature and stirred overnight. The reaction was quenched by water at 0 ^{o}C. All of the organic solvents were removed and the organic precipitate was collected by filtration. The crude product was washed with hexane and methanol to give pure compound **4-1** as a white solid (1.35 g, 65% yield). ^{1}H NMR (500 MHz, $CDCl_3$, ppm): δ = 3.97 (s, 3H); ^{13}C NMR (125 MHz, $CDCl_3$, ppm): δ = 160.91, 142.57, 131.70, 109.82, 52.78. HR MS (EI): calcd for $C_{10}H_6Br_2O_4S_2$ (M^+), 413.8054; found, 413.8053 (error: -0.24 ppm).

Compound 4-2

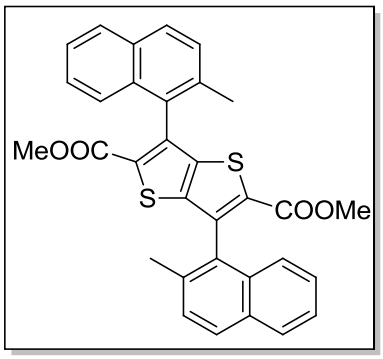

2-methylnaphth-1-yl boronic acid (744 mg, 4.00 mmol), compound **4-1** (414 mg, 1.00 mmol), K_2CO_3 (552 mg, 4.00 mmol) and one drop of aliquat 336 were dissolved in toluene (18 mL) methanol (6 mL) and water (6 mL). $Pd(PPh_3)_4$ (60 mg) was added as a catalyst and the mixture was refluxed for 12 h. After cooling down, the mixture was poured into water and extracted with DCM. The organic layer was washed with water and dried over anhydrous Na_2SO_4. The solvent was removed under vacuum and the residue was purified by column chromatography (silica, hexane: DCM = 2: 1) to give a pale yellow solid (295 mg, 55% yield). ^{1}H NMR (500 MHz, $CDCl_3$, ppm): δ = 7.91 (d, *J* = 8.3 Hz, 2H), 7.53-7.30 (m, 4H), 3.56 (s, 3H), 2.37 and 2.32 (s, 3H); ^{13}C NMR (125 MHz, $CDCl_3$, ppm): δ =161.78, 143.18, 138.92, 134.18, 134.11, 133.68, 132.05, 131.76, 129.39, 129.37, 128.72, 128.52, 128.50, 128.21, 126.50, 126.46, 125.13, 125.09, 124.79, 124.67, 52.14, 20.37, 20.26. HR MS (EI): calcd for $C_{32}H_{24}O_4S_2$ (M^+), 536.1116; found, 536.1108 (error: -1.49 ppm).

Compound 4-3

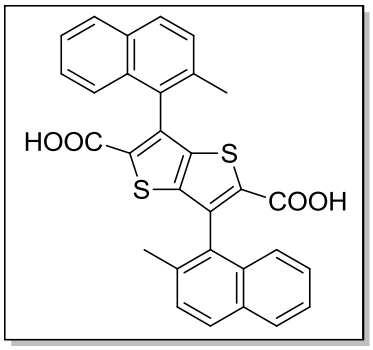

Compound **4-2** (536 mg, 1.00 mmol) was dissolved in methanol and THF (20 mL, 1:1 v/v), followed by the addition of sodium hydroxide (400 mg, 10.00 mmol). This mixture was heated at reflux overnight. The solvent was removed under reduced pressure after the reaction was completed. To the residue then 10% hydrochloric acid solution was added. The precipitate formed was collected by filtration and washed with water and a little amount of DCM, then dried in vacuum to afford product **4-3** as a pale yellow solid (498 mg, 98% yield). ^{1}H NMR (500 MHz, DMSO-d_6, ppm): δ = 13.17 (br, 2H), 8.05-7.93 (m, 4H), 7.61-7.55 (m, 2H), 7.55-7.40 (m, 4H) 7.38 (d, *J* = 8.2 Hz, 1H), 7.28 (d, *J* = 8.3 Hz, 1H), 2.29 and 2.24 (s, 6H); ^{13}C NMR (125 MHz, DMSO-d_6, ppm): δ =162.29, 142.13, 137.22, 135.15, 133.82, 133.79, 131.65, 131.22, 129.41, 128.60, 128.44, 128.18, 126.75, 125.24, 125.21, 124.60, 124.36, 19.98, 19.86. HR MS (EI): calcd for $C_{30}H_{20}O_4S_2$ (M^+), 508.0803; found, 508.0808 (error: 0.98 ppm).

Compound 4-4

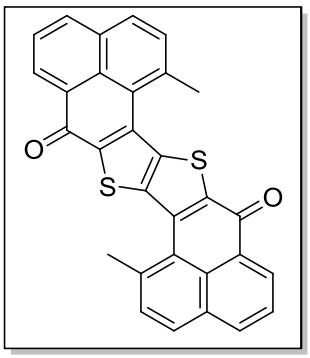

Compound **4-3** (508 mg, 1.00 mmol) was added in anhydrous DCM (20 mL), followed by the addition of excess of thionyl chloride (1 mL). To this mixture anhydrous DMF (1-2 drops) was added at room temperature. The resultant mixture was heated at reflux overnight. During this period the insoluble diacid **4-3** became soluble in DCM. After cooling down the solvent was removed under reduced pressure to afford crude acid chloride. This intermediate compound was dissolved in anhydrous DCM (20 mL) then anhydrous $AlCl_3$ (533 mg, 4.00 mmol) was added carefully at 0 ℃. The resultant mixture was allowed to warm up to room temperature and stirred overnight, then slowly quenched by 10% HCl solution to form a red precipitate. The crude precipitate was rinsed with 10% NaOH, MeOH, hexane and DCM until the washings were colorless, giving **4-4** as an insoluble yellow solid (402 mg, 85% yield). Both ^{1}H NMR and ^{13}C NMR data were not obtained due to its poor solubility. HR MS (EI): calcd for $C_{30}H_{16}O_2S_2$ (M^+), 472.0592; found, 472.0582 (error: -2.11 ppm).

Compound BPT-TIPS

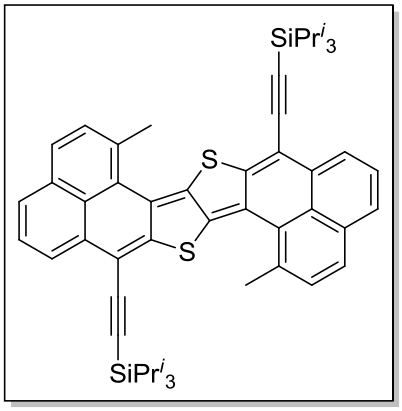

To a solution of triisopropylsilylacetylene (550 mg, 3.00 mmol) in anhydrous THF (20 mL) at 0 ^{o}C was added dropwise *n*-BuLi (1.6 M in hexane, 1.88 mL, 3.00 mmol). The solution was stirred for 30 min at 0 ^{o}C. Then diketone **4-4** (236 mg, 0.50 mmol) was added as solid in one portion. The mixture was slowly warmed to room temperature and stirred overnight. During this period the insoluble diketone disappeared and the solution became clear. The solution was diluted with 30 mL of toluene and then anhydrous $SnCl_2$ (380 mg, 2.00 mmol) was added in portions under argon atmosphere. During this period the color of the reaction mixture became deep blue. Upon completion of the reaction as monitored by TLC, the resulting blue solution was then filtered and the filtrate was subsequently evaporated to dryness. The residue was purified by column chromatography (silica gel, hexane: DCM = 5: 1). Compound **BPT-TIPS** was further purified by recrystallization from MeOH/CH_2Cl_2 as a dark blue solid (181 mg, 45% yield). ^{1}H NMR (500 MHz, $CDCl_3$, ppm): δ = 7.92 (d, *J* = 7.4 Hz, 1H), 7.73 (d, *J* = 8.4 Hz, 1H), 7.64 (d, *J* = 8.0 Hz, 1H), 7.50-7.40 (m, 2H), 2.77 (s, 1H), 1.32-1.21 (br, 21H); ^{13}C NMR (125 MHz,

$CDCl_3$, ppm): δ = 151.74, 142.83, 133.40, 132.20, 131.41, 131.25, 128.41, 127.36, 126.97, 126.93, 126.10, 123.43, 111.13, 103.48, 103.03, 24.82, 18.85, 11.41. HR MS (APCI): calcd for $C_{52}H_{59}S_2Si_2$ $[(M+H)^+]$, 803.3597; found, 803.3578 (error: -2.37 ppm).

References

[1] (a) Z. Sun, Q. Ye, C. Chi and J. Wu, *Chem. Soc. Rev.* 2012, **41**, 7857. (*b*) M. Abe, *Chem. Rev.* 2013, **113**, 7011. (*c*) Z. Sun, Z. Zeng and J. Wu, *Acc. Chem. Res.* 2014, **47**, 2582. (d) T. Kubo, *Chem. Rec.*, 2015, **15**, 218.

[2] Representative examples: (a) A. Shimizu, T. Kubo, M. Uruichi, K. Yakushi, M. Nakano, D. Shiomi, K. Sato, T. Takui, Y. Hirao, K. Matsumoto, H. Kurata, Y. Morita and K. Nakasuji, *J. Am. Chem. Soc.* 2010, **132**, 14421. (*b*) Y. Li, K.-W. Heng, B. S. Lee, N. Aratani, J. L. Zafra, N. Bao, R. Lee, Y. M. Sung, Z. Sun, K.-W. Huang, R. D. Webster, J. T. López Navarrete, D. Kim, A. Osuka, J. Casado, J. Ding and J. Wu, *J. Am. Chem. Soc.*, 2012, **134**, 14913. (*c*) D. T. Chase, B. D. Rose, S. P. McClintock, L. N. Zakharov and M. M. Haley, *Angew. Chem. Int. Ed.*, 2011, **50**, 1127. (*d*) A. Shimizu, R. Kishi, M. Nakano, D. Shiomi, K. Sato, T. Takui, I. Hisaki, M. Miyata and Y. Tobe, *Angew. Chem. Int. Ed.*, 2013, **52**, 6076. (*e*) Z. Zeng, S. Lee, J. L. Zafra, M. Ishida, X. Zhu, Z. Sun, Y. Ni, R. D. Webster, R.-W. Li, J. T. López Navarrete, C. Chi, J. Ding, J. Casado, D. Kim and J. Wu, *Angew. Chem. Int. Ed.*, 2013, **52**, 8561. (*f*) X. Yang, X.; D. Liu and Q. Miao, *Angew. Chem. Int. Ed.*, 2014, **53**, 6786.

[3] (a) T. Takahashi, K. I. Matsuoka, K. Takimiya, T. Otsubo and Y. Aso, *J. Am. Chem. Soc.*, 2005, **127**, 8928. (*b*) J. Casado, R. P. Ortiz and J. T. López Navarrete, *Chem. Soc. Rev.*, 2012, **41**, 5672.

[4] (a) T. M. Pappenfus, R. J. Chesterfield, C. D. Frisbie, K. R. Mann, J. Casado, J. D. Raff, and L. L. Miller, *J. Am. Chem. Soc.*, 2002, **124**, 4184. (*b*) R. J. Chesterfield, C. R. Newman, T. M. Pappenfus, P. C. Ewbank, M. H. Haukaas, K. R. Mann, L. L. Miller and C. D. Frisbie, *Adv. Mater.*, 2003, **15**, 1278. (*c*) Y. Suzuki, E. Miyazaki and K. Takimiya, *J. Am. Chem. Soc.*, 2010, **132**, 10453. (*d*) Q. Wu, R. Li, W. Hong, H. Li, X. Gao and D. Zhu, *Chem. Mater.*, 2011, **23**, 3138.

[5] (a) G. E. Rudebusch, A. G. Fix, H. A. Henthorn, C. L. Vonnegut, L. N. Zakharov and M. M. Haley, *Chem. Sci.*, 2014, **5**, 3627. (b) X. Shi, P. M. Burrezo, S. Lee, W. Zhang, B. Zheng, G. Dai, J. Chang, J. T. López Navarrete, K.-W. Huang, D. Kim, J. Casado and C. Chi, *Chem. Sci.*, 2014, **5**, 4490.

[6] J. E. Anthony, *Angew. Chem. Int. Ed.*, 2008, **47**, 452.

[7] Crystallographic data for **BPT-TIPS**: $C_{52}H_{54}S_2Si_2$. M = 799.25, monoclinic, a = 17.7574(16) Å, b = 14.7085(14) Å, c = 17.0416(15) Å, $\alpha = 90^o$, $\beta = 90.251(5)^o$, $\gamma = 90^o$, V = 4451.0(7) Å^3, T = 100(2) K, space group P 21/c, Z = 4, CuK$_\alpha$ radiation λ = 1.54178 Å, R_1 = 0.0770 ($I > 2\sigma(I)$), $wR(F^2)$ = 0.2043 ($I > 2\sigma(I)$); R_1 = 0.1048 (all data), $wR(F^2)$ = 0.2471 (all data). CCDC No: 1055932.

Chapter 5: Solution-processible *n*-type and Ambipolar Semiconductors Based on Fused Cyclopentadithiophenebis(dicyanovinylene) core

5.1 Introduction

Solution-processable organic semiconductors have attracted considerable attention due to their potential use for low-cost, portable electronic and optoelectronic devices.[1] In recent years, more efforts have been devoted to the design and synthesis of *n*-type and ambipolar semiconductors for organic field effect transistors (OFETs).[2] The key strategy for this type of materials is to appropriately alter the LUMO energy level so that it is close to the work function of the source and drain electrodes and allows efficient electron injection at the semiconductor/electrode interfaces. The general design methods include (*a*) attachment of electron-withdrawing groups such as perfluoroalkyl, CN-, imide, *etc*. onto the *p*-type semiconductors such as acenes and oligo-/polythiophenes,[3] and (*b*) incorporation of electron negative atoms (e.g. imine nitrogen) into the π-conjugated frameworks.[4] In addition, dicyanovinylene-substituted quinoidal arenes/oligothiophenes,[5] indenofluorene,[6] and cyclopentadithiophene[7] have proved to be good *n*-type and ambipolar semiconductors due to their low-lying LUMO energy levels and rigid structures. It was expected that the fused cyclopentadithiophenebis(dicyanovinylene) (**FCPDT**, **Scheme 5.1**) will be a

good skeleton based on the following considerations: (*a*) the molecule has a rigid and largely extended π-conjugated framework, which allows efficient intermolecular π-orbital overlap; (*b*) the electron-withdrawing dicyanovinylene units will lower the LUMO energy level and allow effective electron injection and transport; (*c*) additional S-S interactions in solid state can enhance the molecular order and charge transport; (*d*) alkyl groups can be easily attached onto the termini of the thiophene rings to make the materials soluble and easy to form ordered thin film. Therefore, two FCPDT based compounds, **FCPDT-C16** and **FCPDT-C24** with 2-hexyldecy and 2-decyltetradecyl chains, respectively (**Scheme 5.1**), were prepared and their physical properties, thermal behavior and applications for OFETs were investigated. As expected, both compounds showed ordered self-assembly and good performance in solution processed *n*-channel and ambipolar OFETs.

5.2 Results and discussion

5.2.1 Synthesis

The synthetic route for **FCPDT-C16** and **FCPDT-C24** is shown in **Scheme 5.1**. The Stille coupling reaction between the diethyl 2,5-dichlorothieno[3,2-b]thiophene-3,6-dicarboxylate **5-1**[8] and the alkylated thiophene stannous **5-2**[9] gave **5-3** in 82-85% yield. The electron-withdrawing ester groups increase the reactivity of the C-Cl bonds and allow the Stille coupling to proceed smoothly. The hydrolysis of **5-3**

followed by acidification gave the diacid **5-4**, which was converted into the corresponding carboxylic acid chloride by reaction with thionyl chloride in dry dichloromethane (DCM). Subsequent double Friedel–Crafts acylation with aluminium chloride afforded the desired diketone **5-5** in 30-50% yield. Finally, Knoevenagel condensation between **5-5** and excess malononitrile in the presence of $TiCl_4$ and pyridine provided the target compounds **FCPDT-C16** and **FCPDT-C24** in 60-70% yield. The introduction of shorter aliphatic chains (e.g. dodecyl and 3,7-dimethyloctyl) onto the same FCPDT backbone by a similar method however encountered difficulties in purification due to the very poor solubility of the intermediate diketone compounds and the final products. Hence, branched alkyl chains (2-hexyldecyl and 2-decyltetradecyl) are attached and both **FCPDT-C16** and **FCPDT-C24** are soluble in common organic solvents, which is desirable for solution processed device fabrication.

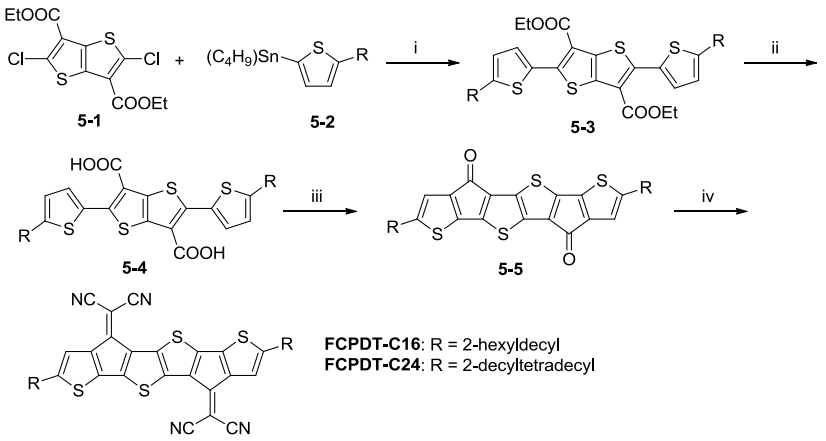

Scheme 5.1 Synthetic route to **FCPDT-C16** and **FCPDT-C24**. *Reagents and conditions*: (i) $Pd(PPh_3)_4$, toluene/DMF, 120 ^oC, 24h, 82~85%; (ii) NaOH, MeOH/THF, reflux, quantitative; (iii) (a) $SOCl_2$, dry dichloromethane, reflux; (b) $AlCl_3$, dry dichloromethane, 0 ^oC - rt., 30~50%; (iv) malononitrile, pyridine, $TiCl_4$, chlorobenzene, 0 ^oC - rt., 60~70%.

5.2.2 Photophysical and electrochemical properties

The UV-vis-NIR absorption spectra of **FCPDT-C16** and **FCPDT-C24** recorded in $CHCl_3$ solution are similar, both showing intense absorption in 300-450 nm with the maxima at 342 and 419 nm, together with a weak and broad band with maximum at 833 nm (**Figure 5.1**). The long-wavelength absorption band is likely accounted for intramolecular charge transfer from electron-donating thiophene units to the electron-withdrawing dicyanovinylene moieties, leading to a small optical energy gap.

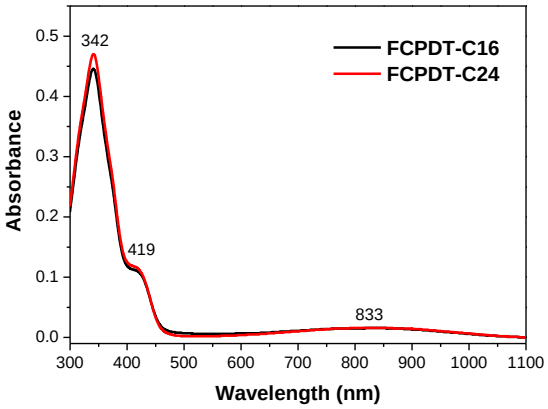

Figure 5.1 UV-vis-NIR absorption spectra of **FCPDT-C16** and **FCPDT-C24** in chloroform (concentration $c = 10^{-5}$ M).

The electrochemical properties of **FCPDT-C16** and **FCPDT-C24** were investigated by cyclic voltammetry (CV) and differential pulse voltammetry (DPV) in DCM solution (**Figure 5.2**). All voltages are referenced with respect to the ferrocene/ferrocenium (Fc^+/Fc) couple. It was found that the alkyl chains had almost no effect on the voltammograms. Both compounds showed two quasi-reversible reduction waves with half-wave potentials $E_{1/2}$ = -1.17 V, -0.98 V for **FCPDT-C16** and $E_{1/2}$ = -1.13 V, -0.98 V for **FCPDT-C24**, and one reversible oxidation wave with $E_{1/2}$ = 0.60 V for both compounds. The HOMO

and LUMO energy levels were estimated to be -5.31 eV and -3.88 eV for **FCPDT-C16** and -5.31 eV and -3.89 eV for **FCPDT-C24**, respectively, based on the corresponding onset of the first oxidation and reduction wave. The electrochemical energy gaps for both compounds were thus determined to be 1.43 eV and 1.42 eV, respectively (**Table 5.1**). The low-lying LUMO energy level of both FCPDT compounds indicates that they can serve as promising candidates for *n*-channel or ambipolar OFETs.

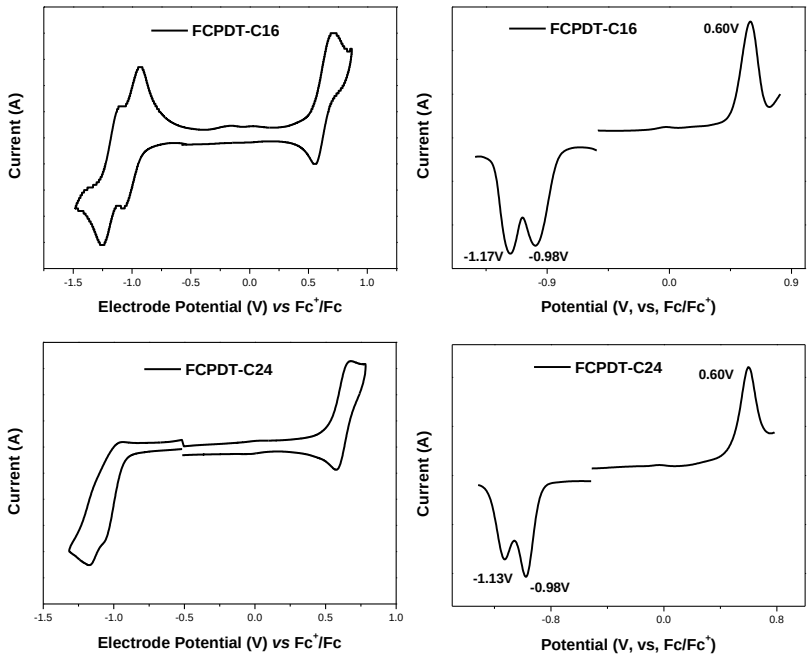

Figure 5.2 Cyclic voltammograms and differential pulse voltammograms of **FCPDT-C16** and **FCPDT-C24** in dry dichloromethane containing 0.1 M Bu_4NPF_6 as the supporting electrolyte, AgCl/Ag as the reference electrode, Au as the working electrode, Pt wire as the counter electrode, and a scan rate of 50 mV s^{-1}. The potential was externally calibrated against the ferrocene/ferrocenium couple.

Table 5.1 Summary of electrochemical properties of compound **FCPDT**[a]

	E_{ox}^{onset} (V)	E_{red}^{onset} (V)	HOMO (eV)	LUMO (eV)	*Eg* (eV)
FCPDT-C16	1.43	-0.92	-5.31	-3.88	1.43
FCPDT-C24	1.43	-0.91	-5.31	-3.89	1.42

[a] HOMO and LUMO energy levels were calculated from the first oxidation and reduction wave onset according to the equations HOMO = - (4.8 + E_{ox}^{onset}) eV and LUMO = - (4.8 + E_{red}^{onset}) eV.

5.2.3 Thermal behavior and molecular packing

The thermal behavior and molecular packing in the solid state were investigated by thermogravimetric analysis (TGA), differential scanning calorimetry (DSC), polarizing optical microscopy (POM) and X-ray diffraction (XRD). TGA measurements revealed that both FCPDT compounds were thermally stable over 335 ℃ with 5% weight loss (**Figure 5.3**). DSC curves of **FCPDT-C16** showed four endothermic transitions at 133.8, 156.3, 166.4 and 196.4 ℃ upon heating and two exothermic transitions at 194.3 and 142.6 ℃ upon cooling. **FCPDT-C24** exhibited two endothermic transitions at 117.1 and 133.9 ℃ upon heating and two exothermic transitions at 134.4 and 90.2 ℃ upon cooling (**Figure 5.4**). Powder XRD diffraction patterns of both compounds at room temperature exhibited many sharp diffraction peaks, indicating a crystalline nature (**Figure 5.5**). Upon heating, both **FCPDT-C16** and **FCPDT-C24** can enter liquid crystalline (LC) phase, as evidenced by the POM images at different temperatures (**Figure 5.6** and **Figure 5.7**). However, the detailed phase structure cannot be simply figured out because the XRD patterns in the LC phases showed broad band (**Figure 5.5**).

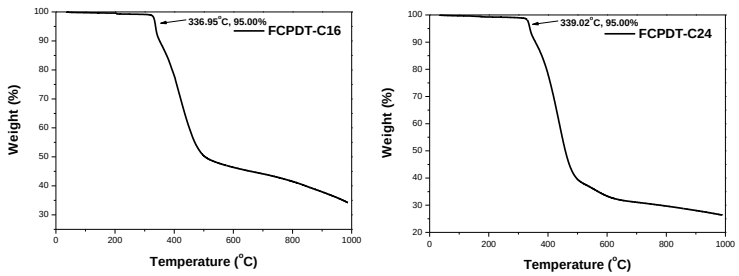

Figure 5.3 Thermogravimetric analysis curves of compound **FCPDT-C16** and **FCPDT-C24** recorded under N_2 at a heating rate of 10 ^{o}C min^{-1}.

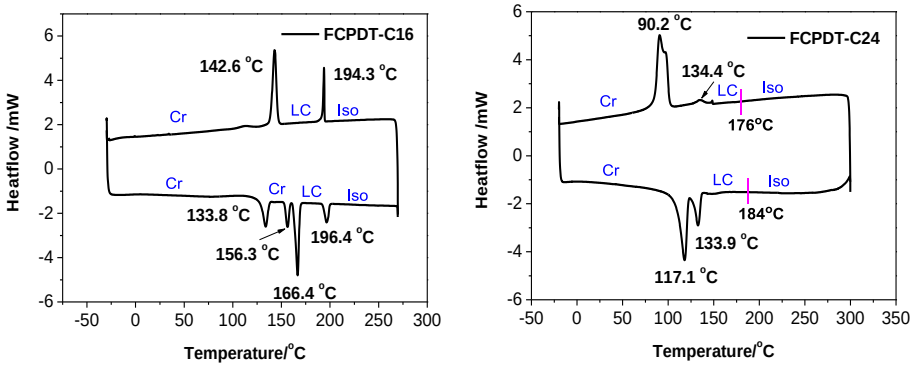

Figure 5.4 Differential scanning calorimetry curves of **FCPDT-C16** and **FCPDT-C24** recorded under N_2 at a heating rate of 10 ^{o}C min^{-1} (Cr: Crystal, LC: Liquid crystal, Iso: Isotropic phase). The isotropic temperature for **FCPDT-C24** can not be observed from DSC curve, but can be determined by polarizing optical microscopy.

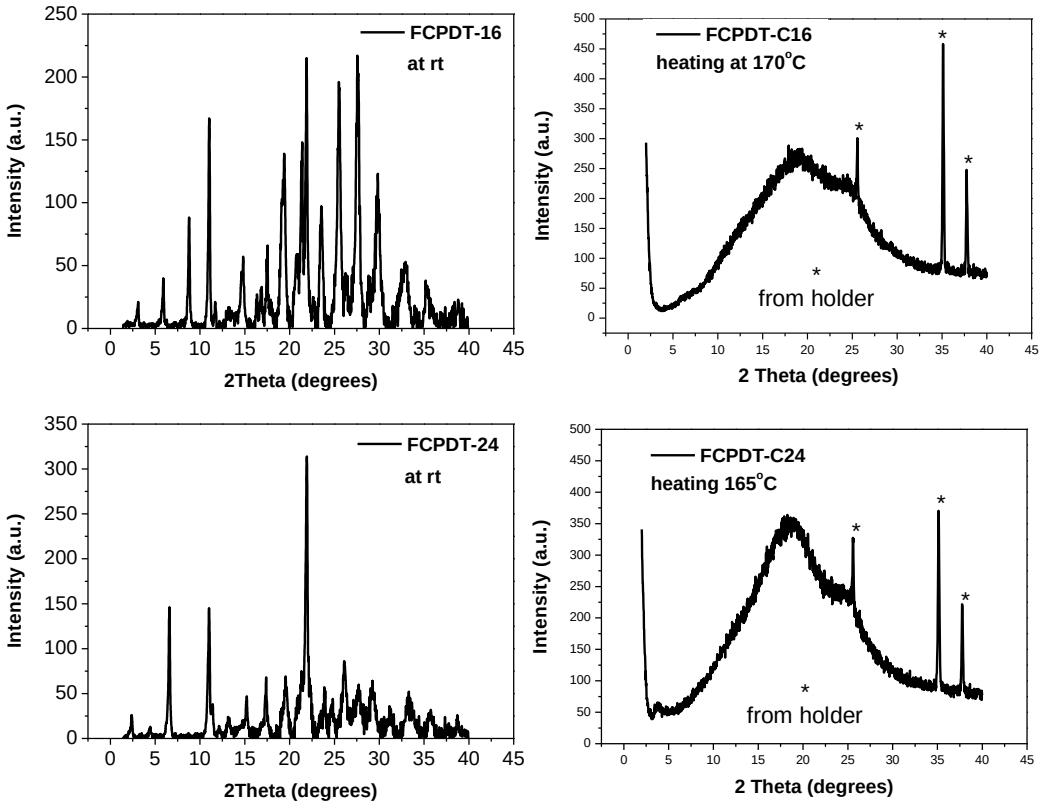

Figure 5.5 Variable-temperature powder XRD patterns for **FCPDT-16** and **FCPDT-24**.

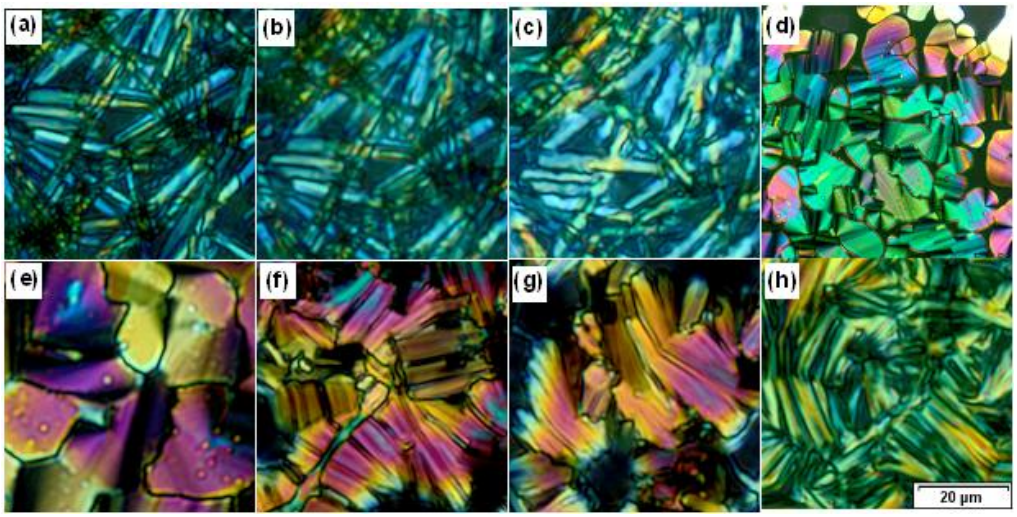

Figure 5.6 POM images of **FCPDT-C16**: (a) heating at 60 ^{o}C; (b) heating at 140 ^{o}C; (c) heating at 160 ^{o}C; (d) heating at 180 ^{o}C; (e) cooling from isotropic phase at 190 ^{o}C; (f) cooling at 150 ^{o}C; (g) cooling at 120 ^{o}C; (h) cooling at 90 ^{o}C. The scale bar is same for all of images.

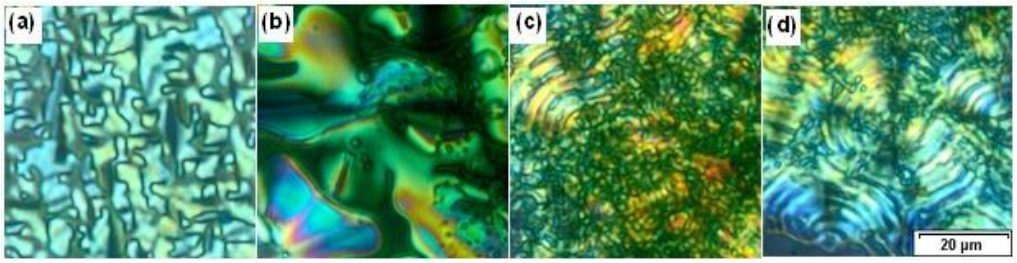

Figure 5.7 POM images of **FCPDT-C24**: (a) heating at 160 ^{o}C; (b) cooling from isotropic phase at 140 ^{o}C; (c) cooling at 120 ^{o}C; (d) cooling at 45 ^{o}C. The scale bar is same for all of imgaes.

5.2.4 *Organic field effect transistor and thin film characterization*

Bottom-gate, top-contact OFETs were fabricated on p+-Si substrates. The SiO_2 dielectric surface was treated with octadecyltrimethoxysilane (OTMS) or octadecyltrichlorosilane (ODTS). Then thin films of **FCPDT-C16** and **FCPDT-C24** were deposited by spin coating or casting from 5-10 mg/mL $CHCl_3$ solutions. The devices were completed by patterning the Au source/drain electrodes using a shadow mask. The OFET device data for the thin films on different substrates measured either under nitrogen or in air, are

summarized in **Table 5.2**. Both compounds showed ambipolar FET behavior, with a major *n*-channel operation. The typical transfer and output curves for the **FCPDT-C16** based OFETs on ODTS modified substrate measured in nitrogen are shown in **Figure 5.8**. No obvious nonlinear behavior at low drain voltage could be observed, indicating a small injection barrier between the LUMO energy level of **FCPDT-C16** and work-function of Au electrodes. At high drain voltage, well defined saturation behavior could be observed. The FET mobility was calculated using the following equation in the saturation regime: $I_D=W/2LC_i\mu(V_G-V_T)^2$, where I_D is the drain current, μ is the field-effect mobility, C_i is the capacitance per unit area of the gate dielectric layer (SiO_2, 200 nm, C_i = 17 nF cm^{-2}), and V_G and V_T are gate voltage and threshold voltage, respectively. W and L are channel width and length, respectively. For compound **FCPDT-C16**, an electron mobility as high as 0.16 $cm^2V^{-1}s^{-1}$ and hole mobility as high as 0.003 $cm^2V^{-1}s^{-1}$ were obtained on ODTS modified devices measured in N_2 conditions after optimization. The electron mobility is about 50× larger than the hole mobility even though injection barrier is larger for electrons than holes, which also indicates good intrinsic electron transport properties for this kind of materials. When exposed to air, the devices showed large degradation (20×) compared to its initial value. When increasing the alkyl chain length from C16 to C24, the device performance decreases significantly from 0.16 $cm^2V^{-1}s^{-1}$ to 0.007 $cm^2V^{-1}s^{-1}$ for electron and from 0.003 $cm^2V^{-1}s^{-1}$ to 4×10^{-4} $cm^2V^{-1}s^{-1}$ for hole mobility

(**Figure 5.9** and **Table 5.2**). The long insulating alkyl chains may suppress effective transport path for charge carriers. When thermal annealing at 100 ^{o}C, the device performance showed almost no change, indicating that this kind of compounds could be a good annealing-free material.

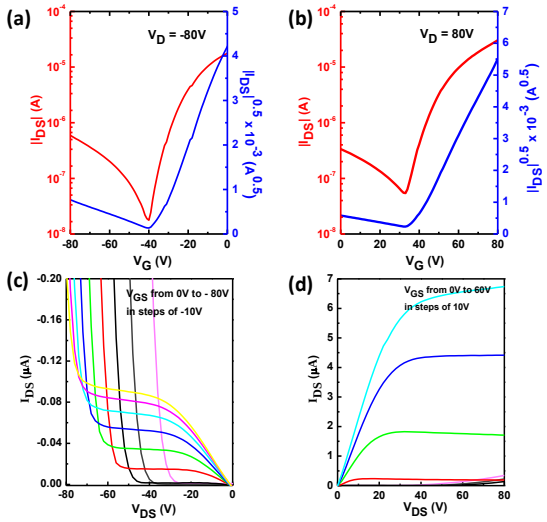

Figure 5.8 The transfer (a, b) and output (c, d) curves of the **FCPDT-C16** thin film on ODTS modified substrates measured in nitrogen.

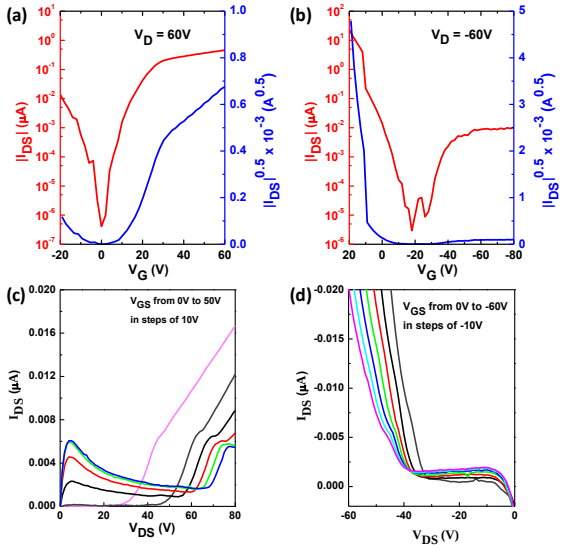

Figure 5.9 The transfer (a, b) and output (c, d) curves of **FCPDT-C24** thin film on ODTS modified substrates measured in nitrogen.

Table 5.2 The electrical parameters of the FET devices.

Compound	Surface modification	electron			hole		
		μ [$cm^2V^{-1}s^{-1}$]	VT [V]	on/off	μ [$cm^2V^{-1}s^{-1}$]	VT [V]	on/off
FCPDT-C16	OTMS (N_2)	0.04	45	10^3	2.5×10^{-4}	-44	10^2
	ODTS (N_2)	0.16	40	10^3	0.003	-40	10^2
	ODTS (air)	0.008	48	10^3	0.001	-12	10^4
FCPDT-C24	OTMS (N_2)	4.2×10^{-4}	12	10^4	1.6×10^{-4}	-25	10^4
	ODTS (N_2)	0.007	10	10^5	4×10^{-4}	-28	10^3
	ODTS (air)	0.002	8	10^4	2×10^{-4}	-13	10^4

The surface morphologies of the thin films with different surface treatments were checked by tapping mode atom force microscope (AFM). The AFM images exhibited granular crystals for both materials on ODTS treated substrates while the crystal size increases with increasing alkyl chain length (**Figure 5.10**). Different surface morphologies formed on OTMS treated substrates, that is, larger ribbon like crystals for **FCPDT-C16** and small crystal network for **FCPDT-C24** were observed (**Figure 5.11**). Two dimensional X-ray diffraction measurements of the thin films on the ODTS modified substrate revealed that both compounds formed highly ordered lamellar packing structure, as evidenced from a series of intense (001), (002), (003) diffraction peaks (**Figure 5.10**). The interlayer distances derived from the (001) diffraction are 2.79 nm and 3.87 nm for **FCPDT-C16** and **FCPDT-C24**, respectively. The former showed more intense diffraction and additional peaks, indicating a higher order, which can explain its superior device performance

than the latter.

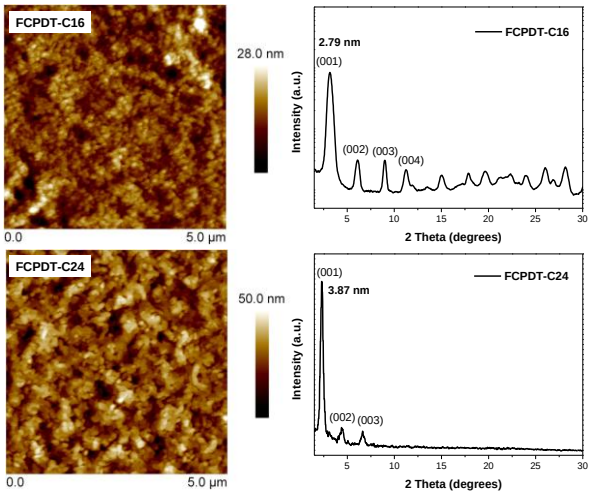

Figure 5.10 AFM images (left, height image) and XRD patterns (right) of the thin films of **FCPDT-C16** and **FCPDT-C24** deposited by spin-coating on the ODTS treated substrates.

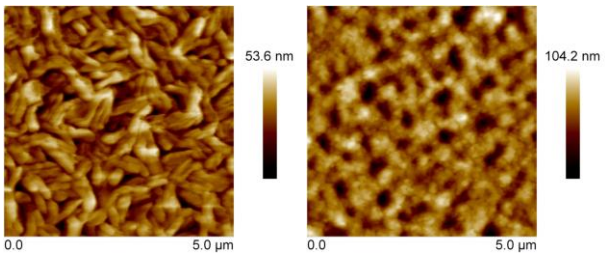

Figure 5.11 AFM images (height image) of the thin films of **FCPDT-C16** and **FCPDT-C24** deposited by spin-coating on the OTMS treated substrates.

5.3 Conclusion

In summary, two new soluble FCPDT-based semiconductors have been synthesized and showed ordered self-assembly in solid state and thin film. Due to the low-lying LUMO energy level, both compounds showed ambipolar FET behaviour with a major *n*-channel operation. Field effect electron mobility as high as 0.16 $cm^2V^{-1}s^{-1}$ was achieved from **FCPDT-C16** by simple solution processing.

5.4 Experiments

5.4.1 General experimental methods

All reagents were purchased from commercial sources and used without further purification. Anhydrous dichloromethane (DCM) and *N*,*N*-dimethylformaldehyde were distilled from CaH_2. Anhydrous toluene and THF were distilled from sodium benzophenone immediately prior to use. The ^1H NMR and ^{13}C NMR spectra were recorded in solution of $CDCl_3$ on Bruker DRX 500 NMR spectrometer with tetramethylsilane (TMS) as the internal standard. Abbreviations for signal coupling are as follows: s, singlet; d, doublet; t, triplet; q, quartet; m, multiplet; br, broad. High-resolution (HR) MALDI-TOFmass spectra were recorded on a Bruker Autoflex instrument. HR ACPI mass spectra were recorded on a MicrOTOF-QII instrument. The device fabrication is as following: The SiO_2/Si substrate was cleaned with acetone and isopropanol, and then immersed in a piranha solution for 8 minutes. Followed by rinsing with deionized water, and then treated with octadecyltrimethoxysilane (OTMS) spin coated from 10 mM trichloroethylene solution, and treated with ammonia vapor for 7h, or octadecyltrichlorosilane (ODTS) immersed in 3 mM hexadecane solution for 16h in N_2.

5.4.2 Detailed synthetic procedures and characterization data

Compound 5-3 (R = 2-hexyldecyl)

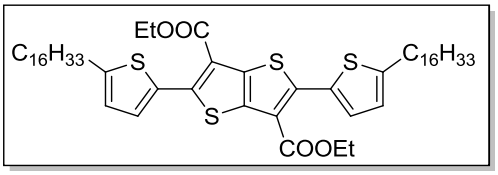

A mixture of compounds **5-1** (706 mg, 2.00 mmol), **5-2** (R = 2-hexyldecyl) (4.78 g, 8.00 mmol) and catalyst $Pd(PPh_3)_2Cl_2$ (231 mg, 5 mol%) in anhydrous DMF (2 mL) and toluene (10 mL) was degassed by three freeze–pump–thaw cycles. The mixture was heated at reflux under argon overnight. The mixture was cooled to room temperature and extracted with $CHCl_3$ (30 mL × 2). The combined organic phase was washed with 10% HCl (50 mL × 1) and brine (50 mL × 1). The organic phase was dried over anhydrous Na_2SO_4 and the solvent was removed under reduced pressure. The crude product was purified by column chromatography (silica gel, hexane: DCM = 8:1) to afford compound **5-3** (1.50 g) as yellow orange oil in 84% yield. ^{1}H NMR (500 MHz, $CDCl_3$, ppm): δ = 7.43 (d, *J* = 6.0 Hz , 2H), 6.76 (d, *J* = 6.0 Hz ,2H), 4.40 (q, *J* = 12.0 Hz, 4H), 2.78 (d, *J* = 11.0 Hz , 4H), 1.42 (t, *J* = 12.0 Hz , 6H), 1.31-1.27 (m, 50H), 0.91-0.85 (m, 12H). ^{13}C NMR (125 MHz, $CDCl_3$, ppm): δ = 161.98, 148.41, 146.91, 136.71, 131.63, 129.70, 125.55, 118.78, 61.19, 40.00, 34.67, 34.63, 33.24, 31.91, 31.88, 31.58, 29.96, 29.62, 29.32, 26.60, 26.58, 22.68, 22.66, 22.64, 14.28, 14.09. HR MALDI_TOF MS: calcd for $C_{52}H_{80}O_4S_4$ (M^+), 896.4939; found, 896.4934 (error: -0.56 ppm).

Compound 5-3 (R = 2-decyltetradecyl)

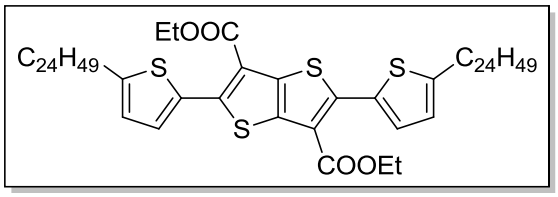

Yellow orange oil, 84% yield.

^{1}H NMR (500 MHz, $CDCl_3$, ppm): δ = 7.42 (d, *J* = 6.3Hz, 2H), 6.76 (d, *J* = 6.3 Hz, 2H), 4.40 (q, *J* = 12.0 Hz, 4H), 2.78 (d, *J* = 11.0 Hz, 4H), 1.41 (t, *J* = 11.8 Hz, 6H), 1.31-1.26 (m, 82H), 0.90-0.85 (m, 12H). ^{13}C NMR (125 MHz, $CDCl_3$, ppm): δ = 162.00, 148.44, 146.92, 136.72, 131.63, 129.70, 125.56, 118.78, 61.20, 40.00, 34.65, 33.24, 31.93, 29.98, 29.70, 29.68, 29.63, 29.36, 26.62, 22.69, 22.67. HR MALDI-TOF MS: calcd for $C_{68}H_{112}O_4S_4$ (M^+), 1120.7443; found, 1120.7438 (error: -0.45 ppm).

Compound 5-4 (R = 2-hexyldecyl)

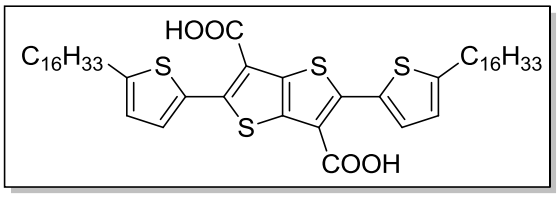

Compound **5-3** (R = 2-hexyldecyl) (897 mg, 1.0 mmol) was dissolved in methanol and THF (30 mL, 1:1 v/v), followed by the addition of sodium hydroxide (400 mg). This mixture was heated at reflux overnight. During this period the orange solid was formed. The solvent was removed under reduced pressure after the reaction was finished. To the residue then concentrated hydrochloric acid was added. The precipitate formed was collected by

filtration and washed with water and a little amount of DCM, then dried in vacuo to afford product **5-4** as a yellow orange sticky solid (800 mg, 95%). The material is carried forward without further purification and characterization.

Compound 5-4 (R = 2-decyltetradecyl)

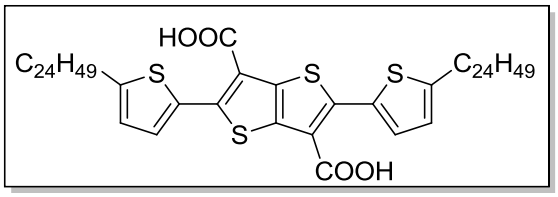

Yellow orange sticky solid 92% yield.

Compound 5-5 (R = 2-hexyldecyl)

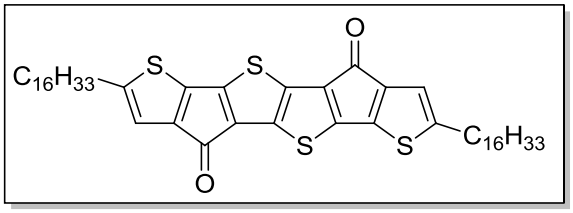

Compound **5-4** (R = 2-hexyldecyl) (1.68 g, 2.00 mmol) was dissolved in anhydrous DCM (20 mL), followed by the addition of thionyl chloride (952 mg, 8.00 mmol). To this mixture anhydrous DMF (1-2 drops) was added at room temperature. The resultant mixture was heated at reflux overnight. The solvent was removed under reduced pressure to afford crude acid chloride. This intermediate compound was dissolved in anhydrous DCM (20 mL) then anhydrous $AlCl_3$ (1.067 g, 8.00 mmol) was added carefully at 0 ℃. The resultant mixture was allowed to warm up to room temperature and stirred

overnight, then slowly quenched by 10% HCl solution, extracted with $CHCl_3$ (30 mL × 2). The combined organic phase was washed with 10% HCl (50 mL × 1) and brine (50 mL × 1). The organic phase was dried over anhydrous Na_2SO_4 and the solvent was removed under reduced pressure. The crude product was purified by column chromatography (silica gel, hexane: DCM = 5:1) to afford compound **5-5** (R = 2-hexyldecyl) (564 mg) as a dark blue solid in 35% yield. ^{1}H NMR (500 MHz, $CDCl_3$, ppm): δ = 6.62 (s, 2H), 2.65 (d, *J* = 6.3Hz, 4H), 1.28-1.26 (m, 50H), 0.90-0.86 (m, 12H). ^{13}C NMR (125 MHz, $CDCl_3$, ppm): δ = 181.02, 151.03, 148.25, 146.97, 140.80, 134.67, 131.32, 119.53, 39.90, 34.77, 33.05, 31.91, 29.93, 29.71, 29.69, 29.67, 29.65, 29.37, 26.60, 22.68, 14.09. HR APCI MS: calcd for $C_{48}H_{68}O_2S_4$ (M^+), 804.4102; found, 804.4108 (error: 0.75 ppm).

Compound 5-5 (R = 2-decytetradecyl)

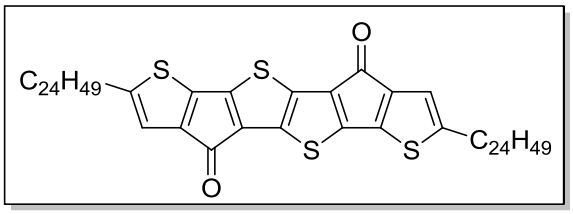

^{1}H NMR (500 MHz, $CDCl_3$, ppm): δ = 6.64 (s, 2H), 2.66 (d, *J* = 7.0 Hz, 4H), 1.28-1.25 (m, 82H), 0.89-0.86(m, 12H). ^{13}C NMR (125 MHz, $CDCl_3$, ppm): δ = 181.44, 151.19, 148.42, 147.06, 140.88, 134.70, 131.45, 119.64, 39.92, 34.82, 33.07, 31.91, 29.90, 29.68, 29.65, 29.64, 29.35, 26.60, 22.68, 14.10. HR APCI MS: calcd for $C_{64}H_{100}O_2S_4$ (M^+), 1028.6606; found, 1028.6612

(error: 0.58 ppm).

Compound FCPDT-C16

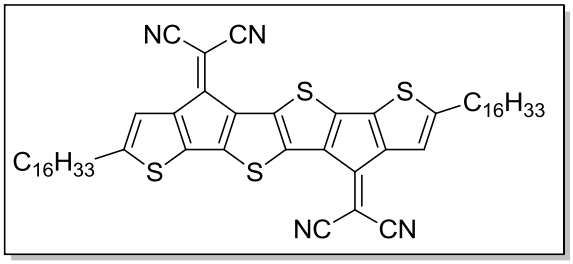

Compound **5-5** (R = 2-hexyldecyl) (403 mg, 0.50 mmol) and malononitrile (0.13 mL, 2.00 mmol) were dissolved in chlorobenzene (10 mL) under nitrogen atmosphere and then $TiCl_4$ (0.23 mL, 2.00 mmol) and pyridine (0.33 mL, 4.00 mmol) were slowly added at 0 ℃. The reaction mixture was allowed to warm up to room temperature and stirred overnight. After adding methanol (10 mL) the crude compound formed as a green precipitate. This crude product was further purified by column chromatography (silica gel, DCM) to give a green solid (305 mg, 68%). ^{1}H NMR (500 MHz, $CDCl_3$, ppm): δ = 7.04 (s, 2H), 2.72 (d, *J* = 11.2 Hz, 4H), 1.28-1.26 (m, 50H), 0.90-0.86 (m, 12H). ^{13}C NMR (125 MHz, $CDCl_3$, ppm): δ = 153.28, 150.38, 148.58, 142.82, 140.63, 135.97, 129.61, 121.68, 113.66, 112.47, 39.91, 35.15, 33.12, 31.90, 31.85, 29.95, 29.60, 29.31, 26.55, 26.51, 22.67, 22.66, 14.11, 14.08. HR APCI MS: calcd for $C_{54}H_{68}N_4S_4$ (M^+), 900.4327; found, 900.4332 (error: 0.56 ppm).

Compound FCPDT-C24

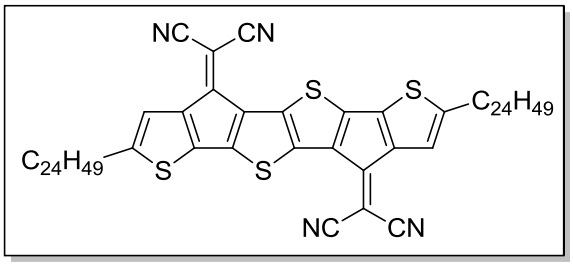

^{1}H NMR (500 MHz, $CDCl_3$, ppm): δ = 7.05 (s, 2H), 2.71 (d, *J* = 11.2 Hz, 4H), 1.27-1.26 (m, 82H), 0.90-0.85 (m, 12H). ^{13}C NMR (125 MHz, $CDCl_3$, ppm): δ = 153.59, 150.18, 148.62, 142.85, 140.60, 135.99, 129.71, 121.67, 113.71, 112.53, 39.91, 35.14, 33.08, 31.92, 29.93, 29.70, 29.67, 29.64, 29.37, 29.35, 26.54, 22.68, 14.11. HR APCI MS: calcd for $C_{70}H_{100}N_4S_4$ (M^+), 1124.6831; found, 1124.6836 (error: 0.44 ppm).

References

[1] For recent reviews, see: (a) M. Bendikov, F. Wudl and D. F. Perepichka, *Chem. Rev.*, 2004, **104**, 4891. (b) J. Wu, *Curr. Org. Chem.*, 2007, **11**, 1220. (c) C. Wang, H. Dong, W. Hu, Y. Liu and D. Zhu, *Chem. Rev.*, 2012, **112**, 2208. (d) Z. Sun, Q. Ye, C. Chi and J. Wu, *Chem. Soc. Rev.*, 2012, **41**, 7857.

[2] (a) J. Zaumseil and H. Sirringhaus, *Chem. Rev*., 2007, **107**, 1296. (b) H. Usta, A. Facchetti and T. J. Marks, *Acc. Chem. Res.*, 2007, **44**, 501. (c) H. Dong, C. Wang and W. Hu, *Chem. Commun.*, 2010, **46**, 5211. (d) C. Wang, H. Dong, W. Hu, Y. Liu, D. Zhu, *Chem. Rev*. 2012, **112**, 2208.

[3] (a) Z. Bao, A. J. Lovinger and J. Brown, *J. Am. Chem. Soc.*, 1998, **120**, 207. (b) H. E. Katz, A. J. Lovinger, J. C. Kloc, T. Siegrist, W. Li., Y. Lin and A.

Dodabalapur, *Nature*, 2000, **404**, 478. (c) M. Yoon, A. Facchetti, C. Stern and T. J. Marks, *J. Am. Chem. Soc.*, 2006, **128**, 5792. (d) Y. Sakamoto, T. Suzuki, M. Kobayashi, Y. Gao, Y. Fukai, Y. Inoue and S. Tokito, *J. Am. Chem. Soc.*, 2004, **126**, 8138. (e) B. A. Jones, M. J. Ahrens, M. Yoon, A. Facchetti and T. J. Marks, *Angew. Chem. Int. Ed.*, 2004, **43**, 6363. (f) X. Gao, C. Di, Y. Hu, X. Yang, H. Fan, F. Zhang, Y. Liu, H. Li and D. Zhu, *J. Am. Chem. Soc.*, 2010, **132**, 3697. (g) H. Qu, W. Cui, J. Li, J. Shao and C. Chi, *Org. Lett.*, 2011, **13**, 924. (h) J. Chang, Q. Ye, K.-W. Huang, J. Zhang, Z. Chen, J. Wu and C. Chi, *Org. Lett.*, 2012, **14**, 2964. (i) Q. Ye, J. Chang, K.-W. Huang, X. Shi, J. Wu and C. Chi, *Org. Lett.*, 2013, **15**, 1194. (j) Q. Ye, J. Chang, K.-W. Huang, C. Chi, *Org. Lett*. 2011, **13**, 5960.

[4] (a) S. Ando, R. Murakami, J. Nishida, Y. Inoue, S. Tokito and Y. Yamashita, *J. Am. Chem. Soc.,* 2005, **127**, 14996. (b) Naraso; J. Nishida, D. Kumaki, S. Tokito and Y. Yamashita, *J. Am. Chem. Soc.*, 2006, **128**, 9598. (c) Y. Liu, C. Song, W. Zeng, K. Zhou, Z. Shi, C. Ma, F. Yang, H. Zhang and X. Gong, *J. Am. Chem. Soc.*, 2010, **132**, 16349. (d) Z. Liang, Q. Tang, R. Mao, D. Liu, J. Xu and Q. Miao, *Adv. Mater.*, 2011, **23**, 5514. (e) O. Tverskoy, F. Rominger, A. Peters, H. J. Himmel and U. H. F. Bunz, *Angew. Chem. Int. Ed.*, 2011, **50**, 3557. (f) C. Tong, W. Zhao, J. Luo, H. Mao, W. Chen, H. Chan and C. Chi, *Org. Lett.*, 2012, **14**, 494. (g) J. Shao, J. Chang, C. Chi, *Org. Biomol. Chem*., 2012, **10**, 7045.

[5] (a) E. Menard, V. Podzorov, S. H. Hur, A. Gaur, M. E. Gershenson and J. A.

Rogers, *Adv. Mater.*, 2004, **16**, 2097. (b) R. J. Chesterfield, C. R. Newman, T. M. Pappenfus, P. C. Ewbank, M. H. Haukaas, K. R. Mann, L. L. Miller and C. D. Frisbie, *Adv. Mater.,* 2003, **15**, 1278. (c) S. Handa, E. Miyazaki, K. Takimiya and Y. Kunugi, *J. Am. Chem. Soc.*, 2007, **129**, 11684.

[6] (a) H. Usta, A. Facchetti and T. J. Marks, *J. Am. Chem. Soc.*, 2008, **130**, 8580. (b) H. Usta, C. Risko, Z. Wang, H. Huang, M. K. Deliomeroglu, A. Zhukhovitskiy, A. Facchetti and T. J. Marks, *J. Am. Chem. Soc.*, 2009, **131**, 5586.

[7] R. P. Ortiz, A. Facchetti, T. J. Marks, J. Casado, M. Z. Zgierski, M. Kozaki, V. Hernandez and J. T. L. Navarrete, *Adv. Funct. Mater.*, 2009, **19**, 386.

[8] S. Ellinger, U. Ziener, U. Thewalt, K. Landfester and M. Möller, *Chem. Mater.*, 2007, **19**, 1070.

[9] T. Kunz and P. Knochel, *Chem. Eur. J.*, 2011, **17**, 866.

Chapter 6: Dipolar Quinoidal Acene Analogues as Stable Isoelectronic Structures of Pentacene and Nonacene

6.1 Introduction

Functionalized acenes/heteroacenes have been demonstrated to be good active materials in organic electronics.[1] However, the lack of efficient synthetic method and the unstable nature of longer acenes/heteroacenes limit their potential applications. Typical decomposition pathways of longer acenes/heteroacenes involve: 1) addition with singlet oxygen to form endoperoxide[2] and further oxidation to the corresponding quinone;[3] 2) Diels-Alder reaction with dienophiles (e.g. alkyne substituents) or [4+4] cycloaddition of the acene backbone.[4] In addition, the solubility issue should be also addressed to obtain characterisable and processible materials. Chemists have developed various strategies to stabilize and solubilize acenes/heteroacenes including: 1) substitution with bulky aryl and silylethynyl groups;[5] 2) substitution with electron-deficient carboximide, fluorine and cyano groups;[6] 3) incorporation of imine-type nitrogen atoms to the backbone;[7] and 4) annulation of cyclopenta-moieties along the zig-zag edges.[8]

Our group has a longstanding interest in acenes/heteroacenes chemistry,[9] and recently we developed a new type of quinoidally conjugated dithia-acenes (e.g., 5,12-dithiapentacene, **Figure 6.1**) which displayed remarkable stability and distinctive electronic properties.[10] The switching from a *cis*-1,3-butadiene

conjugation to a quinoidal conjugation eliminates the possible cycloaddition reactions and at the same time increases the benzenoid character by releasing one additional aromatic sextet ring (highlighted in blue color, **Figure 6.1**), and thus improves the stability and dramatically changes the ground-state electronic structure. It is believed that this concept can be further extended to longer acenes such as highly reactive nonacene which was predicted to have an open-shell singlet diradical ground state (**Figure 6.1**).[11] However, by counting two lone-pair electrons for each sulfur atom, these quinoidal dithia-acenes possess two more π electrons than the corresponding acene derivatives (e.g., 24 πe for 5,12-dithiapentacene while 22 πe for pentacene, **Figure 6.1**). Hence, we became interested in a new type of quinoidal thia-acenes such as A-C by removing one sulfur atom (thus 2 πe) per each *p*-quinodimethane (*p*-QDM) unit and the obtained structures now can be regarded as the isoelectronic structures of the respective acenes (**Figure 6.1**). They are better described as "acene-like molecules" rather than "acenes" because of existence of more than one aromatic sextet rings. Besides the closed-shell quinoidal structure, one open-shell diradical resonance form and one dipolar zwitterionic resonance form are also supposed to contribute to the ground-state structure due to the recovery of one more aromatic sextet ring (**Figure 6.1**). In this chapter, we started to investigate the chemistry, structure and physical properties of the derivatives of A (isoelectronic pentacene) and B (isoelectronic nonacene), **1** and **2**, respectively, and compare them with the

corresponding acenes such as **4** and reported nonacene derivatives.[2b] Bulky mesityl substituents are attached at the methylene site of the *p*-QDM moiety which can stabilze the possible diradical structure. However, instead of the target compound **2**, an isomer **3** was obtained *via* an unusual 1,2-sulfur migration process, which also serves as a good isoelectronic structure of nonacene.

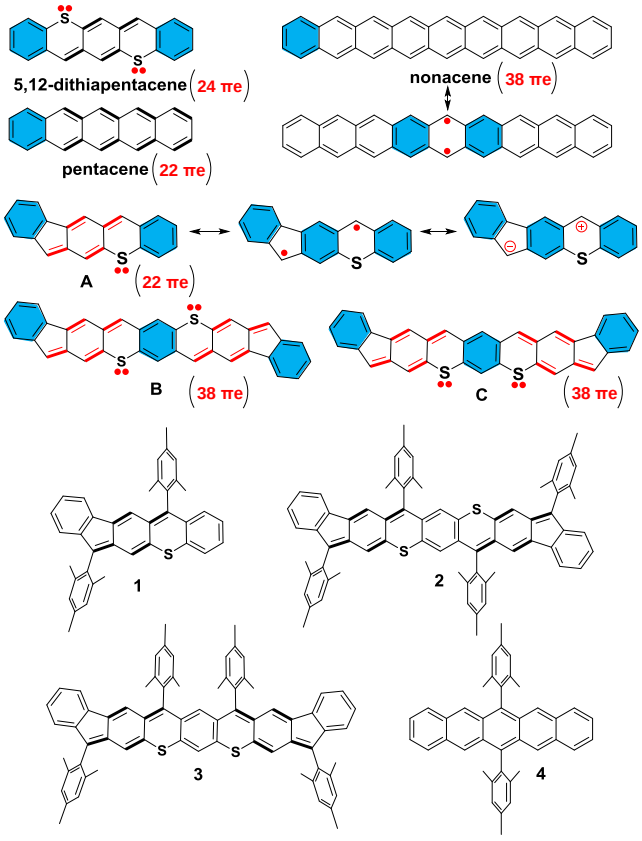

Figure 6.1 Structures of 5,12-dithiapentacene, pentacene, nonacene, and their quinoidal thia-acenes isoelectronic structures.

6.2 Results and discussion

6.2.1 Synthesis

The synthesis of **1-3** was based on an intramolecular Friedel-Crafts-alkylation-followed-by-dehydrogenation strategy (**Scheme 6.1**).

Suzuki coupling between the dibromo- diketone **6-1** and one equivalent of phenylboronic acid gave the key intermediate **6-2** and subsequent nucleophilic substitution with thiophenol in the presence of CuI and K_2CO_3 afforded the asymmetric diketone **6-3**. Reduction of **6-3** gave the diol **6-4** and subsequent BF_3•Et_2O mediated Friedel-Crafts alkylation generated the dihydro-compound **6-5** and finally the target product **1** was obtained by oxidative dehydrogenation by *p*-chloranil in refluxing toluene. Following a similar protocol, reaction between **6-2** and benzene-1,4-dithiol failed to give the desired tetraketone **6-6**. Alternatively, Pd-catalyzed C-S coupling afforded **6-6** in 65% yield. After a similar reduction-Friedel-Crafts-alkylation-dehydrogenation sequence from **6-6**, surprisingly, the *meta*-dithia- isomer **3** instead of the *para*-dithia- compound **2** was obtained in 50% yield over three steps as confirmed by X-ray crystallographic analysis (*vide infra*). The structure of the tetraketone **6-6** was also identified by X-ray crystallographic analysis[12], and re-arrangement reaction likely will not happen during the reduction (with $LiAlH_4$) and oxidative dehydrogenation (with *p*-chloranil) steps. Therefore, the formation of *meta*-dithia compound is likely due to 1,2-sulfur migration *via* a spirocyclic cationic intermediate during the ring cyclization reaction in the presence of BF_3•Et_2O (**Scheme 6.1**).[13] However, the main driving force for this particular migration and the reason for the exclusive generation of **3** rather than the proposed **2** are not clear at this stage. For comparison, the 6,13-dimesityl

pentacene **4** was synthesized according to a published procedure with minor modification.[3a]

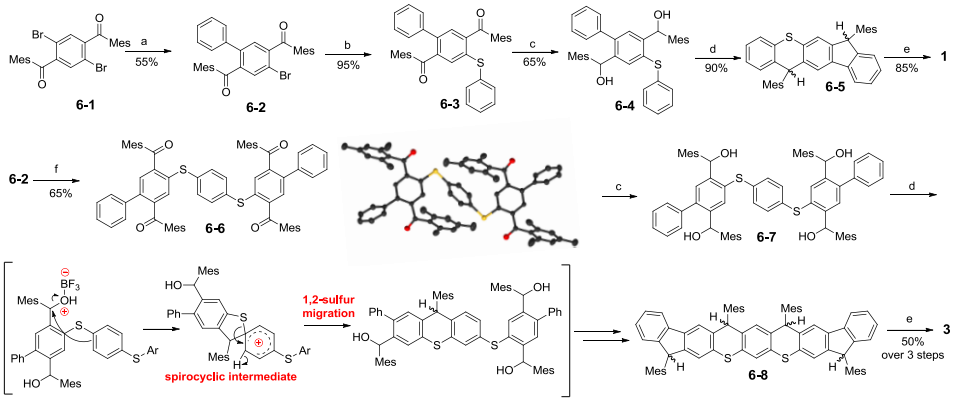

Scheme 6.1 Synthetic route to compound **1** and **3**. *Reagents and conditions*: (a) phenylboronic acid, $Pd(PPh_3)_4$, Na_2CO_3, toluene/water (5:1), 100 ^oC, overnight; (b) thiophenol, CuI, K_2CO_3, DMF, 100 ^oC, overnight; (c) $LiAlH_4$, dry THF, for **6-4**: 0 ^oC – rt. overnight; for **6-7**, 0 ^oC - rt. - 50 ^oC overnight; (d) $BF_3{\cdot}Et_2O$, dry DCM, 0 ^oC - rt., 3 h; (e) *p*-chloranil, toluene, reflux, 5d; (f) benzene-1,4-dithiol, $Pd_2(dba)_3$, dppf, *i*-Pr_2NEt, DMF, 100 ^oC, overnight. Mes: mesityl.

6.2.2 Photophysical and electrochemical properties

1 and **3** are extremely stable in air, in contrast to their corresponding reactive pentacene (such as **4**) and nonacene derivatives.[2b] Compound **1** displays distinctly different absorption spectrum from that of **4** in dichloromethane (DCM), with an intense absorption band at 360 nm and a broad band at 650 nm extending to 900 nm (**Figure 6.2a**). Time-dependent density functional theory (TD DFT) calculations (B3LYP/6-31G*) indicated that the longest-wavelength absorption band is originated from HOMO→LUMO transition (λ_{max} = 677.7 nm, oscillator strength f = 0.1940,). In contrast, the pentacene derivative **4** shows a well-resolved *p*-band with a

maximum at 601 nm. Compound **3** exhibits a similar band structure to that of **1**, but both bands are red-shifted (by 44 nm for the longest absorption band), consistent with an extension of electron delocalization, and in agreement with the TD DFT calculations (λ_{max} = 728.6 nm, f = 0.9865). The corresponding nonacene derivatives show a weak *p*-band with absorption maximum shifted beyond 1000 nm.[2b] The optical energy gap (E_g^{opt}) was determined as 1.34, 1.28 and 2.02 eV for **1**, **3** and **4**, respectively, from the onset of the lowest energy absorption. It was hypothesized that the long-wavelength broad absorption band is attributed to the intramolecular charge-transfer (ICT) and thus the absorption spectra of **1** and **3** have been studied in different solvents (**Figure 6.2c,d**). However, it is found that the positions of the absorption peak for both compounds are almost independent on solvent polarity, indicating that there are only weak ICT in this system. No emission can be observed from molecules **1** and **3**. The HOMO and LUMO profiles of **1** and **3** indeed show some disjoint characters compared to that of **4**, resulting in a significant dipole moment of 3.1436 D and 2.8714 D, respectively (**Figure 6.3**). The broadened and red-shifted absorption bands in **1** and **3** are thus better ascribed to a weak intramolecular donor-acceptor interaction in a quinoidally conjugated skeleton.

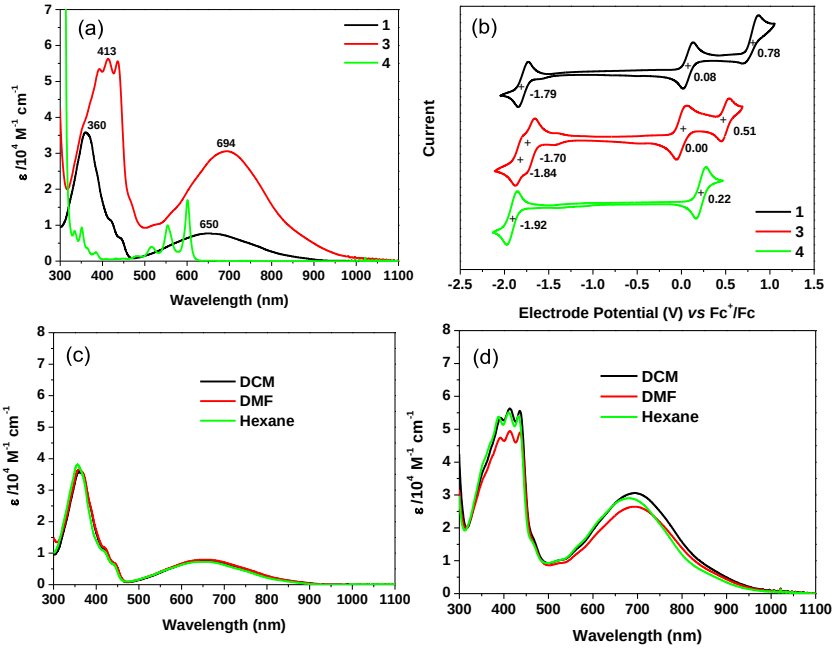

Figure 6.2 (a) UV-vis-NIR absorption spectra of **1**, **3** and **4** recorded in dichloromethane. (b) Cyclic voltammograms of **1**, **3** and **4** in DCM with 0.1 M Bu_4NPF_6 as supporting electrolyte, Ag/AgCl as reference electrode, Pt wire as counter electrode, and scan rate at 50 mV/s. Fc: ferrocene. The electrode potential was externally calibrated by Fc^+/Fc couple. (c) and (d) UV-vis-NIR absorption spectra of **1** and **3** in solvents with different polarity.

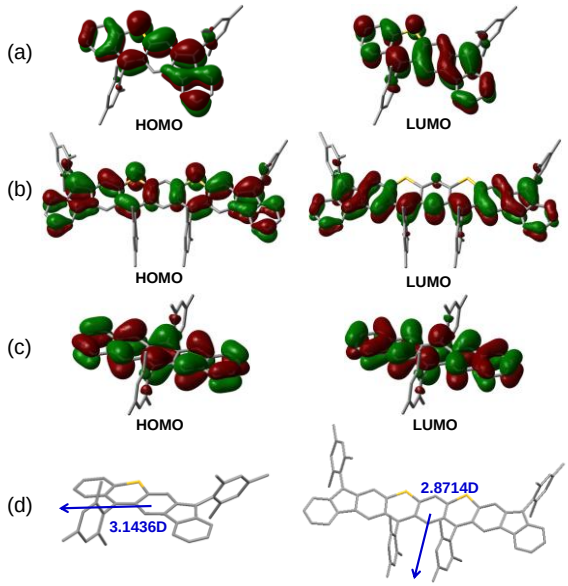

Figure 6.3 Calculated (B3LYP/6-31G*) frontier molecular orbital profiles and energy levels of **1** (a), **3** (b) and **4** (c), and the dipoles of **1** and **3** (d).

Compounds **1** and **3** display excellent amphoteric redox behavior with one or two reversible reduction waves (half-wave potential $E_{1/2}^{red}$ = -1.79 for **1** and -1.84, -1.70 V for **3**, *vs* Fc^{+}/Fc) and two reversible oxidation waves (half-wave potential $E_{1/2}^{ox}$ = -0.08, 0.78 V for **1** and 0.00, 0.51 V for **3**) (**Figure 6.2b**). For comparison, compound **4** exhibits one reversible oxidation wave ($E_{1/2}^{ox}$ = 0.22 V) and one reversible reduction wave ($E_{1/2}^{red}$ = -1.92 V). The HOMO and LUMO energy levels were estimated to be -4.79, -4.72, -4.94 eV and -3.10, -3.20, -2.96 eV for **1**, **3**, and **4**, respectively. The electrochemical energy gap (E_g^{EC}) was thus determined to be 1.69, 1.52 and 1.98 eV for **1**, **3**, and **4**, respectively. The high-lying HOMO energy levels allow us to access the radical cations of **1**, **3** and **4** by oxidative titration with $SbCl_5$ in DCM, and characteristic absorption bands at 419, 638, 974 nm for $\mathbf{1}^{+\bullet}$, 453, 835, 1071, 1224 nm for $\mathbf{3}^{+\bullet}$, and 430, 835, 943, 1195 nm for $\mathbf{4}^{+\bullet}$, were observed (**Figure 6.4**).

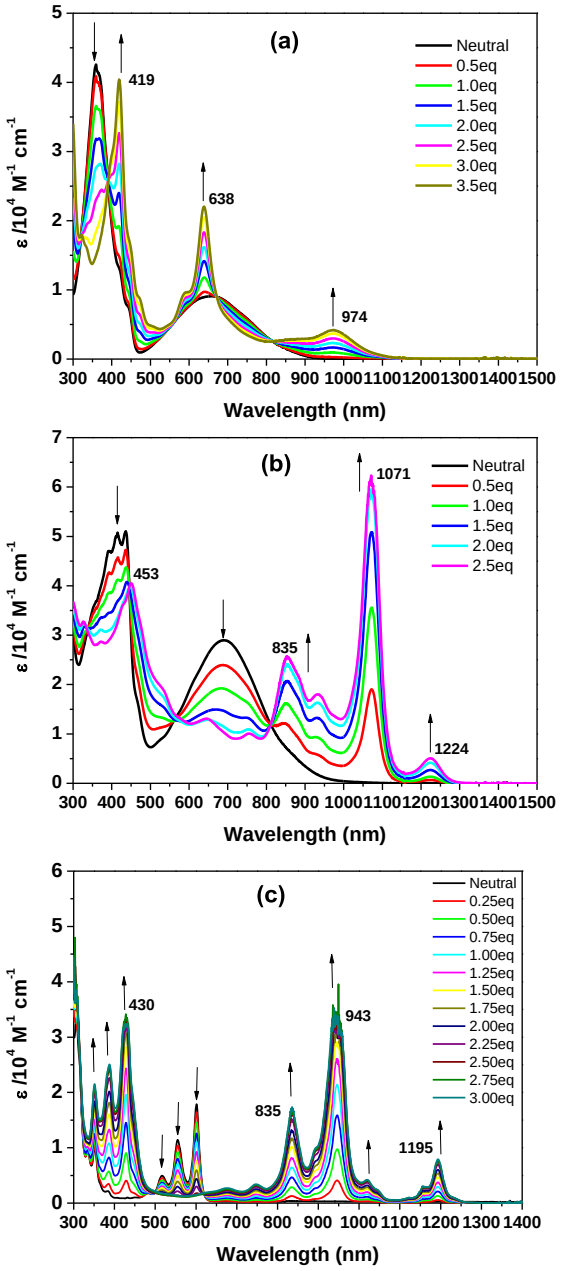

Figure 6.4 Titration with SbCl5 in dry DCM: absorption spectra change from neutral to radical cation for (a) **1**, (b) **3** and (c) **4**. The arrows show the changes of the spectra during the oxidation titration.

6.2.3 Ground-state geometry and electronic structures

Single crystals of **1**, **3** and **4** suitable for X-ray crystallography analysis were successfully grown and analyzed and the ORTEP drawings and 3D packing structures are shown in **Figure 6.5**.[14] The solid state packing of **1** is

highly symmetric (tetragonal; space group $I4_1/a$), even though the molecule itself is asymmetric. The backbone of **1** is essentially planar, with the two mesityl groups oriented almost perpendicularly (torsion angle = 65^o, 88^o) to the backbone. This disrupts the regular π-stacking or herringbone arrangements observed in common acenes/heteroacenes derivatives. Alternatively, molecules of **1** are packed into a square-like tetrameric structure *via* intermolecular dipole-dipole interactions and [C-H•••π] interactions (2.692/2.895 Å) between the methyl groups of one molecule to the π-backbone of another molecule. Such tetrameric structures are further packed into a highly symmetric 3D structure *via* dipole-dipole interactions. No close [S•••S] interaction was observed. In comparison, **3** crystalizes in a triclinic lattice system, with space group P1. One toluene molecule per molecule is incorporated into the crystal lattice. The backbone of **3** is slightly distorted, with the four mesityl rings oriented almost perpendicularly (torsion angle = 71^o, 69^o, 87^o, 82^o) to the backbone. Interestingly, **3** packs in a slipped face-to-face manner mainly *via* [C-H•••S] interactions (2.895/2.994 Å) between one methyl group in one molecule with sulfur atom in the neighboring molecule and [C-H•••π] interactions (2.744/2.780 Å) between methyl groups of one molecule and the π-backbone of another molecule. These interactions suppress the normally observed anti-parallel dipole-dipole interaction in a dipolar molecule. Compound **4** has a slightly distorted backbone with the mesityl groups nearly perpendicular (torsion angle = 78^o) to

the backbone. Due to the bulky substituent, no close π-π interaction was observed. The molecules are packed into a compact structure with tetragonal symmetry, space group $I4_1/a$, mainly *via* intermolecular [C-H•••π] interactions.

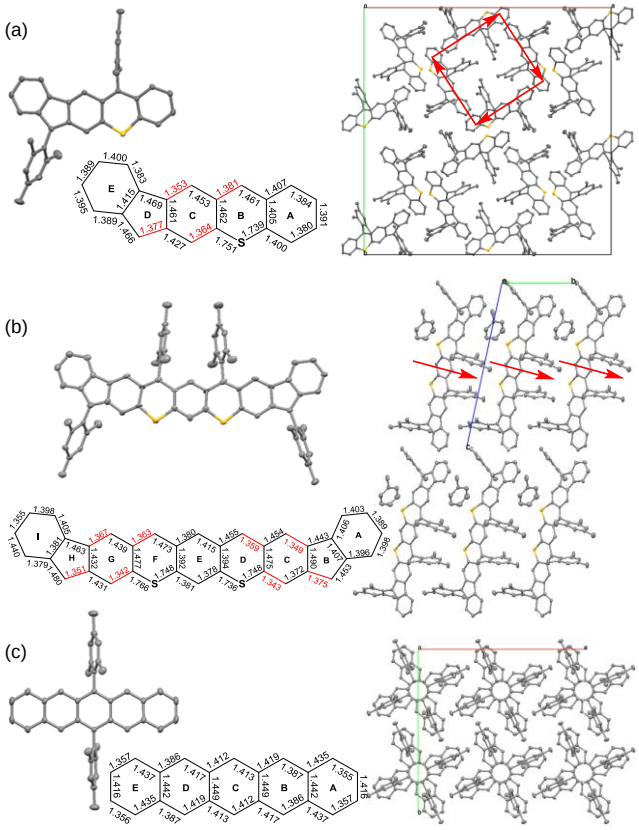

Figure 6.5. X-ray crystallographic structures and 3D packing of **1** (a), **3** (b) and **4** (c), and bond lengths of the π-conjugated core frameworks. Hydrogen atoms are omitted for clarity. The arrows roughly denote the dipole moments.

As mentioned above, dipolar quinoidal polycyclic hydrocarbons could exhibit unique singlet diradical and zwitterionic character and diminished bond length alternation (BLA).[15] Hence, bond length analysis was performed to analyze the ground-state geometry of **1** and **3**, in comparison to that of **4** (**Figure 6.5**). As observed, the central ring C of **1** displays noticeable BLA, indicating a significant quinoidal conjugation. The two terminal rings A and E possess relatively constant bond lengths, implying their large aromatic

character. Similarly, rings C and G of **3** also show large BLA, while the central ring E and the two terminal rings A and I possess relatively constant bond lengths. This confirms that both **1** and **3** have a quinoidal structure in their ground state and have little contribution from the diradical and dipolar zwitterionic resonance forms, which is in well agreement with the UV-vis-NIR absorption spectra in different solvents and DFT calculations. For comparison, the BLA of **4** exhibits a typical diene conjugation motif.

6.3 Conclusion

In summary, two quinoidal thia-acenes **1** and **3** as isoelectronic structures of pentacene and nonacene were successfully prepared and an unusual 1,2-sulfur migration was discovered during the synthesis. The ground-state geometry and electronic properties of **1** and **3** were systematically investigated both experimentally and theoretically. Compounds **1** and **3** show excellent solubility and stability and distinctively different absorption spectra compared to their acene counterparts, which can be explained by their unique dipolar quinoidal structure. No typical π-stacking or herringbone arrangement is observed in the crystalline form of both compounds due to the bulky mesityl substituents. However, a balance between the dipole-dipole interaction and intermolecular [C-H•••π]/ [C-H•••S] interaction result in unique packing structures in solid state. All experimental data and theoretical calculation point to the same conclusion that both **1** and **3** have a typically closed-shell quinoidal structure in their ground state with a small diradical or

bipolar/zwitterionic character. This work again demonstrated the efficiency of the "quinoidal acene" concept and will shed light on the synthesis of stable higher order acenes and heteroacenes in the future.

6.4 Experiments

6.4.1 *General experimental methods*

Refer to the section of *2.4.1 General experimental methods* in chapter 2.

6.4.2 Detailed synthetic procedures and characterization data

Compound 6-1

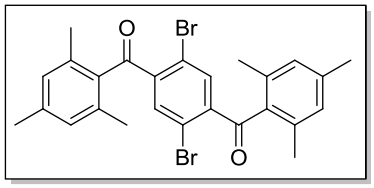

2,5-dibromoterephthalic acid (2.00 g, 6.2 mmol) was added to anhydrous DCM (40 mL), followed by the addition of DMF (2 drops) and excess $SOCl_2$ (3.0 mL). The resultant white suspension was refluxed under argon atmosphere overnight until all solids had dissolved to give a clear yellow solution. After cooling to room temperature, the solvent was removed via rotary evaporation and the reaction mixture further dried under vacuum to yield intermediate 2,5-dibromoterephthaloyl chloride as a yellow solid. The intermediate was re-dissolved in anhydrous DCM (40 mL), followed by the addition of mesitylene (4.47 g, 37.2 mmol) and anhydrous $AlCl_3$ (4.10 g, 30.8 mmol) at 0 ^oC. The mixture was warmed to room temperature and then refluxed under argon atmosphere overnight, then cooled to 0 ^oC and quenched with 10% HCl solution. The mixture was extracted with DCM and the organic layer dried over anhydrous Na_2SO_4. The solvent was removed via rotary

evaporation to give a greenish brown residue. The residue was washed with hexane to yield a yellow-white solid as the crude product. The crude product was purified via column chromatography (silica, hexane: DCM, 3:1 v/v) to yield compound **6-1** as a white, floury solid (2.15 g, 65% yield). ^{1}H NMR (500 MHz, $CDCl_3$, ppm): δ = 7.66 (s, 1H), 6.89 (s, 2H), 2.32 (s, 3H), 2.14 (s, 6H); ^{13}C NMR (125 MHz, $CDCl_3$, ppm): δ =197.44, 142.91, 140.52, 136.75, 135.77, 135.43, 129.25, 119.92, 21.22, 20.12. HR MS (EI): calcd for $C_{26}H_{24}Br_2O_2$ (M^+), 526.0143; found, 526.0125 (error: -3.36 ppm).

Compound 6-2

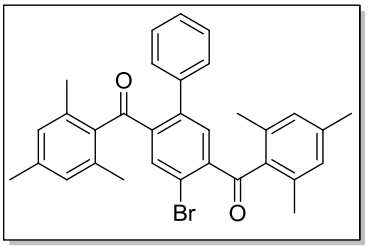

A mixture of compound **6-1** (660 mg, 1.3 mmol), phenylboronic acid (160 mg, 1.3 mmol) $Pd(PPh_3)_4$ (80 mg, 0.07 mmol), and Na_2CO_3 (250 mg, 2.4 mmol) in toluene (35 mL) and H_2O (7 mL) was degassed via three freeze-thaw pump cycles. The mixture was heated at 100 ^{o}C under argon atmosphere overnight, then cooled to room temperature and quenched with 10% HCl solution. The mixture was extracted with DCM, the organic layer dried over anhydrous Na_2SO_4 and the solvent removed via rotary evaporation. The residue was purified via column chromatography (silica, hexane: DCM, 3:1 v/v) to yield compound **6-2** as a light yellow solid (350 mg, 55% yield). ^{1}H NMR (500 MHz, $CDCl_3$, ppm): δ = 7.89 (s, 1H), 7.35 (s, 1H), 7.24-7.17 (m, 3H), 7.11-7.08 (m, 2H), 6.86 (s, 2H), 6.69 (s, 2H), 2.29 (s, 3H), 2.21 (s, 3H), 2.16 (s, 6H), 2.06 (s, 6H); ^{13}C NMR (125 MHz, $CDCl_3$, ppm): δ = 198.71, 198.62, 142.02, 141.99, 141.74, 140.15, 139.86, 138.86, 136.11, 136.02, 135.85, 135.72, 135.54, 133.95, 129.16, 129.09, 128.30, 127.79, 127.56, 120.15, 21.17,

21.01, 20.61, 20.16. HR MS (EI): calcd for $C_{32}H_{29}BrO_2$ (M^+), 524.1351; found, 524.1345 (error: -1.14 ppm).

Compound 6-3

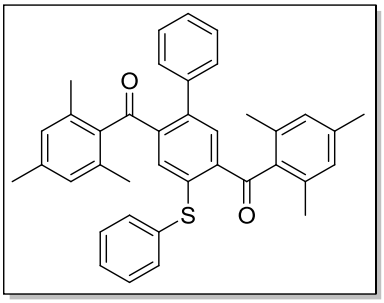

A mixture of compound **6-2** (530 mg, 1.0 mmol), thiophenol (330 mg, 3.0 mmol), CuI (190 mg, 1.0 mmol), and K_2CO_3 (555 mg, 4.0 mmol) in DMF (30 mL) was heated at 100 ^oC under argon atmosphere overnight. After cooling to room temperature, 10% HCl solution was carefully added and the mixture was extracted with EtOAc. The organic layer was dried over anhydrous Na_2SO_4 and the solvent removed via rotary evaporation. The crude product was purified via column chromatography (silica, hexane: DCM, 2:1 v/v) to yield compound **6-3** as a yellow crystalline solid (540 mg, 95% yield). ^1H NMR (500 MHz, $CDCl_3$, ppm): δ = 7.41 (d, J = 7.5 Hz, 2H), 7.35 (s, 1H), 7.33-7.28 (m, 1H), 7.25-7.22 (m, 5H), 7.12-7.10 (m, 2H), 6.88 (s, 1H), 6.85 (s, 2H), 6.56 (s, 2H), 2.28 (s, 3H), 2.23 (s, 3H), 2.15 (s, 6H), 1.89 (s, 6H); ^{13}C NMR (125 MHz, $CDCl_3$, ppm): δ = 200.43, 199.81, 143.64, 140.26, 139.60, 139.14, 138.88, 138.10, 136.37, 136.28, 135.55, 135.02, 134.66, 134.62, 131.70, 130.30, 129.66, 129.22, 128.69, 128.65, 127.86, 127.20, 21.14, 21.06, 19.99, 19.58. HR MS (EI): calcd for $C_{38}H_{34}O_2S$ (M^+), 554.2280; found, 554.2281 (error: 0.18 ppm).

Compound 6-4

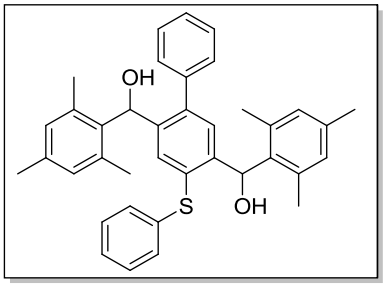

An ethereal solution of $LiAlH_4$ (379 mg, 10 mmol) in anhydrous THF (30 mL) was cooled to 0 ^oC and degassed via three freeze-thaw pump cycles. To the mixture, Compound **6-3** (555 mg, 1.0 mmol) was added in small portions to avoid excessive gas evolution. The reaction mixture was stirred at 0 ^oC for 15 min, then allowed to warm to room temperature and stirred overnight. The mixture was acidified with 10% HCl solution, then filtered to remove all solids. The filtered mixture was extracted with EtOAc, the organic layer was dried over anhydrous Na_2SO_4 and the solvent was removed via rotary evaporation to yield a white solid as the crude product. The crude product was purified via column chromatography (silica, hexane: DCM: EtOAc, 30:15:1 v/v/v) to yield compound **6-4** as two separate diastereomers **6-4a** (195 mg, 33% yield) and **6-4b** (190 mg, 32% yield) (Total: 385 mg, 65% yield). Both diastereomers show similar reactivity and can be used directly (separately or combined) in the next step. Compound **6-4a**: white powder, R_f value: 0.55, ^1H NMR (500 MHz, CD_2Cl_2, ppm): δ = 7.27-7.22 (m, 7H), 7.21-7.18 (m, 2H), 7.15 (s, 1H), 7.13-7.11 (m, 2H), 6.79 (s, 2H), 6.60 (s, 2H), 6.41 (s, 1H), 6.07 (s, 1H), 2.64 (br, 1H), 2.22 (s, 6H), 2.22 (s, 3H), 2.19 (s, 3H), 1.89 (s, 6H), 1.84 (br, 1H); ^{13}C NMR (125 MHz, $CDCl_3$, ppm): δ = 141.46, 140.83, 140.42, 139.75, 137.18, 137.14, 136.65, 136.43, 135.37, 135.02, 134.39, 133.23, 132.30, 131.22, 130.12, 129.89, 129.03, 128.76, 127.94, 127.02, 126.95, 70.69, 70.45, 21.10, 20.91, 20.79, 20.70. HR MS (EI): calcd for $C_{38}H_{38}O_2S$ (M^+),

558.2593; found, 558.2582 (error: -1.97 ppm). Compound **6-4b**: white solid, R_f value: 0.25, ^{1}H NMR (500 MHz, CD_2Cl_2, ppm): δ = 7.27-7.18 (m, 10H), 7.11-7.09 (m, 2H), 6.77 (s, 2H), 6.60 (s, 2H), 6.41 (s, 1H), 6.09 (s, 1H), 2.60 (br, 1H), 2.21 (s, 6H), 2.21 (s, 3H), 2.19 (s, 3H), 1.89 (s, 6H), 1.82 (br, 1H); No ^{13}C NMR spectrum was obtainable due to the poor solubility of compound **6-4b** in $CDCl_3$ and CD_2Cl_2. HR MS (APCI): calcd for $C_{38}H_{38}ClO_2S$ [$(M+Cl)^-$], 593.2287; found, 593.2299 (error: 2.02 ppm).

Compound 6-5

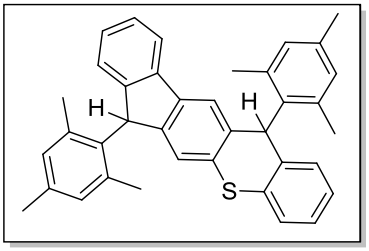

A solution of compound **6-4** (278 mg, 0.5 mmol) in anhydrous DCM (20 mL) was degassed via three freeze-thaw pump cycles. To the mixture, $BF_3{\cdot}Et_2O$ (284 mg, 2 mmol) was added in small portions at 0 ^{o}C under argon atmosphere. The mixture was stirred at 0 ^{o}C for 30 min, then allowed to warm to room temperature and stirred for 3 h. The mixture was cooled to 0 ^{o}C and quenched with H_2O followed by 10% HCl. The mixture was extracted with DCM, the organic layer was dried over anhydrous Na_2SO_4 and the solvent removed via rotary evaporation to yield a colourless oil with brown specks as the crude product. The crude product was purified via flash column chromatography (silica, hexane: DCM 6:1 v/v), to yield compound **6-5** (232 mg, 90% yield) as a pale blue-green flaky solid. The blue-green colour was ascribed to the trace oxidation of compound **6-5** to compound **1** during elution. As such, no clean ^{1}H and ^{13}C NMR spectra were obtainable. HR MS (EI): calcd for $C_{38}H_{34}S$ (M^+), 522.2381; found, 522.2359 (error: -4.21 ppm).

Compound 1

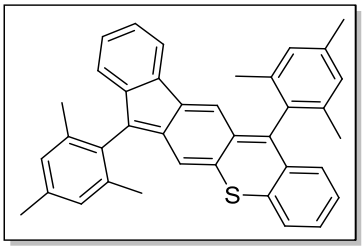

Compound **6-5** (300 mg, 0.6 mmol) was dissolved in toluene (60 mL) followed by the addition of *p*-chloranil (370 mg, 1.5 mmol). The light green-yellow solution was refluxed for 5 d, resulting in the considerable darkening of the solution to dark blue-green. The coloured solution was dried over anhydrous Na_2SO_4 and the solvent was removed via rotary evaporation to yield a dark blue-green residue. The residue was re-dissolved in hexane and purified via flash column chromatography (alumina, hexane: DCM 8:1 v/v) to yield compound **1** (260 mg, 85% yield) as a dark blue-green crystalline solid. ^{1}H NMR (500 MHz, $CDCl_3$, ppm): δ = 7.59 (d, *J* = 7.2 Hz, 1H), 7.27 (m, 1H), 7.24-7.17 (m, 2H), 7.15 (s, 1H), 7.11 (t, *J* = 7.3 Hz, 1H), 7.07 (s, 2H), 7.01 (s, 2H), 7.00-6.93 (m, 2H), 6.79 (d, *J* = 8.2 Hz, 1H), 6.66 (s, 1H), 2.46 (s, 3H), 2.39 (s, 3H), 2.10 (s, 6H), 2.04 (s, 6H); ^{13}C NMR (125 MHz, $CDCl_3$, ppm): δ =144.17, 141.83, 140.70, 137.69, 137.65, 136.96, 136.93, 133.77, 133.50, 133.13, 131.67, 130.72, 130.11, 128.83, 128.57, 128.53, 128.13, 127.81, 126.38, 125.63, 124.65, 123.31, 120.74, 120.34, 119.90, 113.55, 21.25, 21.17, 20.31, 19.93. HR MS (EI): calcd for $C_{38}H_{32}S$ (M^+), 520.2225; found, 520.2224 (error: -0.19 ppm).

Compound 6-6

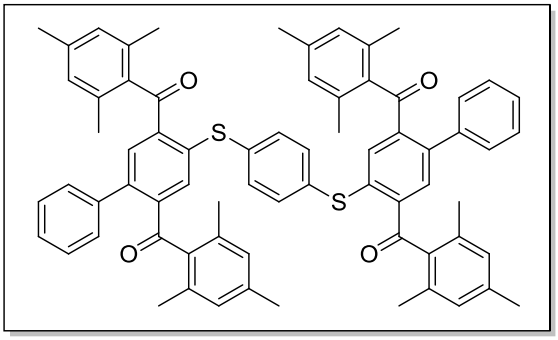

A mixture of compound **6-2** (1051 mg, 2.0 mmol), benzene-1,4-dithiol (142 mg, 1.0 mmol), $Pd_2(dba)_3$ (70 mg, 0.08 mmol), 1,1'-bis(diphenylphosphino)ferrocene (95 mg, 0.17 mmol) and *i*-Pr_2NEt (1.5 mL) in DMF (40 mL) was heated in a sealed tube at 100 ^oC under argon atmosphere overnight. After cooling to room temperature, 10% HCl solution was carefully added and the mixture was extracted with EtOAc. The organic layer was dried over anhydrous Na_2SO_4 and the solvent removed via rotary evaporation. The crude product was purified via column chromatography (silica, hexane: DCM, 4:3 v/v) to yield compound **6-6** as a bright yellow solid (617 mg, 65% yield). ^1H NMR (500 MHz, $CDCl_3$, ppm): δ = 7.42 (s, 2H), 7.30-7.28 (m, 10H), 7.18-7.17 (m, 4H), 6.90 (s, 4H), 6.85 (s, 2H), 6.67 (s, 4H), 2.35 (s, 6H), 2.32 (s, 6H), 2.20 (s, 12H), 1.92 (s, 12H); ^{13}C NMR (125 MHz, $CDCl_3$, ppm): δ = 200.41, 199.55, 142.53, 140.17, 139.49, 139.33, 138.60, 136.41, 136.18, 136.12, 135.83, 135.17, 134.62, 134.60, 133.84, 130.46, 128.78, 128.67, 127.95, 127.32, 21.34, 21.16, 19.96, 19.62. HR MS (APCI): calcd for $C_{70}H_{62}O_4S_2$ (M^-), 1030.4095; found, 1030.4105 (error: 0.97 ppm).

Compound 6-7

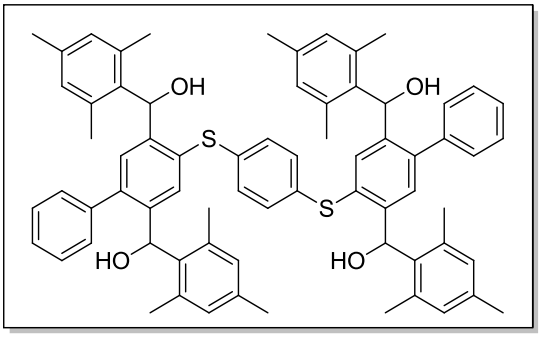

An ethereal solution of $LiAlH_4$ (800 mg, 21.1 mmol) in anhydrous THF (30 mL) was cooled to 0 ^oC and degassed via three freeze-thaw pump cycles. To the mixture, Compound **6-6** (220 mg, 0.21 mmol) was added in small portions to avoid excessive gas evolution. The reaction mixture was allowed to warm to room temperature for 30 mins, then heated at 50 ^oC overnight. After cooling to room temperature, the mixture was quenched with 10% NaOH solution, then filtered to remove all solids. The filtered mixture was extracted with EtOAc, the organic layer was dried over anhydrous Na_2SO_4 and the solvent was removed via rotary evaporation to yield a light yellow solid as the crude product. The crude product **6-7** was used directly for the next step. HR MS (APCI): calcd for $C_{70}H_{70}ClO_4S_2$ $[(M+Cl)^-]$, 1073.4410; found, 1073.4391 (error: -1.77 ppm).

Compound 6-8

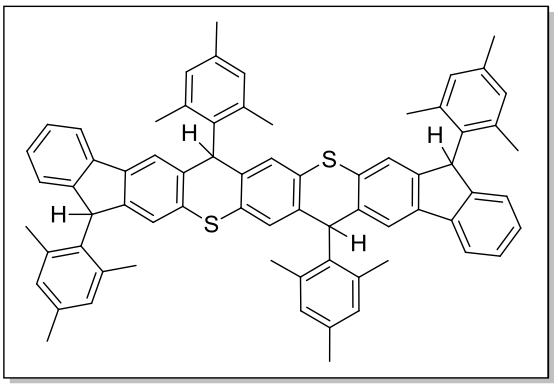

A solution of compound **6-7** (278 mg, 0.5 mmol) in anhydrous DCM (20 mL) was degassed via three freeze-thaw pump cycles. To the mixture, $BF_3{\cdot}Et_2O$ (0.4 mL, xs) was added in small portions at 0 ^oC under argon atmosphere. The mixture was stirred at 0 ^oC for 30 min, then allowed to warm to room temperature and stirred for 3 h. The mixture was cooled to 0 ^oC and quenched with H_2O followed by 10% HCl. The mixture was extracted with DCM, the organic layer was dried over anhydrous Na_2SO_4 and the solvent removed via rotary evaporation to yield a light green oil as the crude product. The crude product was purified via flash column chromatography (silica, hexane: DCM 5:1 v/v), to yield compound **6-8** as a light green solid. The light green colour was ascribed to the trace oxidation of compound **6-8** to compound **3** during elution. As such, no clean ^1H and ^{13}C NMR spectra were obtainable. HR MS (APCI): calcd for $C_{70}H_{63}S_2$ [$(M+H)^+$], 967.4366; found, 967.4337 (error: -3.00 ppm).

Compound 3

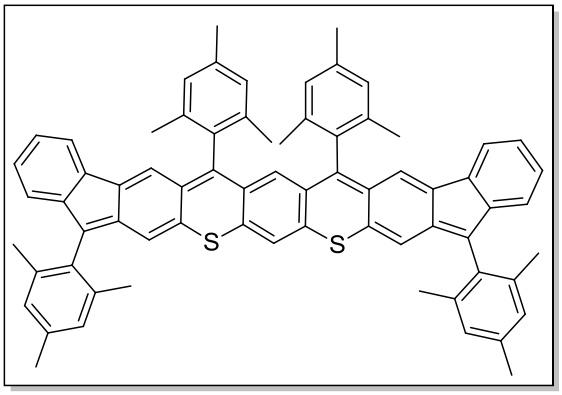

Compound **6-8** (300 mg, 0.6 mmol) was dissolved in toluene (60 mL) followed by the addition of *p*-chloranil (370 mg, 1.5 mmol). The light green solution was refluxed for 5 d, resulting in the considerable darkening of the solution to dark green. The coloured solution was dried over anhydrous Na_2SO_4 and the solvent was removed via rotary evaporation to yield a dark green solid. The residue was re-dissolved in hexane and purified via column

chromatography (silica, hexane: DCM 10:1 v/v) to yield compound **3** (100 mg, 50% yield over 3 steps) as a dark green solid. ^{1}H NMR (500 MHz, benzene-d_6, ppm): δ = 7.42 (s, 2H), 7.16 (d, *J* = 7.5 Hz, 2H), 7.06 (t, *J* = 7.1 Hz, 2H), 7.02-6.80 (m, 4H), 6.90 (s, 4H), 6.83 (t, *J* = 7.2 Hz, 2H), 6.70 (s, 1H), 6.64 (s, 4H), 6.20 (s, 1H), 2.24 (s, 12H), 2.10 (s, 12H), 1.77 (s, 12H); ^{13}C NMR (125 MHz, benzene-d_6, ppm): δ = 144.59, 141.65, 141.59, 137.76, 137.53, 137.27, 136.67, 136.46, 133.70, 133.44, 132.52, 132.10, 131.08, 128.85, 128.47, 125.97, 124.51, 121.12, 120.76, 120.52, 119.76, 115.21, 21.48, 21.25, 20.46, 19.49. HR MS (APCI): calcd for $C_{70}H_{59}S_2$ [$(M+H)^+$], 963.4053; found, 963.4056 (error: 0.31 ppm).

Compound 4

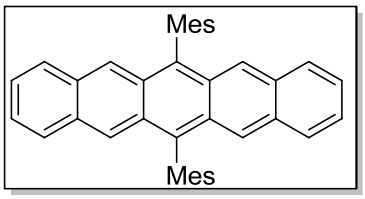

A solution of 2-mesitylmagnesium bromide solution in ether (1 M, 4 mL, 4 mmol) was slowly added to a solution of pentacene-6,13-dione (308 mg, 1 mmol) in THF (30 mL) at 0 ℃ under argon atmosphere. The reaction mixture was allowed to warm to room temperature and stirred for two days. After quenching with 10% HCl (4 mL), $SnCl_2$ (758 mg, 4 mmol) was added in one portion. The color of the reaction became deep purple immediately. The reaction flask was then wrapped in aluminum foil to block ambient light, and the reaction was stirred overnight at room temperature. The resulting deep purple solution was extracted with ethyl acetate (30 mL), washed with water, and then dried over Na_2SO_4. After solvent evaporation, the crude product was

purified with column chromatography on silica gel (hexane: CH_2Cl_2, 8:1 v/v). Compound **4** was further purified by recrystallization from methanol/ CH_2Cl_2 as a purple solid (260 mg, 50% yield). ^{1}H NMR (500 MHz, $CDCl_3$, ppm): δ = 8.17 (s, 4H), 7.75 (m, 4H), 7.24-7.10 (m, 8H), 2.57 (s, 6H), 1.78 (s, 12H); ^{13}C NMR (125 MHz, $CDCl_3$, ppm): δ = 137.94, 137.23, 135.55, 135.35, 131.42, 128.61, 128.50, 128.27, 124.90, 124.86, 21.39, 19.99. HR MS (EI): calcd for $C_{40}H_{34}$ (M^+), 514.2661; found, 514.2658 (error: -0.58 ppm).

References

[1] See review articles: (a) M. Bendikov, F. Wudl and D. F. Perepichka, *Chem. Rev.*, 2004, **104**, 4891. (b) J. E. Anthony, *Chem. Rev.*, 2006, **106**, 5028. (c) J. E. Anthony, *Angew. Chem., Int. Ed.*, 2008, **47**, 452. (d) Z. Sun, Q. Ye, C. Chi and J. Wu, *Chem. Soc. Rev.*, 2012, **41**, 7857. (e) K. Takimiya, I. Osaka, T. Mori and M. Nakano, *Acc. Chem. Res.*, 2014, **47**, 1493.

[2] (a) S. H. Chan, H. K. Lee, Y. M. Wang, N. Y. Fu, X. M. Chen, Z. W. Cai and H. N. C. Wong, *Chem. Commun.* 2005, 66. (b) B. Purushothaman, M. Bruzek, S. R. Parkin, A. F. Miller and J. E. Anthony, *Angew. Chem., Int. Ed.*, 2011, **50**, 7013.

[3] (a) I. Kaur, W. Jia, R. P. Kopreski, S. Selvarasah, R. Dokmeci, C. Pramanik, N. E. Mcgruer and G. P. Miller, *J. Am. Chem. Soc.*, 2008, **130**, 16274. (b) B. Kohl, F. Rominger and M. Mastalerz, *Angew. Chem., Int. Ed.*, 2015, **54**, 6051.

[4] (a) O. Berg, E. L. Chronister, T. Yamashita, G. W. Scott, R. M. Sweet and J. Calabrese, *J. Phys. Chem. A*., 1999, **103**, 2451. (b) B. Purushothaman, S. R. Parkin and J. E. Anthony, *Org. Lett.,* 2010, **12**, 2060.

[5] (a) J. E. Anthony, D. L. Eaton and S. R. Parkin, *Org. Lett.,* 2002, **4**, 15. (b) M. M. Payne, S. R. Parkin and J. E. Anthony, *J. Am. Chem. Soc.*, 2005, **127**, 8028. (c) D. Chun, Y. Cheng and F. Wudl, *Angew. Chemie., Int. Ed.,* 2008, **47**, 8380. (d) H. Qu and C. Chi, *Org. Lett.,* 2010, **12**, 3360. (e) W. Fudickar and T. Linker, *J. Am. Chem. Soc.,* 2012, **134**, 15071.

[6] (a) Y. Sakamoto, T. Suzuki, M. Kobayashi, Y. Gao, Y. Fukai, Y. Inoue, F. Sato and S. Tokito, *J. Am. Chem. Soc.,* 2004, **126**, 8138. (b) H. Qu, W. Cui, J. Li, J. Shao and C. Chi, *Org. Lett.,* 2011, **13**, 924. (c) S. Katsuta, D. Miyagi, H. Yamada, T. Okujima, S. Mori, K. I. Nakayama and H. Uno, *Org. Lett.,* 2011, **13**, 1454. (d) S. Katsuta, K. Tanaka, Y. Maruya, S. Mori, S. Masuo, T. Okujima, H. Uno, K.-I. Nakayama and H. Yamada, *Chem. Commun.*, 2011, **47**, 10112.

[7] (a) B. Gao, M. Wang, Y. Cheng, L. Wang, X. Jing and F. Wang, *J. Am. Chem. Soc.*, 2008, **130**, 8297. (b) U. H. F. Bunz, *Chem. Eur. J.*, 2009, **15**, 6780. (c) U. H. F. Bunz, J. U. Engelhart, B. D. Lindner and M. Schaffroth, *Angew. Chemie., Int. Ed.,* 2013, **52**, 3810. (d) U. H. F. Bunz,. *Acc. Chem. Res.,* 2015, **48**, 1676.

[8] (a) J. D. Wood, J. L. Jellison, A. D. Finke, L. Wang and K. N. Plunkett, *J. Am. Chem. Soc.,* 2012, **134**, 15783. (b) A. Naibi Lakshminarayana, J. Chang, J.

Luo, B. Zheng, K.-W. Huang and C. Chi, *Chem. Commun.*, 2015, **51**, 3604.

[9] (a) H. Qu and C. Chi, *Curr. Org. Chem.*, 2010, **14**, 2070. (b) Q. Ye and C. Chi, *Chem. Mater.*, 2014, **26**, 4046.

[10] Q. Ye, J. Chang, X. Shi, G. Dai, W. Zhang, K. W. Huang and C. Chi, *Org. Lett.*, 2014, **16**, 3966.

[11] (a) M. Bendikov, H. M. Duong, K. Starkey, K. N. Houk, E. A and Carter F. Wudl, *J. Am. Chem. Soc.*, 2004, **126**, 7416. (b) C. Tönshoff and H. F. Bettinger, *Angew. Chem., Int. Ed.*, 2010, **49**, 4125.

[12] Crystallographic data for tetraketone **6-6**: $C_{70}H_{62}O_4S_2$. M_w: 1031.37; triclinic; space group P -1; a = 11.2659(10) Å, b = 11.9309(10) Å, c = 14.1185(12) Å, α = 73.490(3)^o, β = 79.741(3)^o, γ = 63.446(2)^o; V = 1624.6(2) Å^3; Z = 2; ρ_{calcd} = 1.054 Mg/m^3; R_1 = 0.0774, wR_2 = 0.2052 (I > 2σ(I)); R_1 = 0.1424, wR_2 = 0.2241 (all data). CCDC No. 1059907. X-ray-quality crystal was obtained by slow diffusion of acetonitrile into chloroform solution.

[13] (a) G. Capozzi, G. Melloni, G. Modena and M. Piscitelli, *Tetrahedron Lett.*, 1968, **9**, 4039. (b) G. Capozzi, G. Melloni and G. Modena, *J. Chem. Soc. C, 1,* 1970, 2621. (c) G. Capozzi, G. Melloni and G. Modena, *J. Org. Chem.*, 1970, **35**, 1217. (d) M. S. Newman, *Acc. Chem. Res.*, 1972, **5**, 354. (e) G. Capozzi, G. Melloni and G. Modena, *J. Chem. Soc., Perkin Trans. 1,* 1973, 2250.

[14] (a) Crystallographic data for **1**: $C_{38}H_{32}S$. M_w: 520.69; tetragonal; space group I 41/a; a = 36.884(2) Å, b = 36.884(2) Å, c = 8.1964(5) Å, α = 90^o, β =

90°, γ = 90°; V = 11150.4(15) Å^3; Z = 16; ρ_{calcd} = 1.241 Mg/m^3; R_1 = 0.0413, wR_2 = 0.0989 (I > 2σ(I)); R_1 = 0.0519, wR_2 = 0.1047 (all data). CCDC No. 1059905. (b) Crystallographic data for **3** (with one toluene molecule): $C_{70}H_{58}S_2$,C_7H_8. M_w: 1055.41; triclinic; space group P 1; a = 7.9224(5) Å, b = 8.8963(5) Å, c = 21.6521(13) Å, α = 101.408(4)°, β = 94.312(4)°, γ = 97.130(4)°; V = 1476.50(16) Å^3; Z = 1; ρ_{calcd} = 1.187 Mg/m^3; R_1 = 0.1194, wR_2 = 0.2727 (I > 2σ(I)); R_1 = 0.1441, wR_2 = 0.2868 (all data). CCDC No. 1059906. (c) Crystallographic data for **4**: C_{40} H_{34}. M_w: 514.67; tetragonal; space group I4$_1$/a; a = 21.8964(12) Å, b = 21.8964(12) Å, c = 12.0694(9) Å, α = 90°, β = 90°, γ = 90°; V = 5786.7(8) Å^3; Z = 8; ρ_{calcd} = 1.182 Mg/m^3; R_1 = 0.0558, wR_2 = 0.1450 (I > 2σ(I)); R_1 = 0.0768, wR_2 = 0.1600 (all data). CCDC No. 1408042.

[15] See review articles: (a) Z. Sun and J. Wu, *J. Mater. Chem.*, 2012, **22**, 4151. (b) A. Shimizu, Y. Hirao, T. Kubo, M. Nakano, E. Botek and B. Champagne, *AIP Conf. Proc.*, 2012, **1504**, 399. (c) M. Abe, *Chem. Rev.*, 2013, **113**, 7011. (d) Z. Sun, Z. Zeng and J. Wu, *Acc. Chem. Res.*, 2014, **47**, 2582. (e) T. Kubo, *Chem. Rec.*, 2014, **15**, 218. (f) Z. Zeng, X. Shi, C. Chi, J. T. López Navarrete, J. Casado and J. Wu, *Chem. Soc. Rev.*, 2015, DOI: 10.1039/c5cs00051c

Chapter 7: An Isoelectronic Isomer of Pentacene: Synthesis, Crystallographic Analysis, Optical and Electronic Properties of Benzo[4,5]cyclohepta[1,2-*b*]fluorene

7.1 Introduction

"Aromaticity", a very important and fundamental chemical concept, has a history of more than one and a half centuries, which began with the fractional distillation of coal extracts benzene by Faraday in 1825.[1] Aromatic compounds can be divided into two types, alternant and non-alternant.[2] In the past century, a great effort has been devoted to the synthesis of the alternant aromatic compounds and the study of aromaticity involved in these compounds. However, studies on non-alternant aromatic compounds are very few and now attract an increasing interest in this field due to both the modern synthetic and characteristic methods together with the theoretical interests and potential applications in organic electronics of such non-alternant aromatic compounds.[3] Azulene, a structural isomer of naphthalene, is one of the most representative non-alternant aromatic compounds (**Figure 7.1**). The most obvious difference between azulene and naphthalene is the intense blue color of azulene, whereas naphthalene is colorless. The difference in color arises from the fact that they are two-type aromatic compounds, alternant and non-alternant, with unique and differential electronic configurations and molecular orbital characteristics.[4] Another obvious difference between azulene

and naphthalene is their polarity that azulene has a permanent dipole moment of 1.08 D (debye) despite the fact that the C-H bond is almost nonpolar. This difference in polarity arises from the fact that azulene somewhat has a zwitterionic aromatic resonance structure in its ground state according to Hückel's rule. Hence, the intrinsic dipole moment of azulene can be explained by considering both the neutral and zwitterionic structure as being in resonance with each other (**Scheme 7.1**).

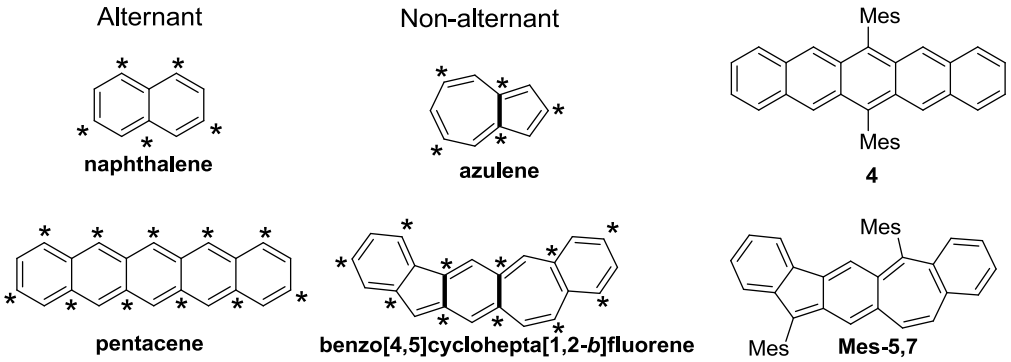

Figure 7.1 Examples of alternant and non-alternant compounds discussed in this work.

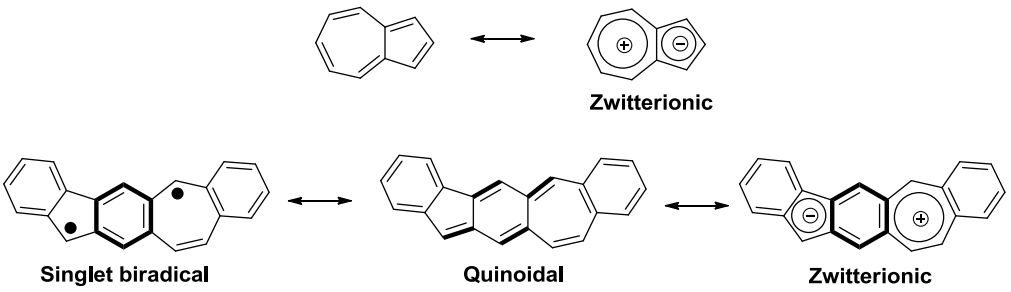

Scheme 7.1 Resonance forms of azulene and benzo[4,5]cyclohepta[1,2-*b*]fluorene.

Herein, we report a new non-alternant aromatic compound, benzo[4,5]cyclohepta[1,2-*b*]fluorene which is a structural isomer of pentacene with the same molecular formula. Benzo[4,5]cyclohepta[1,2-*b*]fluorene is comprised of one *p*-quinodimethane (*p*QDM) at the central and two different fusion motifs, indene and benzo[7]annulene, at both sides. We target this

compound for several reasons: 1) referring to the above discussion of the obvious difference between alternant aromatic compound (naphthalene) and non-alternant aromatic compound (azulene), the special difference of the properties (chemical & physical) between pentacene and benzo[4,5]cyclohepta[1,2-*b*]fluorene is of interest; 2) the polarity of benzo[4,5]cyclohepta[1,2-*b*]fluorene is unknown and thus is of interest because, similar to azulene, according to Hückel's rule benzo[4,5]cyclohepta[1,2-*b*]fluorene also somewhat has a zwitterionic aromatic resonance structure in its ground state (**Scheme 7.1**); 3) the ground-state geometry and electronic structure of benzo[4,5]cyclohepta[1,2-*b*]fluorene are also of interest as recent studies demonstrated that quinoidal polycyclic hydrocarbons (PHs) could show some singlet biradical character.[5] From this aspect there should be at least three resonance forms, i.e., singlet biradical, quinoidal and zwitterionic resonance forms may at the same time contribute to the ground state of benzo[4,5]cyclohepta[1,2-*b*]fluorene (**Scheme 7.1**). Thus it is of particular interest to investigate that which resonance form would dominate in its ground state.

The parent benzo[4,5]cyclohepta[1,2-*b*]fluorene is predicted to be unstable thus its derivative in which the most reactive sites are kinetically blocked by mesityl group (**Mes-5,7**) was designed and synthesized (**Figure 7.1**). Mesityl substituted pentacene (**4**) was also designed and synthesized as a

comparison (**Figure 7.1**). Our studies showed that non-alternant aromatic benzo[4,5]cyclohepta[1,2-*b*]fluorene derivative (**Mes-5,7**) displayed distinctively different ground-state electronic structure and physical properties from its alternant aromatic counterpart mesityl substituted pentacene (**4**).

7.2 Results and discussion

7.2.1 Synthesis

The synthetic route to **Mes-5,7** is depicted in **Scheme 7.2**. Firstly, 2,5-dibromo-*p*-xylene underwent mono-side Suzuki coupling reaction with phenyl boronic acid to give **7-1** in 60% yield. **7-1** was subsequently converted to **7-2** through three-step reactions involving oxidation, acidification and esterification in a very good yield. **7-2** then coupled with phenylacetylene through sonogashira coupling reaction to afford **7-3** in 90% yield. Subsequently, palladium carbon hydrogenation of the triple bond in **7-3** in the presence of hydrogen gave **7-4** in a quantitative yield. The hydrolysis of **7-4** produced the diacid **7-5** which was treated with $SOCl_2$ and then $AlCl_3$ to give **7-6** in an overall 80% yield. After introduction of the double bond by NBS bromination followed by dehydrobromination gave diketone **7-7** in about 75% yield. Finally, addition of Grignard reagent 2-mesitylmagnesium bromide and reduction of the intermediate diols with $SnCl_2$ gave **Mes-5,7** in a 35% yield. **4** was also synthesized according to a published procedure[6] with minor modification (refer to Chapter 6). Both compound **Mes-5,7** and **4** showed

good stability and solubility in common organic solvent and their structures were unambiguously confirmed by X-ray crystallographic analysis (*vide infra*).

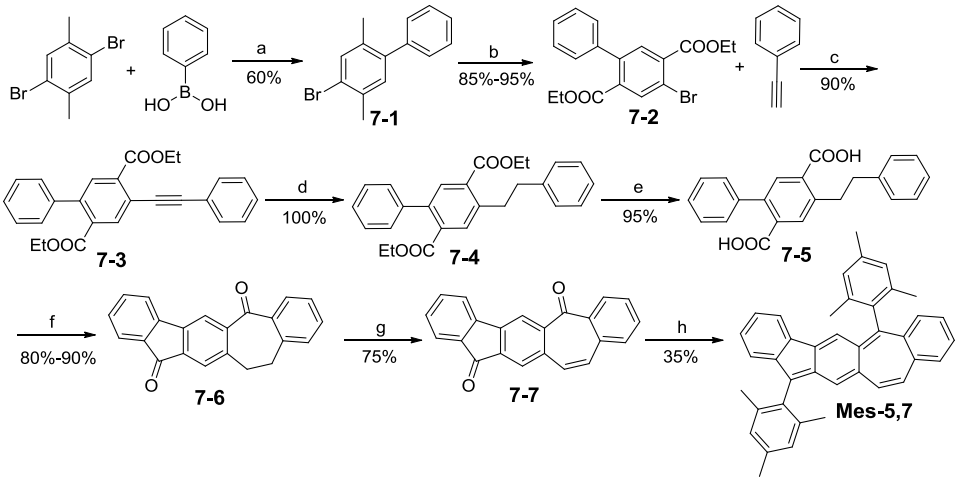

Scheme 7.2 Synthetic route to **Mes-5，7**. *Reagents and conditions*: (a) $Pd(PPh_3)_4$, Na_2CO_3, toluene /water (2:1), reflux overnight; (b) i) $KMnO_4$, pyridine, water, reflux overnight; ii) conc. HCl solution; iii) ethanol, conc. H_2SO_4, reflux overnight; (c) $Pd(PPh_3)_2Cl_2$, CuI, Et_3N, THF, reflux overnight; (d) Pd/C, H_2, THF, heat at 50 ^oC overnight; (e) i) NaOH, EtOH, reflux overnight; ii) 10% HCl (aq.); (f) i) $SOCl_2$, DMF, dry dichloromethane, reflux; ii) $AlCl_3$, dry dichloromethane, 0 ^oC - rt., overnight; (g) i) NBS, dibenzoyl peroxide, CCl_4, reflux overnight; ii) 2) DBU, DMF, 80 ^oC, 6 h; (h) i) 2-mesitylmagnesium bromide, THF, 0 ^oC - rt., overnight; ii) $SnCl_2$, conc. HCl solution, r. t..

7.2.2 Photophysical and electrochemical properties

The UV-vis-NIR absorption spectra of compounds **Mes-5,7** and **4** were recorded in diluted dichloromethane solutions (**Figure 7.2a**). **Mes-5,7** and **4** displayed distinctive band features that two well differentiated groups of bands are observed for **Mes-5,7** contrast to the typical acene band profile of **4** with typical α, β and p bands. The differential absorption spectra give them a distinctive appearance, i.e., **Mes-5,7** is deep green while **4** is deep purple. The first sharp and intense band, at 400 nm in **Mes-5,7**, is contributed from

HOMO-1→LUMO transition (*f*=1.147, 336.5 nm by TD DFT). The second absorption in **Mes-5,7** is at 650 nm (HOMO→LUMO, *f*=0.2505, 548.9 nm by TD DFT) with band edges almost close to 1000 nm. The origin of such low band gap absorptions is of interest and it is hypothesized to be attributed to the intramolecular charge-transfer (ICT) arising from its dipolar/zwitterionic character (**Scheme 7.1**). Thus, the absorption spectrum of **Mes-5,7** has been studied in different solvents (**Figure 7.2b**), as strong solvatochromism is a widely used criterion to identify an ICT state. It is found that the positions of the low band gap absorption peak for **Mes-5,7** is almost independent on solvent polarity indicating a very weak ICT character in this system, and thus, no significant bipolar/zwitterionic contribution to its ground state.

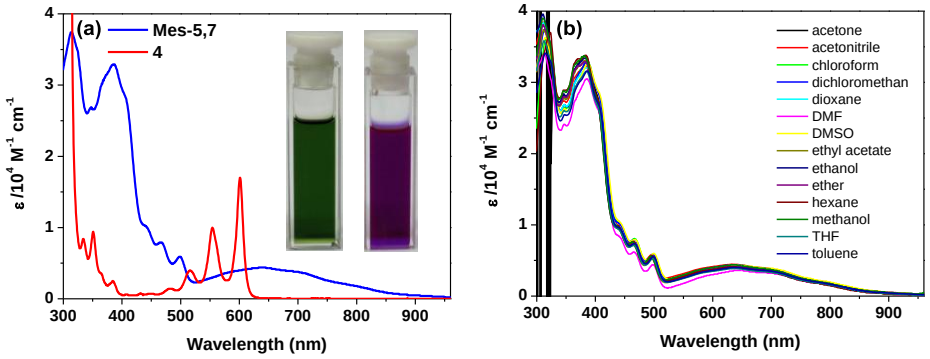

Figure 7.2 (a) UV-vis-NIR spectra of **Mes-5,7** and **4** recorded in dichloromethane; (b) UV-vis-NIR spectra of **Mes-5,7** in various organic solvents. Insert are the photos of the solution.

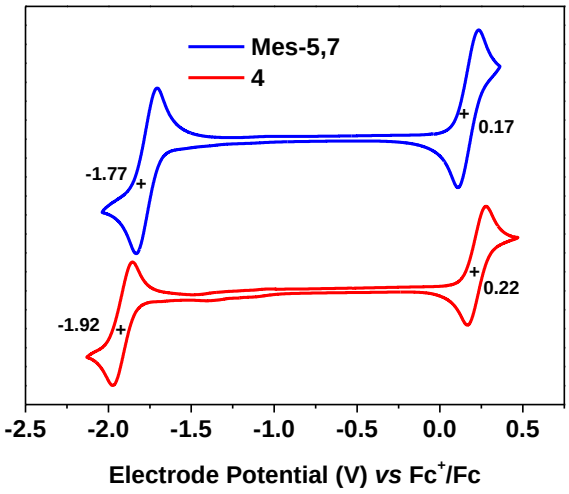

Figure 7.3 Cyclic voltammograms of **Mes-5,7** and **4** in DCM with 0.1 M Bu_4NPF_6 as supporting electrolyte, Ag/AgCl as reference electrode, Pt wire as counter electrode, and scan rate at 50 mV/s. The potential was externally calibrated against the ferrocene/ferrocenium redox couple.

The electrochemical property of **Mes-5,7** and **4** was investigated by cyclic voltammetry (CV) in DCM solution (**Figure 7.3**). All voltages are referenced with respect to the ferrocene/ferrocenium (Fc^+/Fc) couple. Both compounds display excellent amphoteric redox behavior with one reversible reduction waves (half-wave potential $E_{1/2}^{red}$ = -1.77 for **Mes-5,7**, -1.92 V for **4**) and one reversible oxidation waves (half-wave potential $E_{1/2}^{ox}$ = 0.17 V for **Mes-5,7** and 0.22 V for **4**). The HOMO and LUMO energy levels were estimated to be -4.86, -3.12 eV and -4.93, -2.98 eV for **Mes-5,7** and **4**, respectively. The electrochemical energy gap was thus determined to be 1.74 eV and 1.95 eV for **Mes-5,7** and **4**, respectively (**Table 7.1**).

Table 7.1 Summary of the photophysical and electrochemical data[a]

Comp	$E_{1/2}^{ox}$ (V)	$E_{1/2}^{red}$ (V)	HOMO (eV)	LUMO (eV)	E_g^{EC} (eV)	E_g^{opt} (eV)
Mes-5,7	0.17	-1.77	-4.86	-3.12	1.74	1.46
4	0.22	-1.92	-4.93	-2.98	1.95	2.00

[a] HOMO and LUMO energy levels were calculated from the first oxidation and reduction wave onset according to the equations HOMO = - (4.8 + E_{ox}^{onset}) eV and LUMO = - (4.8 + E_{red}^{onset}) eV.

7.2.3 Ground-state geometry and electronic structures

Single crystals suitable for X-ray crystallographic analysis were obtained for **7-7**, **Mes-5,7** and **4** by slow diffusion of methanol into their solution. **7-7** crystallizes in a monoclinic lattice system, with space group P c. **7-7** is not planar, which arranges into a columnar packing pattern (top view, a). The columns then further adopt a lamellar structure. In contrast, after nucleophilic addition with mesityl group into **7-7** and aromatization, the obtained **Mes-5,7** is essentially planar, with two mesityl groups oriented almost perpendicularly to the backbone, which gives rise to its excellent solubility in common organic solvent. **Mes-5,7** crystallizes in a monoclinic lattice system, with space group P 21/n. No close π-stacking was observed for **Mes-5,7**. Though the quality of the crystallographic data is not good enough, the noticeable bond length alternation (BLA) found in the central *p*-quinodimethane (*p*QDM) part indicates its significant quinoidal conjugation. This is in well agreement with the result of UV-vis-NIR measurement of **Mes-5,7** in different solvents discussed above and the sharp NMR signal of **Mes-5,7**, which indicates its rare zwitterionic or singlet biradical character. **4** crystallizes in a tetragonal

lattice system, with space group I 41/a. **4** is planar, which arranges into a compact structure with tetragonal symmetry. In contrast to **Mes-5,7**, no significant bond length alternation (BLA) was observed in **4**.

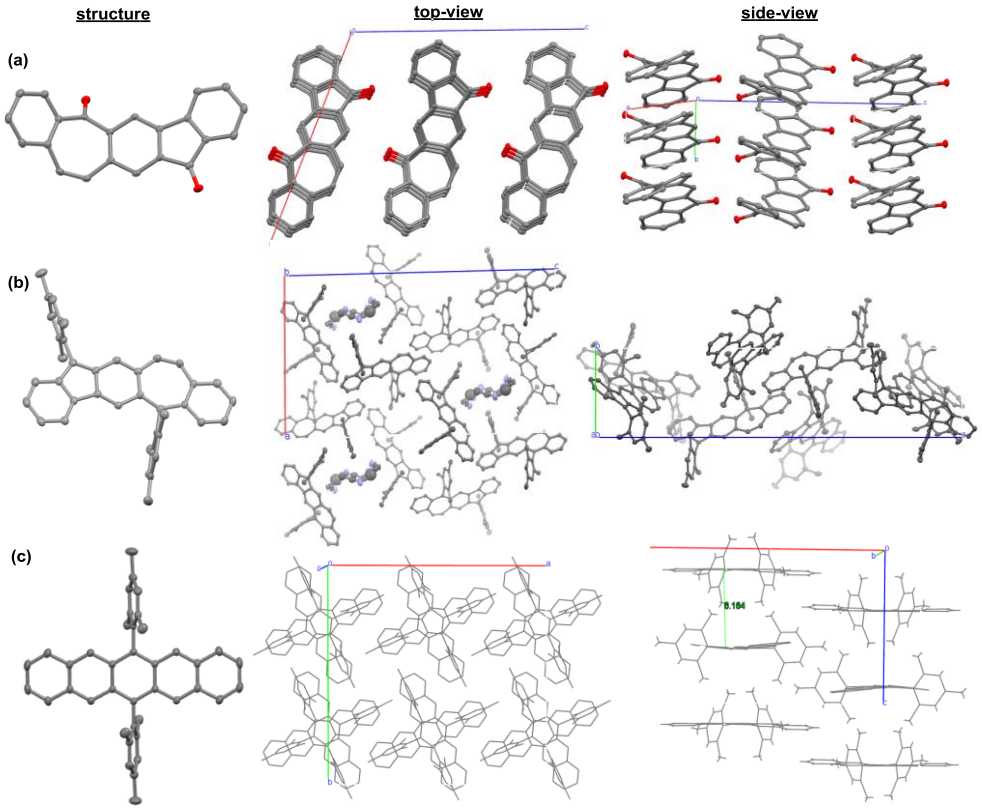

Figure 7.4 X-ray crystallographic structures and packing structures of (a) diketone **7-7**, (b) **Mes-5,7** and (c) **4**. Hydrogen atoms are omitted for clearance.

7.3 Conclusion

In summary, a new class of non-alternant aromatic compound, benzo[4,5]cyclohepta[1,2-*b*]fluorine (**Mes-5,7**), that contains linearly annulated 6-5-6-7-6 ring system was successfully synthesized. Its acene isomer mesityl substituted pentacene (**4**) was also designed and synthesized as a comparison. The crystal structure of **Mes-5,7** indicates its typical quinoidal structure while **4** adopts a typical diene conjugation. No typical π-π stacking is found in both two crystalline forms. Both compounds showed excellent

solubility and stability. Compared to normal alternant aromatic compound **4**, **Mes-5,7** displayed a distinctive UV-vis-NIR absorption band with long wavelength tail to almost 1000 nm. This special band gap absorption peak for **Mes-5,7** is almost independent on solvent polarity. The preliminary results of this work demostrted that this non-alternant aromatic compound **Mes-5,7** could be regarded as typical quinoidal system with quinoidal resonance form dominating in its ground-state, at the same time, with scarce zwitterionic and singlet biradical character.

7.4 Experiments

7.4.1 General experimental methods

Refer to the section of *2.4.1 General experimental methods* in Chapter 2.

7.4.2 Detailed synthetic procedures and characterization data

Compound 7-1

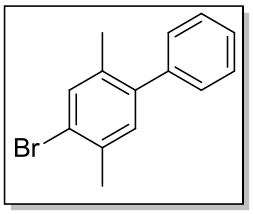

Phenyl boronic acid (2.43 g, 20 mmol), 2,5-dibromo-*p*-xylene (16 g, 60 mmol) and Na_2CO_3 (4.3 g, 40 mmol) were dissolved in toluene (100 mL) and water (50 mL),. $Pd(PPh_3)_4$ (400 mg) was added as a catalyst and the mixture was refluxed for 12 h. After cooling down, the mixture was poured into water and extracted with ethyl acetate. The organic layer was washed with water and

dried over anhydrous Na_2SO_4. The solvent was removed under vacuum and the residue was purified by column chromatography (silica, hexane) to give compound **7-1** as colorless oil (3.1 g, 60% yield). ^{1}H NMR (500 MHz, $CDCl_3$, ppm): δ = 7.44 (s, 1H), 7.41 (t, *J* = 7.5 Hz, 2H), 7.37-7.32 (m, 1H), 7.28 (d, *J* = 7.9 Hz, 2H), 7.09 (s, 1H), 2.39 (s, 3H), 2.21 (s, 3H); ^{13}C NMR (125 MHz, $CDCl_3$, ppm): δ =141.08, 140.89, 134.93, 134.63, 133.68, 132.00, 128.97, 128.13, 126.98, 123.44, 22.24, 19.64. HR MS (EI): calcd for $C_{14}H_{13}Br$ (M^+), 260.0201; found, 260.0196 (error: -1.92 ppm).

Compound 7-2

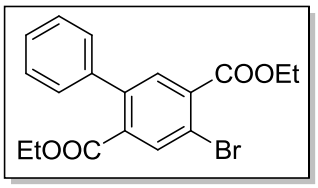

To a refluxing solution of compound **7-1** (2.6 g, 10 mmol) in 20 mL pyridine and 80 mL water was slowly added an excess of $KMnO_4$ (about 15 g) by portions over 3 hours. The reaction mixture was then refluxed overnight. After cooling down the resulting mixture was filtrated. Concentrated HCl solution was added to the filtrated solution to afford the title diacid compound as a white solid. The crude diacid compound was dried under vacuum and used without purification for next step.

The dried diacid compound obtained above was dissolved in anhydrous ethanol (30 mL). Concentrated H_2SO_4 (5 mL) was slowly added as a catalyst to the reaction mixture, and the mixture was heated to reflux overnight. After

cooling down, the mixture was poured into water and extracted with ethyl acetate. The organic layer was washed with water and dried over anhydrous Na_2SO_4. The solvent was removed under vacuum and the residue was purified by column chromatography (silica, hexane: ethyl acetate, 15:1 v/v) to give compound **7-2** as a waxy solid (3.4 g, 90% yield). ^{1}H NMR (500 MHz, $CDCl_3$, ppm): δ = 8.08 (s, 1H), 7.75 (s, 1H), 7.42-7.37 (m, 3H), 7.36-7.28 (m, 2H), 4.42 (q, *J* = 7.0 Hz, 2H), 4.11 (q, *J* = 7.3 Hz, 2H), 1.40 (t, *J* = 7.0 Hz, 3H), 1.01 (t, *J* = 7.1 Hz, 3H); ^{13}C NMR (125 MHz, $CDCl_3$, ppm): δ =166.55, 165.49, 141.31, 139.39, 135.13, 134.64, 134.59, 133.01, 128.19, 127.81, 119.95, 62.01, 61.55, 14.14, 13.57. HR MS (EI): calcd for $C_{18}H_{17}BrO_4$ (M^+), 376.0310; found, 376.0311 (error: 0.27 ppm).

Compound 7-3

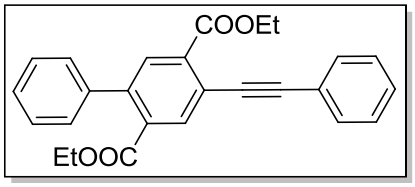

Compound **7-2** (1.13 g, 3 mmol), phenylacetylene (460 mg, 4.5 mmol) CuI (18 mg) and $Pd(PPh_3)_2Cl_2$ (30 mg) were dissolved in THF (30 mL) and Et_3N (10 mL). The resulting solution was deoxygenated by freeze-thow-pump for three times and then slowly warmed to room temperature. The reaction was refluxed for 12 h. After cooling down, the mixture was poured into 10% HCl solution and extracted with ethyl acetate. The organic layer was washed with 10% HCl solution and dried over anhydrous Na_2SO_4. The solvent was

removed under vacuum and the residue was purified by column chromatography (silica, hexane: ethyl acetate, 25:1 v/v) to give compound **7-3** (1.08 g, 90% yield). ^{1}H NMR (500 MHz, $CDCl_3$, ppm): δ = 8.07 (s, 1H), 7.98 (s, 1H), 7.62-7.58 (m, 2H), 7.45-7.32 (m, 8H), 4.44 (q, *J* = 7.0 Hz, 2H), 4.13 (q, *J* = 7.2 Hz, 2H), 1.41 (t, *J* = 7.0 Hz, 3H), 1.04 (t, *J* = 7.0 Hz, 3H); ^{13}C NMR (125 MHz, $CDCl_3$, ppm): δ =167.44, 165.57, 141.45, 139.88, 135.20, 134.12, 133.92, 132.52, 131.74, 128.71, 128.39, 128.29, 128.19, 127.78, 123.04, 122.54, 95.40, 87.33, 61.58, 61.45, 14.31, 13.63. HR MS (EI): calcd for $C_{26}H_{22}O_4$ (M^+), 398.1518; found, 398.1501 (error: -4.27 ppm).

Compound 7-4

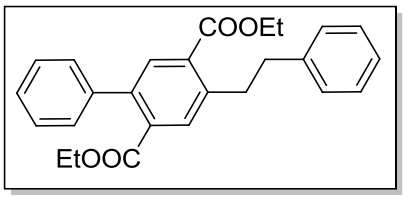

Compound **7-3** (1.6 g, 4 mmol) was dissolved in 50 mL dry THF. To the resulting solution was added an excess of 10% Pd/C (0.6 g). The reaction mixture was kept at an atmosphere of H_2 maintained by an inflated balloon, and heated to 50 ^{o}C. Upon completion of the reaction as monitored by TLC (This reaction usually takes about 1 day to 3 days.), the reaction solution was filtrated to remove the Pd/C. The filtrated solution was concentrated and dried under reduced pressure to give the pure compound **7-4** (1.6 g, 100% yield). ^{1}H NMR (500 MHz, $CDCl_3$, ppm): δ = 7.89 (s, 1H), 7.68 (s, 1H), 7.43-7.36 (m, 3H), 7.35-7.27 (m, 6H), 7.24-7.20 (m, 1H), 4.39 (q, *J* = 7.0 Hz, 2H), 4.10 (q, *J*

= 7.2 Hz, 2H), 3.31 (m, 2H), 2.96 (m, 2H), 1.39 (t, *J* = 7.2 Hz, 3H), 1.00 (t, *J* = 7.2 Hz, 3H); ^{13}C NMR (125 MHz, $CDCl_3$, ppm): δ =168.18, 166.82, 142.23, 141.61, 140.44, 139.88, 134.02, 132.61, 132.21, 132.18, 128.48, 128.38, 128.07, 127.36, 125.99, 61.26, 61.18, 37.96, 36.16, 14.28, 13.59. HR MS (EI): calcd for $C_{26}H_{26}O_4$ (M^+), 402.1831; found, 402.1836 (error: 1.24 ppm).

Compound 7-5

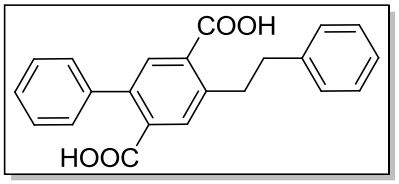

Compound **7-4** (1.6 g, 4 mmol) was dissolved in 60 mL ethanol, followed by the addition of an excess of sodium hydroxide (2 g). This mixture was heated to reflux overnight. The solvent was removed under reduced pressure after the reaction was completed. To the residue then 10% hydrochloric acid solution was added. The precipitate formed was collected by filtration and washed with water and hexane, then dried in vacuum to afford compound **7-5** (1.3 g, 95% yield). ^{1}H NMR (500 MHz, DMSO-d_6, ppm): δ = 13.17 (br, 1H), 7.78 (s, 1H), 7.69 (s, 1H), 7.45-7.41 (m, 2H), 7.39-7.35 (m, 3H), 7.33-7.28 (m, 4H), 7.22-7.18 (m, 1H), 3.24 (m, 2H), 2.87 (m, 2H); ^{13}C NMR (125 MHz, DMSO-d_6, ppm): δ =169.12, 168.04, 141.65, 141.61, 139.80, 138.33, 134.99, 132.38, 132.08, 131.39, 128.31, 128.26, 128.22, 127.42, 125.93, 37.33, 35.53. HR MS (EI): calcd for $C_{22}H_{18}O_4$ (M^+), 346.1205; found, 346.1199 (error: -1.73 ppm).

Compound 7-6

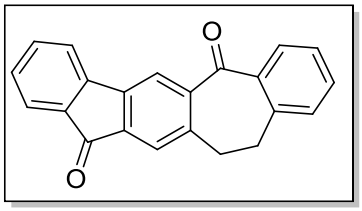

Compound **7-5** (1.39 g, 4 mmol) was added in anhydrous DCM (30 mL), followed by the addition of excess of thionyl chloride (3 mL). To this mixture anhydrous DMF (1-2 drops) was added as catalyst at room temperature. The resultant mixture was heated to reflux overnight. During this period the insoluble diacid **5** became soluble in DCM. After cooling down the solvent was removed under reduced pressure to afford crude acid chloride. This intermediate compound was re-dissolved in anhydrous DCM (30 mL) then anhydrous $AlCl_3$ (2.1 g, 16 mmol) was added carefully at 0 ℃. The resultant mixture was allowed to warm up to room temperature and stirred overnight, then slowly quenched by 10% HCl solution and extracted with DCM. The organic layer was washed with water and dried over anhydrous Na_2SO_4. The solvent was removed under vacuum and the residue was purified by column chromatography (silica, hexane: DCM, 1:1 v/v) to give compound **7-6** as pale yellow solid (1.0 g, 81% yield). ^{1}H NMR (500 MHz, $CDCl_3$, ppm): δ = 8.05-8.02 (m, 2H), 7.66 (d, *J* = 7.5 Hz, 1H), 7.57 (d, *J* = 7.0 Hz, 1H), 7.53-7.45 (m, 3H), 7.36 (t, *J* = 8.0 Hz, 1H), 7.30 (t, *J* = 7.80 Hz, 1H), 7.25 (d, *J* = 7.1 Hz, 1H), 3.22 (m, 4H); ^{13}C NMR (125 MHz, $CDCl_3$, ppm): δ = 195.45, 193.33, 144.20, 144.00, 143.01, 142.18, 142.03, 137.62, 136.79, 135.20,

134.20, 132.88, 130.76, 129.72, 129.15, 126.79, 125.05, 124.45, 121.86, 120.68, 34.71, 34.54. HR MS (EI): calcd for $C_{22}H_{14}O_2$ (M^+), 310.0994; found, 310.0990 (error: -1.30 ppm).

Compound 7-7

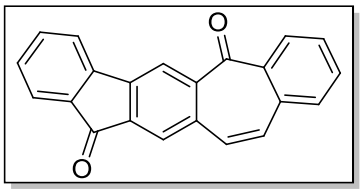

Compound **7-6** (620 mg, 2 mmol), NBS (392 mg, 2.2 mmol) and dibenzoyl peroxide (20 mg) were dissolved in 50 mL CCl_4, and the mixture was refluxed for 12 h. After cooling down the resulting mixture was filtrated. The filtrated solution was concentrated and dried. The residue was re-dissolved in 30 mL dry DMF. Then 1,8-Diazabicyclo[5.4.0]undec-7-ene (DBU) (0.31 mL) was slowly added to the above solution. The resulting mixture was heated to 80 ℃ for 6 hours. After cooling down, the mixture was poured into 10% HCl solution and extracted with large amount of DCM. The organic layer was washed with 10% HCl solution and dried over anhydrous Na_2SO_4. The solvent was removed under vacuum and the residue was purified by column chromatography (silica, hexane: DCM, 2:1 v/v) to give compound **7-7** as a yellow solid. Compound **7-7** was further purified by recrystallization from MeOH/CH_2Cl_2 as a golden solid (462 mg, 75% yield). ^{1}H NMR (500 MHz, $CDCl_3$, ppm): δ = 8.33 (s, 1H), 8.21 (d, J = 7.7 Hz, 1H), 7.84 (s, 1H), 7.75-7.66 (m, 3H), 7.63-7.55 (m, 3H), 7.37 (t, J = 7.3 Hz, 1H), 7.11 (m, 2H);

^{13}C NMR data was not obtained due to its poor solubility. HR MS (EI): calcd for $C_{22}H_{12}O_2$ (M^+), 308.0837; found, 308.0839 (error: 0.65 ppm).

Compound Mes-5,7

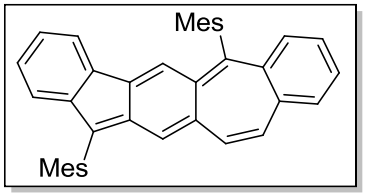

A solution of 2-mesitylmagnesium bromide solution in ether (1 M, 1.8 mL, 1.8 mmol) was slowly added to a solution of compound **7-7** (100 mg, 0.3 mmol) in THF (30 mL) at 0 ℃ under argon atmosphere. The mixture was slowly warmed to room temperature and stirred overnight. During this period the solution became clear and colorless. The reaction was quenched with 10% HCl solution (10 ml) and extracted in $CHCl_3$. The organic layer was dried (Na_2SO_4), filtered, and evaporated to dryness under vacuum. After that the crude diol was re-dissolved in dry THF (50 mL) and degassed with argon. Saturated $SnCl_2$ solution in 37% HCl solution (0.3 mL) was then slowly added to the mixture, and the reaction was stirred overnight. During this period the color of the reaction mixture became green. The resulting green solution was then poured into water and extracted with ethyl acetate. The organic layer was washed with water and dried over anhydrous Na_2SO_4. The solvent was removed under vacuum and the residue was purified by column chromatography (silica, hexane: DCM, 8:1 v/v). Compound **Mes-5,7** was further purified by recrystallization from CH_3CN/CH_2Cl_2 as a dark solid (54

mg, 35% yield). ^{1}H NMR (500 MHz, $CDCl_3$, ppm): δ = 7.56 (d, *J* = 7.3 Hz, 1H), 7.29 (d, *J* = 7.0 Hz, 2H), 7.22-7.15 (m, 3H), 7.06-6.96 (m, 6H), 6.88 (d, *J* = 8.3 Hz, 1H), 6.62 and 6.59 (s, 2H), 6.42 and 6.40 (s, 1H), 2.47 (s, 3H), 2.39 (s, 3H), 2.07 and 2.04 (s, 12H); ^{13}C NMR (125 MHz, $CDCl_3$, ppm): δ = 147.49, 144.04, 139.66, 139.58, 138.44, 137.71, 137.03, 137.00, 136.94, 136.68, 136.38, 135.20, 133.41, 133.23, 132.01, 131.93, 131.68, 130.88, 129.70, 129.46, 128.53, 128.10, 127.94, 127.90, 124.26, 123.69, 123.37, 120.20, 119.95, 21.24, 21.17, 20.31, 19.90. HR MS (EI): calcd for $C_{40}H_{34}$ (M^+), 514.2661; found, 514.2658 (error: -0.58 ppm).

References

[1] M. Faraday, *Phil. Trans. Roy. London*, 1825, 440.

[2] An aromatic compound is alternant (*e.g*. naphthalene) if stars can be placed on alternating π-centers with no two stars adjacent, whereas it is non-alternant (*e.g*. azulene) if two or more adjacent centers receive stars as illustrated in **Figure 7.1**.

[3] (a) Y. Tobe, *Chem. Rec.*, 2014, **15**, 86. (b) H. Miyoshi, S. Nobusue, A. Shimizu and Y. Tobe, *Chem. Soc. Rev.*, 2015 DOI: 10.1039/C5CS00185D.

[4] R. S. H. Liu, *J. Chem. Ed.*, 2002, **79**, 183.

[5] (a) Z. Sun and J. Wu, *J. Mater. Chem.*, 2012, **22**, 4151. (b) Z. Sun, Q. Ye, C. Chi and J. Wu, *Chem. Soc. Rev.*, 2012, **41**, 7857.

[6] I. Kaur, W. Jia, R. P. Kopreski, S. Selvarasah, R. Dokmeci, C. Pramanik, N.

E. Mcgruer and G. P. Miller, *J. Am. Chem. Soc.*, 2008, **130**, 16274.